JOURNAL OF

ELECTROANALYTICAL

CHEMISTRY

AND INTERFACIAL ELECTROCHEMISTRY

International Journal devoted to all Aspects
of Electroanalytical Chemistry, Double Layer
Studies, Electrokinetics, Colloid Stability, and
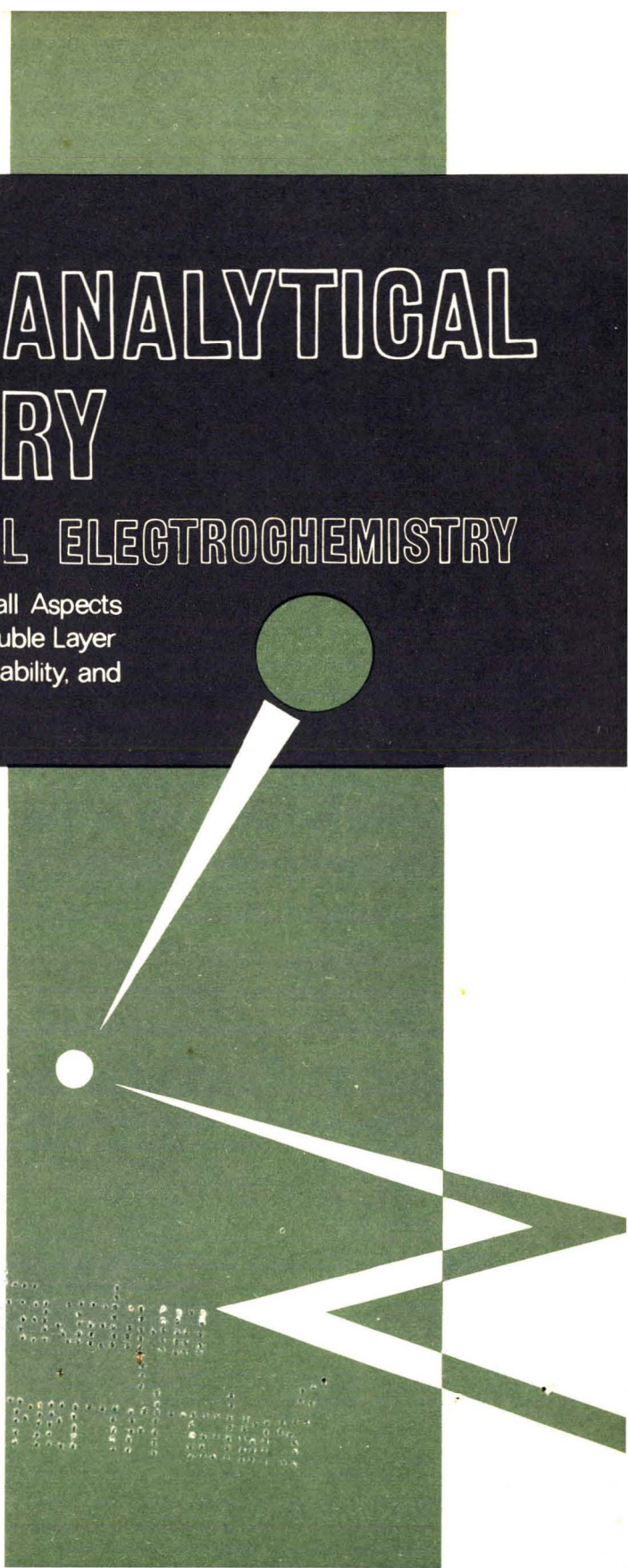Electrode Kinetics.

GENERAL INFORMATION

Types of contributions

(a) Original research work not previously published in other periodicals (regular papers).
(b) Reviews on recent developments in various fields.
(c) Short communications.
(d) Preliminary notes.

A Preliminary Note is a brief report of work which has progressed to the stage when it is considered that the science of chemistry would be advanced if the results were made available as soon as possible to others working on the same subject. Preliminary Notes can in general be published within 4–8 weeks of their acceptance by the editor although this implies that proofs cannot be sent to the author(s). The publisher will attend to correction of the proof but it should be remembered that errors in the manuscript will also appear in the published Note. Preliminary Notes, clearly marked as such, must be sent to Dr. R. Parsons (address given below).

Languages: Papers will be published in English, French or German.

Submission of papers

Papers should be sent to one of the following Editors:
> Dr. R. PARSONS, Department of Chemistry, The University, Bristol BS8 1TS, England.
> Dr. R. DE LEVIE, Department of Chemistry, Georgetown University, Washington, D.C. 20007, U.S.A.
> Dr. R. H. OTTEWILL, Department of Chemistry, The University, Bristol BS8 1TS, England.

For rapid handling papers originating from the American continent should be sent to Dr. DE LEVIE, those of colloid interest to Dr. OTTEWILL, and all others to Dr. PARSONS.

Authors should preferably submit two copies in double-spaced typing on pages of uniform size. Legends for figures should be typed on a separate page. The figures should be in a form suitable for reproduction, drawn in Indian ink on drawing paper or tracing paper, with lettering etc. in thin pencil. The sheets of drawing or tracing paper should preferably be of the same dimensions as those on which the article is typed. Photographs should be submitted as clear black and white prints on glossy paper. Standard symbols should be used in line drawings, the following are available to the printers:

▼ ▽ ■ ⊓ ● ◎ ▪ ▫ ⬦ ▣ ▪ + ×

All references should be given at the end of the paper. They should be numbered and the numbers should appear in the text at the appropriate places.
A summary of 50 to 200 words should be included.

Reprints

Fifty reprints will be supplied free of charge. Additional reprints (minimum 100) can be ordered at quoted prices. They must be ordered on order forms which are sent together with the proofs.

Publication

The *Journal of Electroanalytical Chemistry and Interfacial Electrochemistry* appears monthly. For 1970, each volume has 3 issues and 4 volumes will appear.
Subscription price: Sfr. 318.75 (U.S. $ 75.—) per year incl. postage. Additional cost for copies by air mail available on request. For subscribers in the U.S.A. and Canada, 2nd class postage paid at New York, N.Y. For advertising rates apply to the publishers.

Subscriptions should be sent to:

THE CHEMISTRY OF TITANIUM AND VANADIUM

AN INTRODUCTION TO THE CHEMISTRY OF THE EARLY TRANSITION ELEMENTS

by R. J. H. CLARK, University College, London (Great Britain)

Monograph 11 in the series Topics in Inorganic and General Chemistry edited by P. L. Robinson

With the development of techniques for handling air-sensitive materials, many aspects of the chemistry of titanium and vanadium have developed very rapidly, most noticeably in the last ten years. This is the first book to summarise and critically assess these developments, and to point to likely areas for further research. The chemistry of these two elements is in many ways very similar and the comparisons drawn within this book help to focus attention on the similarities.
The book is devoted to the preparations, properties and structures of the various compounds of titanium and vanadium. Many possible avenues for further research are indicated in the text.

Contents: 1. Discovery, isolation, general and elementary properties of titanium and vanadium. 2. Halides and oxyhalides. 3. Complexes of titanium (IV), vanadium (IV) and (V). 4. Complexes of tervalent titanium and vanadium. 5. Complexes of titanium and vanadium in the oxidation states two, and lower. 6. Spectra and magnetism of titanium and vanadium complexes. 7. Metal oxo species. 8. Organometallic compounds. 9. Oxides, sulphides and other binary compounds. 10. Other topics. Appendix. Subject index.

$5\frac{1}{2}$ x $8\frac{1}{2}$", xi + 327 pages, 67 tables, 35 illus., 1055 lit.refs., 1968
Dfl. 65.00, £8.10.10.

Elsevier Publishing Company

AMSTERDAM - LONDON - NEW YORK

Differential Thermal Analysis

In two volumes
Volume 1 Fundamental Aspects

Edited by R. C. Mackenzie

February 1970, xvi + 776 pp., 240s.

An authoritative and critical assessment of the present state of Differential Thermal Analysis.
Definitive data are given for a very large range of compounds, materials and processes, and the effects of various, often little appreciated, factors on DTA are assessed. Of particular interest to R and D personnel and pure scientists in chemistry, physics, mineralogy, earth sciences and biology.

Polarography of Metal Complexes

David R. Crow

July 1969, xiv + 204 pp., 65s.

Covers all aspects of the polarography of complexed metal ions in solution, emphasising the versatility of polarographic techniques as applied to the study of coordination compounds; as well as all the important methods available for the study of metal-ligand equilibria in solution, and the determination of stability constants.

Academic Press
London and New York

Berkeley Square House
Berkeley Square
London W1X 6BA, England

111 Fifth Avenue, New York
NY 10003, U.S.A.

A New Important
Encyclopaedic
Work of Reference

COMPRE- HENSIVE CHEMICAL KINETICS

edited by C.H. BAMFORD F.R.S.,
and C.F.H. TIPPER

The aim of this series is to cover
in a critical way the practice
and theory of kinetics and the
kinetics of inorganic and organic
reactions in the gas and condensed
phases or at interfaces.
Each chapter is written by an
expert in the field so that the series
as a whole will serve as a direct
source of reference and
information over the whole range
of kinetics.
The vast amount of material
scattered through the literature
has never before been gathered
together and presented in this
accessible form.

Subscribers who place a standing order
for the whole series before
December 15, 1969 will be entitled
to an overall 15% discount.

Elsevier Publishing Company

Volume 1. The Practice of Kinetics

1. Experimental methods for the study of slow reactions (L. Batt)
2. Experimental methods for the study of fast reactions (D.N. Hague)
3. Experimental methods for the study of heterogeneous reactions (D. Shooter)
4. The detection and estimation of intermediates (R.P. Wayne)
5. The treatment of experimental data (D. Margerison)

7 x 10", xiii + 450 pages, 32 tables, 161 illus., 1174 lit. refs., 1969, Dfl. 95.00, £10.15.0
SBN 444-40673-5

Volume 2. The Theory of Kinetics

1. Kinetic characterization of complex reaction systems (Z.G. Szabó)
2. Chain reactions (V.N. Kondratiev)
3. Theory of the kinetics of elementary gas phase reactions (R.P. Wayne)
4. Theory of elementary reactions in solution (I.D. Clark and R.P. Wayne)
5. Theory of solid phase kinetics (L.G. Harrison)

7 x 10", xiii + 462 pages + index, 16 tables, 77 illus., 794 lit. refs., 1969
SBN 444-40674-3

Volume 3. Formation and Decay of Excited Species

1. Effect of low energy radiation (C.S. Burton and W.A. Noyes, Jr.)
2. Effect of high energy radiation (G. Hughes)
3. The chemical production of excited states (T. Carrington and D. Garvin)
4. The transfer of energy between chemical species (A.B. Callear and J.D. Lambert)

7 x 10", 1969, in preparation
SBN 444-40676-x

The series as a whole will comprise about 25 volumes divided into a number of sections:

Section 1. The practice and theory of kinetics (3 volumes)
Section 2. Decomposition and isomerisation reactions (2 volumes)
Section 3. Inorganic reactions (2 volumes)
Section 4. Organic reactions (6 volumes)
Section 5. Polymerization reactions (2 volumes)
Section 6. Oxidation and combustion reactions (2 volumes)
Section 7. Selected elementary reactions (2 volumes)

Other sections are planned on heterogeneous reactions, solid state reactions, and kinetics and technological processes.

STUDY OF THE KINETICS OF ELECTROCHEMICAL REACTIONS BY THIN-LAYER VOLTAMMETRY

III. ELECTROREDUCTION OF THE CHLORIDE COMPLEXES OF PLATINUM(II) AND (IV)

ARTHUR L. Y. LAU AND ARTHUR T. HUBBARD

Department of Chemistry, University of Hawaii, Honolulu, Hawaii 96822 (U.S.A.)

(Received August 18th, 1969; in revised form October 7th, 1969)

In a previous study[1] in which thin-layer electrochemical techniques were employed it was shown that $PtCl_6^{2-}$ is reduced to $PtCl_4^{2-}$ at platinum electrodes in 1 F chloride supporting electrolyte and to the metal in 1 F sodium perchlorate (eqns. 1 and 2).

$$PtCl_6^{2-} + 2e^- \xrightarrow{\text{1 F Cl}^-} PtCl_4^{2-} + 2\ Cl^- \qquad\qquad E^0 = 0.41 \text{ V NaCE} \quad (1)$$

$$PtCl_6^{2-} + 4e^- \xrightarrow{\text{1 F NaClO}_4} Pt + 6\ Cl^- \qquad\qquad E^0 = 0.43 \text{ V NaCE} \quad (2)$$

$PtCl_4^{2-}$ is reduced readily to the metal only when halide is absent from the supporting electrolyte (eqn. 3).

$$PtCl_4^{2-} + 2\ e^- \xrightarrow{\text{1 F NaClO}_4} Pt + 4\ Cl^- \qquad\qquad E^0 = 0.45 \text{ V NaCE} \quad (3)$$

In view of recent studies of the electrochemistry of platinum complexes[2], it appears that the halide dependence of $PtCl_6^{2-}$ electroreduction, eqns. (1)–(3), may be understood in terms of specific adsorption of reactive species at the electrode surface prior to and during the electron transfer step. In some instances electron transfer may proceed through a bridging halogen. The present studies are directed toward verifying this conjecture and extending it to other halide and halo-ammine complexes of Pt(II) and (IV). It appears that thin-layer electrochemical techniques[2,3] are uniquely suited to the exploration of the influence of the electrochemical double layer and reactant structure on the course of reactions at solid electrodes.

1. STOICHIOMETRY OF $PtCl_6^{2-}$ ELECTROREDUCTION

Thin-layer current–potential curves[3] for reduction of $PtCl_6^{2-}$ and $PtCl_4^{2-}$ in supporting electrolytes containing various concentrations of chloride appear in Fig. 1, from which it is apparent that chloride inhibits the electroreduction of $PtCl_4^{2-}$ and, to a lesser extent, of $PtCl_6^{2-}$. Since the rate constant for the electroreduction of $PtCl_4^{2-}$ is about an order of magnitude smaller than that for $PtCl_6^{2-}$ at equal chloride concentrations and the relevant standard potentials are similar, $PtCl_4^{2-}$ electro-
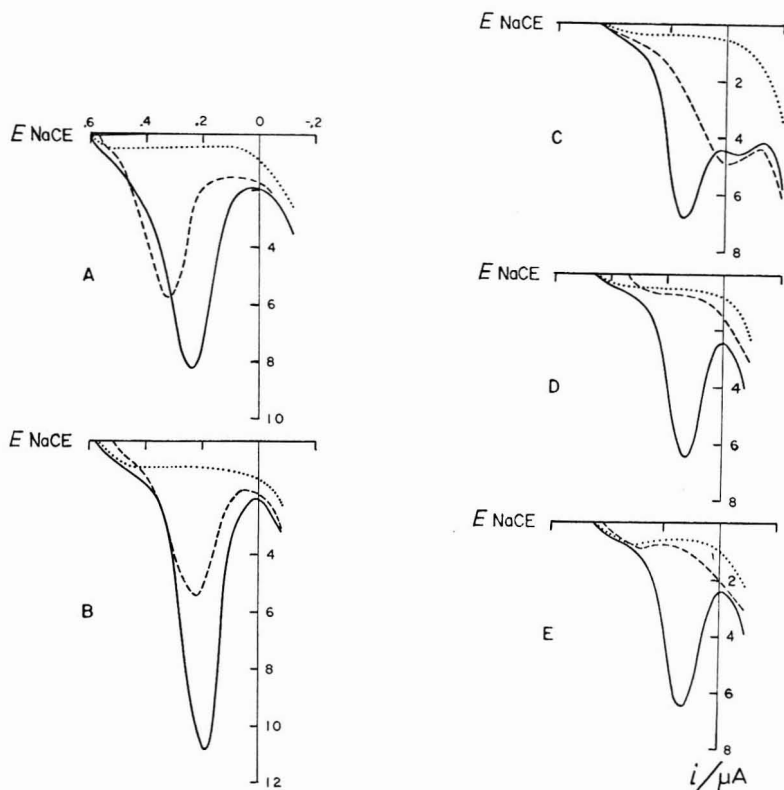
Fig. 1. Thin-layer current–potential curves for reduction of $PtCl_6^{2-}$ and $PtCl_4^{2-}$ at platinum electrodes. Initial chloride concn.: (A) 0.00; (B) 10; (C) 100; (D) 300; (E) 1000 mF. Experimental conditions: reactant solns. contained 1 mF Pt(IV) (solid curves) or Pt(II) (broken curves), 10 mF $HClO_4$, NaCl as indicated above, and sufficient $NaClO_4$ to maintain a constant ionic strength of 1.01. Thin-layer volume $V = 2.18$ μl in Curve A and 2.43 otherwise; platinum electrode area $A = 1.00$ cm^2; soln. layer thickness $l = 26.5$ μm; rate of potential sweep $r = 2$ mV s^{-1}; soln. temp. $T = 297 \pm 0.5°$K. Potentials were measured and reported relative to a 1 F NaCl calomel electrode (NaCE).

reduction occurs at more negative potentials and is masked to a greater extent by reduction of the solvent. That the electroreduction of $PtCl_6^{2-}$ leads to $PtCl_4^{2-}$ in 1 F chloride supporting electrolyte but proceeds all the way to the metal at low chloride concentrations[1] is thus consistent with the suggestion that $PtCl_6^{2-}$ is reduced initially to $PtCl_4^{2-}$ at *all* chloride concentrations, but that if 1 F chloride is present, the further reduction of $PtCl_4^{2-}$ to the metal is postponed to relatively negative values of the potential and is masked by reduction of the solvent, whereas if chloride is absent, $PtCl_4^{2-}$ is reduced as soon as it is formed and $PtCl_6^{2-}$ reduction proceeds quantitatively to the metal.

Equations for the thin-layer current–potential curve resulting from stepwise reduction of a single reactant were derived in ref. 3 and are reproduced here in eqns. (4)–(6).

$$_c i = n_2 F V r C_1^0 G + n_2 F A^* k_2^0 C_1^0 H^{-1} \exp \left[\frac{-(\alpha n_0)_2^* F}{RT} (E - E_2^0) \right] \int_{E_i}^{E} GH \, dE \quad (4)$$

where

$$G \equiv \frac{n_1 A^* k_1^0 C_1^0}{n_2 Vr} \exp\left\{ \frac{-(\alpha n_0)_1^* F}{RT}(E - E_1^0) + \frac{A^* k_1^0 RT}{(\alpha n_0)_1 FVr} \times \right.$$

$$\left. \exp\left[\frac{-(\alpha n_0)_1^* F}{RT}(E - E_1^0)\right]\right\} \quad (5)$$

$$H \equiv \exp\left\{ \frac{A^* k_2^0 RT}{V(-r)(\alpha n_0)_2^* F} \exp\left[\frac{-(\alpha n_0)_2^* F}{RT}(E - E_2^0)\right]\right\} \quad (6)$$

Graphs of eqn. (4) for values of the parameters $(\alpha n_0)_i^*$ and $*k_i^0$ taken from Table 1 appear in Fig. 2. Asterisks identify values of the rate parameters uncorrected for the
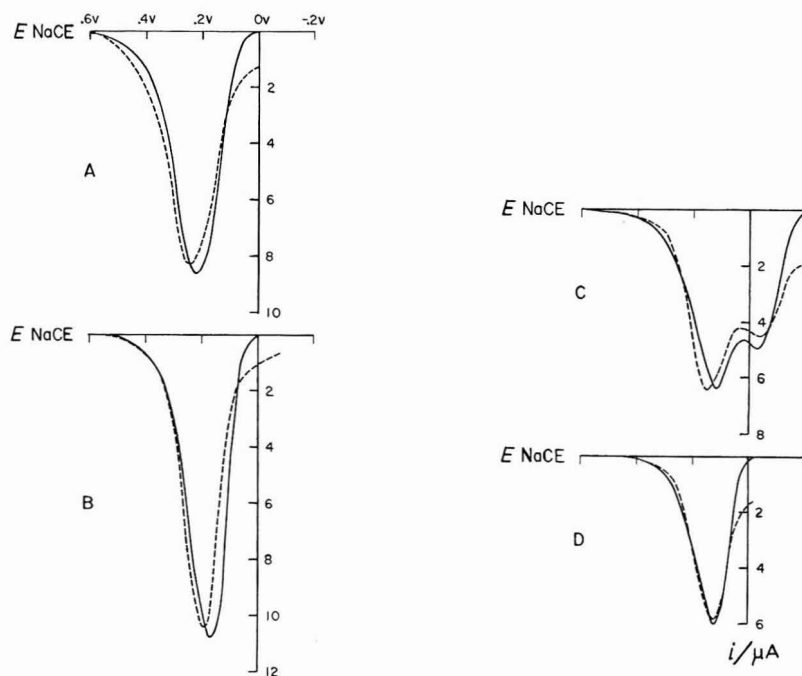

Fig. 2. Theoretical thin-layer current–potential curves for stepwise reduction of $PtCl_6^{2-}$: Graphs of eqn. (3) for values of $(\alpha n_0)^*$ and $*k^0$ taken from Table 1.

	$(\alpha n_0)_1^*$	$(\alpha n_0)_2^*$	$*k_1^0/cm\ s^{-1}$	$*k_2^0/cm\ s^{-1}$
A	0.29	0.38	6.1×10^{-6}	8.1×10^{-6}
B	0.37	0.32	3.48×10^{-6}	3.4×10^{-6}
C	0.37	0.32	1.48×10^{-6}	1.6×10^{-7}
D	0.45	—	5.91×10^{-7}	$\leqq 2 \times 10^{-9}$

(---) Experiment curves after correction for background current (cf. Fig. 1). (——) theoretical curves. The following values of the exptl. parameters were assumed in making the plots (the symbols used are defined in Fig. 1): $n_1 = n_2 = 2$; $V = 2.18\ \mu l$ in Curve A and 2.43 otherwise; $r = 2$ mV s^{-1}; $C_1^0 = 1.00$ mF; $A = 1.00$ cm^2; $E_1^0 = 0.40$ V NCE; $E_2^0 = 0.45$ V NCE; $T = 298 \pm 0.5\ °$K.

TABLE 1

ELECTROREDUCTION OF $PtCl_6^{2-}$ AND $PtCl_4^{2-}$

Data from thin layer current–potential curves

Reactant	Chloride/mF	$_c i_1/\mu A$	$_c E_1/V$ NCE	$_c i_P/\mu A$	$_c E_P/V$ NCE	$(\alpha n_0)_1^*$	$*k_1^0/cm\ s^{-1}$	$(\alpha n_0)_2^*$	$*k_2^0/cm\ s^{-1}$
$PtCl_6^{2-}$	0^a			8.0	0.24	0.29	6.1×10^{-6}		
	10^a			10.2	0.20	0.37	3.5×10^{-6}		
	100^b	4.2	0.20	(5.0)	(0.14)	0.37	1.5×10^{-6}		
	300			5.9	0.12	0.45	5.9×10^{-7}		
	1000			5.8	0.11	0.44	5.7×10^{-7}		
$PtCl_4^{2-}$	0			5.2	0.31			0.38	8.1×10^{-6}
	10			4.4	0.23			0.32	3.4×10^{-6}
	100			4.4	-0.01			0.32	1.6×10^{-7}
	300^c			—	—			—	$\leqq 10^{-9}$
	1000^c			—	—			—	$< 10^{-9}$

The symbols employed are as follows:

$_c i_1$ and $_c E_1$ = current and potential of first inflection point of the thin layer current–potential curve.

$_c i_P$ and $_c E_P$ = cathodic peak current and potential.

$(\alpha n_0)_i^*$ and $*k_i^0$ = rate parameters uncorrected for double layer effects for $PtCl_6^{2-}$ ($i=1$) and $PtCl_4^{2-}$ ($i=2$).

Experimental conditions: The reactant solution contained 1 mF $PtCl_6^{2-}$ or $PtCl_4^{2-}$, NaCl as indicated, 10 mF $HClO_4$ and sufficient $NaClO_4$ to adjust the ionic strength to 1.01. Other conditions were as in Fig. 1.

Notes: ᵃ $(\alpha n_0)^*$ and $*k^0$ values for Pt(IV) in 10 and 0 mF Cl⁻ solutions were calculated assuming a single-step reaction in which $n=4$ (eqns. 11 and 12).

ᵇ $(\alpha n_0)^*$ and $*k^0$ were calculated at the inflection point using eqns. (14) and (15).

ᶜ Calculation of $(\alpha n_0)^*$ and $*k^0$ was prevented by a large interfering current due to reduction of the solvent.

effects of the diffuse double layer. The similarity of the experimental and calculated curves, Fig. 1 and 2, respectively, supports the correctness of the stepwise reaction path.

Cyclic thin-layer current–potential curves allow independent values of α^* and n_0 to be determined for irreversible couples so long as the cathodic and anodic reactions correspond to the same stoichiometric equation. That such is not the case for the aquo–chloro-complexes of Pt(II) and (IV), however, can be readily seen from the thin-layer current–potential curve obtained for $PtCl_4^{2-}$ in 1 F $HClO_4$ (Fig. 3). The initial (anodic) half-cycle corresponds to eqn. (7),

$$PtCl_4^{2-} + 2\,H_2O \rightarrow trans\text{-}Pt(H_2O)_2Cl_4 + 2e^- \tag{7}$$
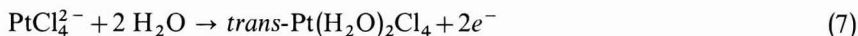
whereas the return cathodic half-cycle corresponds to eqn. (8), $i.e.$,

$$trans\text{-}Pt(H_2O)_2Cl_4 + 2e^- \rightarrow trans\text{-}Pt(H_2O)_2Cl_2 + 2Cl^- \tag{8}$$
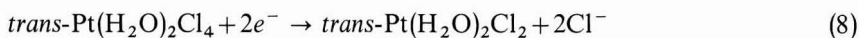
removal of a $trans\text{-}dichloro$-axis accompanies reduction of $Pt(H_2O)_2Cl_4$. The second anodic half-cycle then corresponds to eqn. (9).

$$trans\text{-}Pt(H_2O)_2Cl_2 + 2Cl^- \rightarrow trans\text{-}Pt(H_2O)_2Cl_4 + 2e^- \tag{9}$$
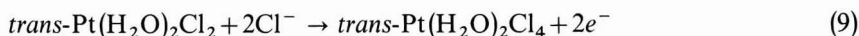
The $stereochemical$ course of eqns. (7)–(9) is not proved by these studies and is merely inferred from recent experiments[2,4] involving chloro–ammino-complexes of Pt(II) and (IV). That Pt(II) is electro-oxidized more readily in the presence of chloride (eqn. (6)) than in its absence (eqn. (4)) is to be expected since complexes of the type $Pt(NH_3)_m(Cl)_{4-m}^{m-2}$ and $Pt(NH_3)_m(NO_2)_{4-m}^{m-2}$ invariably exhibit such behavior. Therefore, independent values of $^*\alpha$ and n_0 cannot be obtained directly from cyclic current–potential data for $PtCl_4^{2-}$, although it should be noted that Pt(IV)/Pt(II) couples for which the analysis is possible yield, after correction for the effects of the double layer, $\alpha = ca.\ \frac{1}{2}$ and $n_0 = 1$.
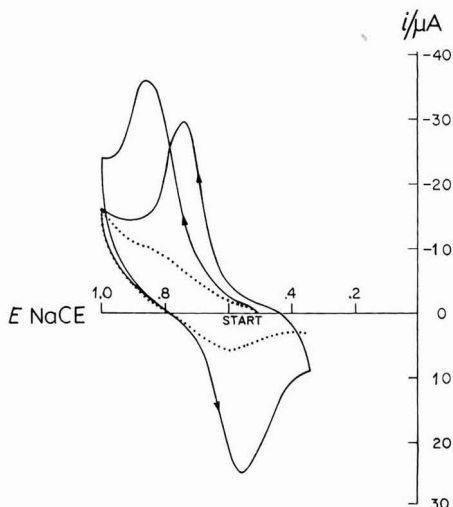

Fig. 3. Cyclic thin-layer current–potential curve for $PtCl_4^{2-}$ in chloride-free solution at a platinum electrode. Experimental conditions: The reactant soln. was 5 mF $PtCl_4^{2-}$ in 1 F $HClO_4 + 1$ F $NaClO_4$, used immediately after dissolution; $V = 2.18\ \mu l$; other conditions as in Fig. 1. (——) 5 mF $PtCl_4^{2-} + 1$ F $HClO_4 + 1$ F $NaClO_4$; ($\cdots\cdots$) 1 F $HClO_4 + 1$ F $NaClO_4$.

2. THE EFFECT OF THE ELECTROCHEMICAL DOUBLE LAYER ON THE KINETICS OF THE ELECTROREDUCTION OF $PtCl_6^{2-}$ AND $PtCl_4^{2-}$

Values of $*k^0$ and $*(\alpha n_0)$ for reduction of $PtCl_6^{2-}$ and $PtCl_4^{2-}$, obtained from thin layer voltammetric data as described below, are given in Table 1.

At large chloride concentrations $PtCl_4^{2-}$ is reduced at more negative potentials than $PtCl_6^{2-}$ and the individual components of the current resulting from reduction of these species are distinguishable (two distinct peaks are observed), allowing the current–potential curve to be analyzed as for reduction of single reactants in independent steps[3] by means of eqns. (10)–(12):

$$_ci = nFA*k^0 C_{ox}^0 \exp\left\{ \frac{-*(\alpha n_0)F}{RT}(E-E^0) + \frac{ART*k^0}{*(\alpha n_0)FVr} \times \right.$$
$$\left. \exp\left[\frac{-*(\alpha n_0)F}{RT}(E-E^0)\right]\right\} \quad (10)$$

$$*(\alpha n_0) = \frac{2.718RT \, _ci_p}{nF^2 V(-r) C_{ox}^0} \quad (11)$$

$$*k^0 = \frac{2.718 \, _ci_p}{nFAC_{ox}^0} \exp\left[\frac{2.718 \, _ci_p(_cE_p - E^0)}{nFV(-r)C_{ox}^0}\right] \quad (12)$$

$_ci_p$ and $_cE_p$ are the cathodic peak current and potential, respectively.

When the concentration of chloride is small, $PtCl_6^{2-}$ and $PtCl_4^{2-}$ are reduced over the same range of potentials; their contributions to the total current are inseparable, requiring, in principle, the use of eqn. (4) to obtain the kinetic parameters. In practice, the analysis can be simplified by means of suitable approximations: if $*k_2^0$ for $PtCl_4^{2-}$ is sufficiently large in comparison with $*k_1^0$ for $PtCl_6^{2-}$, then $PtCl_4^{2-}$ is reduced to the metal as rapidly as it is formed, a single peak is observed in the current–potential curve, and eqn. (10) can be used for the analysis with n set equal to 4. Or, if the magnitude of $*k_1^0$ is larger than $*k_2^0$ but by less than an order of magnitude, two overlapping peaks are observed and advantage can be taken of the fact that the initial $PtCl_4^{2-}$ concentration is zero so that the current resulting from reduction of $PtCl_4^{2-}$ is negligible during the initial portion of the current–potential curve and eqn. (10) can be employed in that region. The first inflection point $(_cE_I, \, _ci_I)$ of the current–potential curve is particularly convenient for evaluation of $*k^0$ and $*(\alpha n_0)$, since at the inflection point:

$$\left(\frac{d^2 \, _ci}{dE^2}\right)_{E = \, _cE_I} = 0 \quad (13)$$

and combining eqns. (10) and (13) leads to simple equations for the parameters $*(\alpha n_0)$ and $*k^0$ in terms of the measured current and potential, $_ci_I$ and $_cE_I$, at the first inflection point:

$$*(\alpha n_0) = \frac{3.84RT \, _ci_I}{nF^2 V(-r) C_{ox}^0} \quad (14)$$

$$*k^0 = \frac{3.84 \,_c i_I}{nFAC_{ox}^0} \exp\left[\frac{3.84 \,_c i_I(_c E_I - E^0)}{nFV(-r)C_{ox}^0}\right]$$ (15)

Equations (10)–(15) were used to obtain the values of $*k^0$ and $*(\alpha n_0)$ appearing in Table 1; both $*k_1^0$, and $*k_2^0$ decrease with increasing chloride concentration.

A pronounced minimum appears in the limiting current region of polarograms obtained for $PtCl_6^{2-}$ and $PtCl_4^{2-}$, which has been attributed by Frumkin[5] to a rapid decrease in the potential ϕ_2 of the plane of closest approach (p.c.a.) of the reactant species with decreasing applied potential in that region. It is commonly accepted that a negative shift in the value of ϕ_2 leads to a smaller activity $_2a_{ox}$ of anionic reactants at the p.c.a. than in the bulk solution (eqn. (16)),

$$_2a_{ox} = a_{ox} \exp\left[\frac{-Z_{ox}F}{RT}\phi_2\right]$$ (16)

to dissipation of a fraction of the applied potential across the diffuse double layer (eqn. (17)),

$$k_f = k^0 \exp\left[\frac{-(\alpha n_0)F}{RT}(E - E^0 - \phi_2)\right]$$ (17)

and thus to a smaller value of the apparent rate constant $*k^0$ than would be observed otherwise[6,7]. Analogous, though not necessarily identical behavior is expected with platinum electrodes. Since chloride is strongly adsorbed at platinum electrodes at sufficiently large chloride concentrations over the range of potentials of interest here[6], the values of ϕ_2 corresponding to a given applied potential can be presumed to become increasingly negative and the reduction rate smaller as the chloride concentration is increased.

3. THE EFFECT OF SPECIFICALLY ADSORBED HALIDE ON THE ELECTROREDUCTION KINETICS OF $PtCl_6^{2-}$ AND $PtCl_4^{2-}$

Inspection of the values of the standard electrochemical rate constant $*k^0$ in Table 1 reveals that reduction of $PtCl_4^{2-}$ is hindered to a much greater extent by addition of chloride ions to the solution than is reduction of $PtCl_6^{2-}$. Since the ionic charges of these reactants are identical and the applied potentials (and hence the values of ϕ_2) are similar, the observed difference indicates that these reactions proceed by markedly different paths. A quantitative study of the influence of ϕ_2 on these reactions would be highly desirable, but must await the arrival of suitable double layer data.

On the basis of experiments at mercury electrodes, Frumkin and co-workers[5] have suggested that $PtCl_4^{2-}$, being a planar molecule, is located closer to the electrode surface than is the octahedral ion $PtCl_6^{2-}$ and is thus more drastically influenced by the potential ϕ_2. In contrast, Thirsk and co-workers[8] have presented data which show that a large fraction of the observed cathodic current at mercury electrodes in platinum chloride solutions results from catalytic reduction of H^+ at the edge of the electrodeposited platinum phase. The possibility of complicated behavior stemming from the fact that platinum chlorides may chemically oxidize the mercury surface has been pointed out by Laitinen and Onstott[9]. Studies of platinum chloride reduction by

means of a thin layer electrode having a pure mercury surface[10] are in progress which may be useful in mediating between the several conflicting explanations appearing in the earlier literature.

The influence of chloride ions on the electroreduction of $PtCl_6^{2-}$ at platinum electrodes is probably limited to a negative shift in ϕ_2 produced by adsorbed chloride ions: $*k_1^0$ is virtually independent of chloride concentration above $300\,mF$ as would be expected, in keeping with the above suggestion, since the electrode surface probably becomes saturated with adsorbed chloride at sufficiently high concentrations, leading to chloride-independent values of ϕ_2 and $*k^0$.

In contrast, the influence of chloride ions on $PtCl_4^{2-}$ electroreduction is probably *not* primarily due to a negative ϕ_2 effect. The observed dependence is most pronounced at high chloride concentrations where the chloride-dependence of ϕ_2 would be expected to be small. Instead, chloride ions may hinder the reaction by occupying adsorption sites in the compact double layer which might otherwise be employed for the formation of an adsorbed transition state species, thus decreasing the apparent electrode area $*A$ and the apparent standard rate constant $*k_2^0$. Hindrance of metal deposition by adsorbed halides has been cited by other workers[11].

It is of interest to estimate by means of a simple competitive-adsorption model the extent to which chloride might be expected to hinder the electroreduction of $PtCl_6^{2-}$ and $PtCl_4^{2-}$. Suppose that the following conditions are met:

(1) the reactivity of $PtCl_4^{2-}$ and $PtCl_6^{2-}$ toward *vacant sites* at the electrode is independent of the chloride concentration, apart from changes in ϕ_2;

(2) the extent of coverage of the surface (*i.e.*, of the compact double layer) by adsorbed $PtCl_6^{2-}$ and $PtCl_4^{2-}$ is negligible in comparison with that due to chloride; that is,

$$_1\theta_{PtCl_4^{2-}} + {_1}\theta_{PtCl_6^{2-}} \ll {_1}\theta_{Cl^-}$$

where $_1\theta \equiv$ interfacial excess/interfacial excess at saturation, in the compact double layer.

The cathodic current is given by eqn. (23)

$$_ci = nF \; *Aa_{ox} \, *k^0 \, \exp\left[\frac{-*\alpha n_0 F}{RT}(E - E^0)\right] \tag{23}$$

The apparent standard electrochemical rate constant is given by eqn. (24).

$$*k^0 = \frac{2.718 \, _ci_p}{nF \; *AC_{ox}^0} \exp\left[\frac{2.718 \, _ci_p(_cE_p - E^0)}{nFV(-r)C_{ox}^0}\right] \tag{24}$$

$*A$ denotes the portion of the total electrode area available at any instant for adsorption of $PtCl_6^{2-}$ and $PtCl_4^{2-}$. Since $PtCl_6^{2-}$ is specifically adsorbed, if at all, at single adsorption sites, the probability of a suitable site remaining available despite competitive adsorption of chloride is proportional to $(1 - {_1}\theta_{Cl})$. The apparent electrode area $*A$ for $PtCl_6^{2-}$ is given by eqn. (25):

$$*A(\text{for } PtCl_6^{2-}) = A[1 - {_1}\theta_{Cl}] \tag{25}$$

Formation of the transition state for reduction of $PtCl_4^{2-}$ appears to require close range interaction between platinum atoms of the complex and the electrode surface and, barring extreme distortion of the planar molecule, between chloride ligands

and surface atoms as well; thus, the adsorption site required by a $PtCl_4^{2-}$ ion may consist of a group of five to nine adjoining surface atoms. Now the probability of an individual surface atom being chloride-free at any instant is proportional to $1 - {}_1\theta_{Cl}$ and that of some number m of adjoining atoms being available to $(1 - {}_1\theta_{Cl})^m$, so that $*A$ is given by eqn. (26).

$$*A \text{ (for } PtCl_4^{2-}) = A[1 - {}_1\theta_{Cl}]^m \qquad (m = 5\text{--}9) \tag{26}$$

Graphs of eqns. (25) and (26) appear in Fig. 5. Equation (26) predicts a rapid decrease in $*A$ for $PtCl_4^{2-}$ as ${}_1\theta_{Cl}$ approaches 0.5 in agreement with the observed chloride dependence of the electroreduction rate constant (Table 1).
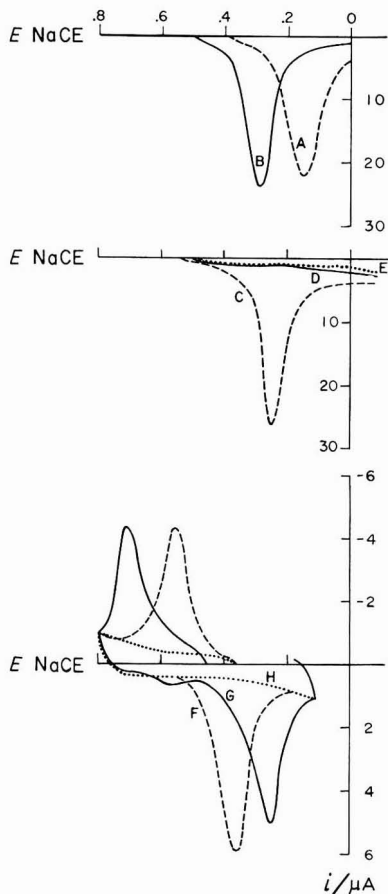
Fig. 4. Thin-layer current-potential curves for reduction of Pt(IV) and Pt(II) at platinum electrodes prior to and following treatment with iodide solution: (A) 1 mF $PtCl_6^{2-}$ in 1 F $HClO_4^-$ + 1 F NaCl at clean platinum electrode, (B) 1 mF $PtCl_6^{2-}$ in 1 F $HClO_4^-$ + 1 F NaCl at iodide-treated platinum electrode, (C) 1 mF $PtCl_4^{2-}$ in 1 F $HClO_4$ at clean platinum electrode, (D) 1 mF $PtCl_4^{2-}$ in 1 F $HClO_4$ at iodide-treated platinum electrode, (E) 1 F $HClO_4$ at clean platinum electrode, (F) 1 mF $Pt(NH_3)_4^{2+}$ in 1 F $HClO_4$ + 10 mF NaCl + 990 mF $NaClO_4$ at clean platinum electrode, (G) 1 mF $Pt(NH_3)_4^{2+}$ in 1 F $HClO_4$ + 10 mF NaCl + 990 mF $NaClO_4$ at iodide-treated platinum electrode, (H) 1 F $HClO_4$ + 10 mF NaCl + 990 mF $NaClO_4$ at clean platinum electrode. Experimental conditions: $V = 7.57$ μl in curves A–E and 1.40 in curves F–H. Other conditions were as in Fig. 1.
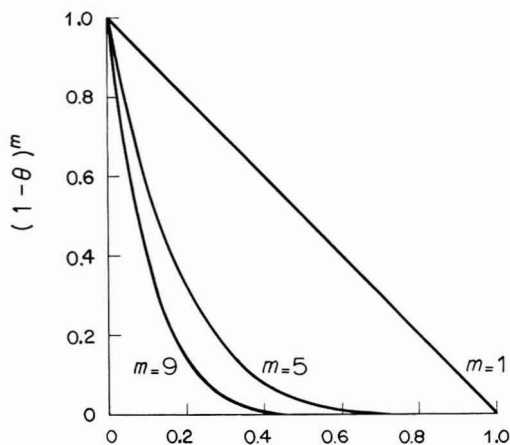
Fig. 5. Graphs of $(1 - \theta)^m$ vs. θ; see eqns. (25) and (26) in the text.

Qualitative evidence that the electroreduction reactions of $PtCl_6^{2-}$ and $PtCl_4^{2-}$ are mechanistically different has been obtained by comparing their rates at platinum electrodes and at platinum electrodes pretreated with iodide. Iodide is adsorbed irreversibly in monolayer amounts at platinum electrodes in the form of an uncharged species which is not electro-active at potentials from 0.0–0.9 V SCE[12]. Thus, reduction of $PtCl_4^{2-}$ would be expected to proceed more slowly at iodide-treated than at clean electrodes due to blocking of the compact layer by adsorbed halogen; reduction of $PtCl_6^{2-}$ would be influenced in the same direction but to a lesser extent. Thin layer current–potential curves for reduction of $PtCl_6^{2-}$ and $PtCl_4^{2-}$ obtained with clean and with iodide-treated electrodes (Fig. 4) display the expected trend. Electro-reduction of $PtCl_4^{2-}$ is completely prevented by the iodide pretreatment; in contrast, reduction of $PtCl_6^{2-}$ is actually enhanced somewhat since the adsorbed neutral species leads to a decrease in the amount of specifically adsorbed chloride, causing ϕ_2 to have more positive values than otherwise, and leading to a net increase in reaction rate (eqn. (16)).

Experiments with iodide-treated electrodes have led to the recognition of an error in a previous communication[1] in which it was claimed that $1F$ $HClO_4$ prevents the reduction of $PtCl_4^{2-}$. In fact, such an effect due to perchloric acid has not been observed in any of the present experiments. The earlier result can be understood only if the electrodes employed in those experiments were allowed to become poisoned with traces of iodide ion or iodine in use at that time in other studies[12]; iodide or iodine concentrations as low as 10^{-6} M, and total amounts of the halogen as small as $5 \cdot 10^{-10}$ mol in the solutions employed would have been adequate to produce the observed result.

In a recent study of $PtCl_6^{2-}$ electroreduction at conventional platinum electrodes from unstirred $3F$ H_2SO_4 solution containing various concentrations of chloride, Kravtsov and Simakov[13] observed a decrease in reduction rate with increasing chloride concentration which they attributed to participation of the species "$PtCl_5^-$" in the rate-limiting step; presumably $PtCl_5^-$ was formed in a rapid prior chemical reaction such as eqn. (20) or (21):

$$PtCl_6^{2-} = PtCl_5^- + Cl^- \tag{20}$$

$$PtCl_6^{2-} + H_2O = Pt(H_2O)Cl_5^- + Cl^- \tag{21}$$

However, the rates of reactions 20 and 21 are surely too small to account for the observed rates of reduction because hydrolysis of $PtCl_6^{2-}$, which is extensive at equilibrium, occurs only slowly in the absence of intense ultraviolet irradiation[1,14]; this is in conflict with the implicit prediction of eqns. (20) and (21) that formation of $Pt(H_2O)Cl_5^-$ from $PtCl_6^{2-}$ should be rapid. In particular, samples of K_2PtCl_6 dissolved in water (0.5–10 mF) and stored in the dark under a nitrogen atmosphere were not appreciably hydrolyzed over a period of two weeks (*i.e.*, $\bar{m} \ll 0.1$, eqn. (22)),

$$PtCl_6^{2-} + \bar{m}H_2O = \sum_m a_m Pt(H_2O)_m Cl_{6-m}^{m-2} + \bar{m}Cl^- \tag{22}$$
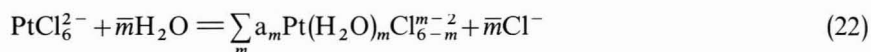
although hydrolysis became noticeable ($\bar{m} \leq 2.2$) after a much longer period; that equilibrium is eventually achieved is indicated by the fact that $\bar{m}$ gradually decreases after sodium chloride is added to the hydrolyzed solutions. When the samples were stored under normal laboratory illumination, appreciable hydrolysis occurred within about one week, as previously reported[1]; normal laboratory illumination had no effect, however, on the electrochemical behavior of $PtCl_6^{2-}$ solutions used immediately after preparation from solid K_2PtCl_6.

4. THE ROLE OF LIGANDS IN REDUCTION OF Pt(IV) COMPLEXES

Earlier studies[2,4] have reported that chloride greatly accelerates the oxidation of Pt(II) complexes in the series $Pt(NH_3)_m(NO_2)_{4-m}^{m-2}$ (eqn. (23));

$$Pt(NH_3)_m(NO_2)_{4-m}^{m-2} + X + Cl^- = Pt(NH_3)_m(NO_2)_{4-m}XCl^{m-1,2} + 2e^- \tag{23}$$

$(X \equiv H_2O \text{ or } Cl^-)$
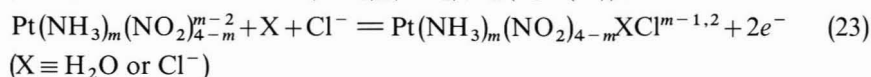
the rate data obtained were consistent with a bridged-intermediate model (eqn. (24)).
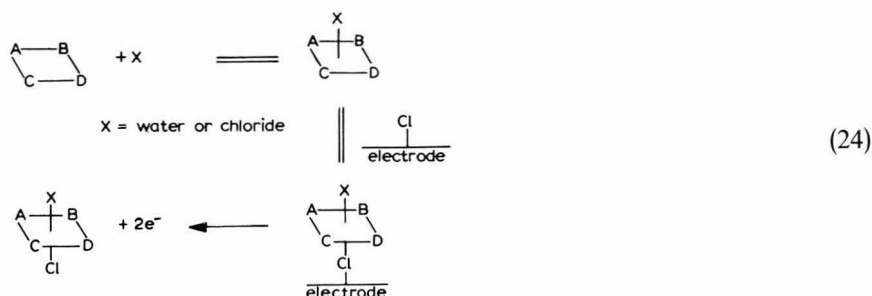
A prediction of the bridged-intermediate model is that Pt(IV) complexes containing one or more halide or similar ligands should exhibit larger reduction rates than ones not having such ligands. This expectation has been realized in the few instances thus far studied[2]. For example, members of the series $Pt^{IV}(NH_3)_m(NO_2)_{4-m}XCl^{m-1,2}$ are readily reduced to $Pt^{II}(NH_3)_m(NO_2)_{4-m}$ (where X is H_2O, NH_3, NO_2^- or Cl^-; $m=0$, 1, 2, 3, 4), whereas $Pt(NO_2)_3(NO_3)_3^{2-}$ and $Pt(NH_3)_6^{4+}$ are completely unreactive toward reduction at platinum electrodes.

A further prediction of the bridged-intermediate model is that the group

opposite the bridging group (X in eqns. (23) and (24)) should have little or no influence on the kinetics of reduction, apart from a small effect due to variation of the reactant activity at the outer Helmholtz plane with the ionic charge of the reactive species (eqn. 13)). Thus, $Pt(NH_3)_5Cl^{3+}$ [15] and $trans$-$Pt(NH_3)_4Cl_2^{2+}$ are expected *and observed* to be about equally reactive, even though $X = NH_3$ in the former case and Cl in the latter.

5. EXPERIMENTAL

The thin-layer electrodes employed for this study were of the type described recently[2], in which the thin layer of solution was confined between the inside wall of a length of precision bore tubing and a platinum rod uniformly positioned within the tubing.

A calomel electrode, prepared with 1 F NaCl instead of KCl to avoid precipitation of $KClO_4$ at the junction, served as the reference electrode (denoted NaCE). The potential of this electrode was 65 mV more positive than a calomel electrode prepared with saturated KCl (SCE) when the intervening electrolyte was 1 F $HClO_4$.

A conventional multi-purpose electrochemical circuit based on operational amplifiers and relays having mercury-wetted contacts was employed.

Prior to each experiment the electrodes were pre-treated as follows: (a) oxidation at 1.2 V NaCE for 60 s, accompanied by thorough rinsing in 1 F $HClO_4$; (b) reduction at 0.0 V NaCE for 60 s; (c) five repetitions of (1) and (2); (d) reduction at 0.4 V NaCE for 120 s. This procedure appears to remove adsorbed halide while leaving the electrode with a minimum of adsorbed hydrogen and oxygen.

SUMMARY

The kinetics and stoichiometry of the electroreduction of $PtCl_6^{2-}$ and $PtCl_4^{2-}$ at platinum electrodes are consistent with a negative shift in the potential ϕ_2 of the outer Helmholtz plane of $PtCl_6^{2-}$ ions brought about by the adsorption of chloride ions, and with competition between chloride and $PtCl_4^{2-}$ for adsorption sites in formation of an adsorbed Pt(II) intermediate species. The present data pertaining to Pt(IV) compounds are suggestive of ligand-bridged charge transfer, whereas reduction of $PtCl_4^{2-}$ appears to require short-range interaction between the electrode and the entire reactant complex.

REFERENCES

1 A. T. HUBBARD AND F. C. ANSON, *Anal. Chem.*, 38 (1966) 1887.
2 J. R. CUSHING AND A. T. HUBBARD, *J. Electroanal. Chem.*, 23 (1969) 183.

3 A. T. HUBBARD, *J. Electroanal. Chem.*, 22 (1969) 165.
4 W. R. MASON AND R. C. JOHNSON, *J. Electroanal. Chem.*, 14 (1967) 345.
5 A. N. FRUMKIN, *Trans. Faraday Soc.*, 55 (1959) 156.
6 V. E. KAZARINOV AND N. A. BALASHOVA, *Russ. Chem. Rev.* (English translation), 34 (1965) 730.
7 P. DELAHAY, *Double Layer and Electrode Kinetics*, Interscience, New York, 1965, p. 47.
8 R. D. GILES, J. A. HARRISON AND H. R. THIRSK, *J. Electroanal. Chem.*, 20 (1969) 47.
9 H. A. LAITINEN AND E. I. ONSTOTT, *J. Am. Chem. Soc.*, 72 (1950) 4565.
10 A. T. HUBBARD AND F. C. ANSON, *Anal. Chem.*, 40 (1968) 615.
11 See, for example, E. SCHMIDT, H. R. GYGAX AND P. BOHLEN, *Helv. Chim. Acta*, 49 (1966) 733.
12 A. T. HUBBARD, R. A. OSTERYOUNG AND F. C. ANSON, *Anal. Chem.*, 38 (1966) 692.
13 V. I. KRAVTSON AND B. V. SIMAKOV, *Vestn. Leningr. Univ., Ser. Fiz. i Khim.*, No. 2 (1964) 90.
14 R. DREYER, I. DREYER AND D. RETTIG, *Z. Physik. Chem. Leipzig*, 224 (1963) 199.
15 *Gmelin's Handbuch der Anorganischen Chemie*, Vol. 68, part D, 1957, p. 484.

THE EFFECT OF THE SOLVENT USED FOR THE INTERNAL REFERENCE ELECTRODE SYSTEM ON THE RESPONSE CHARACTERISTICS OF HYDROGEN-RESPONSIVE GLASS ELECTRODES IN AQUEOUS AND PARTIALLY AQUEOUS BUFFER SOLUTIONS**

A. E. BOTTOM* AND A. K. COVINGTON

Department of Physical Chemistry, School of Chemistry, University of Newcastle upon Tyne, Newcastle upon Tyne, NE1 7RU (England)

(Received August 5th, 1969)

Our recent work with the glass electrode has been directed towards the reinvestigation of some of the accepted facts about glass electrode behaviour and performance, which we believe to be insufficiently firmly established, but which nevertheless have been perpetuated by continual repetition in recent monographs. Many of these facts stem from investigations of thirty years ago and have not been checked with modern techniques and instrumentation.

In work to be reported in detail elsewhere a study has been made of the time response and behaviour of representative commercial hydrogen-responsive glass electrodes in acid[1,2] and in alkaline solutions[3]. During the course of this and other studies small errors of 0.005–0.02 pH were observed in certain buffer solutions where the concentration of the buffer constituents was low[4]. Recently one of us has been concerned with the study of glass electrodes in heavy water solutions[5].

In this paper we have made a study of the effect of varying the inner filling of the glass electrode. It has always been assumed that apart from (a) determining the "null-punkt" of the electrode and hence its suitability for use with certain pH meters, and (b) allowing temperature effects to be reduced, the only property of the internal reference electrode system was to provide a constant, or at least only slowly varying, potential[6]. On the other hand, there have been reports recently[7–10] that, for potentiometric titrations in partially aqueous or (almost) non-aqueous media, it was advantageous to use the same solvent medium on the inside of the electrode as on the outside. For example, Badoz-Lambling *et al.*[7] claimed that an acetonitrile-filled electrode gave more reproducible and more rapidly attained potentials for titrations in that solvent. Douheret[8] also claimed faster response and more precise determinations for methanol media. Similar statements have been made for titrations in dimethylsulphoxide[9,10] and dimethylformamide[11]. It was suggested many years ago that mercury was quite adequate as an internal filling[12] and this was confirmed for the titrations in dime-

---

* Present address: Electronic Instruments Ltd., Richmond, Surrey, England.
** An account of this work was presented at the IMEKO Symposium on Electrochemical Sensors held at the University of Chemical Industry, Veszprém, Hungary, October 3rd–5th, 1968.

thylsulphoxide[10]. More recently a coating of solid electrolyte has been used commercially[13].
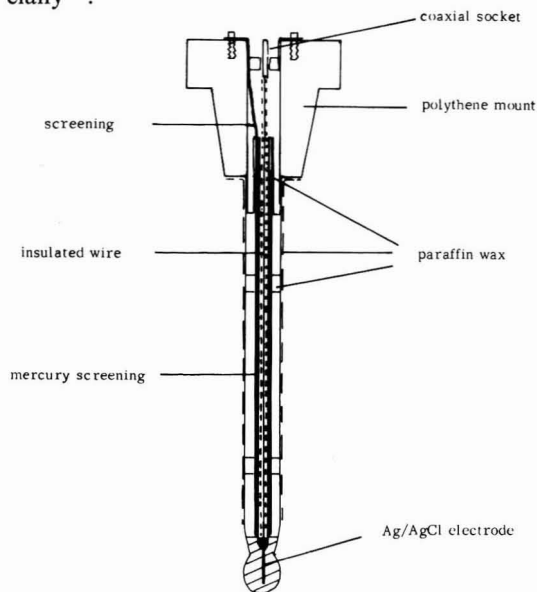

Fig. 1. Detail of glass electrode construction.

Most of these studies were titrimetric and not extensive, nor were the detailed results, when presented, particularly convincing. We have therefore commenced a more detailed study, of which the preliminary results are presented here. We have used as inner reference the reliable electrode system $Cl^-|AgCl|Ag$, varying only the solvent medium and the electrolyte mixture containing the chloride ion. A few mercury-filled electrodes were tested for comparison. Glass electrodes were tested by direct comparison against the hydrogen electrode in the same solution using a third electrode as a check on the reliable behaviour of the hydrogen electrode[2-4]. Of the three possible techniques[4] for varying the composition and nature of the solution in contact with a glass electrode: (a) titration (b) flow systems (c) transfer between solutions containing pre-equilibrated reference electrodes, the last has been preferred as it relates to the usual practice adopted for pH measurements. Some of the experiments were designed also to investigate the effect of conditioning the electrodes in different solvent   mixtures.

EXPERIMENTAL

Electrode blanks, that is stems and bulbs, were kindly provided by the Corning Glass Works, Medfield, Mass., U.S.A. and W.G. Pye & Co. Ltd., Cambridge, England. The first were of two types, a yellow and a white glass[14]. All electrodes were made from lithia-based glasses. Each set of blanks was selected from the same batch production so as to be as nearly similar in composition as possible. Electrode blanks were mounted as shown in Fig. 1.

Electrodes obtained from reputable manufacturers were used in preference

to home-made electrodes to counter any criticism that the latter could be of poor quality and of unspecified behaviour. The Corning 'yellow' glass is the basis of the Corning Type 476020 Triple Purpose electrode tested in previous work[4] and found to show only small errors in NBS standard buffers. The behaviour of typical Pye electrodes was also known to be within the British Standard Specification[15]. The procedure of using a number of identical virgin electrode blanks with different fillings was considered preferable to that of changing the internal filling of a given electrode, because it is well known that the previous solution contacts (electrode history) particularly with other solvents can effect the behaviour of the outside surface of the glass electrode.

A three compartment electrode vessel was used[4], six of which were placed side by side in an air thermostat controlled at $25.00 \pm 0.05°C$. Cell voltages were opposed by a potentiometer and the difference of less than 10 mV was fed to the input of a vibrating condenser electrometer and the output displayed on a potentiometric recorder. Hydrogen and silver–silver chloride electrodes, prepared by standard techniques, were allowed one hour to reach equilibrium before testing of glass electrodes was commenced. Wash solutions were stored in plastic wash-bottles in the thermostat. The optimum washing time was 10 s. Analytical grade reagents were used where possible and the non-aqueous solvents re-distilled after standing over molecular sieve. Resistance measurements were made by the d.c. method of Eckfeldt and Perley[16]. Glass electrodes already assembled and filled were stored in the chosen conditioning solvent for at least two weeks before tests were commenced.

RESULTS

Four series of experiments were performed. In the first the Corning "yellow" glass and Pye electrodes with various fillings (See Table 1) were transferred successively between 0.1 m HCl and (except for P12) four aqueous standard buffer solutions. In the second, nine Corning "yellow" glass electrodes with three different fillings were tested in six acid and buffer solutions in 95 wt% methanol–water solvent, and after a month's interval the experiment was repeated with the same electrodes in 50 wt% methanol–water. In both experiments each electrode with a particular filling was given one of three conditioning treatments (for details see Tables 2 and 3). In the last series of experiments, four Corning "white" glass electrodes were similarly tested in 95 wt% DMF–water mixtures with alternative conditioning (Table 4). In this last series aqueous hydrochloric acid solutions were included as no information was available about water–DMF transfers whereas a previous study had been made of water–methanol transfers[17]. This particular choice of solvents was made because methanol is thought to enter the gel layer of the glass electrode, whereas, since it is a non-hydroxylic solvent, DMF may not solvate glass.

The reproducibility of the results was always reasonable (± 1 mV) when the same sequence of transfer was repeated with the partially aqueous solvents, but it was poor when a different testing sequence was employed. The appearence of several entries in Tables 2 and 4 for the same transfer gives some indication of the reproducibility obtained. This finding is not surprising and supports the statement made earlier of the effect of electrode history on subsequent behaviour.

Some explanation of the method of presenting the results in Tables 1–4 is

ห้องสมุด กรมวิทยาศาสตร์

TABLE 1

EFFECT OF VARIOUS INTERNAL FILLING SOLUTIONS ON THE ERRORS OF TWO TYPES OF ELECTRODE GLASS (ΔE_f in mV)

| Electrode transfers[a] | | Electrode No. | | | | | | | | | |
Solution	pa_H[b]	P12 Mercury	P13 0.1 m HCl in water	P14 0.1 m HCl in 20% ethanol	P15 0.1 m HCl in 60% ethanol	P17 0.1 m HCl in 50% dioxan	C5 Mercury	C6 0.1 m HCl in water	C7 0.1 m HCl in D_2O	C8 0.1 m NaCl in an acetate buffer	C9 0.1 m HCl in 60% ethanol
0.1 m HCl	1.095	—	—	—	—	—	—	—	—	—	—
Satd. potassium hydrogen tartrate	3.557	—	0.4	0.2	6	1.0	0	−0.1	0	0.5	0
0.025 m Equimolal phosphates	6.777	0.5	1.2	1.8	8	2.0	0.2	0.7	0.6	0.5	0.4
0.01 m Borax	9.127	1.5	1.0	2.2	7	1.2	0.2	0.3	0.3	0.8	0.8
Satd. calcium hydroxide	12.454	—	4.2	3.7	16	4.0	0.5	0.4	0	0.4	1.8
0.1 m HCl	1.095	−2.2	−7.8	−8.4	−38	−8.2	−1.0	−1.4	−0.5	−2.4	−3.0
Electrode resistance/MΩ		—	260	105	—	110	—	170	110	155	—

[a] Transfers from solution immediately above in this column. [b] pa_H is defined in ref. 24a.

TABLE 2

EFFECT OF INTERNAL FILLING AND CONDITIONING ON THE ERRORS OF GLASS ELECTRODES IN 95 WT% METHANOL–WATER MIXTURES (errors in mV)

Conditioned in	Filling	0.1 m HCl in water	0.1 m HCl in 50% methanol	0.1 m HCl in 95% methanol
Water		CI	CII	CIII
		$a(s)$–$a(s) \cdot F$ $\Delta E_e = 0$		
		$a(s)$–$b(s) \cdot F$ $\Delta E_e = 0$	Very sluggish in	
		$b(s)$–$b(s) \cdot F$ $\Delta E_e = 0$	all solutions	————
		$R = 370$	$R = 370$	$R = 360$
50% Methanol		CIV	CV	CVI
			$a(s)$–$b(s) \cdot E$ $\Delta E_e = 7$	$a(s)$–$a(s) \cdot C_1$ $\Delta E_f = 20$
		membrane punctured(?)	$\Delta E_f = 5$	$a(s)$–$b(s) \cdot C_1$ $\Delta E_f = 150$
		$R = 20$	$b(s)$–$b(s) \cdot E$ $\Delta E = 1$	$b(s)$–$b(s) \cdot C_2$ $\Delta E_f = 8$
95% Methanol		CVII	CVIII	CIX
		$a(s)$–$b(s) \cdot F$ $\Delta E_e = 0$	$a(s)$–$b(s) \cdot E$ $\Delta E_e = 10$	$a(s)$–$b(s) \cdot C_1$ $\Delta E_f = 135, 115$
		$b(s)$–$b(s) \cdot F$ $\Delta E_e = 0$	$b(s)$–$b(s) \cdot E$ $\Delta E_e = 4$	130, 110
				$b(s)$–$b(s) \cdot C_2$ $\Delta E_f = -20$
				$\Delta E_i = -5$

Key: $a_1(s) = 0.1$ m HCl ($pa_H{}^* = 1.27$): $a_2(s) = 0.01$ m HCl ($pa_H{}^* = 2.13$).
  $b_1(s) = 0.049$ m HAc, 0.049 m KAc, 0.05 m KCl ($pa_H{}^* = 7.62$); $b_2(s) = 0.03$ m HAc, 0.03 m KAc, 0.05 m KCl ($pa_H{}^* = 7.64$); $b_3(s) = 0.015$ m HAc, 0.015 m KAc, 0.05 m KCl ($pa_H{}^* = 7.65$); $b_4(s) = 0.005$ m HAc, 0.005 m KAc, 0.05 m KCl ($p_H{}^* = 7.67$) (see also Fig. 4).
  R = resistance in MΩ.
* $pa_H = -\log m_H \cdot {}_s\gamma_H$ (for nomenclature see ref. 24b). Based on E^0 data of Oiwa[25].
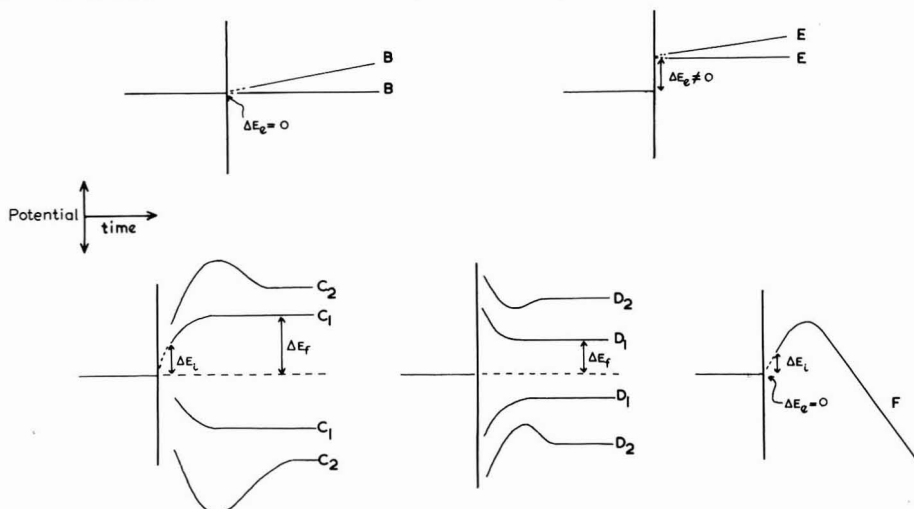
Fig. 2. Classification of potential–time transient forms.

necessary. We shall refer to: ΔE the difference in potential readings between the cells; glass|Solution I|H_2, Pt and glass|Solution II|H_2, Pt, and in particular to:

  ΔE_i the initial error, the difference between the first measured potential in the

TABLE 3

EFFECT OF INTERNAL FILLING AND CONDITIONING ON THE ERRORS OF GLASS ELECTRODES IN 50 WT% METHANOL–WATER MIXTURES (errors in mV)

Conditioned in ╲ Filling	0.1 m HCl in water	0.1 m HCl in 50% methanol	0.1 m HCl in 95% methanol
Water	CI a(s)–a(s)·F $\Delta E_i=4$ $\Delta E_e=0$ $R=370$	CII Very sluggish in all solutions $R=370$	CIII a(s)–a(s)·F $\Delta E_e=0(?)$ a(s)–b(s)·D$_1$ $\Delta E_f=0(?)$ $R=360$
50% Methanol	CIV membrane punctured (?) $R=20$	CV a(s)–a(s)·F $\Delta E_e=0$ a(s)–b(s)·F $\Delta E_e=0$	CVI a(s)–a(s)·D$_2$(?) $\Delta E_f=-6$ b(s)–b(s)·C$_2$ $\Delta E_f=-6$ a(s)–b(s)·F $\Delta E_e=0(?)$
95% Methanol	CVII a(s)–a(s)·F $\Delta E_c=0(?)$ a(s)–b(s)·F $\Delta E_e=0(?)$	CVIII a(s)–b(s)·F $\Delta E_c=0$ $\Delta E_i=4$ b(s)–b(s)·F $\Delta E_e=0$ $\Delta E_i=7$	CIX a(s)–a(s)·E $\Delta E=-4$ a(s)–b(s)·C$_1$ $\Delta E_f=30$ b(s)–b(s)·C$_1$ $\Delta E_f=-4$

Key: a$_1$(s) = 0.10 m HCl (pa$_H$* = 1.16); a$_2$(s) = 0.01 m HCl (pa$_H$* = 2.08).
  b$_1$(s) = 0.05 m HAc, 0.05 m KAc, 0.05 m KCl (pa$_H$* = 5.53); b$_2$(s) = 0.015 m HAc, 0.015 m KAc, 0.05 m KCl (pa$_H$* = 5.53) (see also Fig. 4).
  R = resistance in MΩ.
* pa$_H$ = $-\log m_H \cdot {}_s\gamma_H$ (for nomenclature see ref. 24b). Based on E^0 data from ref. 26.

TABLE 4

EFFECT OF INTERNAL FILLING AND CONDITIONING ON THE ERRORS OF GLASS ELECTRODES IN 95 WT% DMF–WATER MIXTURES (errors in mV)

Conditioned in ╲ Filling	0.1 m HCl in water	0.075 m HAc, 0.02 m KAc, satd. KCl in 95% DMF
Water	C11 a(w)–a(w) B $\Delta E=0$ a(s)–a(s) E $\Delta E=-50$ a(s)–b(s) E $\Delta E=-5, 20$ a(w)–b(s) E $\Delta E=4$ a(w)–a(s) E $\Delta E=2, 20$ b(s)–b(s) E $\Delta E=2, 8, 6$ $R=400$	C12 a(s)–a(s) D$_1$ $\Delta E_f=120$ a(s)–b(s) E $\Delta E=150, 110, -20$ (C$_2$) b(s)–b(s) E $\Delta E=2, 10$(C$_2$) a(w)–b(s) C$_2$ $\Delta E_f=10$ $R=220$
95% DMF	C13 a(w)–a(w) C$_2$ $\Delta E_f=10$ a(w)–a(s) C$_1$ $\Delta E_f=160, 130$ a(s)–a(s) C$_2$ $\Delta E_f=20, -30, -25$ a(s)–b(s) C$_2$ $\Delta E_f=50, 60$	C14 a(w)–a(s) C$_1$ $\Delta E_f=25, 40$ (C$_2$) a(s)–a(s) D$_2$ $\Delta E_f=10$ a(s)–b(s) D$_2$ $\Delta E_f=30, 30$ (E) b(s)–b(s) E $\Delta E=5$ a(w)–b(s) C$_1$ $\Delta E_f=80$

Key: a$_1$(w) = 0.0095 m; a$_2$(w) = 0.095 m HCl in water.
  a$_1$(s) = 0.01 m; a$_2$(s) = 0.10 m HCl in DMF.
  b$_1$(s) = 0.0075 m HAc + 0.002 m KAc + 0.007 m KCl (satd.); b$_2$(s) = 0.075 m HAc + 0.02 m KAc + 0.007 m KCl (satd.) (see also Fig. 5).
  R = resistance in MΩ.

second solution and the last in the previous solution;

ΔE_f the final error, the difference between the final steady readings in the two solutions—in some solutions steady readings are never observed;

ΔE_e the extrapolated error, the difference between the potential extrapolated to the time of transfer and the final steady reading in the previous solutions.

A previous classification of glass electrode potential–time transients[1] has been extended[3] and slightly modified. We refer to the following transient types (Fig. 2):

A. a rapid change over the first few minutes which is probably electrical rather than electrochemical in origin (not shown in Fig. 2);

B. a zero or slight, and approximately linear, change which gives $\Delta E_e = 0$;

C. a rapid change with $|\Delta E_f| > |\Delta E_i|$ the rate of which slowly decreases (C_1) but sometimes turning points are observed (C_2);

D. as C but with $|\Delta E_f| < |\Delta E_i|$;

E. as B but $\Delta E_e \neq 0$;

F. which is peculiar to this work, and has $\Delta E_e = 0$, shows a turning point and at time t, $\Delta E_t = 0$ (Fig. 2).

For some transients of types B and E which do not vary with time, $\Delta E_i = \Delta E_f = \Delta E_e$ and these are referred to simply as ΔE in the Tables. Transient feature A is ignored. The distinction between A/B, A/E and C_1 or D_1 transients is sometimes not clear and is indicated by a query mark in the Tables.

In Tables 2–4, transfers between acids or buffers in the same solvent always refer to the transfer of the electrode *to* the solution of *lower* hydrogen ion concentration.

DISCUSSION

The performance of the Corning electrode with 0.1 m HCl aqueous filling (C6) (see Table 1) was only slightly inferior to that found for this type of electrode in previous studies[4]. The errors shown by the corresponding Pye electrode (P13) were greater in the intermediate pH range, and in the calcium hydroxide buffer ten times larger. These errors are, however, within the acceptable limits laid down in the British Standard Specification[15].

Table 1 shows that for the Corning electrode C5–C9, different fillings have no effect except for the 60% ethanol-filled electrode (C9) in calcium hydroxide buffer. Electrodes P12–P17 show larger errors than the Corning electrodes but the errors are much greater for P15, P17 with partially aqueous fillings. Results are shown graphically for three electrodes (P14, P15, C9) in Fig. 3. Electrode P18 with 80% ethanol filling showed rapid variation of potential with time and was unusable. Otherwise, the transient forms were C_1 or D_1, and the results cannot be attributed to continuous rapid changes in the potential of the internal reference system. The mercury-filled electrodes did show some instability but this took the form of large discontinuous jumps of potential, caused perhaps by vibration, afterwards settling to steady values and giving similar behaviour to aqueous-filled electrodes.

The results given in Table 2 show that in 95% methanol, a 50% methanol-filled electrode (CV) soaked in 50% methanol is the best (on the criterion of E type transients), and those in Table 3 suggest that an aqueous-filled, water-soaked electrode (CI) is best for the 50% mixture. The results for electrodes CV, CVI in 95% methanol
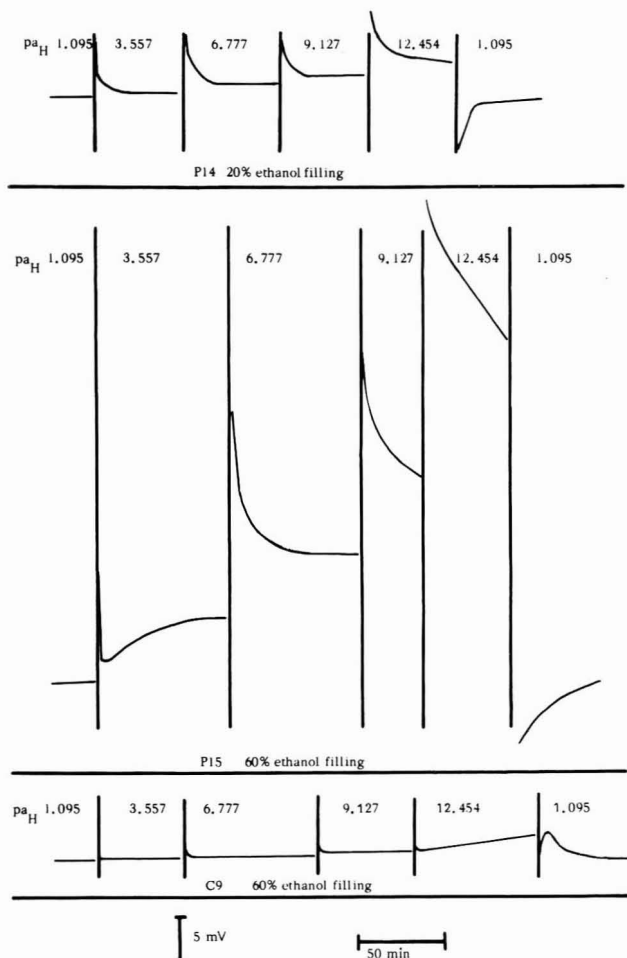
Fig. 3. Behaviour of electrodes P14, P15, C9 in six aqueous buffers.

and CV in 50% methanol are illustrated in Fig. 4. Unfortunately tests were not possible for some electrodes and as no electrode blanks of the same type were available for replacement, the experiments could not be repeated. As mentioned previously, transient type F is peculiar to these partially aqueous systems and consists effectively of two linear regions the first leading to $\Delta E_e = 0$. It is suggestive of two competing processes occurring.

The results for DMF mixtures (Table 4 and Fig. 5) show that the aqueous-filled water-soaked electrode (C11) is superior in behaviour to the other three. It was noticed that contact with 0.095 m HCl in DMF was detrimental to the behaviour of the electrodes and results were less reproducible after the electrodes had been in contact with this solution. The solubility of silver chloride in the acid (but not the buffer) solutions is such as to preclude the use of the silver–silver chloride electrode in 95% DMF–water solutions. This finding is in accord with that of previous workers[18-21].
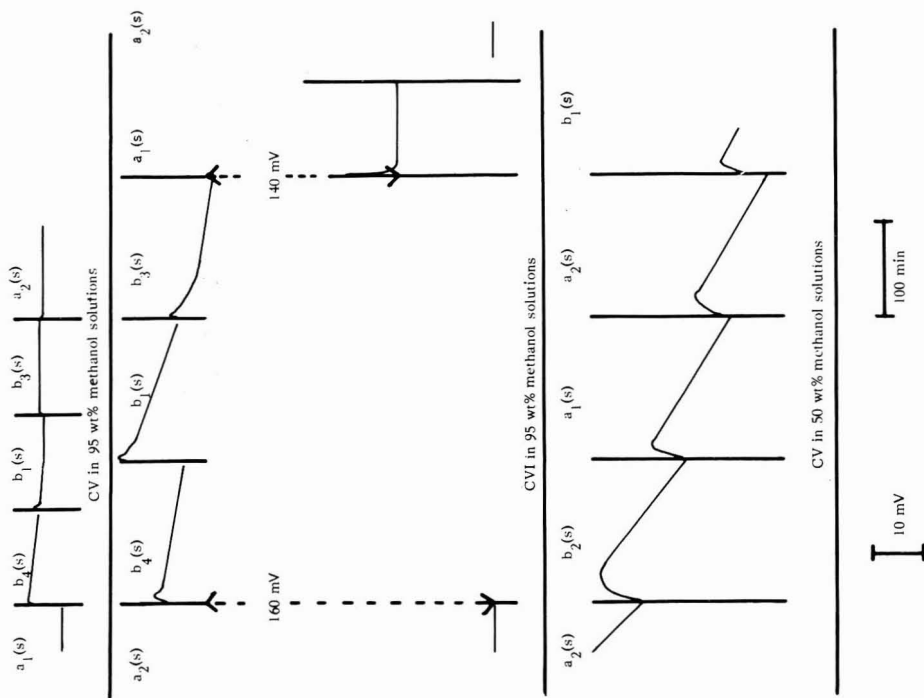
Fig. 4. Behaviour of electrodes CV and CVI in 95 wt % methanol–water and CV in 50 wt % methanol–water. (Solutions are identified in key to Tables 2 and 3).
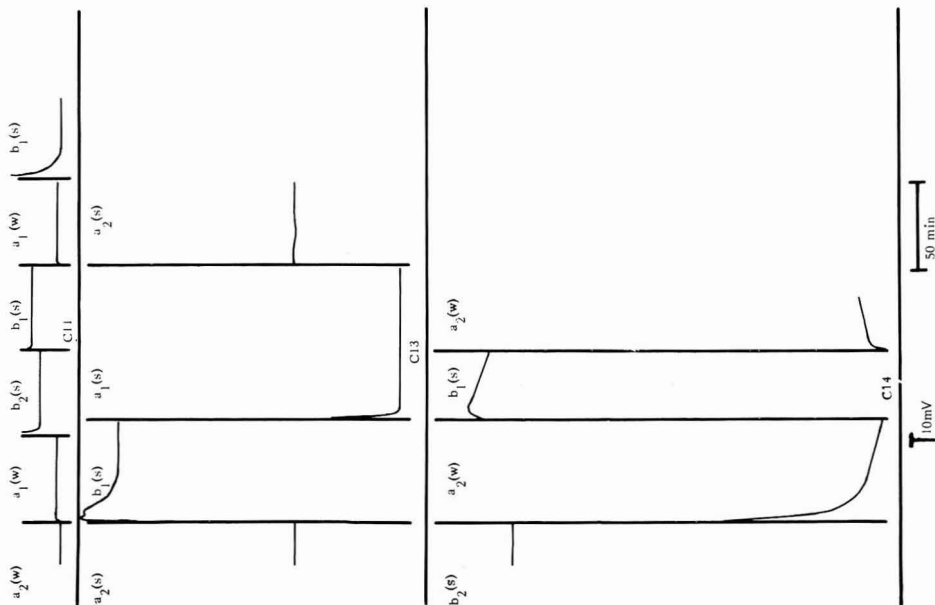
Fig. 5. Behaviour of electrodes C11, C13 and C14 in 95% DMF–water. (Solutions are identified in key to Table 4).

CONCLUSIONS

Change of glass electrode filling from aqueous to partially aqueous, affects not only the time response but the errors observed with nominally identical electrodes. It is not our intention to speculate here on the reasons for the observed behaviour before further experiments have been carried out. It is, however, difficult in view of these results to sustain the hypothesis that the potentials at the inner and outer surfaces of a glass electrode arise independently. This hypothesis is the basis of all theories of the glass electrode and experimentally derives from a rather unconvincing experiment of Dole[22]. It is tempting to explain the results by diffusion of hydrogen ions right through the glass but we do not believe this occurs, as it is inconsistent with the known properties of glass and electrolysis experiments with glass membranes[23] which led to the three layer model of the glass electrode. Neither do we believe that microcracks in the electrodes can be responsible for the observations. Our results support the general statements of some previous investigators that the response time of electrodes is changed when partially aqueous fillings are used. Their conclusions that it is preferable to use the same solvent medium inside as outside cannot be substantiated. We believe that titration curves are not the best form of evidence on which to base such conclusions and that apparently more pronounced inflections can be the result of adventitious drifts in asymmetry potential.

SUMMARY

An investigation of the time effects and time-dependent errors of hydrogen-responsive glass electrodes in various aqueous standard buffer solutions, and in hydrochloric acid and acetate buffer solutions in methanol–water and dimethyl-formamide (DMF)–water mixtures, has been made when the solvent used for the inner reference electrode system has been varied. Whilst some changes have little or no effect, some solvent mixtures profoundly alter the response characteristics and the observed errors.

REFERENCES

1 W. H. BECK, J. CAUDLE, A. K. COVINGTON AND W. F. K. WYNNE-JONES, Proc. Chem. Soc., (1963) 110.
2 W. H. BECK, J. CAUDLE AND A. K. COVINGTON, University of Newcastle upon Tyne, unpublished results, 1964.
3 W. H. BECK, P. J. BUCK AND A. K. COVINGTON, University of Newcastle upon Tyne, unpublished results, 1967.
4 W. H. BECK, A. E. BOTTOM AND A. K. COVINGTON, Anal. Chem., 40 (1968) 501.
5 A. K. COVINGTON, M. PAABO, R. A. ROBINSON AND R. G. BATES, Anal. Chem., 40 (1968) 700.
6 R. G. BATES in D. J. G. IVES AND G. J. JANZ (Eds.), Reference Electrodes, Academic Press, New York, 1961, p. 257.
7 J. BADOZ-LAMBLING, J. DESBARRES AND J. TACUSSEL, Bull. Soc. Chim. France, (1962) 53.
8 G. DOUHERET, Bull. Soc. Chim. France, (1966) 3341.
9 J. A. MARTIN AND J. DUPERIS, Bull. Soc. Chim. France, (1968) 138.
10 C. D. RITCHIE AND R. E. USCHOLD, J. Am. Chem. Soc., 89 (1967) 1721.
11 C. D. RITCHIE AND R. H. MEGERLE, J. Am. Chem. Soc., 89 (1967) 1447.
12 M. R. THOMPSON, Bur. Std. J. Res., 9 (1932) 833.
13 J. H. RISEMAN AND R. A. WALL, to Corning Glass Works, U.S. Patent, 3306837 (1967).
14 J. W. ROSS AND N. C. HEBERT, to Corning Glass Works, Canadian Patent 772,767 (1967).

15 British Standard Specification, (1965) 2586.

16 E. L. ECKFELDT AND G. A. PERLEY, *J. Electrochem. Soc.*, 98 (1951) 37.

17 J. C. BURNS, King's College, Newcastle upon Tyne, unpublished work, 1961.

18 M. TEZE AND R. SCHAAL, *Bull. Soc. Chim. France*, (1962) 1372.

19 G. P. KUMAR AND D. A. PANTONY in G. J. HILLS (Ed.), *Polarography 1964*, Vol. 2, MacMillan, London, 1966, p. 1061.

20 B. CASE AND R. PARSONS, *Trans. Faraday Soc.*, 63 (1967) 1224.

21 R. D. LANIER, *J. Phys. Chem.*, 69 (1965) 2697.

22 M. DOLE, *J. Am. Chem. Soc.*, 53 (1931) 4260.

23 G. HAUGAARD, *Nature*, 140 (1937) 66; *J. Phys. Chem.*, 45 (1941) 148; *Compt. Rend. Trav. Lab. Carlsberg*, 22 (1938) 199.

24 R. G. BATES, *Determination of pH*, Wiley, New York, 1964; (a) p. 23; (b) p. 225.

25 I. T. OIWA, *J. Phys. Chem.*, 60 (1956) 754.

26 M. PAABO, R. A. ROBINSON AND R. G. BATES, *J. Chem. Eng. Data*, 9 (1964) 374.

SIMULTANEOUS DETERMINATION OF THE DIFFUSION COEFFICIENT OF THE DEPOLARIZER AND THE NUMBER OF ELECTRONS INVOLVED IN PROCESSES AT HEMISPHERICAL PLATINUM ELECTRODES

C. BIONDI AND L. BELLUGI

Istituto di Chimica Generale ed Inorganica, Università degli Studi, Roma (Italy)

(Received July 29th, 1969)

INTRODUCTION

In recent years, there has been a revival of interest in solid electrode voltammetry and many papers and some monographs have appeared. Among the reasons for this interest is the applicability of solid electrodes in the positive region of potentials, and for the study of systems at high temperatures, where the DME cannot be utilized.

In order to minimize convective effects, some workers have used electrodes at which the concentration gradient, generated during the electrolysis, is periodically destroyed. With these electrodes, current–voltage curves that resemble the familiar DME polarograms can be recorded.

Among the electrodes for which the periodical renewal technique has been utilized are cylindrical[1] and spherical electrodes[2], for which the proper equations for the current have been shown to be substantially applicable.

There is a significant difference between the equations for the current at spherical and cylindrical electrodes and that for the current at planar electrodes: in the latter equation the diffusion coefficient appears at the power of one-half; in each of the other equations it is present in more than one term, and with different exponents. This, in principle, should permit the simultaneous evaluation of the values of n and D from current–time experiments at spherical and cylindrical electrodes, a possibility precluded for the processes at plane electrodes, for which a separate determination of D (or its estimation) is often necessary in order to establish the value of n (conversely, a previous knowledge of n is necessary in order to evaluate the value of D for the depolarizer).

Particularly simple in this respect is the equation which relates the instantaneous current to the time for an electrochemical process controlled by spherical diffusion[3]; it has the following form:

$$i_t = a + bt^{-\frac{1}{2}} \tag{1}$$

where $a = nCDFAr^{-1}$ and $b = nCD^{\frac{1}{2}}FA\pi^{-\frac{1}{2}}$. $A\,(\text{cm}^2)$ and $r\,(\text{cm})$ are the area and the radius of the electrode, respectively, n is the number of the electrons involved in the process, $C\,(\text{mM l}^{-1})$ and $D\,(\text{cm}^2\,\text{s}^{-1})$ are the concentration and the diffusion coefficient of the depolarizer, F is the Faraday constant (C) and t is the time (s). With these units, the current i_t is expressed in μA.

A plot of i_t vs. $t^{-\frac{1}{2}}$ should then give, if the equation for spherical diffusion is obeyed, a straight line of intercept a and slope b.

Once the area and the radius of the spherical electrode and the concentration of the electroactive species are known, it is possible to calculate n and D by solving the systems: $a = nCDK_a$, $b = nCD^{\frac{1}{2}}K_b$ $(K_a = FAr^{-1}, K_b = FA\pi^{-\frac{1}{2}})$.

Cozzi and coworkers[2] have proposed an apparatus, for which the model of the spherical diffusion is applicable, that uses an hemispherical platinum electrode with periodic renewal of the interphasal layer.
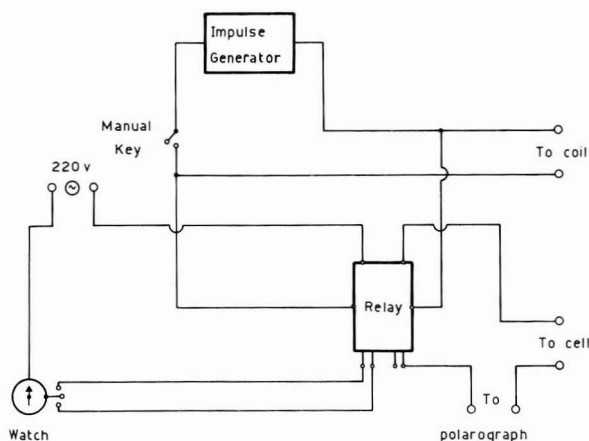
Fig. 1. Electrical circuit.

In order to test the practical feasibility of the simultaneous evaluation of n and D, we have utilized Cozzi's instrument, the electrical circuit of which has been partly modified (Fig. 1) in order to reach conditions for which the validity of the eqn. (1) can reasonably be expected.

OPERATING CONDITIONS

The modification introduced in the polarographic circuit has been suggested by the fact that it is not possible to describe exactly how the concentration of the depolarizer at the interphase changes with time, when the solution is momentarily stirred and the interphase is destroyed. As a consequence, during this time interval neither the value of the instantaneous current, nor the quantity of electricity, can be accurately described by an equation. This difficulty may be overcome by opening the electrolytic circuit (to avoid the current flow and the consumption of depolarizer), whenever the interphase is renewed (Fig. 2). Under these conditions, the current starts to flow only when the concentration of the depolarizer at the interphase has again reached the same value as in the bulk of the solution.

Thus, the electrode process, with consumption of depolarizer, takes place in the time interval, $\tau = T - t_0$, where T (the period) is the time between two successive runs of the piston which stirs the solution, and t_0 (the impulse time) is the time during which the piston is forced out from its rest position and the polarographic circuit is kept open. Under these conditions, the equation for the instantaneous current is still
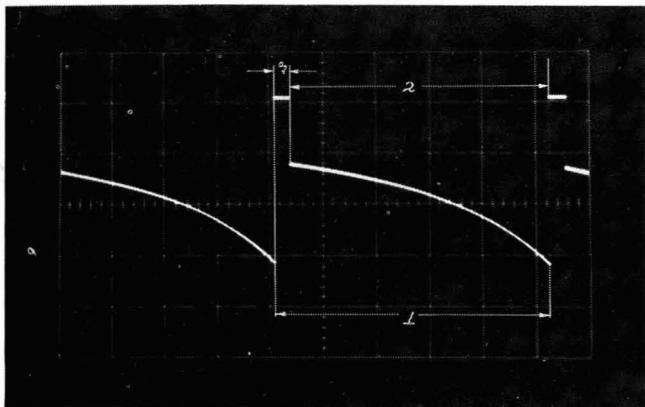
Fig. 2. Oscillogram of the current–time curve of 1.5×10^{-3} M KI in 0.1 M KNO$_3$ and 5×10^{-2} M H$_2$SO$_4$. Electrode I; $E = 0.600$ V. Ordinates 5 μA/div.; abscissae 1 s/div. $T = 5.15$ s; $t_0 = 0.30$ s.
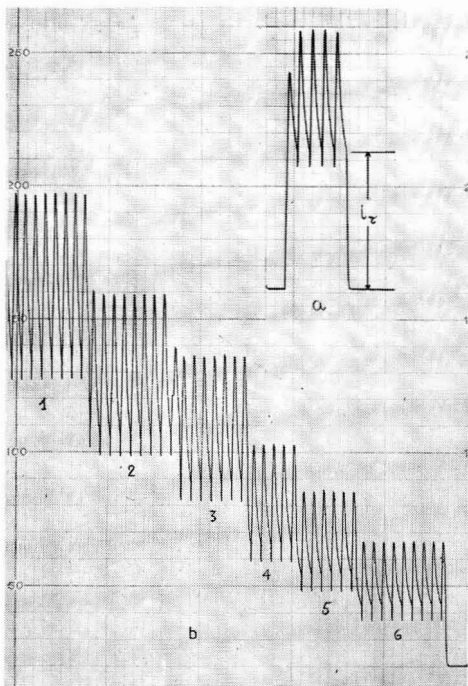

Fig. 3. (a) Current intensities for 1×10^{-3} M K$_4$Fe(CN)$_6$ in 0.1 M NaOH; electrode I, 20° C, $t_0 = 0.30$ s, $T = 12.54$ s, 0.400 V (see text). (b) Current intensities recorded with different sensitivities (same conditions as in (a)). Number of curve, sensitivity (μA mm^{-1}), height (mm), current intensity (μA). (1) 0.06, 114.0, 6.84; (2) 0.08, 85.0, 6.80; (3) 0.10, 68.0, 6.80; (4) 0.15, 45.5, 6.82; (5) 0.20, 34.0 (6.80); (6) 0.30, 23.0, (6.90).

given by (1) while that for the current just before the opening of the circuit is:

$$i_\tau = a + b\tau^{-\frac{1}{2}} = a + b(T - t_0)^{-\frac{1}{2}} \qquad (2)$$

The equation for the average current, obtained from eqn. (1) by integration between $t = 0$ and $t = \tau = T - t_0$ (which gives the quantity of electricity flowing during every period), followed by division by T, is:

$$\bar{\imath} = a\tau/T + 2b\tau^{+\frac{1}{2}}/T \approx a + 2b\tau^{-\frac{1}{2}} \qquad (3)$$

In order to evaluate the values of n and D for a depolarizer, it is necessary to obtain a and b from current–time measurements. In our experimental conditions, however, the value of a represents only a small fraction of the total current, so that in the following evaluation of the data, a is the quantity that contributes most to the error with which n and D are calculated. In order to decrease the error in a, it is then necessary to operate in such a way that its weight on the total current is the highest attainable. With a given electrode, this result can be reached by measuring i_τ since, as can be seen by a comparison of eqns. (1), (2) and (3), for given values of T and t_0, both $\bar{\imath}$ and i_τ carry a smaller relative contribution from a than the instantaneous current at the end of the period.

Moreover, of all the i_t values the one that can be measured with the highest precision (relatively to time) is i_τ, since at time τ the current drops suddenly as a result of the opening of the polarographic circuit (Figs. 2 and 3).

In view of these considerations, we have evaluated our data on the basis of eqn. (2).

EXPERIMENTAL

The electrolysis cell is essentially a glass vessel in which a Teflon piston is inserted; such a cell has been described in detail by Cozzi et al.[2]. An external coil, coaxial with the iron core piston, can be energized by an impulse generator so that, at every impulse, the piston moves, a valve opens and some of the solution is pushed against the hemispherical platinum electrode. In this way the depleted interphase is efficiently destroyed. The motion of the piston lasts only a few hundredths of a second after which the valve closes and, after a time t_0 from the beginning, the piston returns to its rest position without further stirring of the solution.

The electrical circuit used is shown in Fig. 1 which differs from the original[2] in that a relay has been added. This relay is driven by the same impulse generator that energizes the coil. Thus, when the piston moves the polarographic circuit opens and closes again only after the impulse time t_0 has elapsed. This time interval was fixed, after some trial experiments, at 0.30 s.

The values of t_0 and τ were measured by an electrical chronometer. To increase the period (the generator allows only values up to about $T = 13$ s to be used), a manual key, which opens the circuits of the coil and of the relay, was added. Current intensities were recorded by a Sargent polarograph model XXI; a saturated calomel electrode was used as a reference. The temperature was maintained for all experiments at $25.0 \pm 0.1°$C, unless stated otherwise. The geometrical characteristics of the electrodes were measured with a microscope:

electrode I: radius, 6.3×10^{-2} cm; height of the spherical segment, 7.3×10^{-2} cm; area, 2.9×10^{-2} cm^2.

electrode II : radius, 9.9×10^{-2} cm ; height of the spherical segment, 10.9×10^{-2} cm ; area, 6.8×10^{-2} cm^2.

Before each experiment the electrodes were treated for a few minutes at room temperature with $1:4$ HNO$_3$. For the OH$^-$ experiments, however, the electrodes were prepolarized for 60 s at $+2$ V vs. SCE.

The species were studied (after having first recorded their i–V curves) so that a constant voltage corresponding to conditions of diffusion current could be applied. The potentials reported here are uncorrected for IR drop.

In order to ensure that true values of i_τ were obtained, we applied a method analogous to that used by Vecchi[4] in the case of the dropping mercury electrode, by recording i_τ several times for each experiment, with decreasing galvanometer sensitivity. In this way, if the highest sensitivities used had given an i_τ value that was too large (because of a lag in the pen response time of the recorder) a lower sensitivity could be reached where, from that point on, the i_τ value became constant. With our recorder this condition was obtained when the i_τ values produced pen displacements of the order of 120 mm or less from the zero (Fig. 3b).

The value of the current at the time τ was averaged from several measurements and results with reasonably small deviations for $(i_\tau)_{Av.}$ could be obtained. In our evaluation of data we have excluded values of i_τ corresponding to pen displacements of less than 40 mm.

For each experiment, several different values of the period T (from about 4 s to about 35 s) were selected ; longer values of T resulted in noticeable convective effects.

For eqn. (2) to be applicable, it is necessary that the solution becomes quiet again before the end of every impulse, during the first portion of which the liquid is stirred. To ensure that this condition was fulfilled, an experiment was carried out with a slightly modified circuit.

Two manual keys, not shown in Fig. 1, were added in such a way that the value of the first i_τ could be obtained without previously stirring the solution, while the following values were recorded with the apparatus operating normally. Figure 3a shows the recorded current intensities for K$_4$Fe(CN)$_6$ in 0.1 M NaOH under this particular condition ($t_0 = 0.30$ s).

Since the value of the first i_τ obtained coincides with the following ones, it can be concluded that the value of t_0 selected permits the re-establishment of satisfactory conditions of homogeneity and quiet at the electrode after the sudden motion of the piston.

RESULTS AND DISCUSSION

Figure 4 shows the application of eqn. (2) to the values of anodic current intensities obtained for solutions of K$_4$Fe(CN)$_6$, KI and NaOH, with electrode I; analogous results were obtained for the same depolarizers, with electrode II.

The values of a and b of eqn. (2), obtained from the intercepts with the vertical axis and from the slopes of the straight lines of Fig. 4, are plotted in Fig. 5 (together with the results for electrode II), as functions of the quantities nCD and $nCD^{\frac{1}{2}}$, respectively. These quantities can be calculated, since n and D for such depolarizers are known : Fe(CN)$_6^{4-}$ in 0.1 M NaOH, $n=1$ and[5] $D=0.66 \times 10^{-5}$ cm^{2}s^{-1} ; I$^-$ in
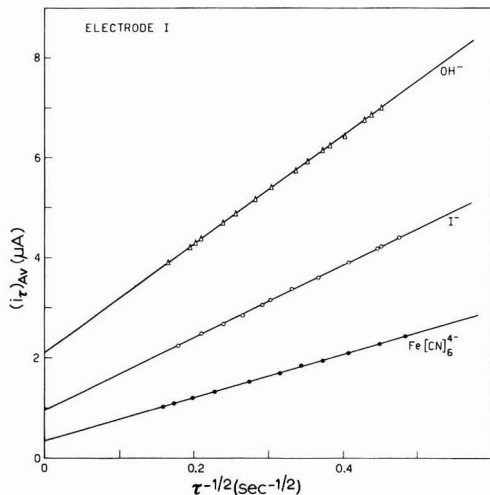
Fig. 4. Application of eqn. (2) to the anodic currents of 1×10^{-3} M solutions of $K_4Fe(CN)_6$ (in 0.1 M NaOH, 0.400 V), KI (in 0.1 M KNO$_3$, plus 0.05 M H$_2$SO$_4$, 0.600 V) and NaOH (in 1 M KNO$_3$, 1.340 V).
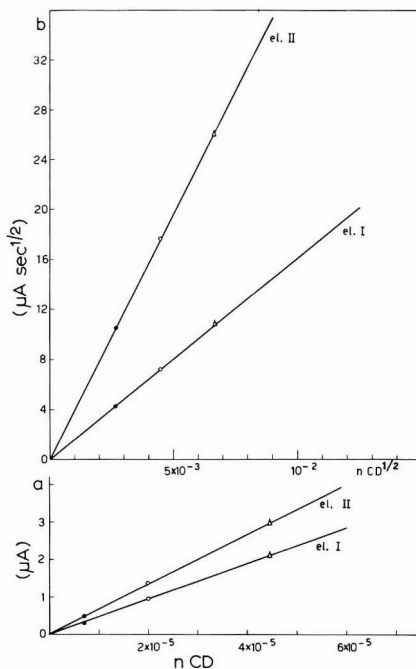
Fig. 5. Plots of exptl. values a and b for both electrodes *vs.* calcd. values of nCD and $nCD^{\frac{1}{2}}$. (●)$K_4Fe(CN)_6$, (○)KI, (△) NaOH.

0.1 M KNO$_3$ and 5×10^{-2} M H$_2$SO$_4$, $n=1$ and[6] $D=1.99 \times 10^{-5}$ cm^{2}s^{-1}; OH$^-$ in 1 M KNO$_3$, $n=1$ and[7] $D=4.45 \times 10^{-5}$ cm^{2}s^{-1}. Straight lines are obtained, passing through the origin, of slopes corresponding to the experimental electrode constants $K_a=FAr^{-1}$ and $K_b=FA\pi^{-\frac{1}{2}}$.

The plots of Fig. 5 may be considered as calibration curves since the quantities, $nCD=a/K_a(=\alpha)$ and $nCD^{\frac{1}{2}}=b/K_b(=\beta)$, for new systems could be evaluated by interpolation once the corresponding experimental values of a and b had been determined. The diffusion coefficient and the number of electrons can be calculated from α and β if C is known. On the other hand a knowledge of C is not necessary in order to obtain D, since the ratio $\alpha/\beta=D^{\frac{1}{2}}$.

The experimental and calculated values of K_a and K_b are reported in Table 1; the agreement between measured and calculated quantities is rather satisfactory since it is known that generally for solid electrodes electrochemical and geometrical surfaces do not coincide[8]. Moreover, the height of the spherical segments emerging

TABLE 1

Electrode constants	$K_a \times 10^4/C$ cm mol^{-1}		$K_b \times 10^3/C$ cm^2 mol^{-1}	
Electrode	Exptl.	Calcd.	Exptl.	Calcd.
I	4.66 ± 0.07	4.4	1.62 ± 0.1	1.6
II	6.62 ± 0.01	6.7	3.95 ± 0.03	3.7

from the glass cannot be measured very precisely, since the contour of their bases, embedded in the glass, is not perfectly circular.

The method outlined here has been applied to the reduction of the I_3^- ion. Some preliminary experiments have shown that the temperature coefficient of the current intensities for the I_3^- reduction is of the order of 1% per degree, so that it can be concluded that the electrode process is probably diffusion-controlled.

The results at 25°C with both electrodes, for a solution 1.22×10^{-3} M I_3^- in 0.1 M KI $(E = -0.200$ V), plotted as those in Fig. 4, gave straight lines from which the following values of a and b were obtained:

electrode I: $a = 1.28$ μA, $b = 13.3$ μA s$^{\frac{1}{2}}$
electrode II: $a = 1.86$ μA, $b = 32.4$ μA s$^{\frac{1}{2}}$

Using the graphs in Fig. 5 it can be shown that:

electrode I: $nCD = 2.77 \times 10^{-5}$ electrode II: $nCD = 2.80 \times 10^{-5}$
$nCD^{\frac{1}{2}} = 8.26 \times 10^{-3}$ $nCD^{\frac{1}{2}} = 8.22 \times 10^{-3}$

From these values, one obtains for the I_3^- reduction:

electrode I: $n = 2.02$, 10^5 $D = 1.15 \pm 0.03$ cm^2 s^{-1}
electrode II: $n = 1.98$, 10^5 $D = 1.14 \pm 0.03$ cm^2 s^{-1}.

We found that the reduction of the triiodide ion involves two electrons in agreement with the reaction $I_3^- + 2\,e \rightarrow 3\,I^-$ [9].

For the diffusion coefficient of the I_3^- ion, Gregory and Riddiford report[10] the value $D = 1.13 \times 10^{-5}$ cm^2 s^{-1} at 25°C, in 0.1 M KI; this value agrees with that found later by Newson and Riddiford[11].

The good approximation we found can be justified by the precision that can be reached in the measurement of the current intensities i_τ: with these electrodes, the double-layer charging current is quite small and most of the time negligible when compared to the total current.

The currents at each time τ are measured at several sensitivities and their average values, $(i_\tau)_{Av.}$, retain a probable error minor of 0.5%. The probable errors pertaining to the quantities discussed in this paper (Table 2), have been calculated by conventional methods[12].

The value of $D^{\frac{1}{2}}$ is obtained from the ratio $aK_b/bK_a = \alpha/\beta$, so that upon substitution in the relation $b = K_b nCD^{\frac{1}{2}}$ (4) the value of n can be evaluated. The precision

TABLE 2

Probable errors (%)

$(i_\tau)_{Av.}$	< 0.5	β	1
a	2–3	$D^{\frac{1}{2}}*$	2–3
b	1	n^{**}	4–5
K_a	2	$D^{\frac{1}{2}}***$	1–2
K_b	1	D^{***}	2–4
α	2–3		

* From the ratio, $aK_b/bK_a = \alpha/\beta$
** From $b = K_b nCD^{\frac{1}{2}}$
*** From $b = K_b nCD^{\frac{1}{2}}$, with non-fractional n.

of the value of $D^{\frac{1}{2}}$ first obtained can be improved once the value of n has been calculated by considering that the latter is necessarily non-fractional. Then, by re-applying relation (4), values of D can be obtained with probable errors less than 5%.

Since solid electrodes permit the exploration of an extended range of positive potentials, the present method could be useful, particularly for the investigation of organic systems for which D values cannot usually be evaluated from conductivity data; moreover, the determination of D (but not of n) is possible when the concentration of the electroactive species is unknown.

ACKNOWLEDGEMENT

SUMMARY

Current–time curves at hemispherical platinum electrodes with periodic renewal of the diffusion layer have been recorded in conditions which permit the use of the spherical diffusion equation.

Since the current intensities are related to two separable exponential terms for the diffusion coefficient of the depolarizer, the number of electrons involved in the electrolytic processes, and the diffusion coefficients of the species studied can be determined simultaneously.

The method has been applied with good results to the reduction of the I_3^- ion.

REFERENCES

1 S. ROFFIA AND E. VIANELLO, *J. Electroanal. Chem.*, 12 (1966) 112.
2 D. COZZI, G. RASPI AND L. NUCCI, *J. Electroanal. Chem.*, 12 (1966) 36; L. BUSULINI AND P. CESCON, *Ann. Chim. (Rome)*, 56, 7 (1966) 852.
3 P. DELAHAY, *New Instrumental Methods of Analysis*, Wiley (Interscience), New York, 1954, p. 69.
4 E. VECCHI, *Ric. Sci. Suppl.*, 2 (1956) 27.
5 J. C. BAZAN AND J. A. ARVIA, *Electrochim. Acta*, 10 (1965) 1025.
6 A. L. BEILBEY AND A. L. CRITTENDEN, *J. Phys. Chem.*, 64 (1960) 177.
7 R. LANDESBERG, W. GEISSLER AND S. MÜLLER, *Z. Chem.*, (1961) 169.
8 R. N. ADAMS, *Electrochemistry at Solid Electrodes*, M. Dekker, Inc., New York, 1969, p. 56.
9 E. A. HOGGE AND M. B. KRAICHMAN, *J. Am. Chem. Soc.*, 76 (1954) 1431.
10 D. P. GREGORY AND A. C. RIDDIFORD, *J. Chem. Soc.*, (1956) 3756.
11 J. D. NEWSON AND RIDDIFORD, *J. Electrochem. Soc.*, 108 (1961) 695.
12 H. MARGENAU AND G. M. MURPHY, *The Mathematics of Physics and Chemistry*, D. Van Nostrand Company, Inc., Princeton, New Jersey, 2nd ed., 1964, p. 515.
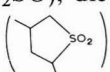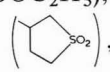
ELECTROCHEMICAL STUDY OF COPPER IONS IN A SERIES OF SULFOXO SOLVENTS

JOE L. HANLEY AND REYNOLD T. IWAMOTO

Department of Chemistry, University of Kansas, Lawrence, Kansas (U.S.A.)

Except for a study of the behavior of inorganic ions in sulfolane (tetrahydro-thiophene-1,1-dioxide)[1], all of the polarographic investigations conducted to date in organic sulfoxo solvents have been in dimethyl sulfoxide. In this study, we have examined the electrochemical behavior of copper(II) and copper(I) ions in dimethyl sulfoxide ($(CH_3)_2SO$), diethyl sulfite ($C_2H_5OSOC_2H_5$), sulfolane, 2,4-dimethylsulfolane, 3-methylsulfolane, methyl methanesulfonate (CH_3SOCH_3), and diethyl sulfate ($C_2H_5OSOC_2H_5$). The information on the relative order of solvation of copper ions in these solvents provided by the electrochemical study is consistent with nuclear magnetic resonance and infrared spectral data on the coordinating ability of these solvent molecules and the dielectric constant of the solvents—in governing ion-association.

EXPERIMENTAL

Dimethyl sulfoxide (Crown Zellerbach) was purified by two distillations under reduced pressure over calcium hydride, the first and last 10% of the distillates being discarded. Sulfolane (courtesy of Shell Chemical Co.), 2,4-dimethylsulfolane (Aldrich Chemical Co.), and 3-methylsulfolane (Aldrich Chemical Co.) were purified by the following adaptation of the method of Jones[2]: distillation below 100° under reduced pressure (*a*) over crushed sodium hydroxide, (*b*) after treatment with hydrogen peroxide and sulfuric acid and removal of remaining hydrogen peroxide and water (500 ml of sulfolane with 25 ml of 30% H_2O_2 and 25 ml of 96% H_2SO_4), (*c*) from solid sodium hydroxide, and (*d*) twice from calcium hydride. Methyl methanesulfonate and diethyl sulfite, both from Aldrich Chemical Co., and diethyl sulfate, from Matheson Coleman and Bell, were distilled twice *in vacuo*, with the sulfate distilled over anhydrous sodium sulfate. Preparation of methyl methanesulfinate was attempted by the method described by Douglass[3]. Methanesulfinyl chloride was prepared first, then converted to the sulfinate. Despite several attempts, only a small amount of product was obtained. Spectroquality carbon tetrachloride (Matheson Coleman and Bell) was used without further purification.

Copper(II) perchlorate 6-hydrate (G. F. Smith Chemical Co.) was dried at 85°

in vacuo for 30 h. The copper content of the dried salt, determined by electrolysis, was 19.3%, indicating the perchlorate to be the tetrahydrate. The theoretical value for the percentage of copper in the tetrahydrate is 19.0. Boron trifluoride was obtained from The Matheson Co., Inc., and phenol was of reagent grade purity from Mallinkrodt.

Tetraethylammonium perchlorate, Et_4NClO_4, was prepared by adding a slight excess of 70% reagent grade perchloric acid to aqueous 10% tetraethylammonium hydroxide. The product was recrystallized four times from water and dried at 80° *in vacuo* for 48 h. Tetrabutylammonium perchlorate, Bu_4NClO_4, was prepared by treatment of a chloroform solution of tetrabutylammonium bromide with a slight excess of an aqueous silver perchlorate solution $0.10 F$ in perchloric acid. The mixture was filtered to remove the silver bromide, and the filtrate was placed in a separatory funnel. The chloroform layer was washed five times with chloride-free water, then filtered through an ultra-fine sintered glass funnel, and finally evaporated to one-fifth its original volume and cooled. The Bu_4NClO_4 was recrystallized from ethyl acetate and dried *in vacuo* for 24 h at 80°.

Current–potential curves were obtained with a modified Kelley, Jones, Fisher controlled-potential polarograph[4,5]. A three-compartment cell, with fritted glass discs of fine porosity separating the compartments, was used. The working electrode was placed in the center compartment, and the reference electrode and the auxiliary electrode in the other two compartments. A saturated aqueous calomel electrode was the reference electrode. The solutions examined were $0.10 F$ in Et_4NClO_4 or Bu_4NClO_4 and $5 \times 10^{-4} F$ or less in copper(II) perchlorate. Purified nitrogen was used to deaerate the solutions and was passed over the surface of the solutions during measurement. The solutions were examined at room temperature. The rotating platinum electrode was a 2-mm length of platinum wire extending from the tip of a soft-glass tube mounted on a Sargent rotator (*ca.* 600 rev. min^{-1}).

A Varian A-60 nuclear magnetic resonance spectrometer was used to obtain the proton nuclear magnetic resonance spectra of solutions of 1–2% phenol and varying concentrations of the sulfoxo compound in carbon tetrachloride. The solutions contained tetramethylsilane as internal standard and were at 38° when examined. For ^{19}F magnetic resonance spectra of sulfoxo solutions containing boron trifluoride, a Varian HA-100 nuclear magnetic resonance spectrometer operated at 94.1 MHz was used (calibrated by field-modulated side bands). The solutions for this nuclear magnetic resonance study were prepared by bubbling small amounts of boron trifluoride into the solvents (amounts sufficient to give measurable signals). The solutions were placed in nuclear magnetic resonance tubes, and the tubes were sealed and the spectra of the solutions recorded immediately. Trichlorofluoromethane was the internal standard in the ^{19}F magnetic resonance measurements.

Infrared spectra were recorded on a Perkin–Elmer 421 spectrophotometer.

A calibration curve of dielectric constant *vs.* capacitance reading of a Sargent model V chemical oscillometer was used to obtain the dielectric constant of solvents for which no literature values are available.

RESULTS

A summary of the electrochemical data for the reduction of solutions of copper(II) perchlorate in dimethyl sulfoxide (ε, dielectric constant, 46.7)[6], diethyl

sulfite (ε, 15.9)[7], sulfolane (ε, 44)[8], 2,4-dimethylsulfolane (ε, 29.5), 3-methylsulfolane (ε, 28.3), methyl methanesulfonate (ε, 46.5), and diethyl sulfate (ε, 29.2)[9] at the dropping mercury electrode (DME) and rotating platinum electrode (RPE) is presented in Tables 1 and 2, respectively. The results of a proton magnetic resonance study of the donor ability of the sulfoxo compounds are summarized in Table 3. The limiting values of the downfield chemical shifts of the phenolic hydrogen in carbon tetra-chloride solutions containing 1–2% phenol and increasing amounts of the sulfoxo compounds have been determined. Along with this hydrogen-bonding investigation, an examination of boron trifluoride–sulfoxo solvent interaction was also carried out to obtain information on the solvating ability of the sulfoxo solvents. Upfield shifts of the ^{19}F magnetic resonance signal caused by the association of boron trifluoride with donor solvents were obtained and are listed in Table 4. The spectrum of fluorine nuclei spin–spin coupled to a nucleus of spin I, where $I > \frac{1}{2}$, is, in general, expected to have a multiplet with $2I + 1$ lines. Since boron has a spin of $\frac{3}{2}$, a $1:1:1:1$ quartet would be expected for BF_3. The ^{19}F resonance signal of the complexes in the sulfoxo solvents is a singlet, except in dimethyl sulfoxide and diethyl sulfite in which there are small

TABLE 1

POLAROGRAPHIC DATA FOR THE REDUCTION OF COPPER(II) PERCHLORATE IN SOME SULFOXO SOLVENTS[a]

Solvent	$E_{\frac{1}{2} Cu(II), Cu(Hg)}/V$ vs. SCE (slope of log plot/V)	
	0.10 F Et_4NClO_4	0.10 F Bu_4NClO_4
Dimethyl sulfoxide	−0.07 (0.095)	−0.07 (0.080)
Sulfolane	+0.50 (0.089)	+0.46 (0.091)
2,4-Dimethylsulfolane	+0.52 (0.099)	+0.56 (0.100)
3-Methylsulfolane	+0.50 (0.093)	+0.52 (0.100)
Methyl methanesulfonate	+0.63 (0.085)	+0.64 (0.085)
Diethyl sulfate	+0.60 (0.062)	+0.63 (0.052)

[a] The reduction wave for copper(II) ion in diethyl sulfite occurs at about the same potential as that for the anodic wave for the dissolution of mercury (+0.70 V vs. SCE).

second signals of, at this time, unknown origin about 3 ppm upfield and ca. 20% of the intensity of the major signal. The absence of boron–fluorine spin coupling may be attributed to some combination of quadrupole relaxation and rapid exchange between "free" and "coordinated" boron trifluoride[2,11]. Table 5 lists the S–O stretching frequencies of the sulfoxo solvents. Use has been made of the "Lehmann average rule" to obtain the "equivalent S–O stretching frequency" from the symmetric and asymmetric S–O stretching frequencies[12]. Where there were more than one symmetric or asymmetric stretching band, the average values were used to calculate the "equivalent S–O stretching frequency".

DISCUSSION

One-step reduction waves were obtained with the dropping mercury electrode for solutions of copper(II) perchlorate in dimethyl sulfoxide, diethyl sulfite, sulfolane, 2,4-dimethylsulfolane, 3-methylsulfolane, methyl methanesulfonate, and diethyl sulfate, with 0.10 F Et_4NClO_4 or 0.10 F Bu_4NClO_4 as supporting electrolyte. With

TABLE 2

VOLTAMETRIC DATA FOR THE REDUCTION OF COPPER(II) PERCHLORATE AT THE ROTATING PLATINUM ELECTRODE IN SOME SULFOXO SOLVENTS

Solvent	(a) $E_{\frac{1}{2}Cu(II),Cu(I)}/V$ vs. SCE (slope of log plot/V) (b) $E^{0'}_{Cu(I),Cu}/V$ vs. SCE* (slope of log plot/V) (c) $E_{\frac{1}{2}ferricinium,ferrocene}/V$ vs. SCE**		Corr. for differences in liquid-junction potential[†]	
	0.10 F Et_4NClO_4	0.10 F Bu_4NClO_4	0.10 F Et_4NClO_4	0.10 F Bu_4NClO_4
Dimethyl sulfoxide	(a) $+0.04$ (0.067)	$+0.04$ (0.075)	$+0.04$	$+0.04$
	(b) -0.09 (0.065)	-0.08 (0.090)	-0.09	-0.08
	(c) $+0.43$	$+0.44$		
Diethyl sulfite[††]	(a) —	$+0.71$ (0.089)	—	$+0.65$
	(b) —	$+0.50$ (0.070)	—	$+0.44$
	(c) —	$+0.50$		
Sulfolane	(a) $+0.58$ (0.074)	$+0.56$ (0.075)	$+0.62$	$+0.60$
	(b) $+0.48$ (0.064)	$+0.49$ (0.059)	$+0.52$	$+0.53$
	(c) $+0.39$	$+0.40$		
2,4-Dimethylsulfolane	(a) $+0.60$ (0.080)	$+0.60$ (0.081)	$+0.62$	$+0.60$
	(b) $+0.52$ (0.070)	$+0.52$ (0.076)	$+0.54$	$+0.52$
	(c) $+0.41$	$+0.44$		
3-Methylsulfolane	(a) $+0.58$ (0.078)	$+0.58$ (0.078)	$+0.59$	$+0.59$
	(b) $+0.48$ (0.070)	$+0.51$ (0.064)	$+0.49$	$+0.52$
	(c) $+0.42$	$+0.43$		
Methyl methanesulfonate	(a) $+0.71$ (0.063)	$+0.69$ (0.075)	$+0.79$	$+0.78$
	(b) $+0.65$ (0.062)	$+0.66$ (0.064)	$+0.73$	$+0.75$
	(c) $+0.35$	$+0.35$		
Diethyl sulfate	(a) $+0.71$ (0.073)	$+0.74$ (0.072)	$+0.75$	$+0.71$
	(b) $+0.68$ (0.064)	$+0.73$ (0.074)	$+0.72$	$+0.70$
	(c) $+0.39$	$+0.47$		

* $E^{0_1}_{Cu(I),Cu} = E^{0}_{Cu^+,Cu} + (RT/F)\ln f_{Cu^+}$

** Oxidation of ferrocene is reversible at the RPE in all solvents.

[†] Dimethyl sulfoxide (reference solvent); Use $E_{\frac{1}{2}ferricinium,ferrocene}$ vs. SCE (see ref. 10).

[††] Et_4NClO_4 is insoluble in the solvent.

the rotating platinum electrode, two-step reduction waves were observed because of the dependence of the potential of the copper(I),copper couple on the concentration of copper(I). The slopes of plots of E vs. log $(i_d - i)$ for the copper(I),copper couple indicate that this redox system is essentially reversible under voltammetric conditions. The slopes of plots of E vs. $\log[(i_d - i)/i]$ for the copper(II),copper(I) couple are generally not nearly as close to the reversible value of 0.059 V. We feel that the half-wave potentials of the copper(II),copper(I) couple as well as the potentials for the copper(I),copper couple, however, are close to the reversible values and do reflect the general solvating ability of the sulfoxo solvents examined for copper(II) and copper(I) ions. From the potentials, the order of the solvents in decreasing ability to solvate copper(I) ion is: dimethyl sulfoxide $\gg$ diethyl sulfite $>$ sulfolane $\sim$ 2,4-dimethyl-

TABLE 3

PROTON MAGNETIC RESONANCE DATA ON THE DONOR ABILITY OF THE SULFOXO SOLVENTS; HYDROGEN BOND
STUDY WITH PHENOL IN CARBON TETRACHLORIDE

Solvent	Limiting value of δ_{obs} for the phenolic hydrogen at large ratios of concn. of sulfoxo compound to concn. of phenol/ppm
Dimethyl sulfoxide	-8.00
diethyl sulfite	-6.10
sulfolane	-5.95
methyl methanesulfonate	-5.51
diethyl sulfate	-5.42

1–2% phenol; internal standard, tetramethylsilane

TABLE 4

[19]F NUCLEAR MAGNETIC RESONANCE DATA ON THE INTERACTION OF BORON TRIFLUORIDE WITH SULFOXO
SOLVENT MOLECULES

Solvent	Solvated BF_3/ppm relative to CCl_3F
Dimethyl sulfoxide	$+148.6$
Diethyl sulfite	$+145.8$
Sulfolane	$+143.5$
Methyl methanesulfonate	$+140.9$
Diethyl sulfate	$+131.0$

TABLE 5

INFRARED S–O STRETCHING FREQUENCIES OF THE SULFOXO SOLVENTS

Solvent	v_{sym}/cm^{-1}	v_{asym}/cm^{-1}	v_{S-O}/cm^{-1}
Dimethyl sulfoxide			1055
Methyl methanesulfinate			1199
Diethyl sulfite			1205^b
Sulfolane	1105, 1145	1295^a	1210^c
Methyl methanesulfonate	1170	1347	1258^c
Diethyl sulfate	1194	1365, 1386, 1400	1289^c

^{a} Major band, two less intense adjacent bands at 1255 and 1272 cm^{-1}. ^{b} Shoulder at 1190 cm^{-1}. ^{c} $v_{SO} =$ (average v_{sym} + average v_{asym})/2.

sulfolane ~ 3-methylsulfolane > methyl methanesulfonate ~ diethyl sulfate. After adjustment for the differences in solvation of copper(I) ion, the copper(II), copper(I) potential data yield the same order for the solvation of copper(II) ion.

The proton magnetic resonance signal of the hydrogen participating in hydrogen bonding is usually shifted downfield because of the change in magnetic field at the hydrogen[13]. The observed chemical shift, δ_{obs}, reflects the population weighted average of the free and hydrogen-bonded states, i.e.,

$$\delta_{obs} = (1 - \alpha)\delta_{A-H} + \alpha\delta_{A-H---B}$$

In the above expression, α is the fraction of hydrogen-bonded acid. When $\alpha=1$, δ_{obs} equals δ_{A-H--B}. In the absence of "donor-anisotropy" effect, the variation in $\delta_{A-H---B}$ arises from differences in electron donor strengths of the donors[14]. In a proton magnetic resonance study of hydrogen bonding with phenol in methylene chloride, it has been shown that with donors such as dimethyl sulfoxide and sulfolane there does not appear to be any significant "donor-anisotropy" effect[14]. The limiting values of δ_{obs} for the phenolic proton with increasing concentration of sulfoxo compound in carbon tetrachloride (Table 3) indicate the donor strength of the sulfoxo solvents to be: dimethyl sulfoxide $\gg$ diethyl sulfite $>$ sulfolane $>$ methyl methanesulfonate $>$ diethyl sulfate.

The same order is obtained for the coordinating ability of the sulfoxo solvents from the ^{19}F nuclear magnetic resonance data on the interaction of boron trifluoride with the solvents. The upfield shift of the ^{19}F signal indicates increase in electron density at the fluorine nuclei arising from coordination of boron trifluoride to a solvent of strong donor character.

Finally, from the S—O stretching frequencies of dimethyl sulfoxide, methyl methanesulfonate, and diethyl sulfite and the "equivalent S—O stretching frequencies" of sulfolane, methyl methanesulfonate and diethyl sulfate, the following orders of basicity of the sulfoxo solvents may be proposed: dimethyl sulfoxide $>$ methyl methanesulfinate $>$ diethyl sulfite and sulfolane $>$ methyl methanesulfonate $>$ diethyl sulfate. The relationship between the S—O stretching frequencies and the basicity of solvents containing the S—O group has been established by Barnard et al.[15] and Hall and Robinson[16]. In fact, on the basis of these studies the single order: dimethyl sulfoxide $>$ methyl methanesulfinate $>$ diethyl sulfite $>$ sulfolane $>$ methyl methanesulfonate $>$ diethyl sulfate, identical (except for methyl methanesulfinate) with that obtained from the nuclear magnetic resonance studies, should be valid.

The only discrepancy in the results of this investigation is the failure of the potentials of the copper couples in methyl methanesulfonate and diethyl sulfate to reflect the difference, indicated by the nuclear magnetic resonance studies and infrared data, between these two solvents in their ability to solvate copper(II) and copper(I) ions. This situation can be attributed to the difference in dielectric constant of methyl methanesulfonate, 46.5, and diethyl sulfate, 29.2, and the resultant difference in extent of ion-pair formation in the two solvents. Although ion-pair formation between the tetralkylammonium ion and perchlorate ion is expected to be more extensive in diethyl sulfate than in methyl methanesulfonate, the lower concentration of perchlorate ion in diethyl sulfate than in methyl methanesulfonate appears to be more than offset by the larger ion-pair formation constants of copper(II) and of copper(I) ions with perchlorate ion in diethyl sulfate than in methyl methanesulfonate. It should be noted that in spite of a certain amount of ion-pair formation in each of the other solvents, the extents of ion-association in these solvents do not distort, as indicated by the potentials, their relative order to solvate copper(II) and copper(I) ions. Also with regard to ion-pair formation, the similarity of the potentials of the copper couples in Et_4NClO_4 and Bu_4NClO_4 solutions of each of the solvents should be noted.

Interestingly, the potentials of the copper couples in sulfolane and 2,4-dimethylsulfolane indicate essentially no change on introduction of a methyl group on the carbon adjacent to the sulfonyl group in sulfolane in the solvating ability of the

resulting sulfolane for copper(II) and copper(I) ions. The introduction of a methyl group on the β-carbon, as expected, causes no change in the solvating ability of the substituted sulfolane for copper ions.

SUMMARY

The voltammetric behavior of copper(II) ion in dimethyl sulfoxide, diethyl sulfite, sulfolane, 2,4-dimethylsulfolane, 3-methylsulfolane, methyl methanesulfonate, and diethyl sulfate at the dropping mercury and rotating platinum electrodes has been examined. Two-step waves were obtained for the reduction of copper(II) ion at the rotating platinum electrode in all the solvents. However, because of the closeness of the potentials of the copper(II),copper(I) and copper(I),copper(Hg) couples to each other in each solvent, only one-step reduction waves were obtained in all the solvents with the dropping mercury electrode.

From the electrochemical data, the proton magnetic resonance data on hydrogen bonding between phenol and the sulfoxo compounds in carbon tetrachloride, the ^{19}F magnetic resonance study of the solvation of boron trifluoride in the sulfoxo solvents, the stretching frequencies of the $S-O$ group of the sulfoxo compounds, and consideration of the dielectric constant of the sulfoxo solvents, the following order has been established for the ability of the solvents to solvate copper(II) and copper(I) ions: dimethyl sulfoxide > (methyl methanesulfinate) > diethyl sulfite > sulfolane > methyl methanesulfonate > diethyl sulfate.

REFERENCES

1 J. B. HEADRIDGE, D. PLETCHER AND M. CALLINGHAM, J. Chem. Soc., (1967) 684.
2 J. G. JONES, Inorg. Chem., 5 (1966) 1229.
3 I. B. DOUGLASS, J. Org. Chem., 30 (1965) 663.
4 M. T. KELLEY, H. C. JONES AND D. J. FISHER, Anal. Chem., 31 (1959) 1475.
5 M. T. KELLEY, D. J. FISHER AND H. C. JONES, Anal. Chem., 32 (1960) 1262.
6 R. A. HOVERMALE AND P. G. SEARS, J. Phys. Chem., 60 (1956) 1579.
7 P. WALDEN, Z. Physik. Chem., 70 (1910) 569.
8 R. L. BURWELL, JR. AND C. H. LANGFORD, J. Am. Chem. Soc., 81 (1959) 3799.
9 C. P. SMYTH AND C. H. HITCHCOCK, J. Am. Chem. Soc., 54 (1932) 4631.
10 I. V. NELSON AND R. T. IWAMOTO, Anal. Chem., 35 (1963) 867.
11 S. BROWNSTEIN, A. M. EASTHAM AND G. A. LATREMOUILLE, J. Phys. Chem., 67 (1963) 1028.
12 W. J. LEHMANN, J. Mol. Spectry., 7 (1961) 261.
13 C. M. HUGGINS, C. C. PIMENTEL AND J. W. SHOOLERY, J. Phys. Chem., 60 (1956) 1311.
14 D. P. EYMAN AND R. DRAGO, J. Am. Chem. Soc., 88 (1966) 1617.
15 D. BARNARD, J. M. FABIAN AND H. P. KOCH, J. Chem. Soc., (1949) 2442.
16 S. K. HALL AND E. A. ROBINSON, Can. J. Chem., 42 (1964) 1113.

ELECTROCHEMICAL BEHAVIOR OF GOLD IN ACIDIC CHLORIDE SOLUTIONS

J. N. GAUR AND G. M. SCHMID

Department of Chemistry, University of Florida, Gainesville, Fla. 32601 (U.S.A.)

(Received May 16th, 1969)

The effect of chloride ions on the passivity of iron commanded the attention of early electrochemists[1] and has since been investigated many times[2-4]. It is generally assumed that, by a mechanism as yet unknown, chloride ions destroy the passive film either locally, as in pitting, or uniformly and thus lead to increased corrosion. Similar observations were made, *e.g.* on stainless steels[5-8], and on nickel[9]. It has been known for many years, (*cf.* Grahame *et al.*[10]) that chloride ions are strongly adsorbed on mercury, and it is generally assumed that they are adsorbed on other metals as well. Presumably the first step in the destruction of passivity is the adsorption of chloride in preference to the oxygenated species forming the passive film. Evidence for this is lacking but accumulation of radioactive bromide ions has been found in pits formed on iron[11].

The anodic dissolution of gold in chloride solutions occurs with formation of a soluble tetrachloro–gold complex at a standard potential of $+1.00$ V[12]. In acidic, chloride free solutions a potential of 1.0 V is frequently quoted for the start of the formation of an oxide and/or adsorbed "oxygen" film on gold electrodes[13,14]. It seemed worthwhile to try to confirm and to complement the results of a previous study of the gold chloride solution system by Heumann and Panesar[15], to see if the gold dissolution reaction could be passivated by the formation of an oxide or "oxygen" film, and to determine the stability of this passivating film in the presence of chloride ions.

EXPERIMENTAL

The test electrodes were gold beads, about 0.1 cm^2 in apparent area, made at the end of 0.5 mm wires (Engelhardt Industries, Fine Gold) by melting in a hydrogen–air flame. The electrodes were sealed into a Teflon holder with Kel-F-200 wax so that only the bead was exposed to solution. The Teflon holder was mounted in an all Pyrex glass cell which also contained a platinum wire gauze polarizing electrode and, in a side compartment, a saturated calomel reference electrode.

Test solutions were 0.1 M in HClO$_4$ and 100, 50, 10, 8, 6, 4, or 2×10^{-4} M in Cl$^-$. Some experiments were made in solutions containing Br$^-$ instead of Cl$^-$. All solns. were made up from Analyzed Reagent 70% HClO$_4$, Analyzed Reagent KCl or KBr, and triply distilled water prepared by distilling once from alkaline permanganate in Pyrex and twice from a quartz still. The solutions were deaerated and saturated with hydrogen gas taken from a Fisher–Serfass purifier. All gas ducts were made of Teflon

tubing and the cell was water trapped on the inlet and the outlet side. Unless otherwise noted, the solutions were stirred vigorously with a magnetic stirrer and a Teflon stirring bar.

Before each experiment, the test electrode was left for 10 min at $+1.4$ V and for 10 min at -0.4 V. Steady state current potential curves were obtained under potentiostatic control from an Electroscan 30 (Beckman Instruments, Inc.). Currents through a standard resistor were measured, and potentials were monitored with a Keithley 610 BR electrometer. Cyclic voltammetry curves were obtained using the Electroscan 30 potential scan and current recorder. Differential capacity measurements were made in the microsecond range with a single pulse technique[16], using a Tektronix type 549 storage oscilloscope.

All potentials are given with respect to the saturated calomel electrode unless noted otherwise. The experiments were conducted at room temperature. The current due to hydrogen oxidation was negligible in the potential region studied.

RESULTS AND DISCUSSION

Figure 1a shows the triangular sweep voltammetry curve (with vigorous stirring) obtained at 2.4 V min^{-1} on gold in chloride free 0.1 M HClO$_4$. On both the cathodic and the anodic sweep a hydrogen oxidation current is observed in the region -0.1 to $+0.4$ V, in agreement with previous work[17]. On the anodic sweep this is followed by a double layer region (0.5–1.0 V) and by the formation of "adsorbed oxygen", beginning at about 1.0 V[13,14]. The reduction of this adsorbed layer occurs on the cathodic scan at about 0.9 V. The magnitude of this reduction peak depends entirely on the turn-around point of the scan (1.4 V in Fig. 1a) and this was difficult to reproduce with precision with the manual controls provided on the Electroscan.

Addition of chloride ions in concentrations $>2 \times 10^{-4}$ M causes the complete disappearance of the hydrogen oxidation current observed in chloride free solutions (Fig. 1b). This is possibly due to the adsorption of chloride ions at potentials close to and anodic to the zero point of charge of gold[18-20] thus blocking the surface sites necessary for hydrogen oxidation[17].

A new current peak appears on the anodic scan at about 1.2 V. Its height depends on the chloride ion concentration and on the stirring rate. The rise of current to the peak is due to the anodic dissolution of gold, possibly according to:

$$Au + 4\,Cl^- \rightleftarrows AuCl_4^- + 3\,e \tag{1}$$

The equilibrium potential for this reaction with the chloride ion concentrations used here is in the vicinity of 0.8 to 1.0 V[12] and this agrees approximately with the position of the current rise to the peaks on the potential axis. The evolution of chlorine has a standard potential of 1.36 V (vs. NHE)[12] and is thermodynamically not possible at < 1.3 V in our experiments. In fact, chlorine evolution does not seem to occur in this system until oxygen evolution starts at about 1.6 V. Our findings are in good agreement with those of Heumann and Panesar[15]. These authors also discussed the anodic dissolution of gold as Au$^+$ and Au^{3+} and distinguished analytically between the two species. They found predominant dissolution as Au^{3+} at currents >100 μA cm^{-2}. We have not investigated this aspect. Since the currents used here for dissolution of gold are generally >50 μA cm^{-2}, dissolution as Au^{3+} will be assumed for the purpose
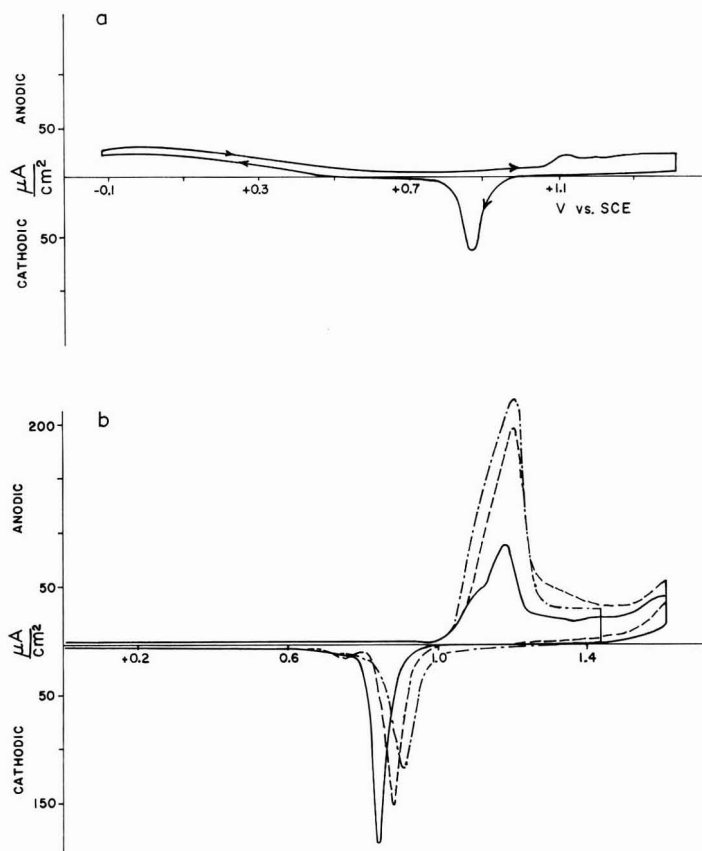
Fig. 1. (a) Triangular sweep voltammetry curve, Au in 0.1 M HClO$_4$, 2.4 V min^{-1}. (b) Triangular sweep voltammetry curves, Au in 0.1 M HClO$_4$ and (——) 4×10^{-4}, (-----) 6×10^{-4}, (—·—) 1×10^{-3} M KCl, 2.4 V min^{-1}.

of discussion.

With reaction (1) and no further complication a limiting diffusion current—and not a current peak—would be expected with the technique used to obtain the curves in Fig. 1b. Moreover, a simple calculation shows that the peak currents observed are lower than the limiting diffusion currents expected on the basis of eqn. (1) by a factor of at least 5. It is interesting to note that the peak position at 1.15 V is independent of the chloride ion concentration and coincides with the formation of "adsorbed oxygen" on the electrode surface (Fig. 1a). This "adsorbed oxygen" film evidently passivates the electrode preventing further dissolution of gold as AuCl$_4^-$.

On the cathodic scan, the presence of this "adsorbed oxygen" film blocks reaction (1) completely. This was shown by re-imposing the anodic scan when the cathodic scan had reached 1.0 V. No current peak was found and the current was comparable to that observed in the double layer region. When this film is finally removed, at about 0.9 V, the potential is already too cathodic for gold dissolution to occur. The reduction peak is shifted to more anodic potentials the higher the chloride

ion concentration. This may reflect a competition for adsorption sites between "adsorbed oxygen" and chloride ions.

A triangular sweep voltammetry curve taken in a solution 4×10^{-4} M in KBr is shown in Fig. 2. Generally, bromide ions are assumed to be more strongly adsorbed than chloride ions[10] and, again, no current due to hydrogen oxidation is observed. The reaction:

$$Au + 4\,Br^- \rightleftarrows AuBr_4^- + 3\,e$$

has a standard potential of 0.87 V ($vs.$ NHE)[12] and consequently a rise in current is seen on the anodic sweep at about 0.8 V. A current plateau follows and the limiting current is much closer to the expected theoretical limiting diffusion current. No passivation of gold is evident. Thermodynamically bromine evolution is possible in this system at about 1.0 V. Either of the small rises in current observed at 1.0 V and at 1.2 V may well be due to this. The ratio of the diffusion limited current for $AuBr^-$
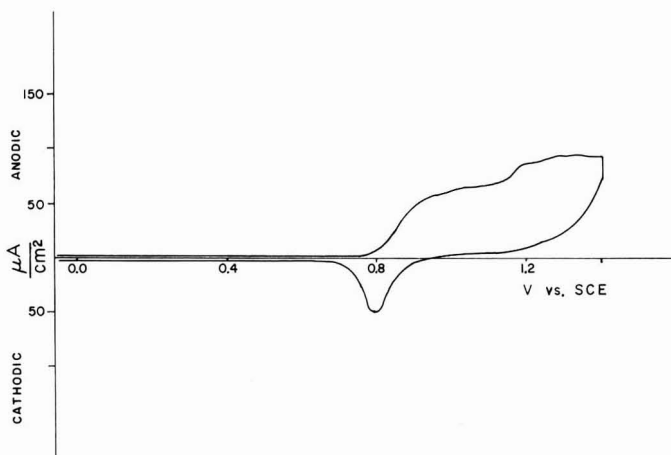
Fig. 2. Triangular sweep voltammetry curve, Au in 0.1 M $HClO_4 + 4 \times 10^{-4}$ M KBr, 2.4 V min^{-1}.

formation to that for Br_2 evolution is $\frac{3}{4}$. No further investigation was made into this aspect. On the cathodic scan a small peak is observed and indicates that some "adsorbed oxygen" still forms and is reduced at about 0.8 V.

The fact that gold can be passivated in solutions containing chloride ions was confirmed by keeping a test electrode in a solution 0.01 M in KCl and 0.1 M in $HClO_4$ for 13 h at 1.1 V. At the end of the experiment the solution was found to contain gold[21] and a uniform thin deposit of gold was obtained on the platinum gauze electrode. No gold was found in solution when an identical system was kept at 1.3 V, again for 13 h and no deposit was obtained on the platinum gauze electrode. Similar experiments in solutions containing KBr demonstrated the dissolution of the electrode at 1.1 V and at 1.3 V.

Steady-state current–potential curves gave results similar to those obtained from triangular sweep voltammetry. Each curve exhibited a peak at 1.1–1.2 V after which the current rapidly fell to low values (Fig. 3). Peak height depended somewhat on chloride ion concentration and stirring rate. The ascending portion of the peaks
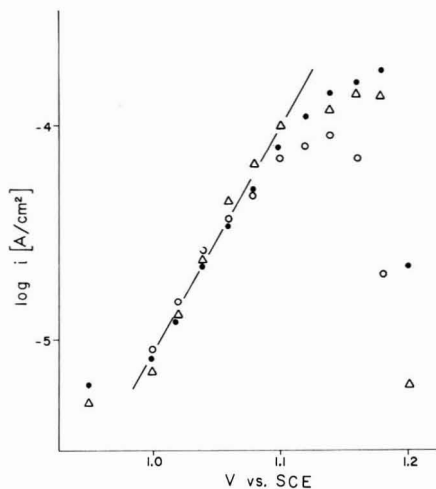
Fig. 3. Steady-state current–potential curves, Au in 0.1 M HClO$_4$ and (○) 4×10^{-4}, (●) 6×10^{-4}, (△) 8×10^{-4} M KCl.

was reasonably linear. Nevertheless, we do not believe the line drawn in Fig. 3 to represent a Tafel line in the usual sense. Rather the rise in current and subsequent decrease seems to be the result of a competition between an increase in current due to increased anodic overvoltage for reaction (1) and a decrease due to increased coverage with "adsorbed oxygen" and the ensuing blocking of the surface to reaction (1). Moreover, apparent exchange currents could not be obtained because the equilibrium potential of reaction (1) in the solutions used here is undetermined (no fixed concentration of AuCl$_4^-$ in solution).

The general shape of the steady-state current–potential curves (and the triangular sweep voltammetry curves) can be calculated from the postulate that reaction (1) does not occur on that portion of the surface covered with "adsorbed oxygen". Considering diffusion and charge transfer overvoltage only, the current for the anodic reaction is given by[22]:

$$i = i_0(1 - i/i_d) \exp(\alpha n F \eta / RT) \tag{2}$$

where the symbols have the usual meaning and i_d is the limiting diffusion current. The latter can be estimated for stirred solutions for reaction (1) using a diffusion coefficient $D = 2 \times 10^{-5}$ cm^2 s^{-1} and a Nernst diffusion layer thickness $\delta = 10^{-3}$ cm. Eqn. (2) can be rewritten:

$$\log[i i_d/(i_d - i)] = \text{const.} + \alpha n F E / 2.3 \, RT \tag{3}$$

The constant on the right can be obtained from the assumption that, *e.g.* at 1.02 V the current observed is given by eqn. (2). It is known from previous work[13,14,23] that the formation of "adsorbed oxygen" starts at about 1.0 V with a monolayer being completed at about 1.2 V, and the coverage, θ, being linear with potential in this potential range. The fraction of the electrode surface available for reaction (1) is then given by:

$$1 - \theta = -5E + 6, \quad 1.0 < E < 1.2 \tag{4}$$

The total current I flowing per apparent cm^2 of electrode area is given by:

$$I = i(1 - \theta) \tag{5}$$

where i is obtained from eqn. (3). Figure 4 shows a comparison between experimental data in 6×10^{-4} M KCl and a plot calculated with $i_d = 1 \times 10^{-3}$ A cm^{-2}, $n = 3$, $\alpha = 0.5$, and const. $= -30.4$ ($i = 1.3 \times 10^{-5}$ A cm^{-2} at 1.02 V). It is seen that the agreement is reasonably good. Since the treatment advanced here is only tentative, an attempt at further curve fitting did not seem justified.

As mentioned above, no gold was found in the electrolyte after the test electrode was kept at 1.3 V for 13 h in acidic, chloride ion containing solutions. This points to a passive film considerably more stable than that on other metals[2-9]. However, the
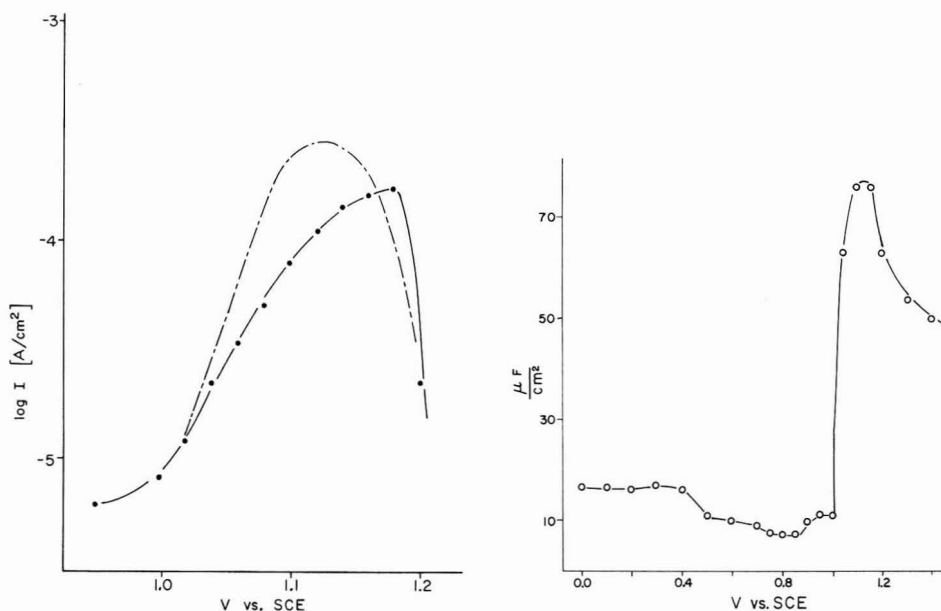
Fig. 4. Steady-state current–potential curve, Au in 0.1 M HClO$_4$ + 6×10^{-4} M KCl. (●—●) experimental, (—·—) calculated from eqn. (5).

Fig. 5. Capacity–potential curve, Au in 0.1 M HClO$_4$ + 1×10^{-3} M KCl.

time stability of the passive film on gold depends on potential and this becomes evident from a comparison of the cathodic sweep experiments (Fig. 1b) with steady-state runs taken in the cathodic direction (not shown). Very little current flows in the sweep experiments at potentials > 1.0 V, whereas the steady-state runs show a current peak almost identical to the one obtained when going in the anodic direction. Apparently, the film of "absorbed oxygen" which, once formed at potentials > 1.2 V, cannot be removed at potentials > 1.0 V (Fig. 1a), soon loses this irreversibility in the presence of chloride ions. To check this, the reverse scan of the sweep experiments was stopped at either 1.05, 1.10, or 1.15 V. In all cases about 10 min were required for the current to reach the value observed at that potential in the steady-state experiments, but this value was not exceeded even after 2 h. This may well reflect competition for

surface sites between chloride ions and "adsorbed oxygen", as indicated above, a steady state being established within a few minutes. At the short times required for a scan the "adsorbed oxygen" film stays intact and remains protective. At longer times, in the range 1.0–1.2 V, the passive film is partially, or wholly, replaced by adsorbed chloride ions and reaction (1) takes place. In solutions containing the more strongly adsorbed bromide ion the coverage with "adsorbed oxygen" is smaller (Fig. 2) and non-protective. Gold dissolution occurs in the potential range studied at potentials >0.8 V.

Figure 5 shows a typical capacity–potential curve obtained in solutions containing chloride ions. It shows the familiar shape expected from previous work[14] in the potential range 0.0–1.0 V. Sharp maxima are observed at 1.1 V. These are indicative of adsorption–desorption reactions such as the formation of "adsorbed oxygen", or the replacement of adsorbed chloride ions with "oxygen", as postulated above. However, we cannot exclude, in the presence of reaction (1), some pseudo-capacity which may have accentuated the peaks. Much smaller peaks are found in chloride ion free solutions[14]. In any case, whatever process causes the capacity maxima to appear, is completed at about 1.2 V and this coincides with the potential at which the electrode is covered with a protective, passivating film.

SUMMARY

The electrochemical behavior of gold was investigated in 0.1 M HClO$_4$ containing 2–100 × 10^{-4} M of KCl or KBr, using triangular sweep voltammetry, steady-state current potential measurements and single pulse differential capacity data. In chloride ion solutions, on the forward scan and ascending steady-state measurements gold dissolution occurs in the range 1.0–1.2 V $vs.$ SCE. A current maximum is found at 1.15 V, this position being independent of chloride ion concentration. Its height depends somewhat on chloride ion concentration and stirring rate, but is lower than the diffusion limited current expected for gold dissolution as AuCl$_4^-$. Gold becomes passive at approximately 1.2 V and no gold dissolution is observed up to 1.4 V. At 1.3 V in 0.01 M KCl, the passive film is stable for at least 13 h. Current–potential curves were calculated with the assumption that the coverage with "adsorbed oxygen" increases linearly from zero at 1.0 V to full at 1.2 V, and that gold dissolution is charge transfer controlled and occurs only at the "oxygen"-free part of the surface. The agreement with experimental data is satisfactory. On the reverse scan of the sweep experiments the gold stays passive; the "adsorbed oxygen" is removed at about 0.8–0.9 V, the potential being larger the larger the chloride ion concentration. The steady-state experiments give current–potential curves similar to those found for ascending potentials; a current peak is observed and gold dissolution takes place at 1.2–1.0 V. The difference between scanning and steady-state experiments is ascribed to competition for adsorption sites between chloride ion and "oxygen" and slow

replacement of "oxygen" by chloride ion. This view is supported by differential capacity measurements. In solutions containing bromide ions the dissolution of gold starts at 0.8 V and the electrode does not become passive up to 1.4 V.

REFERENCES

1 F. HABER AND F. GOLDSCHMIDT, Z. Elektrochem., 12 (1906) 49.
2 U. R. EVANS, J. Chem. Soc., (1927) 1020.
3 B. KABANOV, R. BURSTEIN AND A. N. FRUMKIN, Discussions Faraday Soc., 1 (1947) 259.
4 H. H. UHLIG, J. Electrochem. Soc., 97 (1950) 215C.
5 M. A. STREICHER, J. Electrochem. Soc., 103 (1956) 375.
6 G. M. SCHMID AND N. HACKERMAN, J. Electrochem. Soc., 108 (1961) 741.
7 V. HOSPADARUK AND J. V. PETROCELLI, J. Electrochem. Soc., 113 (1966) 878.
8 A. P. BOND AND E. A. LIZLOVS, J. Electrochem. Soc., 115 (1968) 1130.
9 I. A. AMAR AND S. DARWISH, Electrochim. Acta, 13 (1968) 781.
10 D. C. GRAHAME, M. A. POTH AND J. I. CUMMINGS, J. Am. Chem. Soc., 74 (1952) 4422.
11 K. G. WEIL AND D. MENZEL, Z. Elektrochem., 63 (1959) 669.
12 W. M. LATIMER, Oxidation Potentials, Prentice Hall, Englewood Cliffs, 2nd ed., 1952.
13 H. A. LAITINEN AND M. S. CHAO, J. Electrochem. Soc., 108 (1961) 726.
14 G. M. SCHMID AND R. N. O'BRIEN, J. Electrochem. Soc., 111 (1964) 832.
15 TH. HEUMANN AND H. S. PANESAR, Z. Phys. Chem., 229 (1966) 84.
16 J. S. RINEY, G. M. SCHMID AND N. HACKERMAN, Rev. Sci. Instr., 32 (1961) 588.
17 G. M. SCHMID, Electrochim. Acta, 12 (1967) 449.
18 G. M. SCHMID AND N. HACKERMAN, J. Electrochem. Soc., 110 (1963) 440.
19 H. DAHMS AND M. GREEN, J. Electrochem. Soc., 110 (1963) 466.
20 D. D. BODÉ, JR., T. N. ANDERSEN AND H. EYRING, J. Phys. Chem., 71 (1967) 792.
21 E. B. SANDELL, Colorimetric Determination of Traces of Metals, Chemical Analysis, Vol. 3, Inter-science, New York, 1944, p. 251.
22 K. J. VETTER, Electrochemical Kinetics, Academic Press, New York, 1967, p. 342.
23 R. A. BONEWITZ, J. Electrochem. Soc., 116 (1969) 78C.

INFLUENCE OF NON-SPECIFIC ADSORPTION OF REACTANTS ON THE ELECTRODE IMPEDANCE

B. TIMMER, M. SLUYTERS-REHBACH AND J. H. SLUYTERS

Laboratory for Analytical Chemistry, State University, Utrecht (The Netherlands)

(Received July 18th, 1969)

INTRODUCTION

The coupling of double layer charging and faradaic processes, introduced by Delahay[1], has proved to be an important concept in the study of electrode reactions. The basic equations, given by Delahay, have been used to derive new and more generally valid expressions for the electrode impedance, both for reversible[2,3] and quasi-reversible[4] electrode reactions. From these new expressions for the impedance, it could be deduced that large deviations from classical theory can result, particularly when strong adsorption of reactants at the interface is present. We have presented experimental data for the lead[2] and indium[5,6] electrode reactions with strong *specific* adsorption of the reactants. It was concluded that the new expressions derived for the electrode impedance are in accordance with experimental evidence.

One interesting problem, the importance of *non-specific* adsorption of reactants, remains to be settled. Delahay and coworkers[4,7,8] have argued on the basis of theoretical calculations that non-specific adsorption* can be so large that in some cases significant deviations from classical theory occur. However, experimentally no such departure could be detected for the zinc reaction in 0.1 M KCl[5] nor in 0.1 M NaClO$_4$[9], systems with alleged rather strong non-specific adsorption of Zn^{2+}. We[5] have questioned the original theoretical calculations of Delahay, as has Reinmuth[10]. Recently, Delahay returned to the problem and found from new calculations that for the zinc system in 0.1 M solution no departure can be expected[11].

In this paper, the theoretical double layer calculations are reconsidered. Some necessary conditions are presented for finding experimentally effects caused by non-specific adsorption. The theoretical predictions are tested on the Ba^{2+}/Ba(Hg) reaction in LiCl solutions.

LIST OF SYMBOLS

c_O, c_R	concentration at the electrode of Ox, resp. Red.
c_O^*	concentration of Ox in the bulk of the solution.
c_s	concentration of the supporting electrolyte
c_j	concentration of ion j.

---

* Non-specific adsorption is the adsorption of ions in the diffuse double layer purely by electrostatic interaction with the charge on the electrode.

C_d double layer capacitance.
C_{HF} high frequency capacitance, defined by eqn. (23).
C_{LF} low frequency capacitance, defined by eqn. (24).
D_O, D_R diffusion coefficient of Ox, resp. Red.
E electrode potential.
$E_{\frac{1}{2}}$ halfwave potential.
i_0 exchange current density of the electrode reaction.
j $\sqrt{-1}$, the imaginary unit.
k_{sh} standard heterogeneous rate constant of the electrode reaction.
n number of electrons, involved in the electrode reaction.
p $= \theta/\sigma\omega^{-\frac{1}{2}}$, the irreversibility quotient.
q charge density on the electrode.
u adsorption isotherm parameter, defined by eqn. (25).
u_2 quantity defined by eqn. (3).
Y electrode admittance.
Y', Y'' real and imaginary component of the electrode admittance.
z_j charge of ion j.
Γ_O, Γ_R surface excess of Ox, resp. Red.
θ charge transfer resistance.
σ $\sigma = \sigma_O + \sigma_R$, Warburg coefficient.
σ_O, σ_R Warburg coefficient of Ox, resp. Red, *cf.* eqn. (16).
φ_2 potential of the plane of closest approach.
ψ $= c_O\sqrt{D_O} + c_R\sqrt{D_R}$.
ω angular frequency of sine wave.

Calculation of double layer parameters

     A solution is considered, consisting of solvent plus an oxidized form of an electroactive couple, which is supposed to be a divalent cation. Ox, at a concentration c_O in a supporting electrolyte, consisting of a monovalent cation with concentration c_s and a monovalent anion with concentration $c_s + 2c_O$. The charge density on the electrode is denoted by q and the surface excess of Ox by Γ_O. The derivatives of q and Γ_O with respect to c_O and to the potential of the electrode, E, must be computed for the theoretical calculation of the impedance[4]. It is assumed that the reduced form of the electroactive couple, Red, is not adsorbed at the interface (as might be expected for an amalgam for example) and that therefore Red has no influence on the double layer parameters, although the point of zero charge might change and in this way affect the double layer parameters.

     In order to obtain the necessary partial derivatives, we will use the diffuse double layer theory. In the absence of specific adsorption the following expressions hold for mixed electrolytes[12]

$$q = -2B\left[\Sigma c_j(u_2^{z_j} - 1)\right]^{\frac{1}{2}} \tag{1}$$

where the sum is taken over the ionic species on the solution side of the interface with concentration c_j and charge z_j and

$$B = (RT\,\varepsilon/8\pi)^{\frac{1}{2}} \tag{2}$$

$$u_2 = \exp(-F\varphi_2/RT) \tag{3}$$

with ε the dielectric constant (assumed to be equal to that in the bulk of the solution, whence $B = 9.3 \times 10^{-5}$ C mol$^{-\frac{1}{2}}$ cm$^{-\frac{1}{2}}$) and φ_2 the potential in the plane of closest approach.

The surface excess of Ox is given by[12]

$$\Gamma_{\mathrm{O}} = -\frac{Bc_{\mathrm{O}}}{F} \int_{u_2}^{1} \frac{u^2 - 1}{u[\Sigma c_j(u^{z_j} - 1)]^{\frac{1}{2}}}\, du \tag{4}$$

While eqn. (4) is evaluated numerically by most authors, it can be integrated in closed form to yield[13]

$$\Gamma_{\mathrm{O}} = -\frac{Bc_{\mathrm{O}}^{\frac{1}{2}}}{F} \left[(1+b)^{\frac{1}{2}} - \{u_2(u_2+b)\}^{\frac{1}{2}} + (2-b) \ln\left\{ \frac{1+(1+b)^{\frac{1}{2}}}{(u_2)^{\frac{1}{2}}+(u_2+b)^{\frac{1}{2}}} \right\} \right] \tag{5}$$

where $b = 2 + (c_s/c_{\mathrm{O}})$.

From eqns. (1) and (5) the necessary partial derivatives can be calculated as follows[13]. First we have (note that c_s is always kept constant)

$$\left(\frac{\partial q}{\partial \varphi_2}\right)_{c_{\mathrm{O}}} = \frac{BF}{RT} (\Sigma z_j c_j u_2^{z_j}) [\Sigma c_j(u_2^{z_j}-1)]^{-\frac{1}{2}} \tag{6}$$

$$\left(\frac{\partial q}{\partial c_{\mathrm{O}}}\right)_{\varphi_2} = -B(u_2^2-1)[\Sigma c_j(u_2^{z_j}-1)]^{-\frac{1}{2}} \tag{7}$$

$$\left(\frac{\partial \Gamma_{\mathrm{O}}}{\partial \varphi_2}\right)_{c_{\mathrm{O}}} = -\left(\frac{Bc_{\mathrm{O}}^{\frac{1}{2}}u_2}{RT}\right) \cdot \frac{(u_2+1)}{\{u_2(u_2+b)\}^{\frac{1}{2}}} \tag{8}$$

$$\left(\frac{\partial \Gamma_{\mathrm{O}}}{\partial c_{\mathrm{O}}}\right)_{\varphi_2} = \frac{\Gamma_{\mathrm{O}}}{2c_{\mathrm{O}}} + \frac{Bc_s}{2Fc_{\mathrm{O}}^{\frac{3}{2}}} \left[\frac{1}{(1+b)^{\frac{1}{2}}} - \left(\frac{u_2}{u_2+b}\right)^{\frac{1}{2}} - 2\ln\left(\frac{1+(1+b)^{\frac{1}{2}}}{(u_2)^{\frac{1}{2}}+(u_2+b)^{\frac{1}{2}}}\right) + \right.$$
$$\left. + (2-b)\left\{ \frac{1}{1+b+(1+b)^{\frac{1}{2}}} - \frac{1}{u_2+b+\{u_2(u_2+b)\}^{\frac{1}{2}}} \right\} \right] \tag{9}$$

Of more practical interest are the derivatives, in which φ_2 is replaced by E. This can be performed with the following expressions

$$\left(\frac{\partial q}{\partial E}\right)_{c_{\mathrm{O}}} = \left(\frac{\partial q}{\partial \varphi_2}\right)_{c_{\mathrm{O}}} \times \left(\frac{\partial \varphi_2}{\partial E}\right)_{c_{\mathrm{O}}} \tag{10}$$

$$\left(\frac{\partial \Gamma_{\mathrm{O}}}{\partial E}\right)_{c_{\mathrm{O}}} = \left(\frac{\partial \Gamma_{\mathrm{O}}}{\partial \varphi_2}\right)_{c_{\mathrm{O}}} \times \left(\frac{\partial \varphi_2}{\partial E}\right)_{c_{\mathrm{O}}} \tag{11}$$

$$\left(\frac{\partial q}{\partial c_{\mathrm{O}}}\right)_{E} = \frac{RT}{c_{\mathrm{O}}} \left(\frac{\partial \Gamma_{\mathrm{O}}}{\partial E}\right)_{c_{\mathrm{O}}} \tag{12}$$

$$\left(\frac{\partial \Gamma_{\mathrm{O}}}{\partial c_{\mathrm{O}}}\right)_{E} = \left(\frac{\partial \Gamma_{\mathrm{O}}}{\partial c_{\mathrm{O}}}\right)_{\varphi_2} + \left(\frac{\partial \Gamma_{\mathrm{O}}}{\partial \varphi_2}\right)_{c_{\mathrm{O}}} \times \left(\frac{\partial \varphi_2}{\partial c_{\mathrm{O}}}\right)_{E} \tag{13}$$

where

$$\left(\frac{\partial \varphi_2}{\partial c_{\mathrm{O}}}\right)_{E} = \left[\left(\frac{\partial q}{\partial c_{\mathrm{O}}}\right)_{E} - \left(\frac{\partial q}{\partial c_{\mathrm{O}}}\right)_{\varphi_2}\right] / \left(\frac{\partial q}{\partial \varphi_2}\right)_{c_{\mathrm{O}}} \tag{14}$$

Eqn. (12) is a thermodynamic relation derived by cross-differentiation of the total derivative representation of the surface tension (cf. eqn. (11) of ref. 3).

The relevant partial derivatives can now be calculated if two experimental parameters are known. The best choice is to start with experimental q and $(\partial q/\partial E)c_O$ values, determined with Ox present in solution. The method of obtaining experimental q and $(\partial q/\partial E)_{c_O}$ values is elaborated in the experimental part.

From the q value, φ_2 can be calculated using eqn. (1). Then the partial derivatives of eqns. (6) to (9) can be calculated. The derivative $(\partial \varphi_2/\partial E)_{c_O}$ is calculated from eqn. (10), using the experimentally determined $(\partial q/\partial E)_{c_O}$ value. Next, the derivatives $(\partial \Gamma_O/\partial E)_{c_O}$, $(\partial q/\partial c_O)_E$ and $(\partial \Gamma_O/\partial c_O)_E$ can be calculated from eqns. (11) to (14) and then used in the impedance calculations.

Delahay and coworkers[4,7,8] assumed that φ_2 and $\mathrm{d}\varphi_2/\mathrm{d}E$ are the same in the presence and absence of Ox and they selected φ_2 and $\mathrm{d}\varphi_2/\mathrm{d}E$ from Russell's tables[14], based on Grahame's[15] measurements of double layer parameters in pure NaF solutions. As Reinmuth[10] and the authors[5] have pointed out this is incorrect and leads to too large derivatives, cf. Table 4 columns C and F. Note that the calculated q value $(-37.0~\mu\mathrm{C\,cm}^{-2})$ is too large (experimental value $-26.9~\mu\mathrm{C\,cm}^{-2}$). The calculated double layer capacity is somewhat too low (21.4 vs. 23.3 $\mu\mathrm{F\,cm}^{-2}$). Recently, Susbielles and Delahay[11] used lower φ_2 and $\mathrm{d}\varphi_2/\mathrm{d}E$ values than reported in Russell's tables and concluded that for the zinc system in 0.1 M solution no influence of non-specific adsorption can be expected. However, it is easily verified that with their new φ_2 and $\mathrm{d}\varphi_2/\mathrm{d}E$ values for the zinc system (-51.8 mV and 0.055), too low values for q and $(\partial q/\partial E)_{c_O}$ result, viz. for $c_O=c_R=1$ mM $q=-4.4~\mu\mathrm{C\,cm}^{-2}$ and $(\partial q/\partial E)_{c_O}=6.9$ $\mu\mathrm{F\,cm}^{-2}$ whereas experimentally $q=-10.6~\mu\mathrm{C\,cm}^{-2}$ and $(\partial q/\partial E)_{c_O}=16.0~\mu\mathrm{F\,cm}^{-2}$ were obtained. Therefore, the best procedure is to start with experimental q and $(\partial q/\partial E)_{c_O}$ values, as indicated above. Delahay[11] has made a similar remark recently.

Calculation of the faradaic impedance

Expressions for the electrode impedance, based on the Delahay concept, have been derived by Delahay and coworkers[4] for a quasi-reversible electrode system. The authors assumed adsorption both of the Ox and Red component. For our purposes, we need only consider adsorption of Ox. In that case the real and imaginary component of the electrode admittance $Y = Y' + jY''$, are (eqns. (22) and (23) of ref. 4 with $Y' = 1/R$ and $Y'' = \omega C$)

$$Y' = \frac{\lambda A_\eta (K\xi_r + H\xi_i)}{\xi_r^2 + \xi_i^2} \tag{15a}$$

$$Y'' = \lambda A_\eta \left[\frac{H\xi_r - K\xi_i}{\xi_r^2 + \xi_i^2} + h + l \right] \tag{15b}$$

where

$$\lambda A_\eta = \frac{n^2 F^2}{RT} c_O \left(\frac{\omega D_O}{2} \right)^{\frac{1}{2}} = \frac{1}{2\sigma_O \omega^{-\frac{1}{2}}} \tag{16}$$

$$\xi_r = M(1+Q) - aQ \tag{17}$$

$$\xi_i = M(a+1) + Q(M+a+2) \tag{18}$$

$$K = h(M+2Q) + (a+k)(Mh+Qh-MQ) \tag{19}$$

$$H = M(2Q-h) + Q(a+k)(M+h) \tag{20}$$

TABLE 1

DIMENSIONLESS PARAMETERS IN EQNS.(17) TO (20)

$$M = i_0 / [nFc_O(\omega D_O/2)^{\frac{1}{2}}] = (nF/RT)i_0 \times 2\sigma_O\omega^{-\frac{1}{2}}$$
$$Q = c_R(D_R)^{\frac{1}{2}}/c_O(D_O)^{\frac{1}{2}} = \sigma_O/\sigma_R$$
$$a = (2\omega/D_O)^{\frac{1}{2}}(\partial\Gamma_O/\partial c_O)_E$$
$$h = (2\omega/D_O)^{\frac{1}{2}}(RT/nFc_O)(\partial\Gamma_O/\partial E)c_O$$
$$k = (2\omega/D_O)^{\frac{1}{2}}(1/nF)(\partial q/\partial c_O)_E$$
$$l = (2\omega/D_O)^{\frac{1}{2}}(RT/n^2F^2c_O)(\partial q/\partial E)c_O$$

Where i_0 is the exchange current density of the electrode reaction, σ_O and σ_R the Warburg coefficients of resp. the Ox and Red component, ω the angular frequency of the sine wave, D_O and D_R the diffusion coefficients of Ox and Red and n the number of electrons involved in the electrode reaction.

The dimensionless parameters appearing in eqs. (17) to (20) are given in Table 1. Note that $h = k$, because of the thermodynamic argument eqn. (12).

The classical impedance equations[16] for no adsorption of reactants can be obtained from eqn. (15) by putting $a = h = k = 0$, as has already been shown by Delahay[4]. One gets

$$Y'_{classic} = \frac{1}{\sigma\omega^{-\frac{1}{2}}} \frac{p+1}{p^2+2p+2} \tag{21a}$$

$$Y''_{classic} = \frac{1}{\sigma\omega^{-\frac{1}{2}}} \frac{1}{p^2+2p+2} + \omega \frac{dq}{dE} \tag{21b}$$

where the Warburg coefficient $\sigma = \sigma_O + \sigma_R = \sigma_O(1+Q)/Q$, p the so-called irreversibility quotient and θ is the charge transfer resistance.

$$p \equiv \frac{\theta}{\sigma\omega^{-\frac{1}{2}}} = \frac{2}{M} \frac{Q}{1+Q} \tag{21c}$$

By introducing in eqn. (15) the experimental i_0 value together with partial derivative values, calculated as indicated in the previous section, it is possible to obtain theoretical admittance values in the case of non-specific adsorption of reactants. Comparison of the admittance values calculated in this way with the values calculated from the classical equations (21) can give information about the importance of non-specific adsorption of reactants.

Some other limiting cases of eqn. (15) are of interest. First, if reversibility of the electrode reaction is assumed, taking $i_0 \to \infty$ or $M \to \infty$ in eqn. (15), it can be verified by some rewriting that the reversible equations result, $e.g.$ eqns. (1) and (2) of ref. 3. In a surveyable form they read[2], with $\Gamma_R = 0$,

$$Y'_{rev} = \frac{1}{2\sigma\omega^{-\frac{1}{2}}} + \omega(C_{LF} - C_{HF}) \frac{u}{u^2+2u+2} \tag{22a}$$

$$Y''_{rev} = \frac{1}{2\sigma\omega^{-\frac{1}{2}}} + \omega(C_{LF} - C_{HF}) \frac{2+u}{u^2+2u+2} + \omega C_{HF} \tag{22b}$$

where

$$C_{HF} = \left(\frac{\partial q}{\partial E}\right)_{\Gamma_O} \tag{23}$$

$$C_{LF} = \left(\frac{\partial q}{\partial E}\right)_\psi + nF\frac{\sigma_O}{\sigma}\left(\frac{\partial \Gamma_O}{\partial E}\right)_\psi \tag{24}$$

$$u = \left(\frac{\partial \Gamma_O}{\partial \psi}\right)_E (2\omega)^{\frac{1}{2}} = \frac{a}{1+Q} \tag{25}$$

with

$$\psi = c_O(D_O)^{\frac{1}{2}} + c_R(D_R)^{\frac{1}{2}} = c_O(D_O)^{\frac{1}{2}}(1+Q)$$

If complete irreversibility is assumed, $i_0 \to 0$ or $M \to 0$, it follows from eqn. (15)

$$Y'_{irrev} = \omega(C_{LF} - C_{HF})\frac{u}{u^2 + 2u + 2} \tag{26a}$$

$$Y''_{irrev} = \omega(C_{LF} - C_{HF})\frac{2+u}{u^2 + 2u + 2} + \omega C_{HF} \tag{26b}$$

where, in this case, $u = a$, C_{HF} is given by eqn. (23) and $C_{LF} = (\partial q/\partial E)_{c_O}$. Eqns. (26) are identical to the expressions for the electrode impedance in the case of adsorption of electro-inactive species[16,17], as it should be.

Finally, for relatively small i_0 values, we have for reasonable values of a and $k = h$ (cf. Table 4) $M \ll a$; $M \ll Q$ when $Q \sim 1$ and $k = h \ll a$. In that case eqns. (17) to (20) reduce to

$$\xi_r = -Qa \tag{17a}$$
$$\xi_i = Q(a+2) \tag{18a}$$
$$K = Q(2k + ak - aM) \tag{19a}$$
$$H = Q(2M + aM + ak) \tag{20a}$$

If eqns. (17a) to (20a) are introduced in eqn. (15), the following equations are obtained

$$Y' = \lambda A_\eta M = \frac{1}{\sigma\omega^{-\frac{1}{2}}}\frac{1}{p} \tag{27a}$$

$$Y'' = \lambda A_\eta l = \omega\left(\frac{\partial q}{\partial E}\right)_{c_O} \tag{27b}$$

When in eqn. (21a) $p \gg 1$ (or i_0 small, cf. eqn. (21c)) is assumed, it can be seen that the resulting equation is equal to eqn. (27a). So, for relatively small i_0 values no effects in Y', caused by adsorption of reactants can be found. Also no abnormalities in Y'' can be found, cf. eqn. (27b) or eqn. (21b) with $p \gg 1$, so that it may be concluded that from impedance measurements no indication of non-specific adsorption of reactants can be expected when the electrode reaction is rather irreversible. Note also that when $i_0 \to 0$ holds, no effects can be found, as follows from eqn. (26) with

$$C_{LF} - C_{HF} = \left(\frac{\partial q}{\partial E}\right)_{c_O} - \left(\frac{\partial q}{\partial E}\right)_{\Gamma_O} = \left(\frac{\partial q}{\partial c_O}\right)_E \left(\frac{\partial \Gamma_O}{\partial E}\right)_{c_O} \Big/ \left(\frac{\partial \Gamma_O}{\partial c_O}\right)_E \tag{28}$$

When reasonable values are introduced in eqn. (28), cf. Table 4, it is easily verified that $C_{LF} - C_{HF}$ is small, e.g. $< 0.6\ \mu F\ cm^{-2}$, so that practically $Y'_{irrev} = 0$ and $Y''_{irrev} = \omega C_{LF}$, except when impedances can be measured accurately in a very large frequency

region. Only when the electrode reaction is rather reversible, $e.g.$ $i_0 > 4 \times 10^{-2}$ A cm^{-2} effects of non-specific adsorption can be expected in the a.c. peak potential region, as can be seen from eqn. (22) where $C_{LF} - C_{HF}$ can be as large as 60 μF cm^{-2} for 1 mM solution of Ox in 0.1 M supporting electrolyte, $cf.$ Table 4. The potential dependence of the non-specific adsorption effects is the same as for the specific adsorption case[2,5,6]. Outside of the a.c. peak, no or only very small effects can be expected in the case of non-specific adsorption, $cf.$ eqns. (26) and (28).

In order to verify the foregoing, an electrode system should be studied with the following characteristics.

1. The electrode reaction at a mercury electrode should proceed as reversibly as possible with no kinetic complications; $i.e.$ diffusion and charge transfer should be rate determining.

2. The Ox species must be a divalent (or trivalent) cation that does not form any appreciable amount of complexes with the anions of the supporting electrolyte with a corresponding decrease of the effective charge. The Red species should preferably form an amalgam.

3. The reactants are not specifically adsorbed at the interface, otherwise it will be unlikely that the existence of non-specific adsorption can be verified.

4. The standard potential of the system must be as negative as possible. At these potentials $-\varphi_2$ is large and cations are strongly attracted in the double layer. In the same potential region the supporting electrolyte reduction should not interfere.

5. The electrode reaction should be studied in supporting 1–1 electrolytes of low concentrations, because then $-\varphi_2$ is larger. Moreover, the ratio c_O/c_s can be chosen larger, providing a favourable condition for strong adsorption of c_O.

We thought that the Ba^{2+}/Ba(Hg) reaction in LiCl solutions was a suitable system for testing the importance of non-specific adsorption of reactants. From literature it is known that the half-wave[18] potential is at -1.94 V $vs.$ SCE. The Ba^{2+} wave is d.c. reversible and Li$^+$ ions are reduced at more negative potentials. Barium does not form complexes with Cl$^-$ ions[19]. A complication, however, is the occurrence of maxima[18,20], perhaps unavoidable when the reactants are adsorbed at the interface[25,26].

EXPERIMENTAL

Cell impedances were measured in the usual way, using a cell with a dropping mercury electrode (DME) and a mercury pool electrode connected to the leads of the a.c. bridge described earlier[21]. The potential of the DME was measured against a SCE with a Keithley d.c. voltmeter model 660 A. The cell was kept at 25° C. Solutions were prepared from p.a. LiCl and BaCl$_2 \cdot 2$H$_2$O. The cell solution was de-aerated with tank nitrogen.

In order to minimize the spurious frequency dispersion[9] of the impedance of the DME, a drawn-out capillary was used with a tip diameter of ca 0.5 mm. The drop-time was not controlled externally. The bridge was balanced at a certain time after dropfall (usually 3 s), which was controlled electronically. Measurements were usually performed at frequencies between 480 and 2000 Hz. In that frequency region the series resistance of the cell varies $e.g.$ from 400 Ω at 480 Hz to 390 Ω at 2000 Hz, due to the

spurious frequency dispersion; the series capacitance varies from 0.210 μF to 0.208 μF in the same frequency region.

RESULTS

Barium in 1 M LiCl

In Fig. 1 the d.c. polarogram is presented of a 0.5 mM Ba^{2+} solution in 1 M LiCl. As can be seen, a small maximum is present, which increases with Ba^{2+} concentration[18,20]. Moreover, the lithium and barium wave are reasonably well separated, although at some intermediate potentials there will be some overlap of the two a.c. waves.
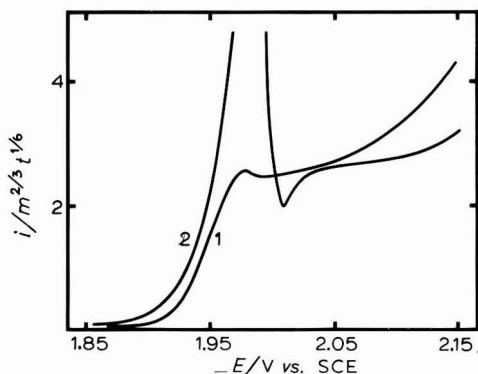
Fig. 1. D.c. polarograms for 0.5 mM Ba^{2+} in 1 M LiCl(1) and 0.1 M LiCl(2). Currents are given at maximum drop life, normalized for $m^{\frac{2}{3}}$ $t^{\frac{1}{6}}$.

Impedances were measured and analysed for 1 M LiCl solutions with 0, 0.5 and 1.3 mM Ba^{2+}. Up to -1.85 V a simple double layer capacitance, C_d, in series with the ohmic resistance of the cell is obtained. Then the barium wave starts; it appeared that the frequency dependence of the impedances at these potentials were in agreement with the classical equations (21). Therefore the double layer capacity was calculated with[2,16]

$$\omega C_d = Y'' - Y'/(p+1) \tag{29}$$

The C_d curves (Table 2) do not change with Ba^{2+} concentration, indicating that no barium adsorption is detectable.

From the experimental charge transfer resistance values obtained from the impedance analysis, the standard heterogeneous rate constant of the electrode reaction, k_{sh}, can be computed. For the barium couple in 1 M LiCl $k_{sh} = (9 \pm 1) \times 10^{-3}$ cm s^{-1} holds. Further $D_O = (9.5 \pm 0.5) \times 10^{-6}$ cm^{2}s^{-1} was calculated and the half wave potential, $E_{\frac{1}{2}}$, is at approx. -1.95 V. From -2.0 V to more negative potentials a gradual transition from the barium to the lithium a.c. wave is found, as can be concluded from the σ values. Note that also at these potentials the double layer capacity can be calculated as usual[2], because[22] both reactions are diffusion controlled in this potential range.

TABLE 2

DOUBLE LAYER CAPACITY VALUES FOR Ba^{2+} SOLUTIONS IN 1 M LiCl

Electrode potential/V	$C_d / \mu F\ cm^{-2}$ 0 mM Ba^{2+}	0.5 mM Ba^{2+}	1.3 mM Ba^{2+}
−0.5	39.1	38.4	40.0
−0.7	22.1	22.0	22.7
−0.9	16.4	16.3	16.6
−1.1	15.3	15.5	15.6
−1.3	16.0	16.0	15.8
−1.5	17.0	17.0	17.1
−1.7	18.9	18.6	19.0
−1.8	20.2	20.0	20.1
−1.9	21.4	21.1	21.7
−1.93	21.7	21.6 ± 0.3	22.4 ± 0.5
−1.96	22.1	22.3 ± 0.3	22.5 ± 1
−2.0	22.4 ± 0.2	22.3 ± 0.2	22.7 ± 0.5
−2.05	22.4 ± 0.3	22.3 ± 0.3	22.7 ± 0.4

TABLE 3

DOUBLE LAYER CAPACITY VALUES FOR Ba^{2+} SOLUTIONS IN 0.1 M LiCl

Electrode potential/V	$C_d / \mu F\ cm^{-2}$ 0 mM Ba^{2+}	0.5 mM Ba^{2+}	1 mM Ba^{2+}	1.5 mM Ba^{2+}
−0.5	25.4	25.6	25.6	25.7
−0.7	18.5	18.6	18.6	18.7
−0.9	16.0	16.1	16.2	16.2
−1.0	15.4	15.5	15.5	15.6
−1.1	15.2	15.3	15.4	15.5
−1.2	15.1	15.3	15.5	15.6
−1.3	15.5	15.7	15.8	16.0
−1.4	15.9	16.2	16.5	16.5
−1.5	16.6	17.0	17.2	17.3
−1.6	17.3	17.9	18.2	18.2
−1.7	18.1	18.8	19.2	19.3
−1.8	19.2	20.1	20.5	20.7
−1.9	20.4	21.0 ± 0.4	22.6 ± 0.2	22.6 ± 0.2
−1.93	20.6	22.2 ± 0.3	22.9 ± 0.4	23 ± 1
−1.96	20.8	22.0 ± 0.5	23.5 ± 1	
−2.0	22.1	21.9 ± 0.5	23 ± 1.5	22 ± 2
−2.05	22.6	22.9 ± 0.3	23.5 ± 0.2	23.7 ± 0.2

Barium in 0.1 *M LiCl*

Figure 1 shows that a large maximum appears in the barium wave in 0.1 M LiCl. It was rather difficult to measure impedances at the maximum and moreover, it must be expected that the normal expressions for the electrode impedance are not valid at these potentials. This was found by evaluating the measured impedances; the computed values for the Warburg impedance were too low, although it was still possible to calculate C_d.

Up to -1.85 V the C_d values were measured directly, as was the case in $1\ M$ LiCl. The C_d curves (Table 3) increase with Ba^{2+} concentration from -1.1 V, indicating that the double layer has changed when Ba^{2+} is present in solution.

Analysis of the electrode impedance at the potentials of the barium wave showed no effect of adsorption other than the change in C_d. The frequency dependence of the impedance was in agreement with the classical equations (21) within experimental error $(\sim 3\%)$, except for potentials in the vicinity of -2.02 V. From the charge transfer resistance values, $k_{sh} = (1.6 \pm 0.3) \times 10^{-2}\ \mathrm{cm\ s^{-1}}$ was calculated for the barium couple in $0.1\ M$ LiCl solution. D_O and $E_{\frac{1}{2}}$ were found to be the same as in $1\ M$ LiCl. No interference of the lithium wave was present, only at very negative potentials $(E < -2.05$ V) does the lithium a.c. wave become significant.

It is possible to obtain the cathodic transfer coefficient β from the two values of k_{sh} in $1\ M$ and $0.1\ M$ LiCl by applying the Frumkin correction[23]

$$k_{sh} = k_{sh}^{true} \times u_2^{z - \beta n}$$

where k_{sh}^{true} is the rate constant corrected for double layer effects and u_2 is as given by eqn. (3). When $z = n = 2$ is introduced together with u_2 values of Table 4 (vide infra), $\beta = 0.83$ is obtained. This value is in agreement with the potential dependence of the charge transfer resistance, calculated from a.c. measurements.

Finally, some experiments have been performed for $1\ mM\ Ba^{2+}$ in $0.1\ M$ tetraethylammonium iodide, because it is known that alkylammonium ions are reduced at very negative potentials, so that no interference with the barium wave occurs[20]. Also the annoying maximum has almost disappeared for $1\ mM\ Ba^{2+}$. From the analysis of the measured impedances it appeared that the classical impedance expressions (21) are obeyed. It was found $k_{sh} \approx 10^{-2}\ \mathrm{cm\ s^{-1}}$, the resulting double layer capacity
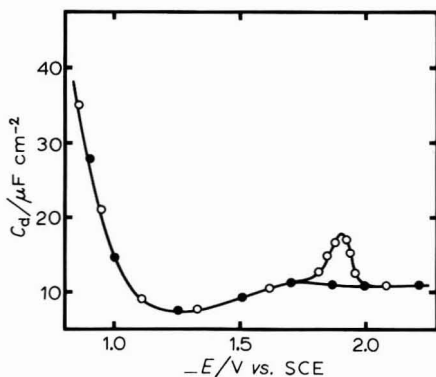
Fig. 2. Double layer capacity curves for $0.1\ M$ ethylammonium iodide with 0, ($\bullet$) and $0.5\ mM\ Ba^{2+}$, ($\bigcirc$).

curves are shown in Fig. 2. In the peak potential region an increase of C_d is found when Ba^{2+} is present in solution, just as would be expected when Ba^{2+} is adsorbed at the interface.

THEORETICAL VERIFICATION OF THE EFFECT OF NON-SPECIFIC ADSORPTION OF BARIUM FROM LiCl SOLUTIONS

In this section the partial derivatives relevant in the calculations of the impe-

dance given by eqn. (15), are computed as outlined in the theoretical part, starting from experimental q and $(\partial q/\partial E)c_O$ values. Comparison of the theoretically calculated impedances with experimental values provides a verification of the theory.

No attempt is made here to calculate theoretically what can be expected for the tetraethylammonium iodide case, because the double layer calculations require a detailed knowledge of the specific adsorption of the supporting electrolyte. Moreover, ion pair formation may complicate matters considerably[24].

Barium in 1 M LiCl

Integration of the C_d curves of Table 2 from the point of zero charge (-0.52 V, obtained from droptime–potential curves) to -1.95 V yields $q = -27.4$ μC cm^{-2} at -1.95 V. From eqn. (1) it follows that $u_2 = 23.4$ when $c_O = 0.5$ mM*. Eqn. (1) may be used directly here, because at -1.95 V there is no specific adsorption of Cl$^-$. The resulting partial derivatives, starting from u_2 and C_d, are shown in Table 4, column A. It can be seen that only a small amount of Ba^{2+} is adsorbed, equivalent to 0.24 μC cm^{-2}, and the partial derivatives are relatively small, as can be expected in 1 M solutions. The low $(\partial q/\partial c_O)_E$ value, -0.013 cm C mol^{-1}, requires special attention. Assuming a linear dependence of q on c_O, (not exactly true, cf. Fig. 3), it would mean a change of -0.007 μC cm^{-2}, when 0.5 mM Ba^{2+} is added to the solution, whereas 0.24 μC cm^{-2} is absorbed. Thus, the net effect of adding Ba^{2+} is the replacement of Li^{1+} in the diffuse double layer with Ba^{2+}, whereas q remains practically constant. A similar argument holds for 0.1 M solution, cf. Table 4.

If the partial derivatives are introduced into eqn. (15), it appears that no difference with the classical equations (21) results for frequencies between 150 Hz and 10 kHz (differences $< 0.5\%$). So, theoretically for 1 M solutions no adsorption of barium, neither specific nor non-specific can be detected in the impedance, in agreement with experimental results. As no specific adsorption of barium is present in 1 M LiCl, it is reasonable to assume that there is also no specific adsorption of barium in 0.1 M LiCl, so that any adsorption effects can be attributed to non-specific adsorption.

Barium in 0.1 M LiCl

The point of zero charge obtained from droptime–potential curves, -0.47 V, was found to be independent of Ba^{2+} concentration. Before it is possible to calculate q by integration of C_d curves, it must be ascertained that C_d is indeed $(\partial q/\partial E)_{c_O}$. Up to -1.85 V this is the case, cf. eqn. (26) with (28) where u and $C_{LF} - C_{HF}$ are small, so that practically $Y' = 0$ and $Y'' = \omega C_{LF} = \omega(\partial q/\partial E)_{c_O}$. At the potentials of the a.c. wave we can assume for the time being that eqns. (17) to (20) are obeyed, so that eqn. (27) holds. Then the measured C_d, eqn. (29), is indeed $(\partial q/\partial E)_{c_O}$ over the whole potential range.

As was the case for 1 M LiCl solutions, we have at $E_{\frac{1}{2}} = -1.95$ V that the surface concentrations of Ox and Red, c_O and c_R are the same and equal to half the bulk concentration of Ox, c_O^*. For the calculation we need q as a function of c_O at -1.95 V. In order to obtain q, e.g. for $c_O = 0.5$ mM, a $(\partial q/\partial E)_{c_O = 0.5\ mM}$ curve should be integrated. Up to -1.85 V this can be done simply by integrating the C_d curve for 0.5 mM Ba^{2+}. From -1.85 V on, the barium wave starts rendering $c_O < c_O^*$. The best

---

* At the halfwave potential, -1.95 V, we have $c_O = c_R = \frac{1}{2}c_O^*$ where c_O and c_R are surface concentrations and c_O^* is the bulk concentration. $c_O = 0.5$ mM corresponds therefore with a 1 mM Ba^{2+} solution.

TABLE 4

DOUBLE LAYER PARAMETERS

Solution	A $1\,mM\,Ba^{2+}$ $+1\,M\,LiCl$	B $1\,mM\,Ba^{2+}$ $+0.1\,M\,LiCl$	C $1\,mM\,Ba^{2+}$ $+0.1\,M\,LiCl$	D $0.5\,mM\,Ba^{2+}$ $+0.1\,M\,LiCl$	E $1.5\,mM\,Ba^{2+}$ $+0.1\,M\,LiCl$	F $1\,mM\,Ba^{2+}$ $+0.1\,M\,LiCl$
$q/\mu C\ cm^{-2}$	-27.4	-26.5	-26.5	-26.3	-26.7	-37.0
$C_d/\mu F\ cm^{-2}$	22.0	23.3	23.3	22.0	23.4	21.4
$(\partial q/\partial E)_{co}/\mu F\ cm^{-2}$	22.0	23.3	24.2	22.7	24.7	21.4
u_2	23.4	126	126	147	113	199
$(\partial\varphi_2/\partial E)_{co}$	3.73×10^{-2}	3.20×10^{-2}	3.34×10^{-2}	3.45×10^{-2}	3.20×10^{-2}	1.96×10^{-2}
$(\partial q/\partial c_o|_E)/cm\,C\,mole^{-1}$	-0.013	-0.333	-0.347	-0.493	-0.266	-0.366
$(\partial\Gamma_o/\partial c_o|_E)/cm$	2.46×10^{-6}	4.00×10^{-5}	4.01×10^{-5}	6.63×10^{-5}	2.84×10^{-5}	5.83×10^{-5}
$(\partial\Gamma_o/\partial E)_{co}/mol\,V^{-1}\,cm^{-2}$	-2.60×10^{-12}	-6.73×10^{-11}	-7.02×10^{-11}	-4.98×10^{-11}	-8.04×10^{-11}	-7.38×10^{-11}
C_{LF}, eqn.(24)/$\mu F\ cm^{-2}$	26.1	85.7	86.2	75.5	89.3	117
$2F\Gamma_o/\mu C\ cm^{-2}$	0.24	7.7	7.7	5.0	9.4	14.1

All calculations are for $E_{\frac{1}{2}}=-1.95\,V$, where the surface concentrations of Ox and Red are the same and equal to half the bulk concentration of Ox. Column F has been calculated according to Delahay[4,7,8], hence u_2 and $(\partial\varphi_2/\partial E)_{co}$ were taken from the supporting electrolyte; the other parameters are calculated, starting from these two values.

procedure would be to integrate at each potential a C_d value for such a bulk concentration that $c_0 = 0.5$ mM. However, this is a laborious procedure and as a good approximation the C_d curve for 0.5 mM Ba^{2+} in the bulk can be integrated also over the a.c. peak potential range, because the increase of C_d (Table 3) is rather small. The error introduced this way is smaller than 0.05 μC cm^{-2} which is much less than the errors introduced by the inaccuracy of the C_d over the whole potential range, e.g. 0.1 μF cm^{-2} error in C_d represents an error of 0.14 μC cm^{-2} in q at -1.95 V.

When the C_d curve for 0.5 mM Ba^{2+} (Table 3) is integrated from -0.47 to -1.95 V, $q = -26.5$ μC cm^{-2} is obtained. With this q value we calculate from eqn. (1), with $c_0 = 0.5$ mM, $u_2 = 126$. The resulting partial derivatives are given in Table 4, column B. Rather large values result, because the barium adsorption is strong (7.7 μC cm^{-2}). Introduction of the partial derivatives in eqn. (15) shows that Y' equals the classical $Y'_{classic}$ of eqn. (21a) within 1% in the measured frequency range, whereas the calculated $C_d = 22.4 \pm 0.3$ μF cm^{-2} has some frequency dependence, but within experimental error. However, it appears that eqn. (27b) is not fulfilled exactly, as a small (0.9 μF cm^{-2}) difference exists between $(\partial q/\partial E)_{c_0}$ and the C_d, calculated from experiment with eqn. (29). Therefore in column C of Table 4, a new set of parameters is given with $(\partial q/\partial E)_{c_0} = C_d + 0.9 = 24.2$ μF cm^{-2}.

TABLE 5

THEORETICAL Y' AND Y'' VALUES FOR 1 mM Ba^{2+} IN 0.1 M LiCl

$\sqrt{\omega}/s^{-\frac{1}{2}}$	$Y'/\Omega^{-1}cm^{-2}$	$Y''/\Omega^{-1}cm^{-2}$	$C_d/\mu F\,cm^{-2}$	$Y'_{classic}/\Omega^{-1}cm^{-2}$	$Y''_{classic}/\Omega^{-1}cm^{-2}$	$C_d/\mu F\,cm^{-2}$
30	0.0950	0.0390	22.3	0.0928	0.0394	23.3
50	0.104	0.0707	22.9	0.103	0.0716	23.3
70	0.108	0.124	23.3	0.108	0.124	23.3
90	0.110	0.198	23.5	0.110	0.197	23.3
110	0.111	0.292	23.6	0.112	0.289	23.3

Y' and Y'' are calculated from eqn. (15) with the values of column C of Table 4 and $k_{sh} = 1.6 \times 10^{-2}$ cm s^{-1}, $D_O = D_R = 9.3 \times 10^{-6}$ cm^2 s^{-1} and $c_0 = c_R = 0.5$ mM. The classical $Y'_{classic}$ and $Y''_{classic}$ are calculated from eqn. (21) with $\partial q/\partial E = 23.3$ μF cm^{-2}. The C_d values are computed from Y' and Y'' with eqn. (29).

The values of q and u_2 should have been changed also somewhat, but this would have given only a small correction. Substitution of the parameters of column C in eqn. (15) yields theoretical values for Y' and Y'' (Table 5), which can be compared with the classical results, eqn. (21). It can be concluded from Table 5 that in the measured frequency range no significant differences can be found between the classical admittance values and values calculated with the new expressions (15) accounting for adsorption effects. So, although Ba^{2+} is rather strongly adsorbed at the interface, no effects can be detected experimentally in the measured frequency range, because of the quasi-irreversibility of the electrode reaction. If the reaction had been reversible, large effects could have been measured, e.g. $C_{LF} - C_{HF} = 62$ μF cm^{-2}, see also discussion.

In Table 4 are presented also sets of parameters for 0.5 and 1.5 mM Ba^{2+} in 0.1 M LiCl. As can be seen from $(\partial \Gamma_0/\partial c_0)_E$ or $nF\Gamma_0$ no linear adsorption isotherm holds. It appeared that a Langmuir isotherm is obeyed for surface concentrations of

Ba^{2+} between 0.25 and 1.5 mM, $viz.$,

$$2F\Gamma_{Ba^{2+}} = \frac{17.4}{1+0.63/c_{Ba^{2+}}(mM)} \ \mu C \ cm^{-2}$$

Again theoretical electrode admittances have been calculated from eqn. (15) and they can be compared with classical values, as has been described for 1 mM Ba^{2+}. Similar results to those in Table 5 are found, showing that also for 0.5 and 1.5 mM Ba^{2+} no adsorption effects can be detected from the electrode admittance.

Finally, the only proof of significant non-specific adsorption of Ba^{2+} can be found in the increase in the double layer capacity, also at the potentials of the a.c.

TABLE 6

EXPERIMENTAL AND THEORETICAL VALUES OF THE CHARGE ON THE ELECTRODE FOR 0.1 M LiCl SOLUTIONS IN THE PRESENCE OF Ba^{2+}

Electrode potential	-0.9 V				-1.1 V			
$c_{Ba^{2+}}/mM$	$-q_{obs}$	$-\Delta q_{obs}$	$-\Delta q_{calc}$	$nF\Gamma_{Ba^{2+}}$	$-q_{obs}$	$-\Delta q_{obs}$	$-\Delta q_{calc}$	$nF\Gamma_{Ba^{2+}}$
0	8.47				11.57			
0.5	8.53	0.06	0.04	0.6	11.65	0.08	0.06	1.3
1.0	8.54	0.07	0.07	1.1	11.67	0.10	0.10	2.1
1.5	8.55	0.08	0.10	1.5	11.70	0.13	0.14	2.8
	±0.05	±0.07			$\pm$ 0.07	±0.10		

Electrode potential	-1.5 V				-1.8 V			
$c_{Ba^{2+}}/mM$	$-q_{obs}$	$-\Delta q_{obs}$	$-\Delta q_{calc}$	$nF\Gamma_{Ba^{2+}}$	$-q_{obs}$	$-\Delta q_{obs}$	$-\Delta q_{calc}$	$nF\Gamma_{Ba^{2+}}$
0	17.81				23.14			
0.5	17.99	0.18	0.13	3.5	23.51	0.37	0.22	6.1
1.0	18.08	0.27	0.21	5.2	23.70	0.56	0.32	8.5
1.5	18.15	0.34	0.26	6.3	23.80	0.66	0.39	10.1
	$\pm$ 0.10	±0.14			$\pm$ 0.13	±0.19		
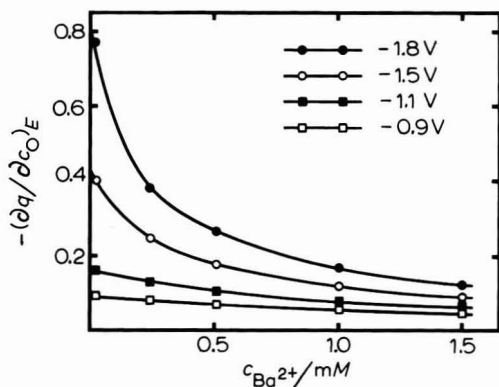
Fig. 3. Values of $(\partial q/\partial c_O)_E$ versus $c_{Ba^{2+}}$ solutions in 0.1 M LiCl at some electrode potentials.

wave of barium, (Table 3). In the following way the increase of C_d can be compared with results obtained from double layer theory. Integration of the C_d curves for the different Ba^{2+} concentrations yields experimental q values as a function of potential (Table 6). From q we calculate u_2 with eqn. (1) and then, following the procedure outlined in the theoretical part, we obtain $(\partial q/\partial c_O)_E$ as a function of potential and Ba^{2+} concentration. In Fig. 3 the results are given for some relevant potentials.

If a curve of Fig. 3 at constant potential is integrated from 0 to some Ba^{2+} concentration c_O, the change in electrode-charge, Δq_{calc}, is found when Ba^{2+} is added to the solution up to a concentration c_O. It appears that a good agreement exists with the experimental Δq_{obs} values (Table 6), except for -1.8 V where the differences are somewhat larger. Considering the uncertainties of the basic double layer equations (1) and (4), *cf.* discussion, especially at -1.8 V with large amounts of adsorbed Ba^{2+}, we can conclude that the increase of C_d values of Table 3 can be explained by assuming Ba^{2+} adsorption in the diffuse double layer according to eqn. (4) or (5).

DISCUSSION

The theoretical double layer calculations are based on the Joshi-Parsons[12] equations (1) and (4). However, these authors found only a poor agreement for their experimental data for aqueous solutions of HCl with $BaCl_2$. Recently, Parsons[27] has discovered a mistake in the analysis of his data. If this mistake is corrected, the experimental data given in ref. 12, agree with Gouy-Chapman theory within experimental error. Thus, it appears that eqns. (1) and (4) are useful expressions for evaluating the double layer parameters for mixed electrolytes. A difficulty with the theory is the fact that ions are considered to be point charges. At large φ_2 values the surface excess values are high and the assumption of point charges becomes doubtful.

Tessari *et al.*[9] have published experimental data on Zn^{2+} in 0.1 M $NaClO_4$. They arrived at the conclusion that no departure from classical behaviour could be detected. We recalculated their results for one case (column D of Table 5 of ref. 9) according to our procedures[16,21]. We also found no departure from the classical equations, but we obtained slightly different and more consistent results, namely $k_{sh} = (4.7 \pm 0.2) \times 10^{-2}$ cm s^{-1} and $\sigma = 27.5 \pm 2 \, \Omega$ cm^2 s$^{-\frac{1}{2}}$ instead of $k_{sh} = (4.4 \pm 0.2) \times 10^{-2}$ cm s^{-1} and $\sigma = 31 \, \Omega$ cm^2 s$^{-\frac{1}{2}}$, as calculated by Tessari. The most important result is that the calculated C_d is independent of frequency and equal to C_d for the supporting electrolyte, showing that also in C_d no adsorption effects can be detected. When the double layer partial derivatives are calculated as indicated and introduced in eqn. (15), it is found that no departure from the classical equations (21) exists, as was found experimentally for the zinc system in 0.1 M $NaClO_4$[9]. The same holds for the zinc system in 0.1 M KCl[5].

Both for the barium couple and zinc couple in 0.1 M supporting electrolyte solution the adsorption of Ox is sufficiently large to give significant departures from classical behaviour, however, only when the electrode reaction is sufficiently reversible. The k_{sh} values for the zinc couple in 0.1 M $NaClO_4$ or 0.1 M KCl (*ca.* 0.05 cm s^{-1}) and for the barium couple in 0.1 M LiCl (*ca.* 0.02 cm s^{-1}) are too low to give deviations in the admittance, as was shown in the experimental part. Theoretical calculations show that $k_{sh} > 0.1$ cm s^{-1} should be fulfilled both for the zinc and barium system in 0.1 M solution in order to yield significant deviations from classical beha-

viour. It was assumed in this calculation that frequencies as low as 200 Hz can be used for accurate measurements. The lower limit of the frequency range is especially important, because at the lower frequencies the adsorption effects are the most important.

From these calculations it also appeared that $Y'/\omega^{\frac{1}{2}}$ is practically independent of frequency when $k_{sh} \approx 0.3$ cm s^{-1}. Therefore one should be careful in the analysis of the impedance when there is suspected adsorption, as the first step of that analysis is the investigation of the frequency dependence of $Y'/\omega^{\frac{1}{2}}$. From the decrease of $Y'/\omega^{\frac{1}{2}}$ with frequency irreversibility can be concluded, cf. eqn. (21a). However, adsorption tends to increase $Y'/\omega^{\frac{1}{2}}$, so that for some k_{sh} values the net effect is that $Y'/\omega^{\frac{1}{2}}$ remains constant, from which it cannot be concluded simply that the electrode reaction behaves reversibly.

In conclusion, it has been shown that theoretical calculations can provide the double layer parameters, necessary for the calculation of the electrode impedance. Unfortunately, the barium electrode reaction appeared to be too irreversible for detecting non-specific adsorption effects in the a.c. peak potential region, although the barium adsorption is rather strong. Possibly, application of lower a.c. frequencies could give additional proof of the theory presented.

At potentials anodic of the peak region a change in C_d with Ba^{2+} concentration was found caused by the non-specific barium adsorption. This change is in quantitative agreement with double layer theory.

SUMMARY

The influence of non-specific adsorption of reactants on the electrode impedance is discussed. A method is proposed for calculating the double layer parameters, starting from experimental values of q and C_d. Substitution of the double layer parameters in the expressions for the electrode impedance, derived by Delahay, makes it possible to predict the importance of non-specific adsorption. It appears that only for rather reversible electrode reactions (rate constant, $k_{sh} > 0.1$ cm s^{-1}) adsorption effects can be expected.

Theoretical predictions have been verified on the system Ba^{2+}/Ba(Hg) in 0.1 and 1 M LiCl solutions. For both solutions no abnormal behaviour was found in the a.c. peak potential region, because the reaction is too irreversible ($k_{sh} = (9 \pm 1) \times 10^{-3}$ cm s^{-1} and $(1.6 \pm 0.3) \times 10^{-2}$ cm s^{-1} for resp. 1 M and 0.1 M LiCl solutions). The double layer capacity increases with Ba^{2+} concentration at potentials anodic of the a.c. peak, because of the non-specific Ba^{2+} adsorption.

REFERENCES

1 P. DELAHAY, J. Phys. Chem., 70 (1966) 2067, 2373.
2 B. TIMMER, M. SLUYTERS-REHBACH AND J. H. SLUYTERS, J. Electroanal. Chem., 18 (1968) 93.

3 P. DELAHAY, *J. Electroanal. Chem.*, 19 (1968) 61.
4 K. HOLUB, G. TESSARI AND P. DELAHAY, *J. Phys. Chem.*, 71 (1967) 2612.
5 B. TIMMER, M. SLUYTERS-REHBACH AND J. H. SLUYTERS, *J. Electroanal. Chem.*, 15 (1967) 343, 452.
6 B. TIMMER, M. SLUYTERS-REHBACH AND J. H. SLUYTERS, *J. Electroanal. Chem.*, 19 (1968) 73.
7 P. DELAHAY AND G. G. SUSBIELLES, *J. Phys. Chem.*, 70 (1966) 3150.
8 P. DELAHAY AND K. HOLUB, *J. Electroanal. Chem.*, 16 (1968) 131.
9 G. TESSARI, P. DELAHAY AND K. HOLUB, *J. Electroanal. Chem.*, 17 (1968) 69.
10 W. H. REINMUTH, *Anal. Chem.*, 40 (1968) 185R.
11 G. G. SUSBIELLES AND P. DELAHAY, *J. Electroanal. Chem.*, 17 (1968) 289.
12 K. M. JOSHI AND R. PARSONS, *Electrochim. Acta*, 4 (1961) 129.
13 W. H. REINMUTH, private communication.
14 C. D. RUSSELL, *J. Electroanal. Chem.*, 6 (1963) 486.
15 D. C. GRAHAME, *J. Am. Chem. Soc.*, 76 (1954) 4821.
16 M. SLUYTERS-REHBACH AND J. H. SLUYTERS in A. J. BARD, (Ed.), *Electroanal. Chemistry*, Vol. 4, Marcel Dekker Inc., New York, in press.
17 A. N. FRUMKIN AND V. I. MELIK-GAIKAZYAN, *Dokl. Akad. Nauk SSSR*, 78 (1951) 855.
18 I. M. KOLTHOFF AND H. P. GREGOR, *Anal. Chem.*, 20 (1948) 541.
19 L. G. SILLÉN AND A. E. MARTELL, *Stability Constants of Metal-ion Complexes*, Special Publication no. 17. The Chemical Society, London, 1964.
20 L. HOLLECK AND A. M. SHAMS-EL-DIN, *J. Electroanal. Chem.*, 17 (1968) 365.
21 M. SLUYTERS-REHBACH AND J. H. SLUYTERS, *Rec. Trav. Chim.*, 82 (1963) 525, 535.
22 B. G. DEKKER, M. SLUYTERS-REHBACH AND J. H. SLUYTERS, *J. Electroanal. Chem.*, 23 (1969) 9.
23 P. DELAHAY, *Double-layer and Electrode Kinetics*, Interscience Publishers Inc., New York, 1965, chapter 7.
24 L. GIERST, J. TONDEUR AND E. NICOLAS, *J. Electroanal. Chem.*, 10 (1965) 397.
25 R. DE LEVIE, *J. Electroanal. Chem.*, 9 (1965) 311.
26 G. C. BARKER AND J. A. BOLZAN, *Z. Anal. Chem.*, 216 (1966) 215.
27 R. PARSONS, private communication.

IMPEDANCES FARADIQUE ET DE COUCHE DOUBLE

I. ESSAI DE SÉPARATION, A POSTERIORI, DES PARAMÈTRES INTERVENANT DANS LA RÉPONSE À UN SIGNAL SINUSOIDAL, D'UNE ÉLECTRODE SIÈGE D'UNE RÉACTION ÉLECTROCHIMIQUE SIMPLE; PROCÉDÉ DE CALCUL

A. M. BATICLE, F. PERDU et P. VENNEREAU

Laboratoire d'Electrolyse du CNRS, 92 Bellevue (France)

INTRODUCTION

Dans toutes les études d'impédance faradique, la grandeur mesurée est toujours l'impédance globale de la cellule, Z_m.

En choisissant une contre-électrode suffisamment grande, cette impédance mesurée ne dépend que de la résistance de l'électrolyte et des connections, de l'impédance faradique proprement dite, et de l'impédance due à la charge de la couche double. Pour pouvoir déterminer les paramètres cinétiques de la réaction électrochimique, il est nécessaire de séparer les différents éléments de l'impédance globale mesurée.

Différents travaux concernant cette séparation sont rapportés dans une publication de D. Britz et H. H. Bauer[1]. Pour ce faire, l'hypothèse admise, la plus ancienne, est que l'impédance de la couche double de l'électrode est une capacité pure déterminée uniquement par la charge de l'électrode, celle-ci n'étant pas affectée par la présence des espèces réagissantes[2]. Par la suite, cette hypothèse a été adaptée[3] dans le cas des électrodes solides en utilisant l'impédance complexe mesurée en milieu électrolyte support seul. Ceci signifie que l'impédance de la couche double n'est plus une capacité pure, mais reste indépendante de la présence des espèces réagissantes.

D'autres travaux[1,4,5] admettent que, la charge de l'électrode dépendant des espèces réagissantes, la capacité de la couche double reste constante, au moins dans un grand domaine de fréquences, mais ne peut être celle mesurée en milieu électrolyte support et, par conséquent, proposent des méthodes de détermination de ces capacités en présence des réactions électrochimiques.

Une autre publication[7] envisage la possibilité d'une capacité dépendant de la fréquence, et propose une méthode de calcul, pour chaque fréquence, de cette capacité variable et de la résistance de transfert de charges.

Dans le cas des électrodes solides, Bump et Remick[6] font une hypothèse particulière sur la loi de variation des termes résistif et capacitif de l'impédance de la couche double en présence de réaction électrochimique.

Les travaux les plus récents de P. Delahay et ses collaborateurs[8] ont montré que la participation des espèces réagissantes à la charge de la couche double entraîne, en régime sinusoïdal, une dépendance de l'impédance de l'électrode, vis-à-vis de la fréquence, différente de la loi classique de Randles.

Nous proposons, dans cet article, une méthode de détermination simultanée des paramètres cinétiques d'une réaction simple (transfert de charge + diffusion des

espèces réagissantes) et de l'impédance de couche double, que cette dernière soit représentée par une impédance complexe ou par une capacité, variables ou non en fonction de la fréquence.

L'impédance globale mesurée Z_m de la cellule peut être représentée par le modèle de la figure 1.
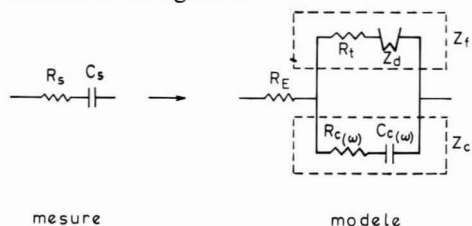
Fig. 1. Représentation du dipôle de mesure et du modèle utilisé dans le calcul.

Les éléments de cette figure ont la signification suivante:

R_S = résistance série mesurée,

C_S = capacité série mesurée,

R_E = résistance de l'électrolyte,

R_t = résistance de transfert de charges;

Z_d = impédance de Warburg = $\sigma \omega^{-\frac{1}{2}}(1-j)$

avec $j = \sqrt{-1}$ et $\sigma = \dfrac{RT}{\sqrt{2}\, n^2 F^2 A^*}\left[\dfrac{1}{C_O D_O^{\frac{1}{2}}} + \dfrac{1}{C_R D_R^{\frac{1}{2}}}\right]$ dans lequel:

A^* est la surface réactionnelle de l'électrode,

C_O et C_R sont les concentrations des espèces oxydées et réduites au sein de la solution,

D_O et D_R sont les coefficients de diffusion des espèces O et R,

R, T, n, F ont leurs significations habituelles.

Soient $R_{c(\omega)}$ la résistance de couche double et $C_{c(\omega)}$ la capacité de couche double. On désignera par θ le déphasage courant tension dans la couche double en écrivant $K = \cotg\,\theta = R_c C_c \omega$, tandis que Z_f représente l'impédance faradique proprement dite, et Z_c représente l'impédance de couche double*.

Nous avons choisi ce modèle afin de l'utiliser comme une première analyse des mesures d'impédance en cinétique électrochimique.

Dans le cas le plus simple ($R_c = 0$, C_c = cte) il se ramène à un circuit de Randles. Mais s'il n'en est pas ainsi le calcul fera apparaître certaines possibilités.

Si l'impédance Z_c (capacité pure ou impédance complexe) est la même que l'impédance de couche double qui a pu être mesurée en milieu support, le comportement des termes faradiques permettra de conclure à un mécanisme réactionnel simple ou non, sans interaction entre la réaction et la charge de la double couche.

Si l'impédance de couche double n'a pu être mesurée en milieu support, certains critères (tels que Z_c indépendant des concentrations des espèces réagissantes) permettront encore de conclure sur le mécanisme réactionnel.

Ce modèle peut être plus particulièrement utile dans le cas des électrodes

---

* Nous avons fait le calcul avec l'impédance série $R_c - j/\omega C_c$. Cette impédance série Z_c ainsi calculée sera aisément transformable pour chaque fréquence en résistance R_{dl} et capacité C_{dl} en parallèle, conformément aux conventions de Delahay[8].

solides pour lesquelles les mesures d'impédance de couche double sont délicates que ce soit en milieu support seul ou en présence d'espèces réagissantes. De plus la signification de la dispersion observée pour Z_c, en fonction de la fréquence, pour ces électrodes, étant inconnue dans la plupart des cas, il semble arbitraire de procéder à une séparation à priori de cette impédance Z_c, de l'impédance globale mesurée en présence de réaction.

Bien entendu en dehors de ces cas simples il faudra reconsidérer le problème à l'aide d'autres modèles et d'autres calculs et, probablement, d'autres expériences.

MÉTHODE

Pour chaque fréquence, l'identification des parties réelles et imaginaires de l'impédance mesurée $Z_m = X + jY$ et de l'impédance du modèle $Z_m = X' + jY'$ conduit au système de deux équations indépendantes:

$$Re = X - X' = 0$$
$$Im = Y - Y' = 0 \tag{1}$$

Re et Im étant fonction des paramètres mesurés $R_{S(\omega)}$ et $C_{S(\omega)}$ et des paramètres à déterminer R_E, R_t, σ, $K_{(\omega)}$ et $C_{c(\omega)}$.

L'élimination de $C_{c(\omega)}$ entre les deux équations de ce système conduit à l'expression suivante de K:

$$K_{(\omega)} = \frac{AR_t^2 + (2A\sigma\omega^{-\frac{1}{2}} - A^2 - D^2)R_t + (2A\sigma\omega^{-\frac{1}{2}} - A^2 - D^2)\sigma\omega^{-\frac{1}{2}}}{DR_t^2 + 2D\sigma\omega^{-\frac{1}{2}}R_t + (2D\sigma\omega^{-\frac{1}{2}} - A^2 - D^2)\sigma\omega^{-\frac{1}{2}}} \tag{2}$$

avec $A = R_S - R_E$ et $D = (\omega C_S)^{-1}$.

Le calcul se décompose alors en deux parties successives: (a) calcul de la résistance de l'électrolyte, de la résistance de transfert et du terme de diffusion σ, et (b) calcul de la résistance et de la capacité de couche double.

Dans la suite du texte, la valeur d'une grandeur $V_{(\omega)}$ pour une fréquence de pulsation ω_i sera notée V_i.

1. *Calcul de la résistance de l'électrolyte R_E, de la résistance de transfert R_t et du terme de diffusion σ*

Il est possible de décrire la fonction $K_{(\omega)}$ par une succession d'échelons considérés pour des valeurs voisines (ω_i, ω_j) de ω. Il sera alors possible d'écrire que $K_i = K_j$ pour chacun des couples (ω_i, ω_j) et d'obtenir à partir de l'équation (2) une expression indépendante de K pour des couples (ω_1, ω_2); (ω_2, ω_3); ... (ω_i, ω_j) ... $(\omega_{(n-1)}, \omega_n)$ dans le spectre des fréquences expérimentales:

$$F(R_E, R_t, \sigma, R_{Si}, R_{Sj}, C_{Si}, C_{Sj}, \omega_i, \omega_j) = 0 \tag{3}$$

Le choix des valeurs de ω_i et ω_j doit répondre à deux conditions: (a) ω_i suffisamment voisin de ω_j pour que la fonction $K_{(\omega)}$ soit décrite avec une précision suffisante; (b) ω_i suffisamment éloigné de ω_j de manière à ce que l'on puisse écrire:

$$\Delta R_S \ll |R_{Si} - R_{Sj}| \quad \text{et} \quad \Delta C_S \ll |C_{Si} - C_{Sj}| \tag{4}$$

où ΔR_S et ΔC_S sont les erreurs commises sur la mesure de R_S et C_S. Une méthode pratique de choix des couples ω_i, ω_j est donnée en appendice I.

On sait que les valeurs des trois grandeurs R_E, R_t et σ sont constantes dans tout le domaine de fréquences. L'expression (3) permettra de déterminer, par itérations successives, ces trois paramètres à condition de connaître approximativement deux de ces paramètres au départ. En général, R_E et σ peuvent être évalués approximativement.

En effet, une valeur approximative de R_E peut être déterminée dans le domaine des hautes fréquences en considérant que $R_{S(\omega \to \infty)} \to R_E$ [8]. Il est possible également d'évaluer R_E par le calcul en tenant compte de la géométrie de la cellule d'électrolyse[9].

Par ailleurs, dans le cas le plus favorable, σ peut être évalué dans le domaine des basses fréquences s'il est possible d'écrire :

$$\left[\frac{\partial R_S}{\partial(\omega^{-\frac{1}{2}})}\right]_{\omega \to 0} = \left[\frac{\partial(1/\omega C_S)}{\partial(\omega^{-\frac{1}{2}})}\right]_{\omega \to 0} = \sigma$$

Si le spectre de fréquences ne peut pas être suffisamment étendu pour que seul, aux basses fréquences, le phénomène de diffusion impose la variation de l'impédance mesurée, nous avons montré[10] que σ peut, malgré tout, être évalué. Rappelons également que la connaissance des coefficients de diffusion des espèces réagissantes permet de calculer σ en assimilant la surface réactionnelle de l'électrode à sa surface géométrique.

Donc, connaissant une valeur approximative de R_E et σ, l'équation (3) ordonnée en R_t permet de calculer la résistance de transfert :

$$\begin{aligned}
(A_iD_j - A_jD_i)R_t^4 + (B_iD_j + A_iE_j - B_jD_i - A_jE_i)R_t^3 + \\
(A_iF_j + C_iD_j + B_iE_j - A_jF_i - C_jD_i - B_jE_i)R_t^2 + \\
(B_iF_j + C_iE_j - B_jF_i - C_jE_i)R_t + (C_iF_j - C_jF_i) = 0
\end{aligned} \qquad (5)$$

avec $\quad A = R_S - R_E$,
$\quad B = 2(R_S - R_E)\sigma\omega^{-\frac{1}{2}} - (R_S - R_E)^2 - (\omega C_S)^{-2}$,
$\quad C = [2(R_S - R_E)\sigma\omega^{-\frac{1}{2}} - (R_S - R_E)^2 - (\omega C_S)^{-2}]\sigma\omega^{-\frac{1}{2}}$,
$\quad D = (\omega C_S)^{-1}$,
$\quad E = 2\sigma\omega^{-\frac{3}{2}}C_S^{-1}$ et
$\quad F = [2\sigma\omega^{-\frac{3}{2}}C_S^{-1} - (R_S - R_E)^2 - (\omega C_S)^{-2}]\sigma\omega^{-\frac{1}{2}}$.

Cette expression montre que la résistance de l'électrolyte intervient toujours dans le calcul de R_t sous la forme d'un terme $(R_{S(\omega)} - R_E)$ où R_S croît quand la fréquence diminue. Si ΔR_E est l'erreur d'évaluation de R_E, l'influence de cette erreur sur le calcul de R_t diminue quand ω diminue et il est possible ainsi de trouver une fréquence au-dessous de laquelle $(R_{S(\omega)} - R_E) \gg \Delta R_E$.

Il est clair, d'autre part, que, dans le domaine des basses fréquences, le calcul de R_t conduit à des valeurs acceptables tant que l'erreur sur l'impédance de diffusion reste négligeable, c'est-à-dire à des fréquences plus basses que celles qui rendent négligeable cette impédance, repoussant d'autant vers les basses fréquences le domaine d'utilisation de la méthode.

En fin de compte, il apparaît que R_t sera calculable dans le domaine des moyennes fréquences, étant bien entendu que les valeurs relatives du courant d'échange apparent et du terme de diffusion constituent une limitation des domaines d'applicabilité de ce calcul. Cependant, raisonner sur les erreurs des évaluations élargit beaucoup ce domaine par rapport aux méthodes basées sur le fait que ce sont les

paramètres cinétiques eux-mêmes qui doivent être négligeables, les uns par rapport aux autres, suivant le domaine des fréquences exploré.

La valeur moyenne de R_t dans son domaine de variation minimum (moyennes fréquences)* permet de préciser R_E et σ. En effet, l'équation (5) ordonnée tour à tour en R_E (5′) et σ (5″) permet de recalculer ces grandeurs en hautes et en basses fréquences à l'aide de cette valeur moyenne de R_t. L'erreur commise sur R_t verra son influence diminuer, sur R_E pour les hautes fréquences, et sur σ pour les basses fréquences. Les valeurs moyennes de R_E et σ déterminées dans leurs domaines respectifs peuvent alors servir à recalculer R_t. Une succession de ces itérations permet ainsi de préciser R_E, R_t et σ de manière à ce que ces grandeurs soient constantes dans tout le spectre des fréquences expérimentales. Le lecteur désirant utiliser ce calcul peut se reporter au texte des équations (5′) et (5″) donné dans l'appendice II.

2. Calcul des paramètres de couche double

Dans le système d'équation (1) $Im(\ldots)=0$ est du premier degré en $K_{(\omega)}$ qui a pour expression:

$$K_{(\omega)} = \frac{(\omega C_{c(\omega)})^{-1}(R_t + \sigma\omega^{-\frac{1}{2}} - A) - A - DR_t}{(\omega C_{c(\omega)})^{-1}(D - \sigma\omega^{-\frac{1}{2}})} \tag{6}$$

Cette expression de K replacée dans l'équation $Re(\ldots)=0$ du système (1) conduit à l'expression suivante de $(\omega C_{c(\omega)})^{-1}$:

$$\frac{1}{\omega C_{c(\omega)}} = \frac{[AR_t^2 + \sigma\omega^{-\frac{1}{2}}(A-D)](D - \sigma\omega^{-\frac{1}{2}}) - [\sigma\omega^{-\frac{1}{2}}(A+D) + DR_t](A - R_t - \sigma\omega^{-\frac{1}{2}})}{(D - \sigma\omega^{-\frac{1}{2}})^2 + (A - R_t - \sigma\omega^{-\frac{1}{2}})^2} \tag{7}$$

En introduisant les valeurs de R_t, R_E et σ précédemment calculées, (6) et (7) permettent de déterminer $C_{c(\omega)}$ et $K_{(\omega)}$ et, par là même, $R_{c(\omega)}$ par l'expression simple $K = \text{cotg } \theta = R_c C_{c(\omega)} \omega$. Remarquons que $K_{(\omega)}$ peut également être calculé indépendamment de $C_{c(\omega)}$ par l'expression (2).

Une telle méthode suppose que les trois grandeurs R_E, R_t et σ soient calculables avec une précision suffisante car les erreurs se répercuteront sur le calcul des paramètres de couche double. Or, suivant les réactions électrochimiques, ces trois termes ont des ordres de grandeurs très différents, entre eux d'une part, et par rapport à l'impédance Z_c d'autre part. Il est donc intéressant de pouvoir calculer les paramètres de couche double en éliminant du calcul la valeur d'un élément mal déterminé. Cet élément peut être éliminé entre les deux équations du système (1), ce qui conduit à la série de systèmes d'équations:

$$\begin{cases} C_{c(\omega)} = f_1(\sigma, R_t, K_{(\omega)}, R_{S(\omega)}, C_{S(\omega)}, \omega) \\ R_E = f_2(\sigma, R_t, K_{(\omega)}, C_{c(\omega)}, R_{S(\omega)}, C_{S(\omega)}, \omega) \end{cases} \tag{8}$$

$$\begin{cases} C_{c(\omega)} = g_1(R_E, R_t, K_{(\omega)}, R_{S(\omega)}, C_{S(\omega)}, \omega) \\ \sigma = g_2(R_E, R_t, K_{(\omega)}, C_{c(\omega)}, R_{S(\omega)}, C_{S(\omega)}, \omega) \end{cases} \tag{9}$$

---

* Si la composante résistive de l'impédance de couche double peut être négligée, la fréquence autour de laquelle R_t sera le moins entaché d'erreur peut être évalué par l'expression: $\omega \simeq 1/3R_t C_c{}^{11}$ en considérant $C_{S(\omega \to \infty)} \sim C_c$ et en évaluant l'ordre de grandeur de R_t dans son domaine de variation minimum lors d'une première itération.

$$\begin{cases} C_{c(\omega)} = h_1(R_E, \sigma, K_{(\omega)}, R_{S(\omega)}, C_{S(\omega)}, \omega) \\ R_t = h_2(R_E, \sigma, K_{(\omega)}, C_{c(\omega)}, R_{S(\omega)}, C_{S(\omega)}, \omega) \end{cases} \tag{10}$$

qui peuvent être résolues après avoir calculé K à partir de l'équation (2). Les expressions f(…), g(…) et h(…) ainsi que le calcul de K sont donnés en appendice III.

Ce dernier calcul peut servir de vérification du premier mode de détermination des paramètres de couche double. Il peut également permettre de préciser un paramètre mal déterminé lors des itérations.

3. *Application de la méthode précédente au cas où la couche double peut être décrite par une capacité seule $C_{c(\omega)}$*

L'élimination de $C_{c(\omega)}$ entre les équations du système (1) écrit avec $K=0$ conduit à l'expression suivante du second degré en R_t:

$$AR_t^2 + [2A\sigma\omega^{-\frac{1}{2}} - A^2 - D^2]R_t + \sigma\omega^{-\frac{1}{2}}[2A\sigma\omega^{-\frac{1}{2}} - A^2 - D^2] = 0 \tag{11}$$

Comme nous l'avons signalé dans une étude précédente[7] cette relation permet de calculer R_t si R_E et σ sont connus avec précision.

Dans le cas contraire il est avantageux de procéder de la manière suivante:

(*a*) R_t étant indépendant de ω peut être dans un premier temps éliminé du calcul en écrivant la condition pour que l'équation (11) admette une racine commune si elle est écrite pour les couples de fréquences ω_i, ω_j précédemment définis.

(*b*) L'expression ainsi obtenue permet de calculer R_t si l'on y introduit la valeur maximum de σ (notée σ_{max}) permettant à l'équation (11) d'admettre au moins une racine réelle et positive.

L'expression de σ_{max} écrite aux basses fréquences se ramène facilement à:

$$\sigma_{max} = \frac{R_S^2 + \omega^{-2}C_S^{-2}}{2R_S\omega^{-\frac{1}{2}}} \tag{12}$$

(*c*) Comme pour la méthode générale, une succession d'itérations effectuées sur l'équation obtenue en (*a*), ordonnée en R_E pour les hautes fréquences et en σ pour les basses fréquences, permet de préciser ces deux grandeurs.

(*d*) L'expression (11) permet alors de calculer facilement R_t, et $C_{c(\omega)}$ sera déterminée par:

$$\frac{1}{\omega C_{c(\omega)}} = \frac{(R_S - R_E)R_t + \sigma\omega^{-\frac{1}{2}}(R_S - R_E - \omega^{-1}C_S^{-1})}{(\omega C_S)^{-1} - \sigma\omega^{-\frac{1}{2}}} \tag{13}$$

Cette dernière expression est obtenue très aisément à partir du système d'équations (1) écrit pour $K=0$.

CONCLUSIONS

La méthode présentée ci-dessus nécessite, de manière évidente, l'utilisation de calculatrices électroniques pour résoudre les équations qui sont, en général, d'un degré élevé. Cependant, les programmes nécessaires restent élémentaires.

L'enchaînement des équations proposé n'est pas exhaustif. Il peut subir des modifications partielles qui seront avantageusement utilisées pour des systèmes électrochimiques particuliers. Il convient de rappeler que le jeu des valeurs relatives

des éléments du modèle électrique a une grande influence sur la précision avec laquelle ces éléments sont déterminables.

Ce mode de calcul peut conduire à trois situations différentes.

Soit il fait apparaître une impédance de couche double identique à celle mesurée en l'absence de réaction, et les valeurs des éléments de l'impédance faradique ainsi déterminées obéissent aux lois classiques du transfert de charges et de la diffusion. Il est alors possible d'affirmer que la réaction électrochimique a bien le mécanisme simple envisagé et que la participation des espèces actives à la charge de la couche double est négligeable.

Soit il fait apparaître une impédance de couche double toujours identique à celle mesurée en l'absence de réaction, mais les valeurs de l'impédance faradique n'obéissent pas aux lois classiques. Il faut alors envisager une complication du mécanisme réactionnel n'impliquant pas de modification de la couche double.

Soit les valeurs de l'impédance faradique déterminées suivent ou non les lois classiques mais l'impédance de couche double apparaît modifiée. Le problème doit alors être repris de façon à donner un sens physique aux variations observées avant de pouvoir conclure à une interaction entre la charge de la couche double et la réaction électrochimique, ou à toute autre complication du mécanisme à l'électrode.

En d'autres termes, cette méthode a vraiment l'avantage de pouvoir calculer les différents éléments du schéma global lorsque celui-ci obéit à des lois simples. La plus grande prudence est nécessaire pour interpréter les résultats qui n'obéissent pas à ces lois.

APPENDICE I

Méthode de détermination des couples de fréquences (ω_i, ω_j)

Si l'équation (4) est résolue pour tous les couples de valeurs ω_i, ω_j possibles dans le spectre des fréquences de mesure, les valeurs de $R_{t(i,j)}$ ainsi trouvées peuvent être disposées suivant le tableau à double entrée de la figure 2. La diagonale principale de ce tableau correspond à des valeurs non déterminées de R_t, $(\omega_i = \omega_j)$. Les valeurs de $R_{t(i,j)}$ situées sur les parallèles à la diagonale principale sont déterminées pour
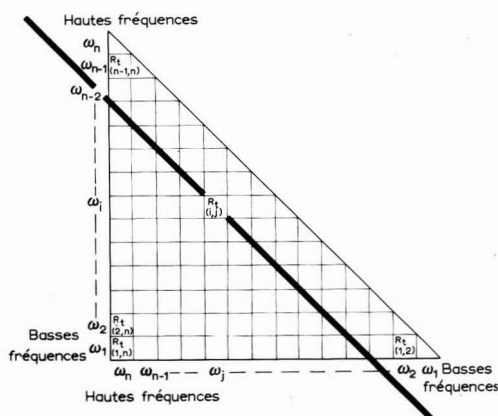
Fig. 2. Tableau permettant le choix des couples de fréquences utilisables pour le calcul.

des fréquences d'autant plus éloignées l'une de l'autre que l'on s'écarte de cette diagonale : elles correspondent à des couples de fréquences, mitoyennes pour la première parallèle, et extrêmes au sommet $R_{t(1-n)}$.

Les conditions (4) impliquent un choix des $R_{t(i,j)}$ situés sur une parallèle suffisamment éloignée de la diagonale principale, mais la précision avec laquelle la fonction $K_{(\omega)}$ doit être décrite implique que ω_i soit suffisamment proche de ω_j pour que l'égalité $K_i = K_j$ ait un sens (donc une parallèle suffisamment proche de cette diagonale principale). La diagonale le long de laquelle une variation minimum de R_t sera observée dans le domaine de fréquences convenable permet ainsi de déterminer les couples de valeurs ω_i, ω_j utilisables dans la suite du calcul.

APPENDICE II

1. *Texte de l'équation* (5') *permettant de calculer* R_E

$$(G_i J_j - G_j J_i)R_E^4 + (H_i J_j + G_i S_j - H_j J_i - G_j S_i)R_E^3 + (G_i L_j + L_i J_j + H_i S_j - G_j L_i - L_j J_i - H_j S_i)R_E^2 + (H_i L_j + I_i S_j - H_j L_i - I_j S_i)R_E + (I_i L_j - I_j L_i) = 0$$

avec :

$$G = -(R_t + \sigma\omega^{-\frac{1}{2}}),$$
$$H = (R_t + \sigma\omega^{-\frac{1}{2}})(2R_S - 2\sigma\omega^{-\frac{1}{2}}) - R_t^2,$$
$$I = R_S R_t^2 + (R_t + \sigma\omega^{-\frac{1}{2}})(2\sigma\omega^{-\frac{1}{2}}R_S - R_S^2 - \omega^{-2}C_S^{-2}),$$
$$J = -\sigma\omega^{-\frac{1}{2}},$$
$$L = R_t^2(\omega C_S)^{-1} + 2R_t\sigma\omega^{-\frac{1}{2}}C_S^{-1} + (2\sigma\omega^{-\frac{1}{2}}C_S^{-1} - R_S^2 - \omega^{-2}C_S^{-2})\sigma\omega^{-\frac{1}{2}} \text{ et}$$
$$S = 2R_S\sigma\omega^{-\frac{1}{2}}.$$

2. *Texte de l'équation* (5'') *permettant de calculer* σ

$$(\alpha_i\delta_j - \alpha_j\delta_i)\sigma^4 + [(\beta_i\delta_j + \alpha_i\varepsilon_j) - (\beta_j\delta_i + \alpha_j\varepsilon_i)]\sigma^3 + [(\lambda_i\delta_j + \beta_i\varepsilon_j + \alpha_i Z_j) - (\lambda_j\delta_i + \beta_j\varepsilon_i + \alpha_j Z_i)]\sigma^2 + [(\lambda_i\varepsilon_j + \beta_i Z_j) - (\lambda_j\varepsilon_i + \beta_j Z_i)]\sigma + \lambda_i Z_j - \lambda_j Z_i = 0$$

avec :

$$\alpha = 2(R_S - R_E)\omega^{-1},$$
$$\beta = [2R_t(R_S - R_E) - (R_S - R_E)^2 - \omega^{-2}C_S^{-2}]\omega^{-\frac{1}{2}},$$
$$\lambda = (R_S - R_E)R_t^2 - (R_S - R_E)^2 R_t(\omega C_S)^{-2},$$
$$\delta = 2\omega^{-2}C_S^{-1},$$
$$\varepsilon = [2R_t\omega^{-1}C_S^{-1} - R_t^2 - \omega^{-2}C_S^{-2}]\omega^{-\frac{1}{2}}, \text{ et}$$
$$Z = R_t^2\omega^{-1}C_S^{-1}.$$

APPENDICE III

Equations permettant de calculer la capacité de couche double C_c *en éliminant du calcul un élément mal déterminé*

Les notations suivantes sont utilisées : $X = (\omega C_{c(\omega)})^{-1}$, $A = R_S - R_E$, $D = (\omega C_S)^{-1}$, $P = R_t + \sigma\omega^{-\frac{1}{2}}$, $K = R_E' C_{c(\omega)}\omega$.

(a) *Calcul de* $C_{c(\omega)}$ *en éliminant* R_E

$$f_1(\ldots) = (1 + K^2)(D - \sigma\omega^{-\frac{1}{2}})X^2 + [2D(PK + \sigma\omega^{-\frac{1}{2}}) - P^2 - \sigma^2\omega^{-1}]X + D(P^2 + \sigma^2\omega^{-1}) = 0 \tag{8}$$

(b) *Calcul de $C_{c(\omega)}$ en éliminant σ*

$$g_1(\ldots) = (1+K^2)(R_t - A + D)X^2 + [(A^2+D^2)(K-1) - 2R_t(KA+D)]X + (A^2+D^2)R_t = 0 \tag{9}$$

(c) *Calcul de $C_{c(\omega)}$ en éliminant R_t*

$$h_1(\ldots) = (1+K^2)(\sigma\omega^{-\frac{1}{2}} - D)X^2 + [A^2+D^2 - 2\sigma\omega^{-\frac{1}{2}}(KA+D)]X + (A^2+D^2)\sigma\omega^{-\frac{1}{2}} = 0 \tag{10}$$

(d) *La relation entre $C_{c(\omega)}$, K, R_t, σ et R_E*

La relation suivante permet de déterminer à postériori la grandeur éliminée du système (1):

$$R_t[A - KX] = X\sigma\omega^{-\frac{1}{2}}(K-1) + \sigma\omega^{-\frac{1}{2}}(D-A) + X(D-KA) \tag{14}$$

(e) *Calcul de K*

L'équation (2) est du deuxième degré en R_E, R_t et σ. Ces trois grandeurs sont indépendantes de ω. L'une d'entre elles, au choix, peut être éliminée dans les couples d'équations (2) écrites pour ω_i et ω_j.

RÉSUMÉ

L'obtention de l'impédance faradique d'une réaction électrochimique passe toujours par la mesure de l'impédance globale de l'électrode. Il n'est pas toujours justifié de séparer de l'impédance globale, l'impédance de double couche mesurée en milieu support seul. Il est aussi des cas où cette impédance ne peut être connue. De plus, pour diverses raisons, elle peut apparaître sous la forme d'une impédance complexe et non d'une capacité. Pour remédier à tout ceci, il est proposé un modèle simple et un procédé de calcul pour déterminer simultanément l'impédance faradique, et l'impédance de couche double. La méthode n'est valable que dans un certain nombre de cas. Mais elle peut apporter des informations précieuses en particulier dans le cas des électrodes solides où l'impédance de couche double est le plus souvent mal connue.

SUMMARY

The faradaic impedance of an electrochemical reaction is always obtained from measurements of the total impedance of the electrode. It is not always justified to separate from the total impedance, the double layer impedance measured in the supporting medium alone. There are also cases where this impedance cannot be measured. Further, for various reasons it can behave as a complex impedance and not as a capacity. To allow for this a simple model is proposed with a procedure for calculating simultaneously the faradaic impedance and the double layer impedance. The method is valid only in certain cases; but it provides valuable information particularly in the case of solid electrodes where the double layer impedance is not well known.

BIBLIOGRAPHIE

1 D. BRITZ ET H. H. BAUER, *J. Electroanal. Chem.*, 16 (1968) 13.
2 J. E. B. RANDLES, *Discussions Farad. Soc.*, (1947) p. 11.
3 F. PERDU, *Thèse*, Paris (1967).
4 J. H. SLUYTERS, *Rec. Trav. Chim.*, 79 (1960) 1092; M. REHBACH ET J. H. SLUYTERS, *Rec. Trav. Chim.*, 80 (1961) 469; 81 (1962) 301; 82 (1963) 525; J. H. SLUYTERS ET R. DE LEEUWE, *Rec. Trav. Chim.*, 83 (1964) 657; A. B. IJZERMANS, M. SLUYTERS-REHBACH ET J. H. SLUYTERS, *Rec. Trav. Chim.*, 84 (1965) 729.
5 R. DE LEVIE, *Electrochim. Acta*, 10 (1965) 395.
6 D. D. BUMP ET A. E. REMICK, *J. Electrochem. Soc.*, 111 (1964) 981.
7 A. M. BATICLE ET F. PERDU, *J. Electroanal. Chem.*, 12 (1966) 15.
8 P. DELAHAY, *J. Phys. Chem.*, 70 (1966) 2373; 71 (1967) 2612.
9 K. J. VETTER, *Elektrochemische Kinetik*, Springer Verlag Berlin, Heidelberg (1961) 299.
10 A. M. BATICLE, F. PERDU ET P. VENNEREAU, *C. R. Acad. Sci. Paris, Ser. C*, 267 (1968) 452.
11 D. J. KOOIJMAN ET J. H. SLUYTERS, *Electrochim. Acta*, 12 (1967) 1579.

THE SPECIFIC ADSORPTION OF OXALATE ANIONS AT THE MERCURY–AQUEOUS SOLUTION INTERPHASE

W. P. RACE

Electrochemistry Research Laboratory, School of Chemistry, The University of Newcastle upon Tyne, Newcastle upon Tyne, NE1 7RU (England)

(Received September 3rd, 1969)

INTRODUCTION

In recent work from these laboratories, anion adsorption on mercury or mercury amalgam electrodes has been inferred at potentials cathodic to those at which anodic films are formed[1-3]. Evaluation of the extent of anion adsorption has previously been carried out using non-thermodynamic assumptions. The present communication deals with the adsorption of oxalate species at a mercury electrode where a more rigorous thermodynamic analysis is possible, and a wide concentration range of $C_2O_4^{2-}$ ions can be achieved by employing suitable ratios of oxalic acid and potassium oxalate, at suitable pH values.

The specific adsorption has been studied using $HClO_4$, and KNO_3 solutions as supporting electrolytes, at concentrations such that the non-specific adsorption of oxalate species in the diffuse double layer is negligible. It was necessary to employ these electrolytes as it was not possible to use the theoretically advantageous fluoride electrolyte, since low pH values cannot be achieved because of the pK of hydrofluoric acid. Consequently, the competitive adsorption of nitrate or perchlorate ions can be expected to impose some limitation on the analysis of oxalate adsorption, particularly when involving behaviour at constant charge on the mercury electrode.

LIST OF SYMBOLS

C_{dl}	Double layer capacitance (μF cm^{-2})
C_b	C_{dl} in base electrolyte alone (μF cm^{-2})
ΔC	$(C_{dl} - C_b)_E$ (μF cm^{-2})
C_p	Parallel circuit capacitance (μF cm^{-2})
c, c_0, c_0'	Concentrations of $H_2C_2O_4$, $C_2O_4^{2-}$, and dissolving species, respectively (M)
D	Diffusion coefficient (cm^2 s^{-1})
E	Potential (V)
ΔG	Standard free energy of adsorption (kcal mol^{-1})
K	Henry's Law constant (cm)
k, k'	Pseudo first order rate constants (s^{-1})
k_0	Composite rate constant (s^{-1})

n	Charge number
q_1	Specifically adsorbed charge (μC cm^{-2})
q_m	Charge on the mercury electrode (μC cm^{-2})
q_b	q_m in the base electrolyte alone (μC cm^{-2})
Δq_m	$(q_m - q_b)$ (μC cm^{-2})
R_p	Parallel circuit interfacial resistance (Ω cm^2)
x_1, x_2	Distance from electrode to IHP and OHP, respectively (cm)
γ	Interfacial tension (dyn cm^{-1})
γ_0	γ at point of zero charge (dyn cm^{-1})
γ_b	γ in the base electrolyte alone (dyn cm^{-1})
$\Delta \gamma$	$(\gamma_b - \gamma)_E$ (dyn cm^{-1})
Γ	Surface concentration of adsorbed species (mol cm^{-2})
$\tau_{D1}, \tau_{D2}, \tau_R$	Relaxation times (s)
$\varphi_m, \varphi_1, \varphi_2$	Potentials at electrode, IHP and OHP, respectively, referred to potential in bulk solution (V)
Φ	Difference in quantity $\gamma + q_m E$ from its value in the base electrolyte, at the same q_m value (dyn cm^{-1})
μ	Chemical potential (kcal mol^{-1})
ω	Angular frequency (s^{-1})

EXPERIMENTAL

Solutions were made up in triply distilled water using AnalaR oxalic acid and potassium oxalate, twice recrystallised AnalaR potassium nitrate, BDH "AristaR" perchloric acid, and BDH potassium hydrogen oxalate. Mercury was purified by prolonged treatment with nitric acid, then distilled twice *in vacuo*. Solutions were deoxygenised using pre-saturated nitrogen, and all measurements were carried out in an air thermostat at 25.0 $\pm$ 0.1°.

Impedance measurements were made using a Wien bridge described previously[4], and a cell containing a hanging mercury drop electrode, symmetrically aligned within a cylindrical platinum subsidiary electrode. The latter was large enough for its impedance to contribute negligibly to that of the cell.

In solutions where the base electrolyte was 1 M or 3 M KNO$_3$, saturated calomel electrodes (SCE) were used as reference electrodes. Hydrogen reference electrodes in 1 M HClO$_4$ were used in the acid solutions.

Solutions of oxalic acid, 0.5, 0.25, ... 0.03125 M, were prepared in 1 M HClO$_4$. The cell impedance was measured at 50 mV intervals from -500 to $+400$ mV (H$_2$), then at decreasing intervals (10 mV–1 mV) up to the limit of anodic polarisation in each solution. The impedance was found to be independent of frequency, except near the anodic limit in the most dilute solution, so most measurements were performed at 1 kHz. At potentials close to the anodic capacity rise, greater sensitivity was obtained when measuring high capacitances by reducing the frequency to 200 Hz, when necessary.

To avoid errors due to the irreproducibility of electrode areas (typically up to 3%, for areas less than 0.01 cm^2), a "calibration" potential was chosen at $+400$ mV. For each solution, the capacitance was determined accurately at this potential, by turning up several drops of known area, and taking the mean of the estimated capaci-

tance per unit area. At other potentials, the drop area was determined before and after the actual measurement, using the calibration potential.

In 3 M KNO$_3$, the conductivity is sufficiently high, so that the capacitative part of the cell impedance is great enough for sensitive capacitance balance to be observed, even when values as high as 1,400 μF cm^{-2} are encountered. The high concentration also leads to the neglect of the diffuse double layer contribution to the oxalate adsorption being a realistic approximation. Solutions of 0.1, 0.05, ... 0.0125 M K$_2$C$_2$O$_4$ in 3 M KNO$_3$ were prepared, and KHC$_2$O$_4$ was added to maintain the ratio K$_2$C$_2$O$_4$: KHC$_2$O$_4$ at 10 : 1. The interfacial capacitance, having been found to be frequency independent, was measured at 5 kHz, at potentials from -450 mV (SCE), at 50 mV intervals to 0 mV, then at diminishing intervals until the limit of anodic polarisation at potentials beyond $+250$ mV.

To determine which species was adsorbed, the anodic branch of the C_{dl}–E curve was determined for each of the following solutions: (a) 0.115 M K$_2$C$_2$O$_4$, 0.013 M KHC$_2$O$_4$; (b) 0.108 M KHC$_2$O$_4$, 0.0102 M K$_2$C$_2$O$_4$; (c) 0.0115 M K$_2$C$_2$O$_4$, 0.00103 M KHC$_2$O$_4$; in 1 M KNO$_3$ as support electrolyte.

The C_{dl}–E curves were also determined for the KNO$_3$ and HClO$_4$ base electrolyte solutions, and in each the potential of the e.c.m. was determined by setting up a streaming mercury electrode in the thoroughly de-oxygenated solutions.

Finally, the potentials of mercury/mercurous oxalate electrodes in the various solutions were determined. Since mercurous oxalate is very photosensitive, it was prepared (from AnalaR mercurous nitrate and oxalic acid) with as little exposure to light as possible, immediately before use, and the potentials were measured in the absence of light.

RESULTS AND DISCUSSION

(i) *Equilibrium properties of the interphase*
        The anodic branches of the C_{dl}–E curves, for the solutions of different ratios of C$_2$O$_4^{2-}$ and HC$_2$O$_4^-$, are shown in Fig. 1, the capacitance being plotted on a logarithmic scale because of the high values encountered near the anodic limit of polarisation. Curves a and b show a displacement of about 45 mV, when the C$_2$O$_4^{2-}$ concentration is decreased by a factor of ten. However, changing the KHC$_2$O$_4$ concentration causes little displacement, b and c. Therefore the species adsorbed is the oxalate anion, C$_2$O$_4^{2-}$, in these solutions. It may also be seen that curve d shows no marked anodic behaviour, comparable with the magnitude of the capacitance rise produced by oxalate adsorption.

For the solutions of oxalic acid in HClO$_4$, the capacitance curves near the e.c.m. did not show any dependence on concentration, and it was concluded that no measurable adsorption of oxalic acid itself occurs at these potentials. Figure 2 shows the anodic branches of the capacitance curves for the respective solutions: (a) of H$_2$C$_2$O$_4$ in HClO$_4$ (b) of K$_2$C$_2$O$_4$ in KNO$_3$. The shift of the C_{dl}–E curves with concentration is the same for each set of data, proving that the same species, *viz.* the C$_2$O$_4^{2-}$ anion, is adsorbed in the oxalic acid solutions. It is shown later that the actual C$_2$O$_4^{2-}$ concentrations in the acid solutions are a factor of $4 \cdot 10^{-5}$ less than the H$_2$C$_2$O$_4$ concentrations, in fair agreement with the predictions from stability constant data. Thus Fig. 2(a) shows data where the adsorbed species is present at much less concen-
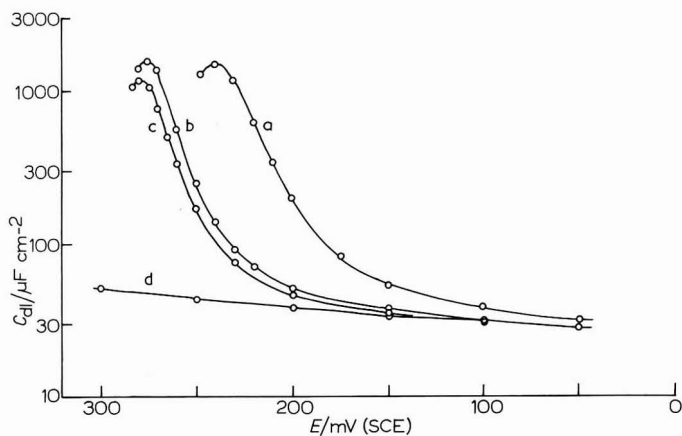
Fig. 1. Anodic branches of the C_{dl}–E curves, illustrating which oxalate species is adsorbed. Curves a, b, and c refer to respective solns. defined under *Experimental*, (d) is for 1 M KNO$_3$ alone.
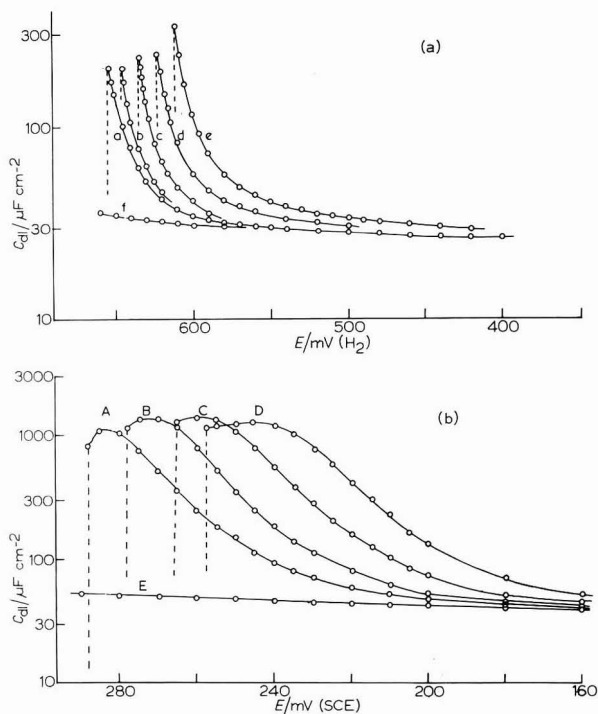
Fig. 2. Anodic branches of C_{dl}–E curves: a. (a–e) H$_2$C$_2$O$_4$ solns. 0.03125…0.5 M, respectively, (f) 1 M HClO$_4$; b. (A–D) K$_2$C$_2$O$_4$ solns. 0.0125…0.1 M respectively, (E) 3 M KNO$_3$.

trations than H$_2$C$_2$O$_4$ or HC$_2$O$_4^-$. In these solutions, no inflexion in the C_{dl}–E curve appears near the anodic limit, but as the capacitance approaches 300 μF cm^{-2} a discontinuity occurs. The capacitance then falls to about 30 μF cm^{-2}; this has been ascribed previously[5] to the formation of a monolayer of the anodic phase (mercurous oxalate) on the mercury surface. The formation potential was reproducible to within 1

mV in separate experiments, yet the decreased capacitance value was markedly dependent on the speed of overshooting the formation potential (see also ref. 6). This suggests that the phase can form with different degrees of ordered "packing" on the metal surface. This view is further substantiated by the tendency for further phase formation, accompanied by a slow decrease of the capacitance with time at constant potential. Such multilayer growth is probably initiated at sites of irregularities in the thin phase already present. On moving anodically from the monolayer formation potential, the capacitance was typically potential independent for about 20 mV, beyond which the multilayer formation potential was reached, and the capacitance fell rapidly with time. The thin phase could be removed on passing cathodic to the formation potential by about 2 mV, when an instantaneous rise of capacitance was seen.

Figure 2(b) shows the corresponding behaviour when the adsorbed species is several orders of magnitude more concentrated. Here, the capacitances achieved are much higher and a capacitance peak reaching 1,400 μF cm^{-2} is shown in all cases. The peak is moved anodically as the $C_2O_4^{2-}$ concentration is reduced, at the rate of about 46 mV per decade of concentration. The peak also then becomes progressively more narrow, and the potential range anodic to the peak is reduced at lower concentrations. This is part of a continuous trend which results in the peak having disappeared entirely at concentrations as low as those represented in Fig. 2(a).

At the higher oxalate concentrations, it was not possible to observe the formation of a thin anodic phase, but after the discontinuity in the C_{dl}–E curves, the capacitance fell rapidly with time, as the multilayer was formed directly. The anodic phase could again be removed with little hysteresis, and the shapes of the C_{dl}–E curves obtained on traversing cathodically coincided exactly with those obtained in the reverse direction.

The dependence on $C_2O_4^{2-}$ concentration of various potentials associated with features of the capacitance curves, is presented in Fig. 3. In both the concentration ranges studied, the mercurous oxalate reversible potential (measured directly) shows a 29.5 mV dependence on log c_0, as is expected for a reversible electrode process involving two electrons. Since for the oxalic acid solutions, the direct calculation of the $C_2O_4^{2-}$ concentration involves the accumulation of errors in stability constant data, and assumptions regarding activity coefficients, it was more practicable to compute these concentrations by assuming a continued 29.5 mV dependence of the reversible potential between the two sets of data. The position of these concentrations was therefore found by obtaining the best agreement with the extrapolated line of this slope through the $K_2C_2O_4$ solution data, assuming this salt to be completely dissociated. Having fixed the relative concentration scales, other potentials can then be examined, as in Fig. 3. It is seen that the phase formation potential remains anodic to the reversible potential throughout the range studied, and shows an overall 31.5 mV shift per decade of concentration.

The potential at which the capacitance had reached a constant value, high enough for a substantial adsorption effect to be included, is shown (taking $C_{dl} = 60$ μF cm^{-2}). Again, a continuous trend is followed over six decades of concentration, this time with a 46 mV per decade dependence. As noted earlier, for the more concentrated solutions, the potential of the capacitance peak also shows this concentration dependence. It may be predicted that as the "peak" line in Fig. 3 is intersected by the "phase"
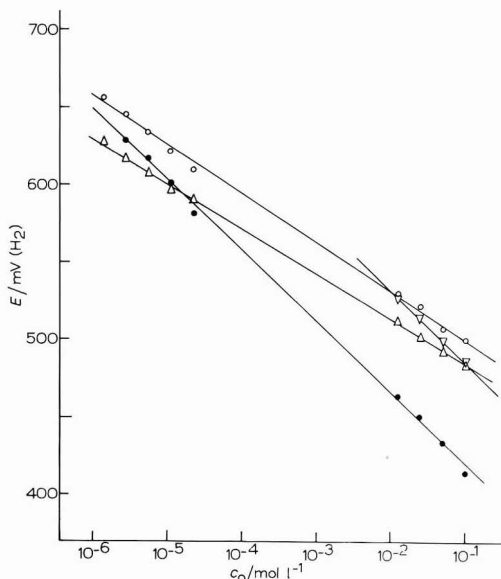
Fig. 3. Variation of characteristic potentials with log c_0: ($\triangle$) oxalate reversible potential, (∇) potential of capacitance peak, ($\bigcirc$) phase formation potential, ($\bullet$) potential at which $C_{dl} = 60$ μF cm^{-2}.

line at progressively lower concentrations, the capacitance peak gradually is over-taken by phase formation, and disappears.

    Since in Fig. 3, both the "constant capacity" line, and the "phase" line show continuous behaviour between the two sets of data, the use of the reversible oxalate potential data to determine the actual oxalate concentrations in the acid solutions, is substantiated.

    To integrate the C_{dl}–E curves to obtain values of the charge on the metal (q_m) and the interfacial tension (γ), it was necessary to determine the potentials of zero charge. The measured values were -542 ± 1 mV (SCE) for the 3 M KNO$_3$ solution, and -250 ± 1 mV (H$_2$) for the 1 M HClO$_4$ solution. It is reasonable to assume that these e.c.m. values can be taken for all the respective solutions within experimental error, since for the oxalic acid solutions, the C_{dl}–E curves were coincident at potentials cathodic to $+100$ mV (H$_2$), and also for the potassium oxalate solutions cathodic to 0 mV (SCE).

    Digital integration using the measured capacitance values gave q_m as a function of E for each solution, at potentials right up to the limit of anodic polarisation. Figure 4 shows the anodic branches of the q_m–E curves for the respective solutions. It is seen that the deviations of these curves from the base electrolyte curve are about an order of magnitude greater for the K$_2$C$_2$O$_4$ solutions than for the H$_2$C$_2$O$_4$ solutions. Also, in the former case, the closed circles represent the charges reached at the potential of the peak in the C_{dl}–E curves, and a slight inflexion in the q_m–E curves is evident near these points. The actual charge achieved at the capacitance peak varies only slightly with concentration of the adsorbing species, while the potential range between the peak and phase formation falls off rapidly as the concentration is decreased, confirming the trend already observed in connection with Fig. 3.
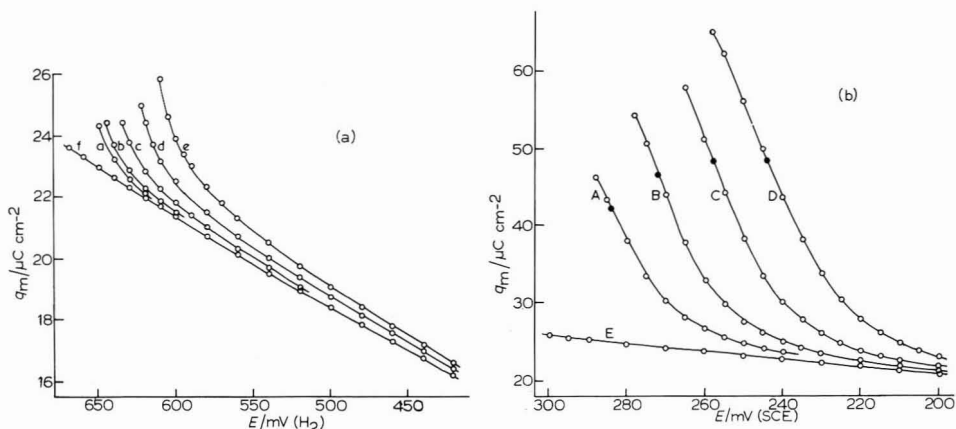
Fig. 4. Potential dependence of q_m: (a) $H_2C_2O_4$ solns., (b) $K_2C_2O_4$ solns. (codes as for Fig. 2), (●) charge at peaks in $C_{dl}-E$ curves.
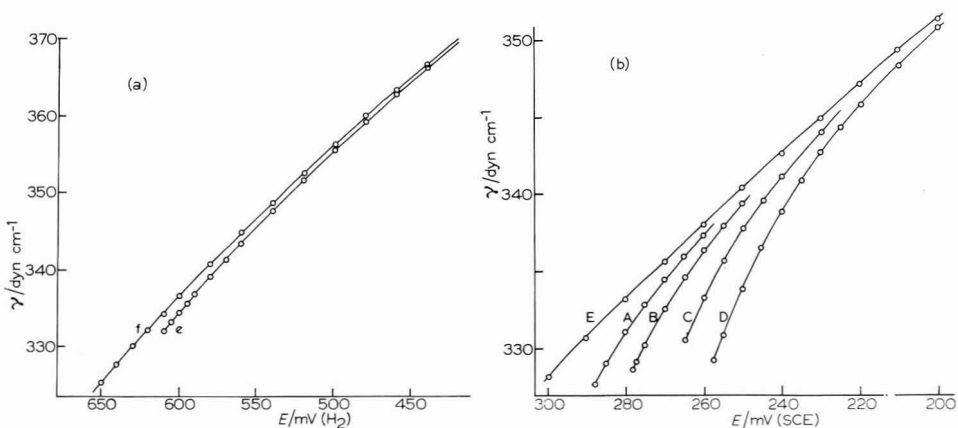
Fig. 5. Potential dependence of the interfacial tension: (a) 0.5 M $H_2C_2O_4$ soln. and 1 M $HClO_4$ soln., (b) $K_2C_2O_4$ solns. and 3 M KNO_3 soln. (Code as for Fig. 2).

To integrate the q_m-E curves to obtain γ values, the interfacial tension value at the e.c.m. (γ_0) was taken as 425 dyn cm^{-1}, after a survey of Gouy's extensive data[7] (the actual γ_0 value is not critical in the subsequent analysis). The extreme anodic branches of the electrocapillary curves are shown in Fig. 5. For the $H_2C_2O_4$ data, only the results for the most concentrated solution, and for the base electrolyte, are shown. It is seen that the γ values are very insensitive to the adsorption, compared with the $C_{dl}-E$ curves. For the $K_2C_2O_4$ solutions, the anodic deviations are shown on an expanded scale, illustrating that to analyse accurately surface tension data as a function of concentration or potential, it is desirable to know the individual γ values to at least five significant figures.

To examine the adsorption isotherm of $C_2O_4^{2-}$ ions, it is necessary to compute either the surface pressure at constant charge, Φ, or at constant potential $\Delta\gamma$ and then to investigate either as a function of c_0. For the oxalic acid solutions, Φ was comput-
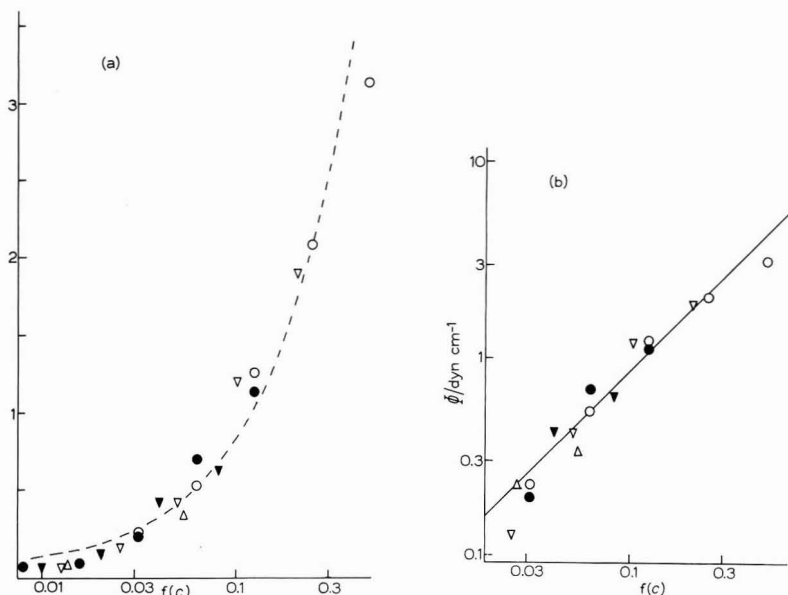
Fig. 6. $H_2C_2O_4$ solns.: (a) dependence of Φ on log concn., broken curve represents Henry's Law; (b) dependence of log Φ on log concn., line of unit slope represents Henry's Law. Code: values of q_m (μC cm^{-2}): ($\bigcirc$) 24, ($\triangledown$) 22, ($\bullet$) 20, ($\blacktriangledown$) 18, ($\triangle$) 16.

ed at q_m values of 16, 18, ... 24 μC cm^{-2} for each concentration. It was found that the curves of Φ against log c_0 could be shifted along the log c_0 axis to give a single coincident curve within experimental error, this being shown in Fig. 6(a). Since the actual magnitude of the Φ scale is less than 4 dyn cm^{-1} (therefore about an order less than in most similar treatments of adsorption[8-11]) the superposibility of the curve segments at different q_m values appears satisfactory. The broken curve drawn through the points is a simple exponential function of log c_0, and would correspond to Henry's Law as the relevant adsorption isotherm. Figure 6(b) shows the corresponding logarithmic $\Phi-c_0$ dependence, the line of unit slope drawn through the points again representing Henry's law. It appears that in the oxalic acid solutions, $C_2O_4^{2-}$ adsorption does not significantly deviate from Henry's Law for any solution. This is not surprising since the actual adsorption achieved is very low compared with most other systems which have been examined quantitatively.

In the case of the $K_2C_2O_4$ solutions, the charge values achieved near the anodic extreme of polarisation are very much higher (*cf.* Figs. 4(a) and (b)). Consequently, Φ could not be determined, since the capacitance data necessary to obtain these q_m values for the base electrolyte are inaccessible to measurement, due to the dissolution of mercury, and eventual phase formation. It was considered impracticable to extrapolate the existing q_m values to more anodic potentials, because of the length of extrapolation required, and the fact that Φ values calculated in this manner were very sensitive even to slight variations in the extrapolation. It was therefore necessary to compute $\Delta\gamma$ values, at constant potential for these solutions. Potentials of $+200$, 210, ... 260 mV (SCE) were taken, to cover the anodic behaviour as completely as possible. In this case the reverse procedure is demonstrated to test for deviations from
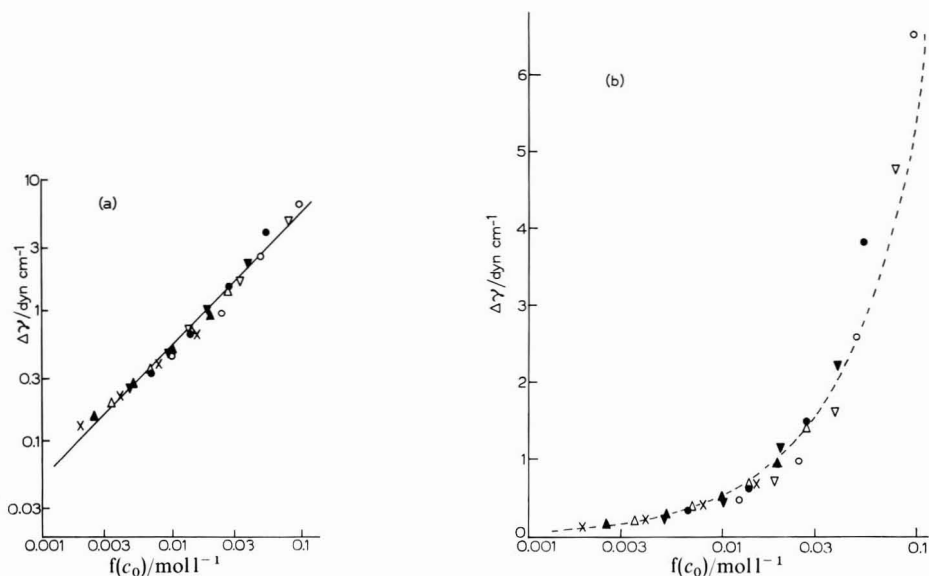
Fig. 7. $K_2C_2O_4$ solns: (a) fitting of $\Delta\gamma$ values to Henry's Law line, (b) corresponding $\Delta\gamma$–log concn. dependence. Code: values of E (mV, SCE): ($\bigcirc$) 260, ($\triangledown$) 250, ($\bullet$) 240, ($\blacktriangledown$) 230, ($\triangle$) 220, ($\blacktriangle$) 210, ($\times$) 200.

Henry's Law. Plots of $\log \Delta\gamma$ against $\log c_0$ were shifted along the $\log c_0$ axis to lie on the best line of unit slope, Fig. 7(a). Then $\Delta\gamma$ was plotted directly as a function of $\log c_0$ and the degree of overlap of the respective curve segments inspected, Fig. 7(b). Most of the data lie near the exponential curve, and such deviations that do occur (mainly at anodic potentials) cannot be unambiguously assigned to any well defined departure from Henry's Law. It is rather unexpected that when relatively high coverages of adsorbed ions are obtained (an adsorption peak in the C_{dl}–E curve usually represents near half coverage) the adsorption still appears to follow so simple a form. However, since at any one potential, only one $\Delta\gamma$ point for one concentration can correspond to the anodic limit of polarisation, the majority of the points in Fig. 7 necessarily relate to lower coverages. The $\Delta\gamma$–log c_0 relationships were also tested for the $H_2C_2O_4$ solutions, and similar behaviour was found.

A probable explanation of the applicability of Henry's Law to the $K_2C_2O_4$ data is that there is considerable nitrate adsorption in addition to the $C_2O_4^{2-}$ adsorption. If the amount of NO_3^- adsorbed depended only slightly on the $C_2O_4^{2-}$ concentration, then those $C_2O_4^{2-}$ ions which are adsorbed may experience a similar electrical environment in the various solutions at constant potential. Thus the analysis would be relatively insensitive to detecting specific interactions between the adsorbed $C_2O_4^{2-}$ ions as deviations from Henry's Law. Similarly, ClO_4^- adsorption in the $H_2C_2O_4$ solutions may enhance the agreement with Henry's Law.

Having established the closeness of the adsorption isotherm to Henry's Law, it is instructive to analyse the actual capacitance data after the manner employed by Parsons[15] and Dutkiewicz and Parsons[16] to study the dependence on charge or potential of the standard free energy of adsorption.

For the $H_2C_2O_4$ data at constant q_m, the relationship
$$\Delta(1/C) = (1/C_b - 1/C_{dl})_{q_m}$$
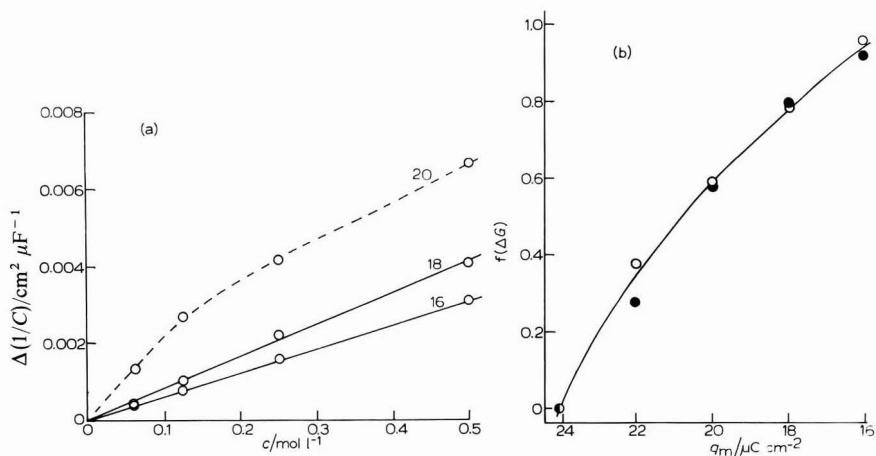
Fig. 8. $H_2C_2O_4$ solns.: (a) dependence on c of $\Delta(1/C)$, lines drawn through data for $q_m = 16, 18 \ \mu C \ cm^{-2}$, broken curve for $q_m = 20 \ \mu C \ cm^{-2}$; (b) charge dependence of $f(\Delta G)$: (○) Δ log concn. from Fig. 6. (●) Δ log d$(\Delta 1/C)$/dc. (Both equivalent to $\Delta(\Delta G/RT)$).

may be applied to investigate the dependence of $\Delta(1/C)$ on c (where C_b is the capacitance in $HClO_4$ alone). This is shown in Fig. 8(a). When such plots take the form of straight lines (as for the data for $q_m = 16, 18 \ \mu C \ cm^{-2}$) the slopes can be used to follow the dependence of the adsorption energy on q_m. In the present work, however, for $q_m \geqq 20 \ \mu C \ cm^{-2}$, the form of the $\Delta(1/C)$–c graph is distinctly curved. This reflects the difficulty in establishing values of C_b without including errors arising from the adsorption of ClO_4^- ions. The data at the highest oxalic acid concentration are unlikely to be seriously affected by such errors, since (for $q_m \geqq 20 \ \mu C \ cm^{-2}$) $C_{dl} \gg C_b$. Thus for these charge values, a tentative estimate of the slope may be taken from the 0.5 M $H_2C_2O_4$ data alone. Figure 8(b) shows the dependence of the logarithm of these slopes on q_m (closed circles). The open circles are derived from the amounts the respective curve segments of Fig. 6(a) had to be moved along the log c axis for coincidence. Both methods show that the free energy of adsorption shows a non-linear dependence on q_m in the necessarily restricted range of charge amenable to analysis.

Since for the $K_2C_2O_4$ solutions it is impossible to obtain C_b corresponding to the much higher q_m values, it is again necessary to examine the data at constant potential. In this case, when Henry's Law is obeyed, it has been shown[15] that log ΔC should depend linearly on E, when ΔG is a linear function of the potential, where $\Delta C = (C_{dl} - C_b)_E$. Figure 9 shows the dependence of log ΔC on E for the four solutions. Apart from slight deviations at both extremely high ($\Delta C > 1,000 \ \mu F \ cm^{-2}$) and low ($\Delta C < 10 \ \mu F \ cm^{-2}$) values, the data lie close to parallel straight lines. This is itself a measure of how closely the data show a linear dependence of the adsorption free energy on potential. The fact that these lines show a 52 mV per decade of concentration shift along the potential axis, rather than the 46 mV dependences noted for Fig. 3 probably indicates an effect of NO_3^- adsorption. A linear potential dependence of the adsorption energy was also derived from the shift of the data of Fig. 7 to fit a single line.

The behaviour of oxalate ions is thus in marked contrast to the behaviour
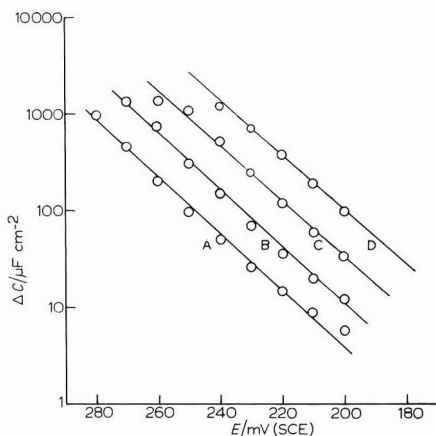
Fig. 9. $K_2C_2O_4$ solns.: dependence of ΔC on E. (Code as in Fig. 2(b)).

found by Payne for NO_3^- [9] and ClO_4^- [10] adsorption, where these ions were studied in solutions containing F^- ions, whose adsorption may usually be discounted. The oxalate adsorption appears to bear closer resemblance to that of I^- in formamide solutions[11]. It is surprising that the larger oxalate ion should show behaviour more nearly like point charges, than the smaller NO_3^- or ClO_4^- ions.

It seems unlikely that this oxalate adsorption behaviour can result solely from competitive adsorption of NO_3^- and ClO_4^- in the solutions studied in the present work, since in both base electrolyte solutions the capacitance remains less than about 50 μF cm^{-2}, whereas the capacitance in the presence of $C_2O_4^{2-}$ adsorption exceeds 1,000 μF cm^{-2} at several points in the $K_2C_2O_4$ solutions data.

When adsorption in the diffuse double layer is neglected or eliminated, it has been shown[1] that for point charges in a continuous dielectric, $(\partial q_m/\partial q_1)_E$ represents an apparent distance ratio $(x_2 - x_1)/x_2$, if the infinite imaging model of the interface is applied[12]. For the $K_2C_2O_4$ solutions, the dependence of $\Delta\gamma$ on log c_0 is shown in Fig. 10 for 6 potentials. Estimates of the distance ratio are then given from the dependence of q_1 (obtained from $(\partial\Delta\gamma/\partial\mu)_E$; Fig. 10) on q_m, which is shown in Fig. 11 for a potential sufficiently anodic for the respective errors in q_1 and q_m to be small. This datum leads to a value of 0.65, and in general at other potentials and concentrations estimated values of the distance ratio lie between 0.5 and 0.7.

An estimate of the ratio of the inner layer potential, φ_1 and the potential difference across the compact layer, $(\varphi_m - \varphi_2)(=\varphi_m$ when the diffuse layer is neglected) may be made from the dependence on potential of the adsorption energy. The (53 mV)$^{-1}$ dependence on potential of the adsorption energy. The (53 mV)$^{-1}$ dependence noted from Fig. 9 and also from the shift of the data along the concentration scale in Fig. 7, lead to $\varphi_1/\varphi_m = 0.55$. This parameter approaches the distance ratio if a linear potential gradient can be applied across the compact layer, an assumption which is unlikely to hold when large doubly charged anions are adsorbed as in the present case.

The Henry's Law constant, $K = \Gamma/c_0$, exhibits a potential dependence reflecting the φ_1 behaviour. For the 0.1 M $K_2C_2O_4$ solution, the present data give $K = 15.4$ cm at 240 mV (SCE). Calculations of K for the oxalic acid solutions show values consis-
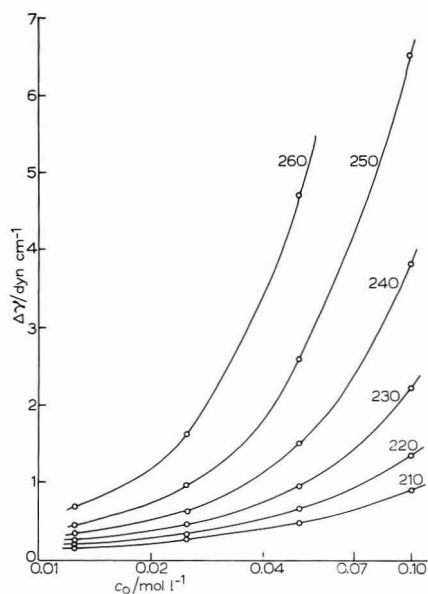
Fig. 10. $K_2C_2O_4$ solns.: dependence of $\Delta\gamma$ on log c_0; numbers above lines denote potentials vs. SCE.
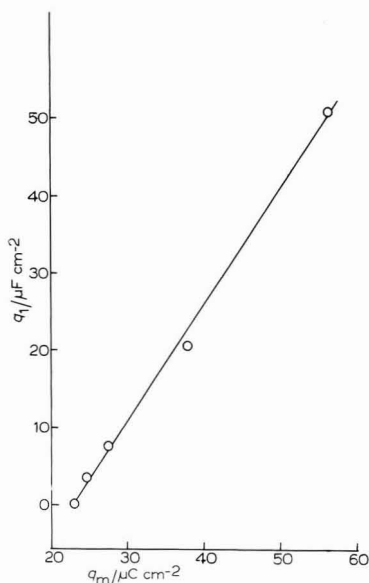
Fig. 11. $K_2C_2O_4$ solns. at 250 mV (SCE): dependence of q_1 on q_m.

TABLE 1

COMPARISON OF ESTIMATES OF "DISTANCE RATIO" PARAMETERS

Quantity	Method of estimation	Solutions	Value
$\dfrac{x_2-x_1}{x_2}$	$\left(\dfrac{\partial q_m}{\partial q_1}\right)_E$	$K_2C_2O_4$ only	0.6 ± 0.1
$\dfrac{\varphi_1}{\varphi_m}$	Shift of isotherm with potential	$K_2C_2O_4$ only	0.56
$\dfrac{\varphi_1}{\varphi_m}$	Total shift of isotherm with potential	$K_2C_2O_4$ and $H_2C_2O_4$	0.82
Assuming $\dfrac{x_2-x_1}{x_2}=\dfrac{\varphi_1}{\varphi_m}$	$\left(\dfrac{\partial E}{\partial \ln a}\right)_{C_{d1}=60\ \mu F\ cm^{-2}}$	$K_2C_2O_4$ and $H_2C_2O_4$	0.65
	$\left(\dfrac{\partial E}{\partial \ln a}\right)_{C_{d1}=1,400\ \mu F\ cm^{-2}}$	$K_2C_2O_4$ only	0.65

tent with a mean potential dependence of $(36\ \text{mV})^{-1}$, over the overall concentration range. Since this differs from the shift of the isotherm in the $K_2C_2O_4$ solutions alone, the adsorption free energy does deviate from a linear potential dependence over the total potential range studied (more than 200 mV).

The final method used to give an estimate of the distance ratio is the less rigorous analysis of the shift of the C_{d1} curves along the potential axis, with decreasing c_0. Table 1 summarises the various estimates outlined above.

Under conditions where the adsorption is governed by Henry's Law, and the adsorption energy is linearly potential dependent, the values of the charge difference Δq_m, between the curves of Fig. 4(b) and the base curves, should show an exponential potential dependence, assuming the distance ratio to vary little with potential in the range studied. This is tested in Fig. 12, where the slope of the line in Fig. 12(a) is near
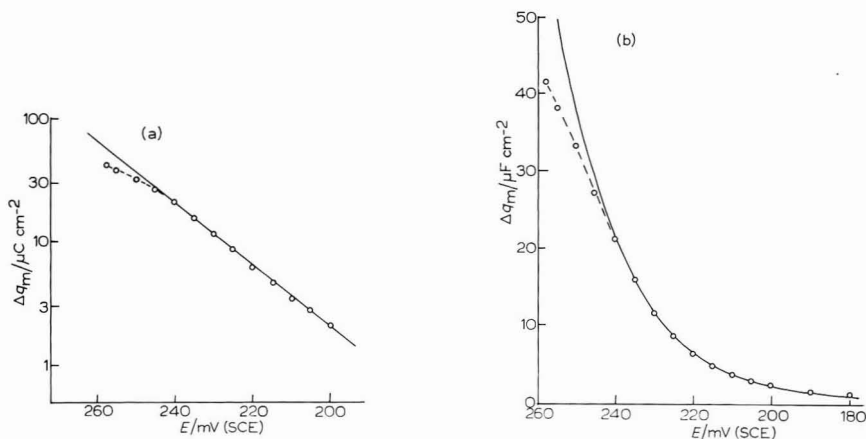
Fig. 12. 0.1 M $K_2C_2O_4$ soln.: (a) potential dependence of log Δq_m, (b) potential dependence of Δq_m. Extrapolated full line and curve refer to Henry's Law behaviour fitted to data at low Δq_m.

to the expected $(46 \text{ mV})^{-1}$ corresponding to the shift of the $C_{dl}-E$ curves. Figure 12(b) shows the close agreement of the data at $\Delta q_m \leq 20 \ \mu C \ cm^{-2}$ with the exponential form. It is also seen that although the deviations at high Δq_m values are significant, they are by no means pronounced. If the various tests of the adsorption isotherm are compared, the observation of a peak in the capacitance curve is by far the most sensitive test for departure from Henry's Law (the law would predict an indefinite exponential increase of C_{dl} with E). The $C_{dl}-E$ curve has the great advantage of acting as a continuous monitor of the interface, all the way to phase formation, whereas Φ or $\Delta \gamma$ can only partially reflect the limiting anodic behaviour.

(ii) Adsorption kinetics

Since it was shown that in the oxalic acid solutions, the adsorbed species was $C_2O_4^{2-}$, the possibility that the rate of dissociation of the acid to form the ions could be reflected in the adsorption kinetics was investigated. Armstrong[13] has recently shown that when a homogeneous reaction in solution is coupled with an adsorption process, the overall kinetics can be examined in terms of three characteristic relaxation times. Two of these are mean times, with a particular distribution about them corresponding to the relaxation of diffusion processes[14]. The third time is a single value characteristic of the kinetics of the homogeneous reaction in solution. Consider the overall reaction:

$$H_2C_2O_4 \underset{k'}{\overset{k}{\rightleftharpoons}} C_2O_4^{2-} + 2H^+$$
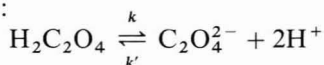
where k and k' are pseudo first order rate constants. Then when c and c_0 are the acid and ion concentrations, respectively, it is predicted that the three times will be given by:

$$\tau_{D1} = \left(\frac{\partial \Gamma}{\partial c_0}\right)_E^2 / D$$

$$\tau_{D2} = \left(\frac{\partial \Gamma}{\partial c_0}\right)_E^2 \left(\frac{c_0}{c_0+c}\right)^2 / D$$

$$\tau_R = \left(\frac{\partial \Gamma}{\partial c_0}\right)_E / k_0^{\frac{1}{2}} D^{\frac{1}{2}}$$

where $k_0 = k(1 + c_0/c)$.

Thus if τ_{D1} and τ_{D2} are substantially separated, as in the case of the oxalic acid solutions, and if τ_R lies between them, the reaction kinetics may be amenable to analysis. Alternatively, as in the present case, where very little frequency dispersion of the impedance is observed, an upper limit may be ascribed to τ_R, and a lower limit for k_0 calculated from the observed values of $(\partial \Gamma/\partial c_0)_E$. To calculate this quantity, it is
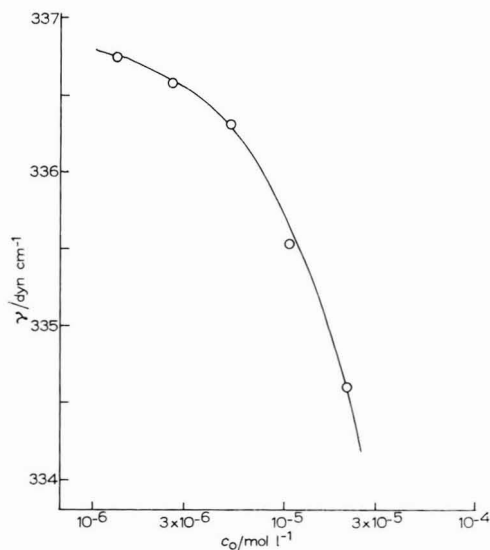
Fig. 13. $H_2C_2O_4$ solns. at $+600$ mV (H_2): dependence of γ on log c_0.

necessary to analyse the dependence of γ on c_0. Figure 13 shows the dependence of γ on log c_0 for the oxalic acid solutions at $+600$ mV (H_2). To obtain $(\partial \Gamma/\partial c_0)_E$ directly from the graph involves taking the slope at several points, and the data corresponding to intermediate concentrations only could be used, thereby omitting the most crucial point which represents the highest concentration near the anodic limit. This point is obviously the best to actually test for the magnitude of any frequency dispersion of the capacitance, which is considerably higher than in the base electrolyte at this potential. A method of making full use of the data of Fig. 13 is as follows. If it is assumed that $\Gamma = Kc_0$, and since $\Gamma = (\partial \gamma/\partial \mu)_E$ it follows that the form of the γ–c_0 relationship is

$$\gamma = \gamma_b - bc_0$$

then

$$\left(\frac{\partial \gamma}{\partial (\log c_0)}\right)_E = \frac{bc_0}{RT}$$

and

$$\left(\frac{\partial \Gamma}{\partial c_0}\right)_E = \frac{b}{RT}$$

To determine the constant b, the values of γ for the highest and lowest concentrations shown in Fig. 13 were fitted numerically to this form of equation. The agreement of the calculated curve drawn through the other points in Fig. 13 is quite adequate. These data then lead directly to the value 4.3×10^{-3} cm for $(\partial \Gamma / \partial c_0)_E$ at 600 mV (H_2).

At this potential, the capacitance in the most concentrated oxalic acid solution was examined as a function of frequency in the range 100 Hz–25 kHz. The capacitance at this potential was about 106 μF cm^{-2}, thus being about 75 μF cm^{-2} higher than in the base electrolyte. Any frequency dispersion arising from relaxation of any process connected with the adsorption would then be expected to be reflected substantially in the measurements of the total interfacial capacitance. Of course, the capacitance is also extremely potential dependent at this point, since the anodic rise is well under way. The results therefore show some random scatter, reflecting the difficulty of returning to exactly the same potential when making successive measurements at different frequencies.
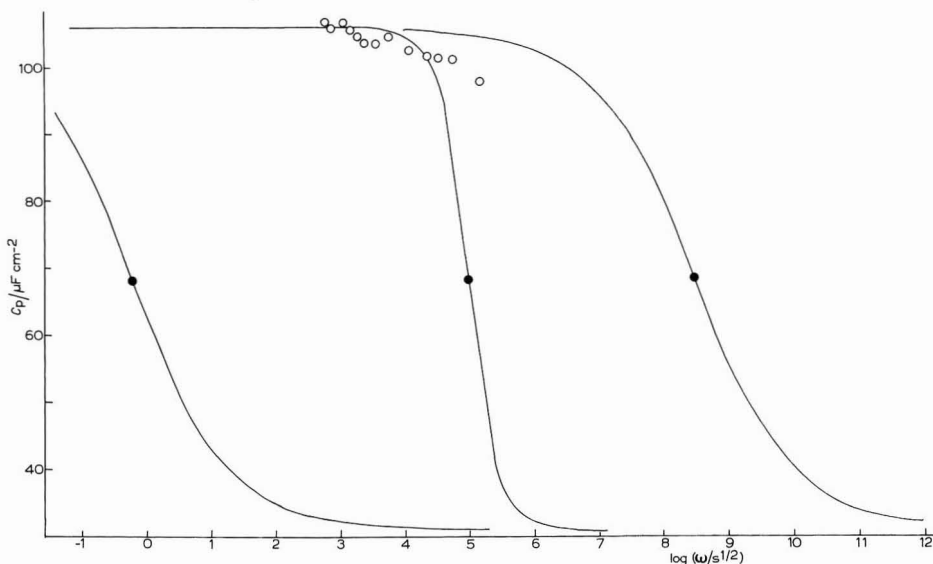
Fig. 14. 0.5 M $H_2C_2O_4$ soln. at 600 mV (H_2): exptl. capacitance values as a function of log ω. Curves drawn through solid circles representing behaviour characteristic of relaxation times: $\tau_{D1} = 1.85$ s, $\tau_R = 10^{-5}$ s, $\tau_{D2} = 3.4 \times 10^{-9}$ s.

Figure 14 shows the predicted dependences of the parallel circuit interfacial capacitance for relaxations where the C_p value falls from 106 to 31 μF cm^{-2} on spanning the relaxation, using the values of τ_{D1} and τ_{D2} pertaining to the value of $(\partial \Gamma / \partial c_0)_E$ already estimated, using the distribution of times postulated previously[14]. The measured frequency dispersion is slight, and could include slight instrumental errors due

to the increasing effect of residual circuit inductance when high capacitances are measured at progressively higher frequencies[4]. The curve drawn near the points corresponds to the maximum value of τ_R which could be compatible with the data, viz. $\tau_R = 10^{-5}$ s. From this it is estimated that the lowest value of k_0 is 1.8×10^{10} s^{-1}, which is not inconsistent with accepted values for the rates of protonation reactions.

It should be pointed out that if the dissociation of oxalic acid does eventually control the adsorption kinetics at much higher frequencies, it may not necessarily be the rate of the homogeneous reaction which is involved, but possibly the rate of a heterogeneous reaction on the mercury surface.

The frequency dispersion in the most dilute oxalic acid solution near the anodic limit, was more pronounced than that shown in Fig. 12. Since in this case the resistance was also observed to be frequency dependent, it was possible to analyse the data quantitatively. The solution resistance, as measured at very high frequency, or cathodic potentials, was subtracted from the series resistance measured at frequencies between 300 Hz and 5 kHz. The remaining resistance term, and the interfacial capacitance were then converted to their equivalent parallel circuit values, and it was found that both C_p and R_p showed a linear dependence on $\omega^{-\frac{1}{2}}$. This shows that a reversible faradaic process is taking place at the mercury electrode[2]. Figure 15 shows
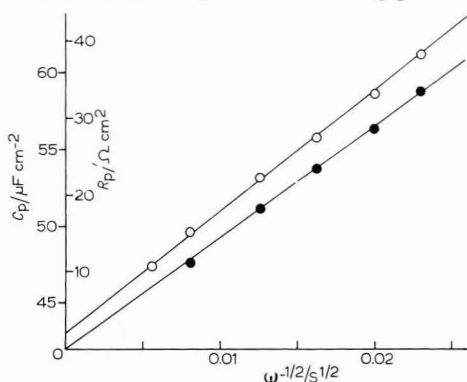
Fig. 15. 0.0313 M H$_2$C$_2$O$_4$ soln. at 640 mV (H$_2$): faradaic impedance analysis.

that the R_p graph extrapolates through the origin at infinite frequency, as required for a reversible process. Moreover, the two estimates of $c_0' D_0^{\frac{1}{2}}$ given from the respective slopes of the lines of Fig. 15, agree, and are identical with the value of the same term for mercury in 1 M HClO$_4$ alone[6]. Thus it is found that as the oxalate concentration becomes very low, the limiting anodic behaviour of mercury tends to its equivalent behaviour in the base electrolyte alone, with the capacity rise due to oxalate adsorption being progressively cut off as the concentration is reduced to values less than 10^{-6} M.

Since the faradaic contribution to the impedance is reduced by about an order of magnitude on moving 30 mV cathodic, only very slight dispersion would be expected at +600 mV (H$_2$). Although the dispersion noted at this potential was too small to be analysed quantitatively, it is probable that it arose mainly from the faradaic process. Thus the minimum reaction relaxation frequency may be considerably higher than the estimate already made, and consequently an even higher minimum value of k_0 is possible.

CONCLUSIONS

The adsorption of oxalate species at a mercury electrode has been studied at potentials up to the limit of anodic polarisation using measurements of the impedance of the interface. The adsorbed species is invariably the $C_2O_4^{2-}$ ion, even when its concentration is much less than those of oxalic acid or the $HC_2O_4^-$ ion.

Under most experimental conditions, the adsorption isotherm is close to Henry's Law, though at extreme anodic potentials there are significant deviations from this form. This adsorption behaviour may result in part from the competitive adsorption of anions from the support electrolytes at anodic potentials.

Near the limit of anodic polarisation, first a monolayer, then a thick film of mercurous oxalate form on the electrode surface. Many of the features connected with adsorption and phase formation, such as the potential of the discontinuity in the $C_{dl}-E$ curves, and the anodic capacitance rise and peak, all show continuous systematic trends through the wide range of $C_2O_4^{2-}$ concentration studied. Only slight departure from a linear dependence of the free energy of adsorption on potential is observed; the non-linear dependence on charge may result partly from competitive adsorption.

In solutions of oxalic acid, the rate of the dissociation reaction to produce $C_2O_4^{2-}$ ions does not impose any significant limit on the overall adsorption kinetics. The slight frequency dependence of the interfacial impedance for the most dilute solutions can be explained solely in terms of the dissolution of mercury, exactly as in the base electrolyte solutions alone.

NOTE ADDED IN PROOF

As De Levie and Pospíšil have recently pointed out (*J. Electroanal. Chem.*, 22 (1969) 277), equations (5) and (6) in ref. 14 were reproduced erroneously. They should have read as follows:

$$C_p = C_\infty + \frac{\Delta C\left[\left(\frac{\partial \Gamma}{\partial c}\right)_\phi \left(\frac{2\omega}{D}\right)^{\frac{1}{2}} + 2\right]}{\left[\left(\frac{\partial \Gamma}{\partial c}\right)_\phi \left(\frac{2\omega}{D}\right)^{\frac{1}{2}} + 1\right]^2 + 1} \tag{5}$$

$$\frac{1}{\omega R_p} = \frac{\Delta C \left(\frac{\partial \Gamma}{\partial c}\right)_\phi \left(\frac{2\omega}{D}\right)^{\frac{1}{2}}}{\left[\left(\frac{\partial \Gamma}{\partial c}\right)_\phi \left(\frac{2\omega}{D}\right)^{\frac{1}{2}} + 1\right]^2 + 1} \tag{6}$$

SUMMARY

The adsorption of $C_2O_4^{2-}$ ions at a mercury electrode follows a Henry's Law isotherm, at potentials cathodic to the formation potential of mercurous oxalate. In solutions when $H_2C_2O_4$, and/or $HC_2O_4^-$ are present at much higher concentrations than $C_2O_4^{2-}$, the adsorbed species is still found to be $C_2O_4^{2-}$ ion. The rate of the adsorption process in oxalic acid solutions is not significantly limited by the kinetics of the acid dissociation reaction.

REFERENCES

1 R. D. ARMSTRONG, D. F. PORTER AND H. R. THIRSK, *J. Electroanal. Chem.*, 16 (1968) 219.
2 R. D. ARMSTRONG, W. P. RACE AND H. R. THIRSK, *J. Electroanal. Chem.*, 19 (1968) 233.
3 R. D. ARMSTRONG, W. P. RACE AND H. R. THIRSK, *J. Electroanal. Chem.*, 23 (1969) 351.
4 R. D. ARMSTRONG, W. P. RACE AND H. R. THIRSK, *Electrochim. Acta*, 13 (1968) 215.
5 R. D. ARMSTRONG AND M. FLEISCHMANN, *Z. Physik. Chem. NF.*, 52 (1967) 131.
6 R. D. ARMSTRONG, W. P. RACE AND H. R. THIRSK, *J. Electroanal. Chem.*, 22 (1969) 207.
7 G. GOUY, *Ann. Chim. Phys.*, 29 (1903) 145.
8 R. PARSONS, *Proc. Roy. Soc. London*, 261A (1961) 79.
9 R. PAYNE, *J. Phys. Chem.*, 69 (1965) 4113.
10 R. PAYNE, *J. Phys. Chem.*, 70 (1966) 204.
11 R. PAYNE, *J. Chem. Phys.*, 42 (1965) 3371.
12 C. A. BARLOW AND J. R. MACDONALD, *J. Chem. Phys.*, 40 (1964) 1535.
13 R. D. ARMSTRONG, *J. Electroanal. Chem.*, 22 (1969) 49.
14 R. D. ARMSTRONG, W. P. RACE AND H. R. THIRSK, *J. Electroanal. Chem.*, 16 (1968) 517.
15 R. PARSONS, *J. Electroanal. Chem.*, 5 (1963) 397.
16 E. DUTKIEWICZ AND R. PARSONS, *J. Electroanal. Chem.*, 11 (1966) 100.

ADSORPTION OF CAMPHOR, CAMPHENE, PINENE, NAPHTHALENE AND NONYLIC ACID AT THE MERCURY–SOLUTION INTERFACE

K. G. BAIKERIKAR AND S. SATHYANARAYANA

Department of Chemistry, Indian Institute of Technology, Bombay, Powai, Bombay-76 (India)

(Received July 14th, 1969)

INTRODUCTION

In a previous communication[1] a theory was proposed for the analysis of differential capacitance curves obtained with compounds undergoing a two-dimensional association during adsorption at the mercury–solution interface. Camphor is typical of this class of compounds. In the present work, experimental data on the adsorption of camphor for different bulk concentrations have been obtained by equilibrium capacitance measurements. In order to correlate molecular structure with the possibilities of two-dimensional association in the double layer, the adsorption of certain other compounds, *viz.* camphene, α-pinene, n-nonylic acid and naphthalene, has also been studied by equilibrium capacitance measurements.

EXPERIMENTAL

Hanging mercury drop electrode (HMDE)

In order to allow for a slow diffusion of the surfactants, a hanging mercury drop electrode was used for equilibrium capacitance measurements. The HMDE was of an all-glass burette-type construction used by Melik-Gaikazyan *et al.*[2]. The capillary tip had a bore diameter of about 100 μ and an external diameter of about one millimeter. The capillary was cut so that the plane of the tip was normal to its axis. The HMDE unit was cleaned with hot chromic acid, then with hot AnalaR sulphuric acid and washed with twice-distilled water. The vacuum stop-cock was greased with Apiezon-N. The burette was filled by suction with hot, twice-distilled water through the capillary and immediately part of the burette was filled by suction with a small amount of redistilled mercury. By careful turning of the stop-cock, a mercury drop could be hung at the tip. The extraordinary sensitivity of the HMDE to temperature fluctuations necessitated a Perspex enclosure for the electrode, the cell and accessories. In addition, the temperature of the room itself was controlled. It was thus possible to keep the area of the hanging mercury drop constant to within $\pm 1\%$ for more than 30 min.

The HMDE unit was cleaned and set up afresh for each experiment. A new mercury drop was taken for capacitance measurement at each potential. After a few experiments with surfactants, the mercury drop was found to become detached spontaneously in a few minutes. It was then necessary to change the capillary.

The area of the mercury drop was measured as follows: if the HMDE is set

up keeping the capillary axis vertical, the mercury drop is under the action of gravity and its shape is that of a prolate spheroid. The area S is therefore given by

$$S = 2\pi b^2 + 2\pi ab\varepsilon^{-1}\sin^{-1}\varepsilon$$

where $2a$ and $2b$ are the lengths of major and minor axes, and $\varepsilon^2 = [1 - (b/a)^2]$; $2a$ and $2b$ were measured precisely to $\pm 0.3\%$ by a vernier microscope kept outside the Perspex enclosure. The area of HMDE was in the range 0.03–0.04 cm^2.

Cell

The cell used was of all-glass construction with suitable inlets through un-greased ground glass joints for the HMDE, reference electrode and surfactant addition unit. Since 0.5 M Na$_2$SO$_4$ solution was employed as the supporting electrolyte in all experiments, a reference electrode of mercury–mercurous sulphate type in 0.5 M Na$_2$SO$_4$ solution was used. This electrode was connected to the cell through a salt bridge with an ungreased stop-cock. The bridge, filled with 0.5 M Na$_2$SO$_4$ solution, terminated in a Luggin capillary close to the HMDE, thus practically avoiding liquid junction potentials. A large platinum cylinder surrounding the HMDE was used as the auxiliary electrode. The observation of the HMDE for area measurement was possible through holes drilled into the platinum cylinder. The latter was lightly amalgamated to keep it well nonpolarised and to minimise any drift in potential. The potential of the HMDE could then be kept constant to within ± 0.5 mV over a period of 30 min. This care is necessary in order to make reliable measurements of capacitance *change* with time at constant potential.

Capacity measurements

The differential capacity measurements were made with the classical bridge method which is essentially the same as that of Grahame[3], in which, as pointed out later by Damaskin[4], there is a significant advantage in using the polarising source of e.m.f. not across the cell but across a diagonal of the bridge. Necessary shielding and careful grounding were provided to minimise parasitic capacitances. A low frequency selective amplifier reduced the noise level such that the capacitance measurements with standard capacitors could be made correct to $\pm 0.2\%$ when the test signal at 45 Hz was of 5 mV amplitude across the standard capacitor (test arm of the bridge). Under the same conditions, capacitance data with HMDE for 1.0 M KCl solution showed a mean deviation of less than $\pm 0.5\%$ when compared with the data of Grahame [5], except at extreme positive potentials. All measurements were carried out at 45 Hz frequency and with 5 mV (r.m.s.) amplitude.

Polarisation circuit

The polarisation circuit was of low resistance (less than 200 Ω). The potential of HMDE was measured correct to ± 0.2 mV against that of the reference electrode using a high resistance potentiometer.

Chemicals

Mercury was purified by prolonged aeration under hot dilute alkali, hot dilute nitric acid and finally under doubly-distilled water. It was then dried, filtered and distilled under vacuum.

Care was taken to prevent contamination of chemicals by surface-active impurities. Doubly-distilled water, the second distillation being carried out over alkaline permanganate in an all-glass assembly, was used to prepare solutions. AnalaR sodium sulphate was recrystallised from this water and ignited in air at about 500°C.

Electrolytic hydrogen was purified by passing it successively through finely divided heated copper catalyst, activated carbon, soda lime and silica gel, in an all-glass unit. The purified gas was bubbled through the solution in the cell for deaeration. A helical coil of glass tube was used to connect the cell with the gas purification unit.

Camphor, camphene and naphthalene were recrystallised once from distilled methanol and then sublimed. Nonylic acid and α-pinene were distilled before use in an all-glass unit. The melting or boiling points of these purified surfactants were in agreement with the literature data.

Procedure

A solution of 0.5 M Na_2SO_4 was used throughout as the base electrolyte. Owing to the low solubility of camphor, a solution of camphor in aqueous methanol (30–50%) was added in the desired quantity to get different concentrations. To a known volume of the deaerated solution in the cell, the camphor solution was added dropwise through a fine capillary tip. This capillary was fused to a reservoir containing the camphor solution and attached to the cell by an ungreased ground glass joint. The dropwise addition of camphor solution was effected by compressing the air space above the camphor solution in the reservoir with a flexible polyethylene cap so that drops were formed and detached slowly from the vertical tip. After the addition of the desired number of drops of camphor solution, hydrogen was bubbled slowly through the solution for one minute to effect mixing.

A similar procedure was adopted for the addition of naphthalene. However, the extremely low solubilities of camphene, α-pinene and nonylic acid permitted only solutions saturated with these compounds to be studied. Furthermore, stirring for about 3 h by bubbling hydrogen gas was necessary to effect mixing in the case of α-pinene and nonylic acid.

RESULTS

(a) Adsorption of camphor

Equilibrium capacitance values are reached within about a minute with different concentrations (excepting the lowest concentrations) of camphor in solution in the region of potentials of maximum adsorption. Figure 1 shows the experimental data*. Discontinuous transitions in the capacitance curves occur at the desorption potentials for each concentration of camphor. Even for the lowest concentration of camphor in solution, the equilibrium capacitance (equilibrium value is reached in about 5–10 min for lower concentrations and in about 1 min for the higher concentrations) in the region of maximum adsorption is that of a monolayer, *i.e.*, equal to the capacitance at the same potential in the solution saturated with camphor. This interesting result is characteristic of a two-dimensional condensed layer as pointed out

---

* The preliminary capacitance data presented in the previous communication[1] are slightly in error with regard to the data for 0.5 M Na_2SO_4 solution. The error arose owing to an unsuspected change in the calibration of the vernier microscope employed for area measurement of HMDE.
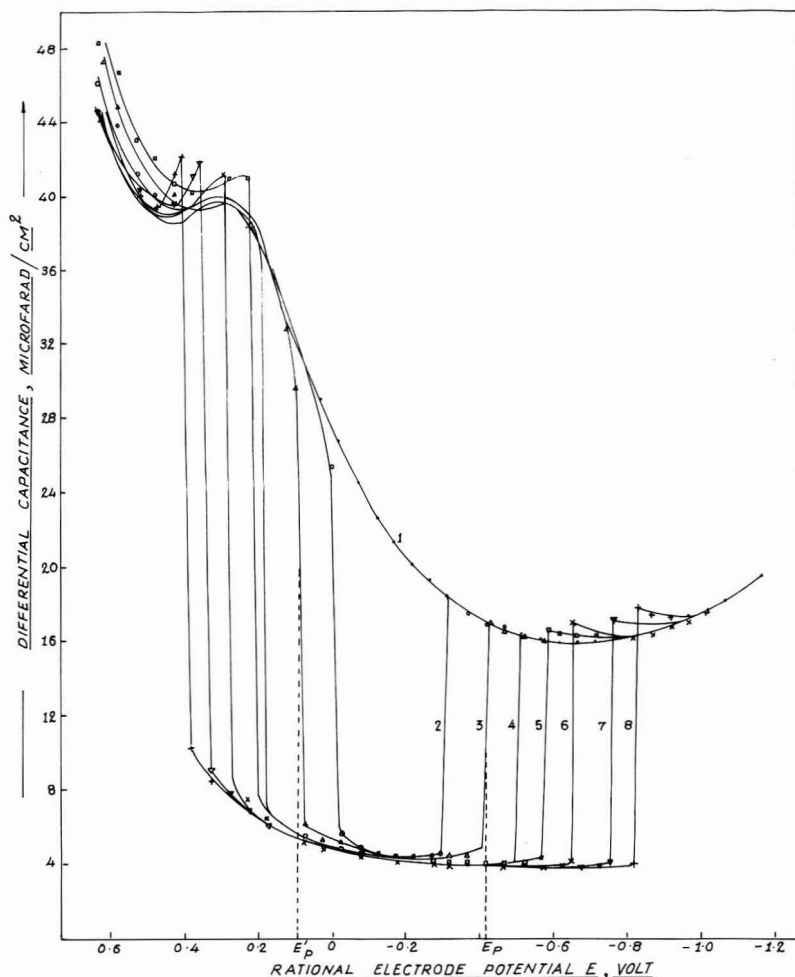
Fig. 1. Differential capacitance–potential curves of a HMDE in 0.5 M Na$_2$SO$_4$ soln. containing camphor at concns.: (1) 0, (2) 5.46×10^{-5}, (3) 8.18×10^{-5}, (4) 13.64×10^{-5}, (5) 21.82×10^{-5}, (6) 35.22×10^{-5}, (7) 88.05×10^{-5}, (8) 176×10^{-5} M. The potential E is expressed $vs.$ the potential of zero charge of mercury in 0.5 M Na$_2$SO$_4$ soln. Frequency: 45 Hz.

in the previous work[1]. The capacitance data at and near the desorption potentials, E_P and E'_P in Fig. 1, however, do not represent equilibrium values. This is to be expected since, for equilibrium to exist along the whole curve, the area enclosed between the curves for the base electrolyte and a given solution must equal the sum of the areas of the capacitance peaks. In the absence of the capacitance peaks, the above condition is not fulfilled. A comparison with our present data shows that the capacitance data for camphor solutions obtained by earlier workers[6-8] with the aid of a dropping mercury electrode are all non-equilibrium values, including the data in the region of maximum adsorption. Likewise, the evaluation of the adsorption isotherm for camphor from capacitance data[6] is incorrect since our present data with HMDE show that the capacitance (and hence coverage) at equilibrium is independent of concentration in

the region of potentials of maximum adsorption.

Figure 2 shows the capacitance data obtained when the solution is saturated with camphor and when the potential of HMDE is changed in steps of about one millivolt only at and near the desorption potentials. At these potentials, the capacitance values *increased* with time, reaching the equilibrium value in about 20 min (Fig. 3). Capacitance peaks for adsorbed camphor are thus experimentally realised under equilibrium conditions of measurement at the desorption potentials. For lower concentrations of camphor in solution, capacitance peaks could not be obtained, since capacitance values always decreased with time to the final value of a monolayer (Fig. 3). In other words, equilibrium coverages of fractions of a monolayer could not be achieved at lower concentrations of camphor in solution. The present observations on the kinetics of adsorption of camphor in solution at a HMDE at
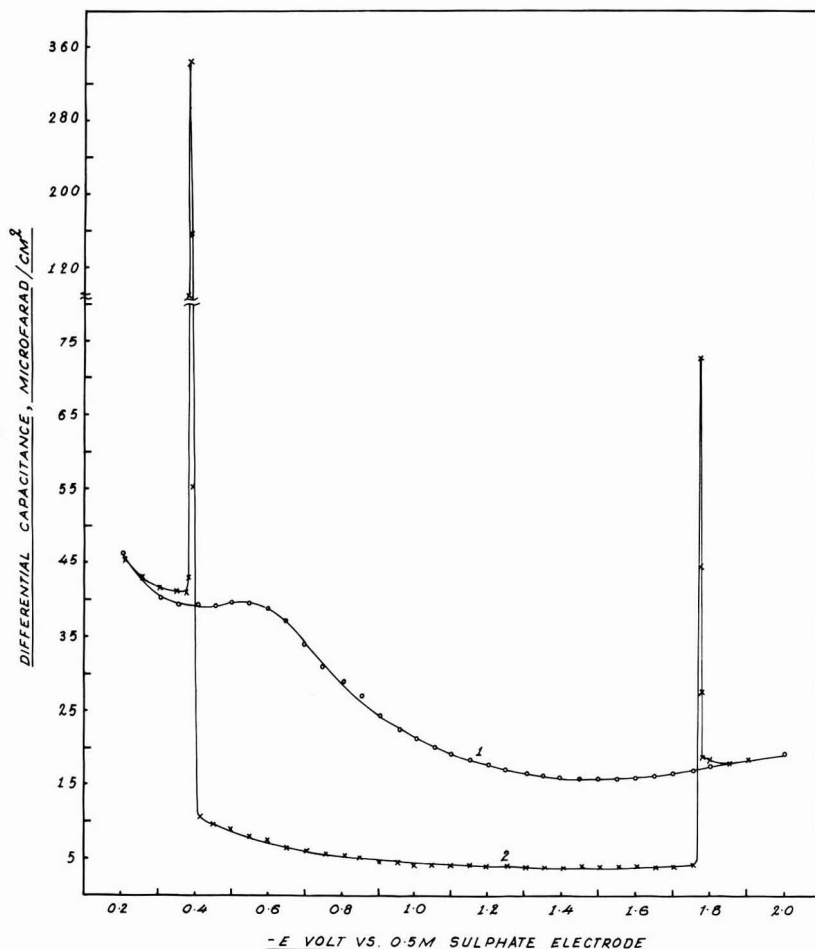
Fig. 2. Differential capacitance–potential curve of a HMDE in: (1) a 0.5 M Na$_2$SO$_4$ soln., (2) 0.5 M Na$_2$SO$_4$ soln. satd. with camphor. Frequency: 45 Hz.
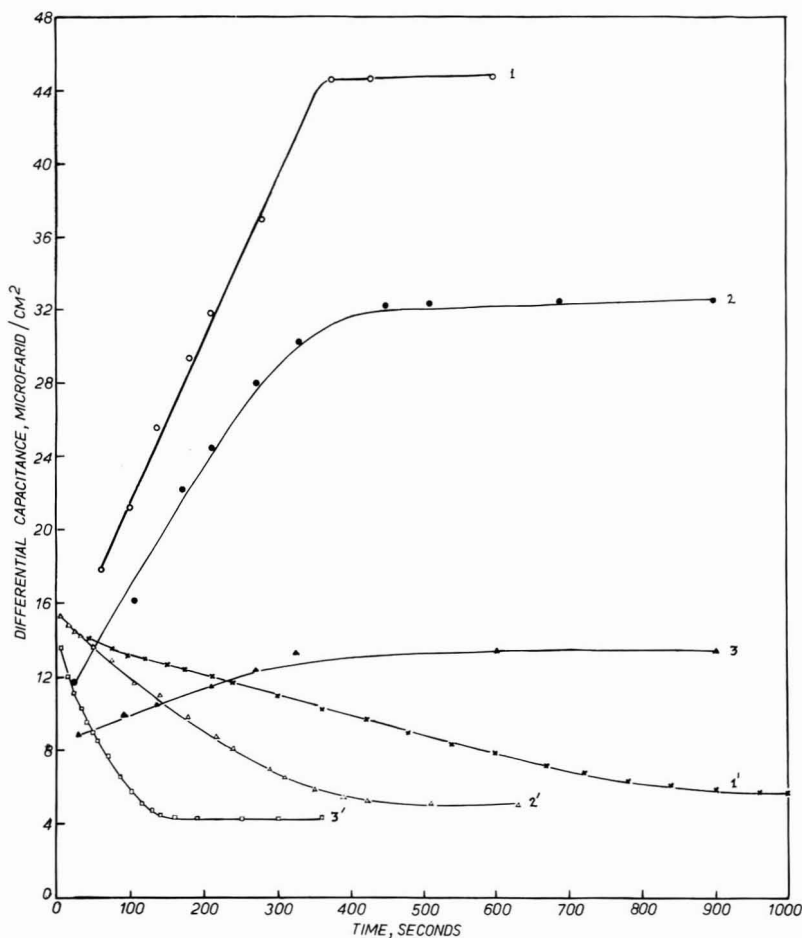
Fig. 3. Time-dependence of capacitance of a HMDE, (a) in 0.5 M Na$_2$SO$_4$ soln. satd. with camphor in the region of cathodic desorption potentials: (1) -1.7743, (2) -1.7755, (3) -1.7730 V; (b) in 0.5 M Na$_2$SO$_4$ soln. containing camphor at concn. 17.08×10^{-5} M in the region of cathodic desorption potentials: (1') -1.3660, (2') -1.3653, (3') -1.3604 V. All potentials refer to the sulphate reference electrode.

different potentials can be, in principle, correlated with a diffusion-controlled approach to adsorption equilibrium at medium coverages. A theoretical study of this observation along with more extensive experimental data on adsorption kinetics will be presented in a subsequent communication.

(b) Adsorption of camphene, α-pinene and nonylic acid

Capacitance data for the adsorption of camphene, α-pinene, and nonylic acid from the corresponding saturated solutions in 0.5 M Na$_2$SO$_4$ were measured as above and are presented in Fig. 4. Characteristic discontinuous transitions at the desorption potentials are observed in the capacitance curves for camphene and α-pinene. The capacitance curve for nonylic acid shows, however, well defined desorption peaks (only the cathodic peak is shown in Fig. 4). As our results for nonylic acid are equilibrium

data obtained after sufficient waiting and with a freshly renewed hanging mercury drop electrode at each potential, they do not show the hysteresis phenomena observed by Lorenz[9].
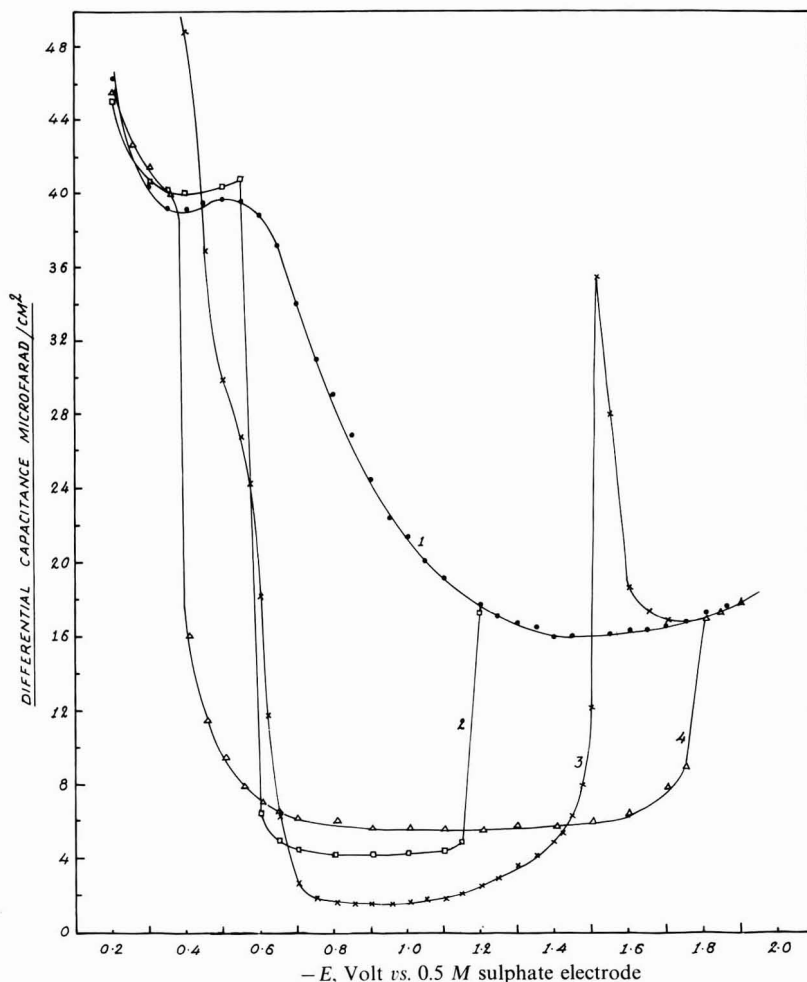
Fig. 4. Differential capacitance–potential curves of a HMDE in : (1) 0.5 M Na$_2$SO$_4$ soln. and in 0.5 M Na$_2$SO$_4$ soln. satd. with (2) camphene, (3) nonylic acid, (4) α-pinene. Frequency : 45 Hz.

(c) *Adsorption of naphthalene*

The capacitance curves for the adsorption of naphthalene from aqueous solution on mercury are shown in Fig. 5. The capacitance values, at equilibrium, in the region of adsorption are dependent on the concentration of naphthalene in solution (unlike that of camphor, see Fig. 1) and the capacitance peaks in the desorption region show smooth change with potential for each concentration (unlike the capacitance "jump" in case of camphor, see Fig. 1).
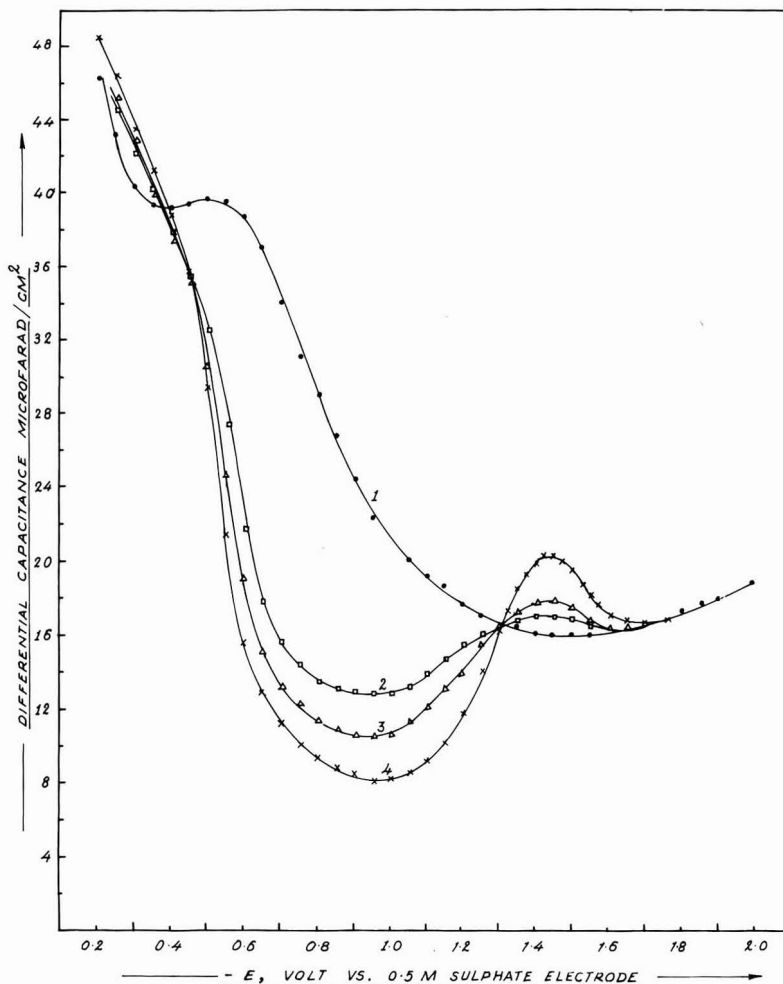
Fig. 5. Differential capacitance–potential curves of a HMDE in 0.5 M Na$_2$SO$_4$ soln. containing naphthalene at concns.: (1) 0, (2) 1.64×10^{-5}, (3) 3.28×10^{-5} M, (4) satd. Frequency: 45 Hz.

DISCUSSION

(a) Camphor

The capacitance data for camphor suggest[1] the existence of a phase transition in the double layer. A method for the evaluation of the adsorption isotherm in the case of a two-dimensional condensation of adsorbed molecules has been proposed by Damaskin and Dyatkina[10]. An important assumption in this method is that the magnitude of the capacitance jump at the critical potentials of desorption, E_P or E'_P (see Fig. 1), is a well defined quantity which may be related to the interaction parameter in the Frumkin adsorption isotherm. However, as seen from Fig. 3, the capacitance values at these potentials are time-dependent; and as seen from Fig. 2, the *equilibrium capacitance* values at these potentials have a large magnitude and no capaci-

tance jump can be recognised. The theoretical approach suggested in ref. 10 cannot therefore be valid in such cases.

An alternative approach to the evaluation of the parameters of the adsorption isotherm in the case of a two-dimensional condensation has been suggested by the present authors[1], based on the Frumkin–Damaskin theory of adsorption pseudo-capacitance[11]. According to this method, if the adsorption is characterised by the following equations (1)–(3)

$$\theta = Bc(1-\theta)\exp(2a\theta) \tag{1}$$

$$C = C_0(1-\theta) + C_1\theta - RT\Gamma_s a''\theta(1-\theta) \text{ in the region } E'_P > E > E_P \tag{2}$$

and,

$$q = q_0(1-\theta) + C_1(E-E_N)\theta - RT\Gamma_s a'\theta(1-\theta) \text{ in the region } |E| > E'_P \text{ or } E_P \tag{3}$$

then, a plot of $(\text{d}\ln c/\text{d}E_P)$ vs. $(q_0 - C_1 E_P)$ gives $RT\Gamma_s$ as the reciprocal slope, and $(C_1 E_N/RT\Gamma_s)$ as the intercept at $q_0 = C_1 E_P$. Here c is the bulk concentration of the surfactant, B the adsorption equilibrium constant, a an interaction parameter, a' and a'' the first and second derivatives of a with respect to potential E, C the differential capacitance, q the charge density on the electrode at E, subscripts 0 and 1 refer to the value of the coverage θ, Γ_s the saturation surface excess of the adsorbate, E_N the adsorption potential and E_P and E'_P the critical potentials of desorption on the cathodic and the anodic sides, respectively. All the potentials are referred to the potential of zero charge of mercury in 0.5 M Na$_2$SO$_4$ solution (-0.830 V vs. 0.5 M sulphate reference electrode).

A successive approximation between (1) and (2) and between (1) and (3) will then permit the calculation of θ, a, etc., at each potential.

The plots of log c vs. E_P and of $(\text{dlog } c/\text{d}E_P)$ vs. $(q_0 - C_1 E_P)$ derived from the data in Fig. 1 are shown in Figs. 6 and 7, respectively. From the region of negative charge densities, where anion specific adsorption is absent (Fig. 7, dashed line), it follows that

$$\Gamma_s = 7.4 \times 10^{-10} \text{ mol cm}^{-2};$$

Molecular area of adsorbed camphor $= 1/\Gamma_s N = 23$ Å^2;

$$E_N = 0.44 \text{ V} \ (= +0.39 \text{ V vs. } 0.5 \ M \text{ sulphate reference electrode})$$

A graphical integration of the capacitance curve in Fig. 2 from the extreme negative potentials towards more positive potentials gives approximately $E_N = -0.40$ V vs. 0.5 M sulphate reference electrode; further, the electrocapillary measurements although found irreproducible as discussed in ref. 1, show that the e.c.m. lies at about -0.40 V vs. 0.5 M sulphate reference electrode for a solution saturated with camphor. The calculated value of E_N above is thus in agreement with experimental values.

The parameters θ, a, etc. at different potentials cannot be evaluated from the data in Fig. 1 using the method proposed above since there is no capacitance change with concentration in the region of adsorption ($E'_P > E > E_P$) and very little of it outside this range. In other words, the adsorption of camphor occurs on an all-or-none basis. Intermediate coverages occur only over a very narrow potential range and isotherm evaluation may be possible by equilibrium measurements in this region.

(b) *Camphene, α-pinene and naphthalene*

The close similarity of capacitance data for camphene and α-pinene to that of camphor shows that these compounds also undergo adsorption with two-dimensional condensation. The ketonic group in camphor is not therefore responsible for the strong interaction on adsorption. On the other hand, the adsorption of naphthalene is not accompanied by any phase transition in the double layer, since, as
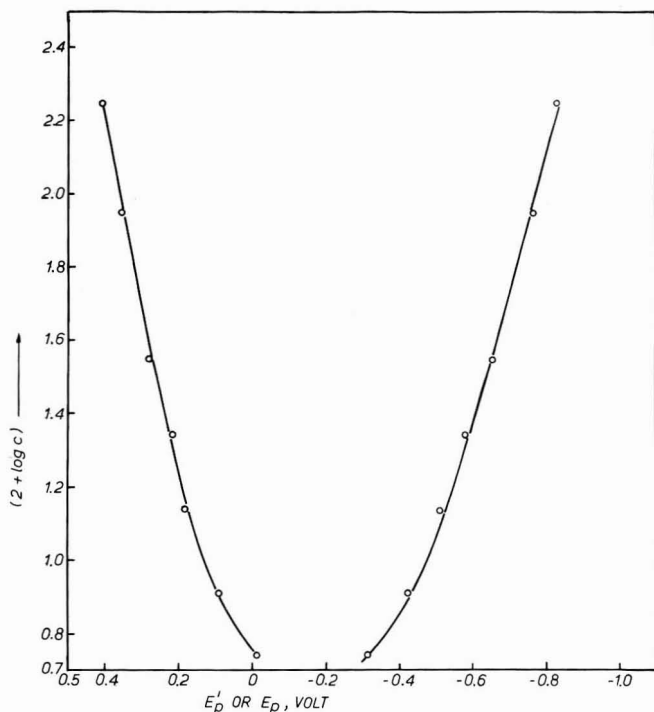
Fig. 6. Plot of log c vs. E'_P (anodic transition potential) or E_P (cathodic transition potential). c is the molar concn. of camphor in soln.

pointed out above, the equilibrium capacitance values change continuously with concentration as well as with potential. Since naphthalene $(C_{10}H_8)$ has the same number of carbon atoms as camphor $(C_{10}H_{16}O)$, camphene $(C_{10}H_{16})$ or α-pinene $(C_{10}H_{16})$, condensation of the latter compounds in the double layer cannot be due to the number of carbon atoms or the large molecular weight.

The tensammetric curves for cyclohexanone adsorption from 1 M KCl solution are given in ref. 12. The smooth variation of capacitance with potential and concentration shows that cyclohexanone is adsorbed on mercury without any condensation.

A comparison of the structures of camphor, camphene and α-pinene, which undergo a phase transition on adsorption, with those of naphthalene and cyclohexanone which do not, shows that a bridged carbon atom in the former class of compounds is perhaps responsible for the two-dimensional condensation effect.

(c) *Nonylic acid*

From the estimated value of the interaction parameter a, it has been concluded[11] that for this long chain compound (and higher homologues) there is a likelihood of adsorption with two-dimensional association. The present data for nonylic acid adsorption (Fig. 4) show that the capacitance change with potential is smooth and the equilibrium capacitance peak from the saturated solution is not as narrow as in the case of camphor. These facts suggest that a two-dimensional association for adsorbed nonylic acid is not as marked as for camphor, camphene and α-pinene.
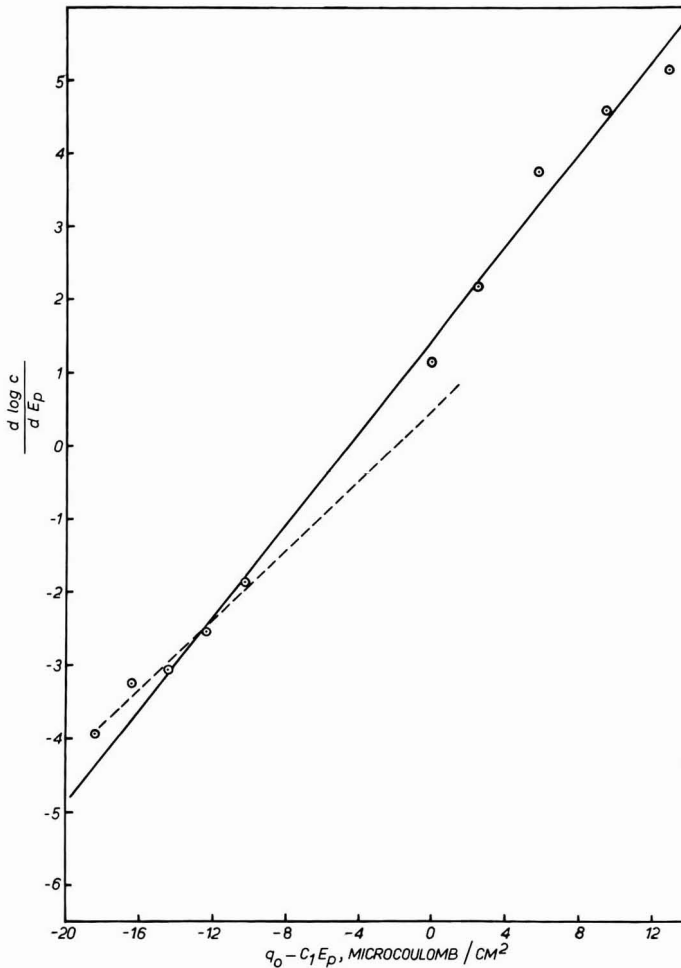
Fig. 7. Plot of $(\mathrm{d}\log c/\mathrm{d}E_P)$ *vs.* $(q_0 - C_1 E_P)$; c and E_P as in Fig. 6; q_0 is charge density on mercury in the base electrolyte; C_1 is the monolayer capacitance with adsorbed camphor.

SUMMARY

The equilibrium capacitance of the interface between mercury and solutions containing camphor has been measured as a function of potential with a hanging drop electrode by using a low frequency (45 Hz) a.c. bridge. The data show that the capacitance in the region of adsorption is always that of a monolayer of adsorbed camphor, independent of its bulk concentration. The capacitance–potential curve for the solution saturated with camphor shows the usual desorption peaks if equilibrium measurements are made at millivolt intervals near the critical potentials of desorption. From a theoretical analysis of the capacitance data, the molecular area on adsorption as well as the adsorption potential for camphor have been calculated. It is shown that camphene and α-pinene are adsorbed like camphor at the mercury–solution interface with phase transition, whereas naphthalene is adsorbed without any phase transition. The capacitance curve for nonylic acid adsorption at the mercury–solution interface is not characterised by any hysteresis if measurements are made at equilibrium on an initially clean surface. A bridged carbon atom in a surfactant, as also a long hydrocarbon chain, seem to give condensed monolayers on adsorption.

REFERENCES

1 S. SATHYANARAYANA AND K. G. BAIKERIKAR, *J. Electroanal. Chem.*, 21 (1969) 449.
2 V. I. MELIK-GAIKAZYAN, V. V. VORONCHIKHINA AND E. A. ZAKHAROVA, *Elektrokhimiya*, 4 (1968) 479.
3 D. C. GRAHAME, *J. Am. Chem. Soc.*, 68 (1946) 301.
4 B. B. DAMASKIN, *Zh. Fiz. Khim.*, 32 (1958) 2199.
5 M. A. V. DEVANATHAN (D. C. GRAHAME's data), *Trans. Faraday Soc.*, 50 (1954) 373.
6 E. O. SHERMAN, *Dissertation Abstr.*, 24 (1963) 488.
7 H. A. LAITINEN, K. EDA AND M. NAKANISHI, *Talanta*, 11 (1964) 321.
8 S. SATHYANARAYANA, *J. Electroanal. Chem.*, 10 (1965) 56.
9 W. LORENZ, *Z. Elektrochem.*, 62 (1958) 192.
10 B. B. DAMASKIN AND S. L. DYATKINA, *Elektrokhimiya*, 2 (1966) 981.
11 A. N. FRUMKIN AND B. B. DAMASKIN in J. O'M. BOCKRIS AND B. E. CONWAY (Eds.), *Sovremennye aspekti elektrokhimii*, Russian translation, YA. M. KOLOTYRKIN (Ed.), Mir, Moscow, 1967, chap. 3.
12 K. TSUJI in T. KAMBARA (Ed.), *Modern Aspects of Polarography*, Plenum Press, New York, 1966, p. 233.

THE ANODIC STRIPPING VOLTAMMETRY OF TRACE SILVER SOLUTIONS EMPLOYING GRAPHITE ELECTRODES APPLICATION TO SILVER ANALYSIS OF RAIN AND SNOW SAMPLES FROM SILVER IODIDE SEEDED CLOUDS

URI EISNER AND HARRY B. MARK, JR.

Department of Chemistry, The University of Michigan, Ann Arbor, Michigan 48104 (U.S.A.)

(Received March 3rd, 1969; in revised form July 8th, 1969)

INTRODUCTION

Anodic stripping voltammetry (ASV) has proved to be a very versatile technique for the determination of trace elements in the concentration range of 10^{-6}–10^{-10} M. The applicability, sensitivity, and limitations of this technique are summarized in detail in two recent and comprehensive reviews by Shain[1] and Barendrecht[2].

Most of the reported analytical applications of ASV have been carried out with the hanging mercury drop electrode provided the elements of interest form amalgams, when deposited, or form anions that react with mercury to form an insoluble film (halides, sulfide)[1,2]. For nobler metals than mercury, a solid electrode must be employed, however. Perone has reported the use of a spectrographic grade graphite electrode (SGE) for the determination of silver[3] and showed that when the concentrations of Ag^+ were less than 10^{-7} M, the subsequent stripping voltammograms showed multiple peaks. As the area under the peak(s) is the parameter measured for analytical evaluation, these multiple peaks impose a difficulty. There is more uncertainty of the position of the base line (background current), as the multiple peaks occur over a large voltage range, which results in lower accuracy and precision in measuring the area. Thus, a sharp and narrow mono peak is favored for higher sensitivity, better precision, and accuracy.

The preparation and pretreatment of a solid electrode are also very critical as they determine the reproducibility and accuracy of the results. This pretreatment may include different kinds of processes: (i) Mechanical, such as grinding and polishing; (ii) Chemical, treatment in acids or bases; and (iii) Electrochemical, subjecting the electrode to deposition and stripping potentials alternately. All these factors have been found to have an effect on the reproducibility of the signal as well as the level of the background current[3–5].

In this work the use of pyrolytic graphite (and other graphite forms) were explored, and the pretreatment, the application procedures and conditions of application, were investigated and defined to enable its use for accurate determinations of trace amounts of silver. The physical nature of the deposited silver on the electrode was also investigated by electron microprobe spectroscopy and the deposit was found to be concentrated on specific sites on the electrode surface.

The pyrolytic graphite electrode (PGE), pretreated in a manner found to

yield the most nearly ideal and reproducible anodic stripping voltammograms, has been used for the determination of trace silver in rain and snow samples. A method is described with which it is possible to analyze samples containing silver concentrations as low as 5×10^{-11} M.

EXPERIMENTAL

Apparatus

      The instrumentation employed was constructed from operational amplifier modules and has been described in detail previously[4]. The scan rates employed in the anodic dissolutions were 10–20 mV s^{-1} as indicated below. The anodic stripping voltammograms were recorded by means of a Moseley autograph model 2D-2M X-Y Recorder. The measuring resistor in the current follower[4] was a 100 kΩ $\pm$ 0.1% wire wound element. For high sensitivity measurements, capacitors of 1–5 μF were connected in parallel with this resistor to reduce the noise level in the current output. The reference electrode system, a saturated calomel electrode (SCE), salt bridge, and auxiliary electrode assemblies are illustrated in Fig. 1. The cell of 30 ml solution capa-
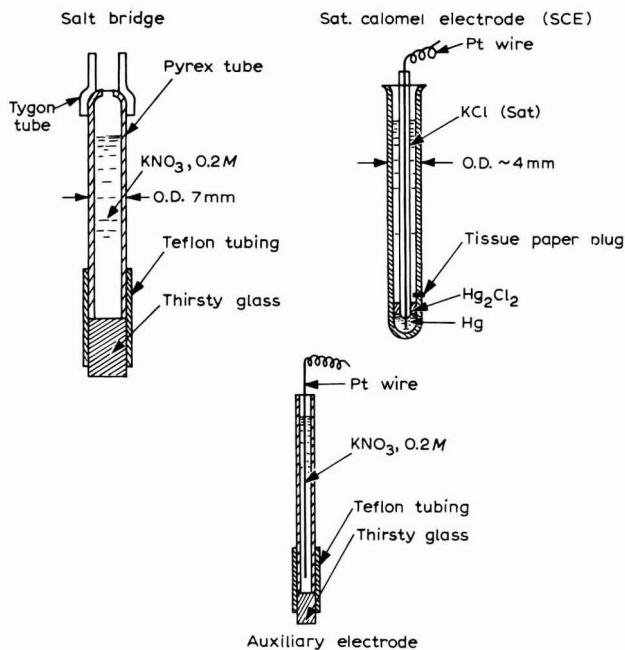
Fig. 1. Schematic diagram of the salt bridge, reference electrode, and auxiliary electrode.

city was constructed from a quartz tube (outside diameter 30 mm). The reference electrode was inserted into the top of the salt bridge. The cell cap was made of Teflon and fitted the cell snugly. Holes were drilled in the cap for insertion of the salt bridge, auxiliary electrode system, and deaeration system. No appreciable surface adsorption of the silver to the cell walls could be detected during the course of any of the anodic stripping analysis experiments (up to a period of 2 h).

Preparation of the electrode

Ceresin wax was melted in a 50 ml distillation flask and the machined pyrolitic graphite rods (6.5 mm in diameter, see ref. 4 for details) were placed into the melt. The distillation flask was then stoppered and connected through a Buchner flask, acting as a trap, to a vacuum system. Air bubbles evolved from the graphite rods, and when no more bubbles could be seen, the flask was opened to the atmosphere and heated to just below the boiling point of the wax. The graphite rods remained in this melt for a few minutes and the vacuum was reapplied. This procedure was repeated until no more bubbles were observed evolving from the surface. The ceresin melt and the rods were then poured into a beaker. The wax was allowed to cool and the rods taken out, when they had a solid coat of wax of about $\frac{1}{2}$ mm. When the rods cooled to room temperature, both ends were cleaved with a razor blade. The pyrolytic graphite rod was then pressed into a thick walled Teflon sleeve[4]. The exposed graphite was ground manually on a No. 600 carborundum paper until it became flush with the holder. It was then polished with a very fine carborundum paper (actually a No. 600 paper used many times previously so that it had become very smooth) which was moistened with ethanol. The ethanol had the effect of removing all the graphite dust from the surface, leaving it very smooth. The rod and sleeve were then transferred to the electrode holder to be used in the cell. Before use and between runs, the electrode was polished with a No. 42 Whatman filter paper mounted on a jeweller's wheel[4]. Towards the completion of the polishing, the paper was moistened with ethanol. The electrode in the cell sample system was connected to the polarization circuit and the potential was scanned anodically from zero volts *vs.* SCE to the point where the background current rose sharply. It was left there until the background current dropped to a steady level (about 1 min). The electrode was then ready for the electrolysis (deposition) step.

The deposition step

The deposition potential employed was -0.60 V *vs.* SCE. A constant stirring rate was attained by means of a magnetic stirrer driven by a 400 rev. min^{-1} synchronous motor and a steady stream of nitrogen (purified according to standard practices[1-4]). The nitrogen flow passed through a narrow polyethylene tube in which a platinum wire was inserted in order to give the tube some rigidity. This tube was placed in a position against the wall of the cell and while the stirrer was on, nitrogen bubbled vigorously in the vicinity of the electrode. The magnetic stirrer was then shut off 15 s before the end of the electrolysis period, but the nitrogen was allowed to flow until the end of the electrolysis period along the walls of the cells. This procedure prevented nitrogen bubbles from adhering to the electrode surface. The nitrogen flow was stopped and the potential then switched to -0.40 V *vs.* SCE.

The stripping step

After a quiescent period of 30 s at -0.40 V during which the current decayed to a steady level, the silver deposit was anodically stripped by means of a linear anodic potential sweep. The area under the peak, which is proportional to the number of coulombs consumed in the stripping process, was measured by weighing the recorder graph paper. The concentration of the sample was determined by adding to the unknown sample solution a known volume of a standard silver solution (standard

addition method) and repeating the determination. Standard solutions were prepared in the same manner as previously described[4].

Reagents

Silver-free NH_4SCN was provided by Dr. J. W. Warberton, University of Nevada, Reno, Nevada. All other reagents were reagent grade and were experimentally shown to present no blank problems. The water employed in making all solutions was passed through a mixed bed ion exchanger and then double-distilled (potassium permanganate was added in the first distillation stage).

RESULTS AND DISCUSSION

The characteristic shapes of the stripping voltammograms of submicro solutions of silver ion depend on the type of graphite electrode used and the composition of the supporting electrolyte. The number of dissolution peaks and their individual shapes are also affected strongly by these conditions, as can be seen in Table 1 and

TABLE 1

EFFECT OF MEDIUM AND ELECTRODE MATERIAL ON THE ANODIC DISSOLUTION VOLTAMMOGRAMS OF SILVER SOLUTIONS

Electrolyte medium	Electrode material	Potential of anodic dissolution peaks/ V vs. SCE
0.15 M NH_4OH and	SGE	−0.02, +0.38
0.15 M NH_4NO_3	PGE	−0.05, +0.30*
NH_4OAc–HOAc (total concn. acetate) =0.30 M	SGE	+0.07, +0.18, +0.65
pH = 5.0	PGE	−0.01*, +0.20, +0.55*
0.15 M NH_4OH and	SGE	−0.17, +0.05, +0.50
0.15 M NH_4OAc (pH ∼ 7)	PGE	+0.10, +0.45*
0.17 M KNO_3	SGE	+0.05, +0.20, +0.40
	PGE	−0.05, +0.17*, +0.40*

* The size of these peaks is very small with respect to the main peak.

Figs. 2 and 3. In general, it was found that more pronounced multiple peaks appear when wax impregnated spectroscopic grade graphic rods, SGE, are used, and that the reproducibility of their shape is poor. It must be emphasized here that the shape of the stripping voltammograms were found to vary drastically when using the SGE, although special care was taken at all times to treat the electrodes in the same way. The relative height of the multiple peaks changed and, on occasion, the disappearance of one of the secondary peaks occurred. On the other hand, it was found that the shape and characteristics of the dissolution peak(s) obtained with the PGE was invariant and reproducible. In general, one main peak appeared and one (or two) relatively small secondary peak(s) were observed, as shown in Figs. 2 and 3. The main peak was also considerably sharper than that obtained with a SGE.
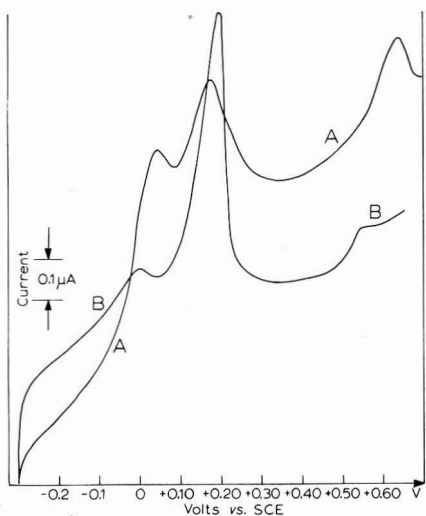
Fig. 2. Anodic stripping voltammograms for a 5×10^{-8} M Ag$^+$ solution in a 0.15 M NH$_4$OAc–HOAc (pH = 5) soln. Sweep rate, 14 mV s^{-1}. The electrodepositions were carried out at -0.60 V $vs.$ SCE for 12 min. (A) SGE, (B) PGE.
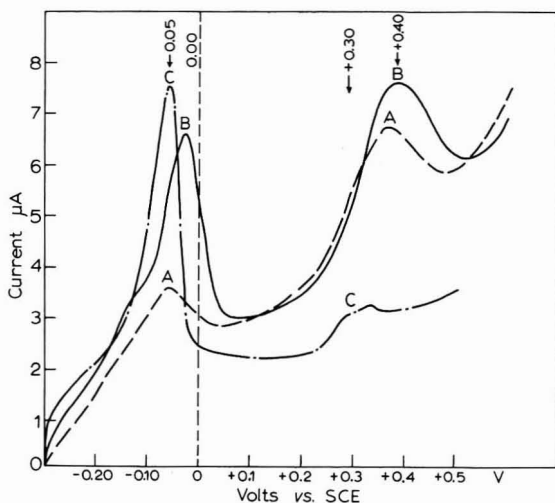
Fig. 3. Anodic stripping voltammogram for a 5×10^{-8} M Ag$^+$ soln. in 0.15 M NH$_4$OH–0.15 M NH$_4$NO$_3$ soln. Sweep rate, 14 mV s^{-1}. The electrodepositions were carried out at -0.60 V $vs.$ SCE. (A) SGE, electrolysis time = 5 min; (B) SGE, electrolysis time = 12 min; (C) PGE, electrolysis time = 5 min.

It is obvious that for analytical work, the PGE is preferable. It must be stressed here that, contrary to the findings of other workers[5], the pyrolytic graphite rods must also be impregnated with wax. This disagreement stems from the differences in current ranges employed. In previously reported studies of the electrochemical behavior of pyrolytic graphite, current levels of the order of 30 μA cm^{-2} (in conventional voltammetry) were used. In comparison, current peaks of the order of 0.03–0.3 μA cm^{-2} were obtained in this work. Accuracy and precision could not be attained with these

low current ranges unless the electrode was wax impregnated. The supporting electrolyte most suitable for silver determination was found to be an ammoniacal buffer of 0.30 M NH_4NO_3–0.60 M NH_4OH solution. The workable voltage span in this solution is from -0.9 to $+0.6$ V $vs.$ SCE. The dissolution voltammograms for silver on PGE in this solution consist essentially of one peak as shown in Fig. 3. Successive electrolysis on the same electrode surface may result in broadening of the peak, but polishing on the filter paper with ethanol restores the peak to its previous sharpness and height.

The phenomenon of multiple anodic dissolution peaks has been observed by various investigators[6–10]. It has been suggested that the peaks appearing at more positive potential than the formal peak potential of an M,M^{+n} couple represents the first layer of metal deposit bound to the electrode which has a different (greater) bonding energy than the normal bonding in the metal lattice[9]. Propst[10], who used a gold electrode, found that a silver deposition corresponding to a full monolayer coverage of the electrode occurs while electrolyzing at a potential of 0.25–0.75 V more positive ("underpotential") than the potential predicted by the Nernst equation for the macro deposition of silver. In the experiments discussed here, the "monolayer" peak could not be produced alone by employing a more positive potential than was
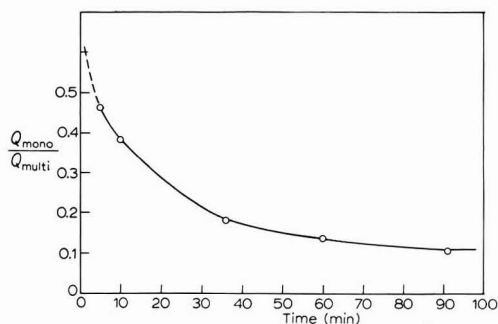
Fig. 4. Variation of the ratio of the area of the "monolayer" peak to the area of the multilayer peak (for the SGE with the ammonia buffer, see Fig. 3).
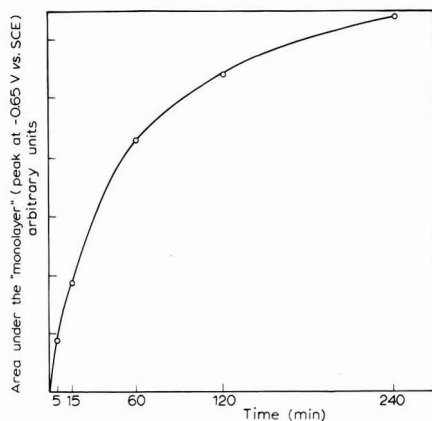
Fig. 5. Variation of the area under the "monolayer" peak at -0.65 V $vs.$ SCE (see Fig. 3) employing a SGE and ammonia buffer, with time.

needed for the normal silver peak. The multiple peaks appeared only whenever the deposition potential was sufficiently negative to produce the "normal" silver anodic dissolution peak.

It was found that (using SGE and ammonia buffer) the "normal" silver peak grows much faster than the "monolayer" peak as a function of electrolyzing time, as shown in Fig. 4. Thus, on the beginning of the electrolysis, the active sites are covered with silver very rapidly. As the electrolysis continues, the multilayer deposit is formed on these sites and, at the same time, coverage of the rest of the surface proceeds, but at a slower pace (Fig. 4). When the electrolysis is carried out for a long enough period, the "monolayer" peak reaches a maximum value as shown in Fig. 5. From results shown in this Figure, it was calculated that the area available for deposition is only about 50% of the total apparent geometric area and, therefore, did not correspond to monolayer coverage. It is interesting to note that this is in good agreement with findings by Matson[11] who studied the mercury film on SGE.

It is of interest to speculate as to why the two types of graphite demonstrate such a large difference in properties. The probable answer can be found in their different structure. The pyrolitic graphite is an almost perfect single crystalline form[4,5]. The graphite plane (two dimensional crystal lattice of fused rings, ab plane) is used as the electrode surface[4]. In the grinding process, the single plane is broken, and the exposed (virtually smooth) surface is really made up of various broken planes. One can assume that there are certain sites on this surface more favored energetically for deposition, but the SGE, on the other hand, is polymicrocrystalline in nature and will have many more active sites. Therefore, the deposition of silver occurs on many sites at once and more deposit of the "monolayer" type deposit is obtained.
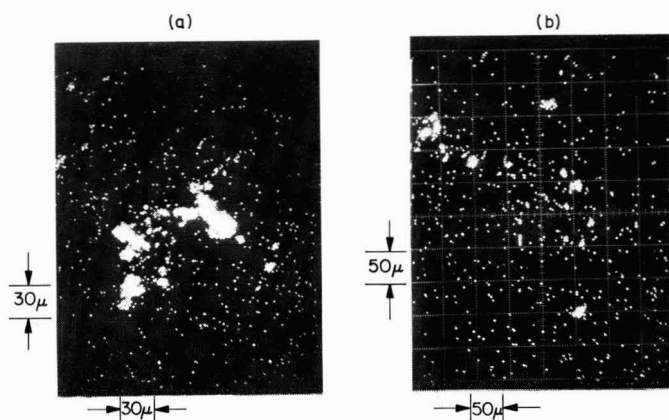
Fig. 6. X-ray fluorescence of a silver deposit on PGE. The deposit was obtained on electrolysis of a 2×10^{-6} M Ag^+, 0.1 M NH_4OAc–0.1 M HOAc soln. at -0.75 V $vs.$ SCE. Electrolysis time, 90 min.

Electron microprobe studies were undertaken to explore further the character of the silver deposit on the electrode. As the sensitivity of the technique is not enough to work with the "monolayer" deposits obtained from solutions of the 10^{-8} M range, an attempt was made to observe the pattern nature of the deposit from higher con-

centration of Ag^+, and to try and correlate these patterns with electrode behavior of the SGE and PGE.

The samples employed were 2×10^{-6} M in Ag^+ and were electrolyzed for 90 min at -0.75 V $vs.$ SCE. When the electrolysis was stopped, the electrode was rinsed with acetone, and a disc for study was cut[4]. When the disc of the pyrolytic graphite (with the silver deposit on it) was viewed through a microscope, a few spots of silver could be found, but in general, the electrode surface appeared homogeneous. These specks of deposit appeared very clearly (Fig. 6, a, b) on the X-ray fluorescence micrographs. Such high concentration silver deposits could not be found on the SGE discs. These discs appeared to be homogeneous all over the surface and the X-ray fluorescence density of these samples was higher than that found for the "homogeneous"
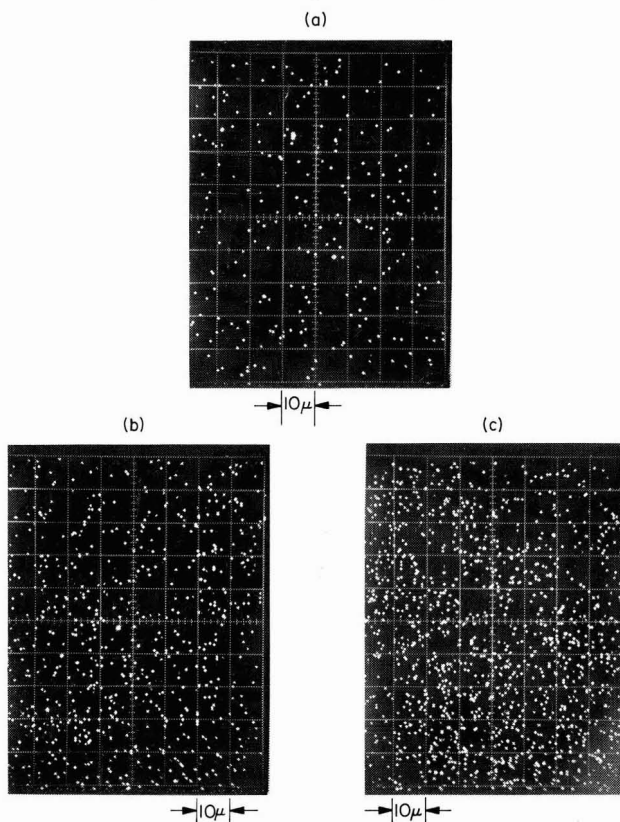
Fig. 7. X-ray fluorescence of silver deposits. Electrolysis at -0.70 V $vs.$ SCE for 90 min from a 5×10^{-6} M Ag^+, 0.1 M NH_4OAc. (a) Blank obtained for PGE disc; (b) "homogeneous" areas of deposit, PGE disc; (c) deposit on SGE.

areas (between spots) for the pyrolytic graphite discs (Fig. 7, a, b, c). Although these experiments show a tendency for a different formation of silver deposits or a difference in the number of active sites on the two graphites, they cannot be directly correlated with the experimental observation and mechanism of multiple dissolution peaks because of the higher deposition concentration used.

APPLICATION OF ANODIC STRIPPING VOLTAMMETRY TO THE DETERMINATION OF SILVER
TRACES IN SNOW SAMPLES

Weather modification by cloud seeding has become a common practice in many regions. The most usual agent used in seeding is crystalline silver iodide. The seeding is performed by either ground-based or airborne generators. Analysis of the snow or rainfall in these regions enables investigation of the effectiveness of the seeding process and indicates the most effective locations for placing the generators in order to modify the precipitations. The expected concentration range of silver in the precipitation is about 10^{-8}–10^{-11} M[12]. The most effective micro method of silver analysis is that developed by Warberton, employing neutron activation (NAA)[12] which utilizes the nuclear reaction ^{109}Ag $(n\gamma)$ ^{110}Ag. As the half life of the resulting ^{110}Ag is 24 s a very sensitive γ spectrum for silver is obtained. A pre-concentration prior to the activation step employs a cation exchange resin which is eluted with 0.1 M NH_4SCN. The detection limit of this method is about 5×10^{-11} M but the accuracy of determinations of lower than 10^{-10} M concentrations is very poor[12]. As will be shown later, ASV is much more sensitive and because of simple instrumentation has the potential of allowing the analysis to be carried out under field conditions.

It was found that concentrations of silver higher than 3×10^{-9} M could be determined by direct ASV. In the case of lower concentrations, a preconcentration step was also employed.

Reproducibility and accuracy of direct ASV were checked on standard silver solutions of 4×10^{-9} M and reproducibility of the peak areas was better than $\pm 5\%$. On standard addition to bring the solutions to 6×10^{-9} M, the agreement between expected and experimental results was better than $\pm 7\%$. Electrolysis duration needed for this concentration level was 15 min.

In order to determine lower Ag^+ concentrations, a preconcentration step, for silver traces, which was also essential to Warberton's method[12], was used in this work. An enrichment factor of about 80 was obtained by using 1 l samples which were passed through a Dowex 50W–X8 cation exchange column of 25.0×10.0 mm, and eluting with 24 ml of 0.04 M NH_4SCN. One ml of a mixture of one part concentrated HNO_3, one part H_2O, and one part NH_4OH was used to bring the total volume to 25 ml. Thus samples as low as 4×10^{-11} M can be determined.

It was found that a high concentration of NH_4SCN (greater than 0.05 M) caused a splitting and broadening of the stripping peaks. On the other hand, in order to obtain good elution efficiency ($>80\%$), the NH_4SCN concentration must be larger than 0.02 M. A 0.04 M NH_4SCN could be used without impairing the efficiency of the elution process and without causing a noticeable change in the stripping voltammograms. Also, single and sharp stripping peaks were developed when the supporting electrolyte was 0.3 M NH_4NO_3–0.6 M NH_4OH.

Typical analytical results

The results of a few sample analyses of precipitation for Ag^+ are reported below to demonstrate the applicability of the above procedures. Snow samples were supplied by M. J. Warberton of the Desert Research Institute, University of Nevada, Reno, Nevada. From previous neutron activation analysis (NAA) of these samples, it was shown that the samples could be divided into 2 groups: Group (A) $[Ag^+] > 10^{-9}$

M and Group (B) $[Ag^+] < 10^{-9}$ M. A set of replicate snow samples from group A, which were designated sample No. 23, were analyzed directly by transferring 25 ml of each sample into the cell and adding to it 1 ml HNO_3 (concentrated HNO_3, diluted 1:1) and 1 ml of concentrated NH_4OH (the resulting solution was 0.3 M NH_4NO_3, 0.3 M NH_4OH). The results are shown in Table 2.

TABLE 2

DIRECT ANODIC STRIPPING ANALYSIS OF SNOW SAMPLES

Sample No. 23	Concn. measured $\times 10^9$ M	Mean concn.	Neutron activation value[12]
	6.8		
	7.2	$7.0 \times 10^{-9} \pm 6\%$	$20 \times 10^{-9} \pm 6\%$
	7.6		
	6.3		

To check further the above values, the concentration was determined after employing the ion exchange enrichment step. In this case 25 ml of sample No. 23 was passed through the ion exchange column and the silver was eluted with 25 ml of 0.04 M NH_4SCN into the cell that held 1 ml of 1:1 diluted concentrated HNO_3 and 2 ml of concentrated NH_4OH. The concentration of silver found was 6.2×10^{-9} M which is in satisfactory agreement with the results found by the direct method.

A set of replicate snow samples from group B, which were designated samples No. 12 and 25, were preconcentrated using the same ion exchange procedures used to concentrate silver from the two sets of samples of group B. As stated above the sample volume was 1000 ml. The results of the analyses are shown in Table 3.

TABLE 3

RESULTS OF ANALYSIS OF GROUP B SAMPLES EMPLOYING A PRECONCENTRATION STEP

Sample No.	Concn. found $\times 10^{11}$ M	NAA[12] results $\times 10^{11}$ M
25	10	7.8
12	4.8	1.1

From these results it can be seen that the ASV merits serious consideration for trace Ag^+ analysis of precipitation samples as a standard method. These preliminary results have not established which method results in the least absolute error in determination of 10^{-11} M or lower concentrations. Further studies are necessary to determine this fact but the analytical procedure as well as instrumentation is far simpler with ASV.

SUMMARY

The characteristics of the anodic stripping curves obtained from 10^{-11}–10^{-7} M Ag^+ have been studied using pyrolytic graphite and wax impregnated spectrographic grade carbon electrodes. It was found that the stripping curves on pyrolytic graphite electrodes (PGE) had essentially only one sharp dissolution peak, while those for wax impregnated carbon (SGE) exhibited multiple dissolution peaks. The nature of the Ag deposits was studied by X-ray fluorescence employing an electron microprobe which showed that PGE had a few preferred sites for deposition but the SGE exhibited a uniform distribution of the deposit. The optimum solution conditions, electrode pretreatments, and procedure are described, as well as the results of the analyses of snow samples containing 10^{-8}–4×10^{-11} M Ag^+.

REFERENCES

1 I. SHAIN in J. M. KOLTHOFF AND P. J. ELVING (Eds.), *Treatise on Analytical Chemistry*, Part I, Vol. 4, Interscience Publishers, New York, 1962.
2 E. BARENDRECHT in A. J. BARD (Ed.), *Electroanalytical Chemistry*, Vol. 2, M. Dekker, New York, 1967.
3 S. P. PERONE, *Anal. Chem.*, 35 (1963) 2091.
4 B. H. VASSOS, Ph. D. Dissertation. Univ. of Michigan, 1964; H. B. MARK, JR., F. J. BERLANDI, B. H. VASSOS AND T. H. NEAL, *Proc. 1965 Intern. Conf.: Modern Trends in Activation Analysis*, Texas A and M Press, 1966.
5 I. FRIED, Ph. D. Dissertation, Univ. of Michigan, 1964.
6 K. GARDINER AND L. B. ROGERS, *Anal. Chem.*, 25 (1953) 1393.
7 M. M. WECHOLSON, *J. Amer. Chem. Soc.*, 79 (1957) 7.
8 B. H. VASSOS AND H. B. MARK, JR., *J. Electroanal. Chem.*, 13 (1967) 1.
9 L. B. ROGERS AND A. F. STEHNEY, *J. Electrochem. Soc.*, 95 (1949) 25.
10 R. C. PROPST, *J. Electroanal. Chem.*, 16 (1968) 319.
11 W. R. MATSON, Ph. D. Dissertation, Mass. Inst. of Tech., 1967.
12 J. A. WARBERTON AND L. G. YOUNG, Reprint Series No. 97, Desert Research Inst., Univ. of Nevada, Reno, Nevada, 1967.

METHOD FOR COMPARING ELECTROCHEMICALLY ACTIVE AREAS OF DIFFERENT CARBON POWDERS

M. L. KRONENBERG

Union Carbide Corporation, Development Department*, Parma Technical Center, Cleveland, Ohio 44101 (U.S.A.)

This investigation was undertaken to find a method for determining the electrochemical activity of powders that are used in making up porous fuel cell electrodes. It was desired that the method be related to the measurement of the electrochemically significant surface area in solution rather than to the standard surface area measurement in a solid–gas system as determined by BET[1]. This is important because in the preparation of porous electrodes the powders are often coated with non-conducting binders and wetproofing materials which cannot be differentiated from active conducting surfaces by surface area measurements. Electrochemical methods such as potential scan coulometry[2-4] have been used to estimate electrochemical surface area but only on finished electrodes and not on the materials making up the electrodes.

Russian workers[5] have recently studied polarization characteristics on various fuels on circulating nickel powders using a diaphragm pump to move the powders through a screen collector. Also, Gerischer[6,7] and others[8,9] have shown that in the presence of H_2, O_2 or other electrochemically active substances considerably higher currents could be drawn from a stirred slurry of metal catalyst powders in contact with a polarized acceptor electrode. Because of transitory and loose contact between the catalyst powders and acceptor electrode and other uncertainties, no clear inter-relationship between the magnitude of current and catalyst activity was reported. Experiments of this nature were conducted in our laboratory with catalyzed and non-catalyzed carbon powders in the presence of hydrogen or oxygen. Typical polarization data for the blank electrolyte and several catalyzed carbon suspensions (characterized by carbon weight) are given in Fig. 1. The results show that a certain fraction of the current results from the reduction of dissolved oxygen unaided by catalyst particles. The observed significant increase in current with increasing amounts of powders is caused either by direct charge transfer between particles and collector or improved transport of oxygen to the collector *via* an adsorption–desorption mechanism. The quantity of oxygen reduced during the polarization run is less than 1% of the oxygen dissolved in the solution[10]. Since the solution alone yielded a relatively high current, it was not possible to use polarization curves as a basis for comparing activities of various powders.

In another approach the high currents normally obtained from solutions

---

* Present address, Union Carbide Corp., Consumer Products Division, Parma, Ohio.

containing no powders were minimized so that better comparisons in activity could be made between powders variously treated. In this method, sample powders are suspended in an acidic or alkaline electrolyte and saturated with the electrochemically reactive gas, *e.g.*, oxygen. After saturation, the O_2 supply is cut off, an inert gas flow is turned on, and the remaining gas is potentiostatically used up at an inert electrode. Once the supply is cut off, the O_2 to be reduced must come from two sources—O_2 dissolved in the solution and O_2 which was adsorbed by the sample powders and later given up to the solution or reduced directly while adsorbed on the particle. After a correction is made for the gas in solution by running a blank on the solution, the amount of gas electrochemically reacted at the electrode is related to the area of active adsorption sites on the powders. The amount of gas electrochemically reacted is measured by the number of coulombs from the current–time curves.
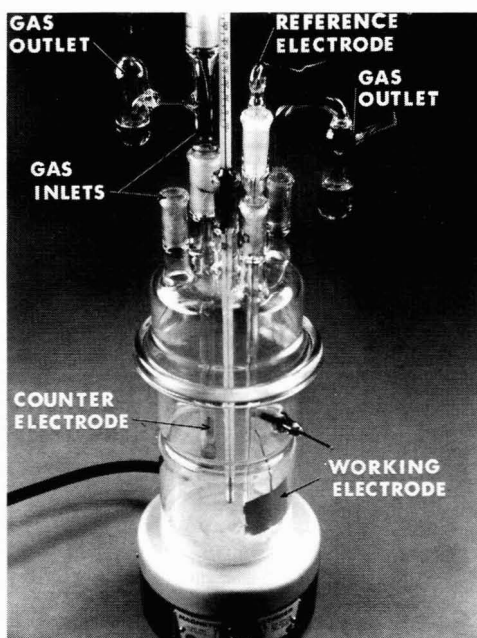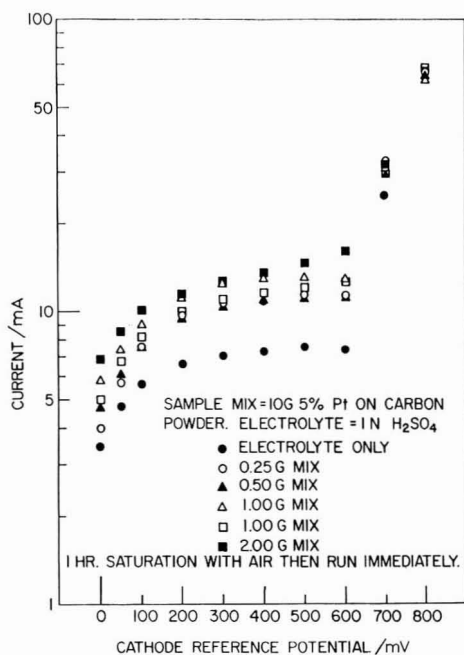
Fig. 1. Polarization curves for Pt-catalyzed carbon powder, in an air-saturated soln.; ref. electrode, Hg/Hg_2SO_4.

Fig. 2. Electrochemical cell used for powder studies.

Figure 2 shows the cell and magnetic stirring apparatus used for most of the runs with carbon powders. The stirrer was operated with a Variac and the speeds corresponding to the Variac settings were obtained by means of a stroboscope. The cell was designed so that the electrodes could be easily changed and a uniform motion of the electrolyte made possible. A plug of polyethylene wool was used in the counter-electrode compartment to prevent particles from entering. To limit undesirable gaseous diffusion, the same atmosphere was maintained over the cell and counter-electrode compartment.

This method was first tried on uncatalyzed carbon powders in 1 N H_2SO_4.

For carbon particles the preferred electrolyte is an acidic electrolyte because carbon particles have a greater tendency to float in high surface tension media such as concentrated caustic solutions and it is preferred that the particles be uniformly dispersed in applying this method. Metal and oxide particles do not have a great tendency to float and the most important consideration in the selection of electrolyte for these materials would be chemical stability (*e.g.*, one would not measure the electrochemically significant surface of zinc in an acid media).

The data presented in Table 1 were run under the following conditions: One gram of sample powders was suspended in a cell containing 400 ml of 1 N H_2SO_4 at ambient temperature. The powders were saturated with air for 30 min. The air was then turned off and replaced with nitrogen at the same flow rate (0.1 SCFH). The powders were stirred at 1000 rev./min during the 20-min run and the potential of the working electrode (10 cm^2 gold) was set at 300 mV negative with respect to a $Hg/Hg_2SO_4/1$ N H_2SO_4 reference electrode. The number of coulombs were obtained by integrating the current–time curve obtained on a Varian G-10 recorder. The 20-min run time for the method is arbitrary, but served for a rapid comparison of relative surface areas, even though the coulometric equivalent of the O_2 reduced during this

TABLE 1

COMPARISON OF BET AND DATA BY ELECTROCHEMICAL METHOD

BET area/m^2 g^{-1}	Type carbon	Q/mC	Q–Q(Blank)/mC
570	0%, S-100	5743 (5130–6360; 6 runs)	5120
270	0%, P-90	3105 (2940–3225; 4 runs)	2482
274.1	7.5%; S-100 Cold Mix	1716 (1566–1879; 3 runs)	1093
195.2	12%; S-100 Cold Mix	1295 (1266–1325; 2 runs)	672
115	20%; S-100 Cold Mix	601 (556–629; 3 runs)	—
236.7	10%; S-100 Hot Mix	1804 (1800–1808; 2 runs)	1181
168.8	20%; S-100 Hot Mix	1102 (966–1170; 3 runs)	479
—	Blank, 1 N H_2SO_4	623 (524–720; 8 runs)	—

period is only a fraction of the quantity initally available. It is important to note that a large fraction of the oxygen originally present in the solution was removed by means of the N_2 sweep which removed a larger percentage from the gas dissolved in the solution than from the gas adsorbed on the carbon, thus increasing the accuracy of the method. A check was always made for the dissolved oxygen by running a blank on the solution. In Fig. 3,A and B are shown typical recorder tapes taken on the blank solution (3A) and the same solution containing 1 g S-100 carbon (3B).

In Table I representative results were obtained on plastic-bonded, wetproofed and nonwetproofed carbon powder used for fuel cells (S-100 and P-90, percent figures refer to plastic content). The average value is given and the range of results and number of runs are given in parentheses. BET surface area measurements are included for comparison.

These preliminary results were encouraging and showed that the method was essentially in qualitative agreement with BET surface area measurements. Both BET and this electrochemical method suggested that S-100 carbon has a larger surface area than P-90 carbon and that incorporation of plastics by the hot-mix method resulted in a greater surface area than the cold-mix method.
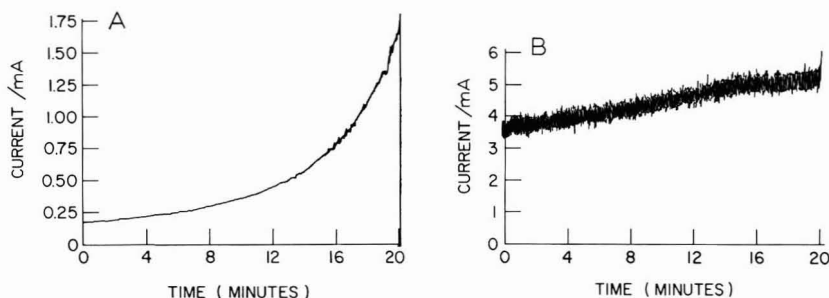
Fig. 3. Recorder tape of current vs. time for coulometric method. (A) Run No. 122: 600 mC (20 min), (B) Run No. 126: 5,240 mC (20 min).

When samples of the above materials were run again several weeks later according to the method described above, the results did not agree with the results summarized in Table 1. A series of experiments was begun, which turned out to be more than 500, to determine the important experimental parameters using this method.

The main difficulty with the method stemmed from the fact that with the use of air to saturate the electrolyte about 22 coulombs-worth of O_2 are available for reduction from a blank solution of electrolyte based on solubility considerations and partial pressure of O_2. Since a blank runs out at about 0.5 coulombs in 20 min it means that about 2–3% of the O_2 available is taken out coulometrically and about 97% by N_2 displacement. This makes the N_2 flow rate, electrolyte stirring rate, and cell geometry more critical than it should be for a practical system. To make the method practical, the amount of O_2 dissolved in the solution had to be reduced to an insignificant amount before the run, and in such a way that the O_2 adsorbed in the carbon was hardly affected. Two approaches were used to accomplish this. One was to reduce the partial pressure of O_2 by using dilute O_2 mixtures, and the other was to precede the coulometric run by an equilibration period under N_2. Both methods yielded reproducible results but the last approach was best for our purposes because it took much less time to run a sample by this method. The nitrogen equilibration period did remove virtually 100% of the oxygen from the solution but left substantial quantities adsorbed on the powders. To get the method to work satisfactorily we had to optimize or, rather, fix certain conditions of N_2 flow rate, electrolyte stirring rate, equilibration time, saturation time, cathode-reference potential, electrode material, electrode preparation, etc.

When these parameters are fixed, the adsorption capacity (number of coulombs obtained) appears to be a linear function of sample size as shown in Fig. 4. The procedure finally adopted is slightly different from the one used to obtain the data in Fig. 4, and is summarized as follows:

1. A 1 g carbon sample is dispersed in 400 ml of 1 N H_2SO_4 and equilibrated (high speed stirring) for 2 h in air (open flask).

2. Sample and solution are then placed in the electrochemical cell and equilibrated at high stirring speed under N_2 for $\frac{1}{2}$ h. This removes oxygen almost completely from the solution (reduces a blank to virtually zero) while a significant quantity of oxygen remains adsorbed on the carbon.
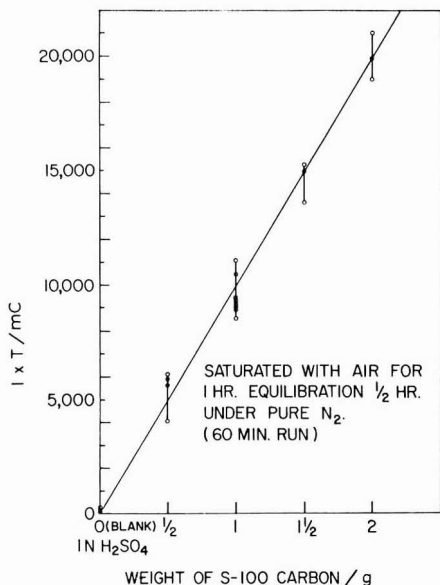
Fig. 4. Dependence of adsorption capacity on sample size.
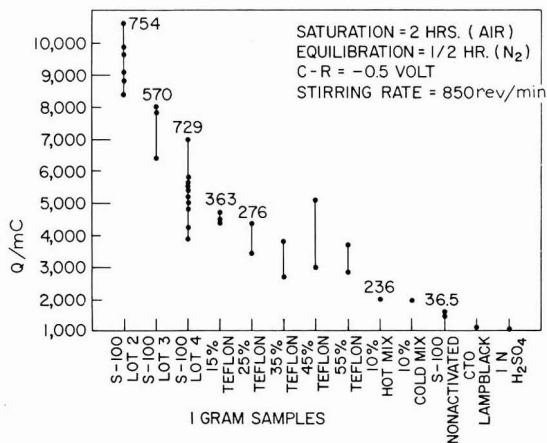
Fig. 5. Relative electrochemically significant surface areas of carbon samples by the coulometric method.

3. The sample is then run potentiostatically at 500 mV negative with respect to a $Hg/Hg_2SO_4/1\ N$ reference under a N_2 sweep using platinum working and counter electrodes.

A number of carbon samples with and without wetproofing plastics were run by this procedure and the results are summarized in Fig. 5. Unfortunately only two of the original polyethylene samples could be run since all others were used up. BET values which were available appear above the coulometric results. The significant information to be derived from the data in Fig. 5 is as follows:

1. The data are in rough qualitative agreement with BET values, but significant differences are apparent (*e.g.*, Lot 2 and Lot 4, S-100 carbon).

2. Samples containing tetrafluoroethylene polymers (Teflon) exhibited a relatively minor decrease in performance as the percent of this material was increased from 15–55%. This is significantly different from the carbon samples which were made up with polyethylene. Here a significant decrease in activity resulted upon increasing the plastic content from 7.5 to 20%.

3. Polyethylene-containing carbons have lower electrochemically significant surfaces than Teflon-containing samples.

Runs were also made with BET standardized samples of high surface area silica and silica-alumina. Contrary to experience with carbons, the contributions of adsorbed oxygen from these materials to the total current was negligible.

It is fairly well accepted among electrochemists that a quantity known as the "differential capacitance" is proportional to the surface area of an electrode and can be obtained from the buildup or decay of electrode potential on closing or opening the circuit of an electrolytic cell[11]. In applying this method to a powder cell with

constant stirring rate, it must be assumed that the particle collision rate with the electrode does not change with time, and agglomerate size does not vary significantly from sample to sample. The measurement is made by obtaining a steady-state potential with a potentiostat and displaying this on an oscilloscope, then rapidly opening the circuit by means of a mercury-wetted relay. The capacitance C is obtained from the reciprocal slope of time $vs.$ potential $(\mathrm{d}t/\mathrm{d}E)$ according to the equation:

$$C = I\mathrm{d}t/\mathrm{d}E \tag{1}$$

where I is the current at $t \approx 0$. A typical picture of an oscilloscope trace showing 3 slopes taken on the same film is shown in Fig. 6. The values obtained for a solution without carbon, and several carbon samples are given in Fig. 7. The high values reflect the relatively high surface area of the carbon powders. Results are in qualitative agreement with those obtained by the coulometric method.
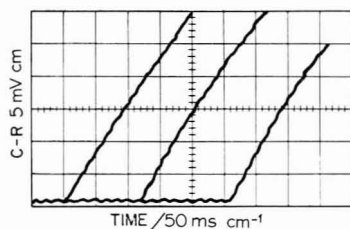
Fig. 6. Oscilloscope trace for differential capacitance measurement (Run No. 634: 1 g S-100, Lot 4). $I = 1.85$ mA; $C = I(\Delta I/\Delta E)$. (1) 11,550, (2) 11,750, (3) 11,850 μF.
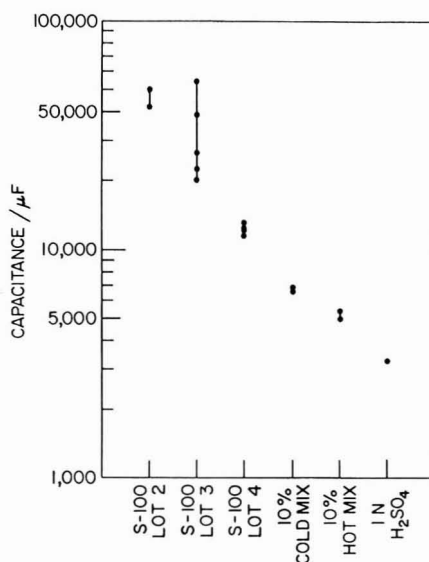
Fig. 7. Differential capacitance data on electrolyte without carbon, and on various carbon samples.

While no detailed study of the discharge mechanism has been undertaken, it is believed that two different mechanisms may be present—one for the direct discharge of dissolved O_2 and another for the discharge of O_2 adsorbed on the carbon. In the latter case electron transfer can occur directly between the carbon particle and the collector as a result of the several hundred millivolt potential difference between them—or the adsorbed O_2 may be gradually released to the solution to replace the dissolved O_2 that was reduced. Since both of these mechanisms would yield values related to electrochemically significant surfaces, a determination of which discharge mechanism prevails is not a necessary prerequisite for using this method.

SUMMARY

The suspended powder experiments described suggest a method for obtaining a relative, electrochemically significant surface area for wetproofed and nonwetproofed carbon powders. It is believed that the method depends on the chemisorption of oxygen on active sites of the carbon and subsequent reduction.

REFERENCES

1 S. BRUNAUER, P. EMMET AND E. TELLER, *J. Am. Chem. Soc.*, 59 (1937) 2682.
2 S. GILMAN AND M. BREITER, *J. Electrochem. Soc.*, 109 (1962) 662.
3 R. OSTERYOUNG, G. LAUER AND F. ANSON, *J. Electrochem. Soc.*, 110 (1963) 926.
4 A. JULIARD AND H. SHALIT, *J. Electrochem. Soc.*, 110 (1963) 1002.
5 A. FASMAN AND D. SOKOLSKII, *Dokl. Akad. Nauk SSSR*, 153 (1963) 653.
6 H. GERISCHER, *Z. Elektrochem.*, 67 (1963) 164.
7 J. HELD AND H. GERISCHER, *Z. Elektrochem.*, 67 (1963) 921.
8 P. BOUTRY, O. BLOCH AND J. BALACEANU, *Compt. Rend.*, 254 (1962) 2583.
9 K. SCHWABE AND A. STASKO, *J. Electroanal. Chem.*, 11 (1966) 308.
10 J. D'ANS AND E. LAX, *Taschenbuch für Chemiker und Physiker*, Springer-Verlag OHG, Berlin, 1943, p. 974.
11 F. BOWDEN AND E. RIDEAL, *Proc. Roy. Soc. London*, A120 (1928) 59.

OXIDE CHEMISTRY AND ELECTROREDUCTION OF NO_3^- IN MOLTEN ALKALI NITRATES

PIER GIORGIO ZAMBONIN

Istituto di Chimica Analitica, Università di Bari, Bari (Italy)

(Received July 31st, 1969)

INTRODUCTION

In spite of the fact that during the last decade the electroreduction of nitrate ions in fused alkali nitrates has been the subject of numerous investigations, some fundamental aspects of the problem are still controversial.

The first study in the field by Hills and Johnson[1], postulated the following reactions:

$$NO_3^- + 2e^- = NO_2^- + O^{2-} \tag{1}$$
$$NO_3^- + e^- = NO_2 + O^{2-} \tag{2}$$

Subsequently, reaction (1) has been reproposed by Swofford and Laitinen[2] to explain a puzzling maximum observable at -1.7 V *vs.* Ag/Ag^+, 0.07 m, reference electrode, when NO_3^- is electroreduced in the presence of sodium (or lithium) ions. In their interesting study, these authors related the current peak to the precipitation of sodium oxide on the cathode and the small after-peak current to the replacement of the precipitate continuously dissolving in the melt. Following the work of Swofford and Laitinen many authors[3-9] considered reaction (1) a satisfactory means for the quantitative production, over a large temperature range, of oxide ions in nitrate melts. Even so, there has been considerable disagreement concerning the chemical or electrochemical behavior of the products of such electrolyses. Finally, Barlett and Johnson[10], on the basis of thermodynamic considerations and of experiments performed in sodium or potassium nitrates, suggested that a mixed process could be involved and proposed that the following cathode processes:

$$NO_3^- + 5e^- = \tfrac{1}{2}N_2 + 3O^{2-} \tag{3}$$

$$2NO_3^- + 8e^- = N_2O + 5O^{2-} \tag{4}$$

$$NO_3^- + 3e^- = NO + 2O^{2-} \tag{5}$$

occur concomitantly with reaction (1).

Equations (1)–(5), postulated in agreement with the conventional Flood and Lux acid–base theory, involve the formation of oxide ion (O^{2-}) assumed to be an inert species. In contrast to all previous work, recent studies[11,12] have shown that oxide ion in nitrate melts is a very unstable species because of the prevalence of the following reactions:

$$O^{2-} + NO_3^- \rightleftharpoons NO_2^- + O_2^{2-} \tag{6}$$

$$O_2^{2-} + 2\,NO_3^- \rightleftharpoons 2\,NO_2^- + 2\,O_2^- \tag{7}$$

These new findings might well serve as a basis for rationalizing the conflicting reports in the literature which were often based on indirect methods of detection of the final products of massive electrolyses.

In the present study the entire problem has been reconsidered on the basis of voltammetric measurements which can discriminate between different steps in the reaction path, from the primary cathodic process to the formation of the final products. All the chemical species involved could be monitored by *in situ* analytical techniques.

EXPERIMENTAL

Solvent

The solvent consisted of a filtered equimolar $(Na,K)NO_3$ melt, dried by applying a vacuum or by bubbling an inert gas through the fused salt. A vacuum or an inert gas atmosphere was maintained over the system during all experiments. Moisture was reduced to a level not exceeding 10^{-5} molal water as ascertained by monitoring (rotating disk electrode—RDE—polarography) the characteristic[2,13,14] cathodic "water wave".

Temperature

The temperature was maintained sufficiently low to avoid secondary reactions involving attack[10] of the electrode surface. In fact, no variation in the weight of large electrodes was detectable at the end of experiments performed under our working conditions. Moreover, as previously reported[12], low temperature favoured well resolved RDE polarographic waves and residual currents.

Apparatus

The platinum-lined electrolysis cell and the electrodes recently described[15] were used for massive electrolysis and simultaneous RDE polarographic measurements. A glass cell was used for voltammetric studies, with a stationary indicator electrode. In this case a suitable window in the thermostatting mantle permitted continuous observation—*via* a ten-fold magnification microscope—of the indicator electrode surface. With such a device and applying a good vacuum, any gas evolution involved in the electrode processes could be efficiently detected. This was ascertained by anodic polarization of solutions containing small concentrations of anions such as CO_3^{2-}, O_2^- and NO_2^-, which give gaseous products. During the massive electrolysis in a wet melt, the desired concentration of water was maintained[13] by bubbling nitrogen at a certain partial pressure of water. The stationary indicator electrode consisted of a circular platinum surface (1.2×10^{-3} cm^2 in area) embedded in the middle of a concentric and coplanar glass surface, by coaxial sealing of a platinum wire in a soft glass tube. The best reproducibility was obtained with the micro-electrode surface horizontal and turned up (by U-bending of the glass tube). Counter and reference electrode $(Ag/Ag^+, 0.07\ m)$ were previously described[15]. RDE polarograms and cyclovoltammograms were obtained with the aid of a home-made electronic polarograph[16] at potential span velocities from 0.2 to 50 V min^{-1}. A three-

electrode system was employed throughout. A conventional set-up with a potentiostat (ARF Products Inc., model APP 8) and a continuous reading gas coulometer was employed for controlled potential massive electrolysis. A Houston X-Y recorder model HR-97 or a Tektronix model 507A oscilloscope were used to record data. Potential assignments were in accordance with the Stockholm Convention[17].

RESULTS

Massive electrolysis in pure $(Na,K)NO_3$

RDE current–voltage curves recorded during and after a massive electro-reduction of NO_3^-, exhibited three polarographic waves. These waves, identifiable by their known[11,12] half-wave potentials, revealed the presence, in the bulk of the melt, of the species: peroxide (O_2^{2-}), superoxide (O_2^-) and nitrite (NO_2^-). The relevant electrode processes are reported in Fig. 1 which shows a family of such steady-state curves sequentially recorded after interruption of a massive electrolysis. The limiting currents related to these polarograms present sensible variations as a function of time: significant findings are outlined below with reference to Fig. 1 that is representative of a series of experiments.

Composite wave I allowed one to determine, at any moment, the exact concentration of O_2^- and O_2^{2-} according to eqns. (8) and (9):
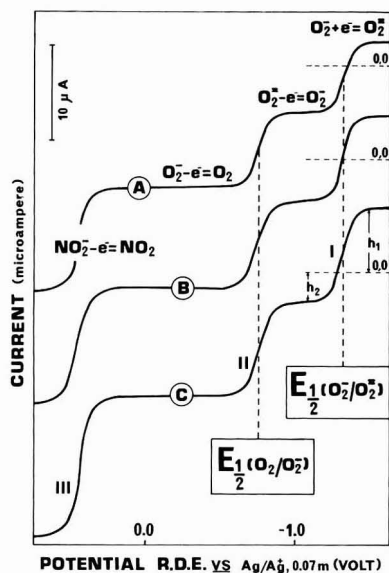
Fig. 1. Sequential RDE polarograms recorded, at different times, starting $(t=0)$ at the end of a massive electroreduction of NO_3^-: (A) $t=0$, (B) $t=25'$, (C) $t=\infty$ (5 h). Zero current axis shifted arbitrarily; curves corrected for residual current and the presence of some NO_2^-, an impurity of the melt; RDE (area 1.7×10^{-2} cm²) rotated at 600 r.p.m. Massive electrolysis performed at 229°C in a dry melt (0.134 kg) vigorously stirred. Potential of the cathode ($\simeq 100$ cm² in area) -1.75 V *vs.* Ag/Ag⁺, 0.07 *m*; duration of the electrolysis ~ 15 min; total equivs. of electricity passed 2.18×10^{-4} (21 C).

$$h_1 = 0.62 \, nFAD_{O_2^-}^{\frac{2}{3}} v^{-\frac{1}{6}} \omega^{\frac{1}{2}} c_{O_2^-} \tag{8}$$

$$h_2 = 0.62 \, nFAD_{O_2^-}^{\frac{2}{3}} v^{-\frac{1}{6}} \omega^{\frac{1}{2}} c_{O_2^-} \tag{9}$$

Symbols in these equations, derived from the Levich relation[18], have their usual significance *viz.*: nF is the number of coulombs per mole, A the area of the indicator electrode (cm^2); D ($cm^2 \, s^{-1}$) the diffusion coefficient for the specified species in a solvent of kinematic viscosity v ($cm^2 \, s^{-1}$); ω the angular velocity (rad s^{-1}) and c the concentration (mol cm^{-3}) of the electroactive species identified by subscripts. The diffusion coefficient data in $(Na,K)NO_3$ solvent have been previously[12] reported. The peroxide concentration, present at the interruption of the massive electrolysis, decreases as function of time and the corresponding concentrations of superoxide and NO_2^- increase (see curves A, B and C). The related kinetic effect tends to an equilibrium situation represented by curve C. Relevant quantitative data are summarized in Table 1. In this Table, columns 6 and 7 compare Q, the equivalents of electricity

TABLE 1

DATA RELEVANT TO CURVES A, B, C IN FIG. 1

Curve	$10^4 \times [O_2^{2-}]/$ mol kg^{-1}	$10^4 \times [O_2^-]/$ mol kg^{-1}	$[NO_2^-]^a/$ mol kg^{-1}	$2[O_2^{2-}] +$ $2[O_2^-]/$ mol kg^{-1}	$\Sigma q = \{2[O_2^{2-}] +$ $[O_2^-]\} G$ eqns. of O_2^- and O_2^{2-} present in soln. $\times 10^4$	Q eqn. of electr. passed $\times 10^4$
A $(t=0)$	6.9	2.4			2.1_5	2.18
B $(t=25')$	5.9	5.0			2.2_5	2.18
C $(t=\infty)$	4.5	7.5	2.5×10^{-3}	2.4×10^{-3}	2.2	2.18

^{a} Value obtained applying eqn. (12) to the equilibrium condition expressed by curve C.

passed during the electrolysis and Σq, the sum of equivalents of O_2^- and O_2^{2-} present in solution when curves A, B and C were recorded. Within the limits of experimental errors, at any time during the experiment, the relation:

$$Q = \Sigma q = \{[O_2^-]_t + 2[O_2^{2-}]_t\} \cdot G \tag{10}$$

was verified. Here, $[O_2^-]_t$ and $[O_2^{2-}]_t$ are the molal concentrations of peroxide and superoxide at a certain time and G is the weight of the melt.

The concentration of nitrite reported in column 4 was obtained by applying* at the equilibrium conditions (curve C), the relation:

---

* The indirect determination of NO_2^-, was necessary because recent findings from our laboratory seem to exclude the possibility of utilizing the limiting current of wave III for quantitative measurement of NO_2^- in the presence of O_2^{2-} or O_2^-. This is due in part to the "concealed limiting current"[19] arising from reactions such as:

$$O_2^{2-} + 2NO_2 = 2NO_3^- \tag{11}$$

An analogous polarographic behaviour also characterizes solutions containing, simultaneously, nitrite and hydroxide ions. For this reason, in Fig. 2 (*vide infra*), the nitrite wave is much smaller than expected on the basis of the actual nitrite concentration detectable by usual[2,13,20] titrimetric methods (P. G. Zambonin: work in progress).

$$\frac{[O_2^-]_{eq}^2 \, [NO_2^-]_{eq}^2}{[O_2^{2-}]_{eq} \, [NO_3^-]_{eq}^2} = K = 6.7 \times 10^{-11} \tag{12}$$

recently[12] obtained for reaction (7) at the same temperature of 229°C.

The nitrite concentrations determined in this way were numerically equivalent (compare columns 4 and 5) to twice the sum of the concentrations of peroxide and superoxide *viz.*:

$$[NO_2^-] \equiv 2\{[O_2^{2-}] + [O_2^-]\} \tag{13}$$

Massive electrolysis of $(Na,K)NO_3$ *containing small quantities of water*

Figure 2 reports a RDE polarogram recorded after a massive electrolysis, performed in a slightly wet melt, under the same experimental conditions (temperature, potential, stirring, etc.) as in the preceding case. The curve differs substantially from that reported in Fig. 1 and did not exhibit any change as a function of time. Salient points are outlined below, with reference to Fig. 2. The cathodic wave, I, is the characteristic water wave[2,13,14], corresponding to a water content of about 0.1–0.2% w/w. The anodic waves, II and III have been attributed to electrooxidation of hydroxide and nitrite ions, respectively, on the basis of their half-wave potential values and
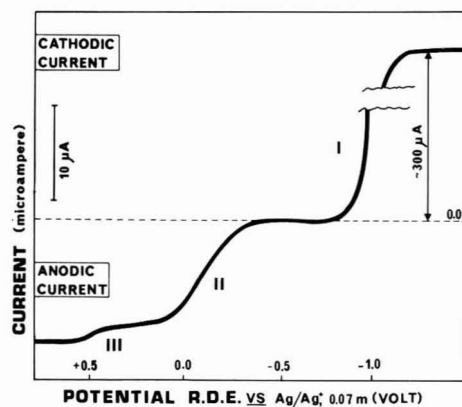
Fig. 2. RDE polarogram recorded after a massive electrolysis performed in the same exptl. conditions of Fig. 1 but with the melt under a partial pressure of water of ~ 10 mm Hg. Curve corrected as in Fig. 1.

confirmed by introducing NaOH and $NaNO_2$ into the solution. There is no trace of peroxide or superoxide ions. Hydroxide and nitrite concentrations determined by literature titrimetric methods[2,13,20] verified, within a few percent, the relation:

$$Q = [OH^-]G = 2[NO_2^-]G \tag{14}$$

where the symbols have the significance previously given, *i.e.*: for each equivalent of electricity an equivalent of OH^- and half an equivalent of NO_2^- were produced.

Voltammetry in pure $(Na,K)NO_3$

The bold-faced curve reported in Fig. 3 represents a typical current–potential profile observed by polarizing the stationary platinum microelectrode cathodically,
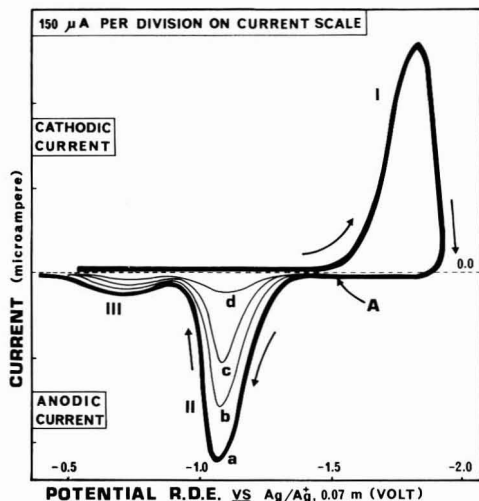
Fig. 3. Current–voltage curves recorded (in the sense of the arrows) using the platinum microelectrode $(A = 2.7 \times 10^{-3} \text{ cm}^2)$ in pure $(Na,K)NO_3$ solvent at 229°C under N_2 atm. Potential scanning (5 V min^{-1}) stopped at point A for the specified lapse of times. (t): (a) 0, (b) 50, (c) 100, (d) 200 s.

and subsequently anodically. The existence and the position of peaks I and II are in agreement with previous reports[1,2,5,21] in the literature. On the contrary, the existence of the smaller peak III—which will be seen to be an important interpretative key— has never been mentioned. Peak potentials of I and II were dependent on the rate of the potential scanning while the peak potential III was found independent. Both II and III were strictly related to a previous electroreduction of the melt, *viz.* to a polarization of the microelectrode in the region of peak I.

The origin of peak II has been related to the oxidation of an insoluble product formed on the electrode during the cathodic process responsible for peak I. This is apparent from Fig. 3 which reports a series of anodic curves recorded, starting from the point A, after the same cathodic polarization, *i.e.* after recording an identical peak I. These curves differ among themselves owing to the fact that the potential scanning was stopped at point A (current equal zero) for different lapses of time. As shown, the area of II decreases on increasing the "waiting time", which allowed a proportional spontaneous dissolution of the precipitate.

Obviously such spontaneous solubilization was also present during the recording of peaks I and II. For this reason, the ratio between areas I and II was found dependent on V, the potential scanning rate. As shown in Fig. 4, for the highest values of V there is a nearly linear dependence of R on V^{-1}. This permitted the extrapolation, at $V^{-1} \rightarrow 0$, of the limiting values of R practically unaffected by spontaneous dissolution. The significance of R_{ext} and its independence of temperature and of the presence of nitrite ion will be discussed later when the nature and the electrochemical behaviour of the precipitate will be described.

The nature of peak III was investigated by the voltammetric study exemplified in Fig. 5. On cathodically polarizing the microelectrode, after recording wave III,

two other waves, IV and V, could be detected. The areas of the three peaks decreased in the order:

$$\text{area III} > \text{area IV} > \text{area V} \qquad (15)$$

and were found dependent on the potential scanning rate. Peak V could also be obtained by reversing the direction of the potential scan immediately after recording peak II; *i.e.* without recording III and IV. The peak potentials of III and IV are symmetric towards the half-wave potential of the polarographically reversible redox couple O_2/O_2^- (see Fig. 1); the peak separation was found to be $\cong 100$ mV, in agreement with the theoretical peak separation for a reversible one-electron process[22] at 229°C. Peak V is separated from the half-wave potential of the reversible couple O_2^-/O_2^{2-} by about -50 mV. As for III, the peak potentials of the waves IV and V were found independent of the potential scanning rate.

In experiments under vacuum conditions, observation of the microelectrode with a microscope during polarization cycles such as that reported in Fig. 5, showed that there was evolution of gas only during the tracing out of peak III.

The findings that emerged from the experiment of Fig. 5 will be discussed in the next section.
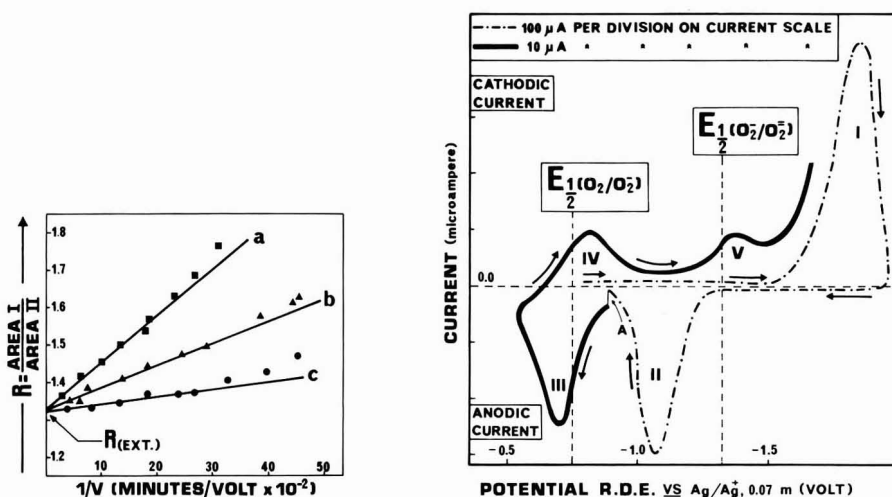
Fig. 4. Plots of $R=$ area I/area II for curves similar to the bold-faced in Fig. 3, *vs.* 1/V, the reciprocal of the potential scanning used to record the curves. (a) Pure melt, $T=280°C$; (b) pure melt, $T=229°C$; (c) melt 0.3–0.5 *m* in NO_2^-, $T=229°C$.

Fig. 5. Current–potential curves recorded, in the sense of the arrows, in the same exptl. conditions of Fig. 3. In A the sensitivity of the recorder was instantaneously switched.

DISCUSSION

The results of the massive electrolysis experiment, summarized by relations (10) and (13), and the kinetic effect apparent from Fig. 1, are consistent with the following interpretation. The electroreduction of NO_3^- generates peroxide ions quanti-

tatively (*via* intermediate steps too fast to be detected by this experiment) according to the overall reaction:

$$2\,NO_3^- + 2e^- = 2\,NO_2^- + O_2^{2-} \tag{16}$$

Further peroxide reacts (slowly) with the solvent to generate superoxide according to reaction (7) until the equilibrium condition expressed by eqn. (12) is reached. These findings immediately exclude the stoichiometries expressed by eqns. (2)–(5) which cannot satisfy the experimental relations (10) and (13). This is confirmed by the observation that, contrary to the requirement of eqns. (2)–(5), no gas is evolved during the recording of peak I.

The reaction paths theoretically permissible, according to massive electrolysis results, are summarized in Fig. 6. In this figure the underlined species represent the final products of the process, *i.e.*: O_2^{2-}, O_2^-, NO_2^-. Na_2O (solid), Na_2O_2 (solid), Na_3NO_3 (solid) are the compounds which could constitute the precipitate on the
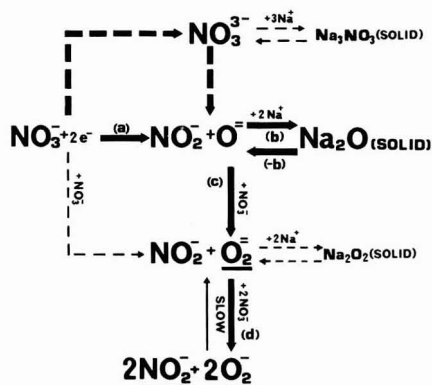
Fig. 6. Reaction path for the electroreduction of NO_3^- on a platinum cathode.

electrode. In fact, each of them could, in theory, precipitate, then dissolve and react with the melt to generate NO_2^-, O_2^{2-} and O_2^- in quantities and ratios required by relations (10) and (13).

Nature and properties of the precipitate

The nature of the precipitate has been deduced as follows. The findings arising from the experiment presented in Fig. 5 are consistent with the presence of superoxide (O_2^-) in close proximity to the microelectrode after recording wave II. In fact, during the recording of III it is oxidized to molecular oxygen and successively (peak IV) regenerated, according to the reversible electroprocess:

$$O_2^- = O_2 + e^- \tag{17}$$

It is reduced to peroxide according to the reversible relation:

$$O_2^- + e^- = O_2^{2-} \tag{18}$$

during the recording of V. In this context, the progressive decreasing of the area from III to V, expressed by relation (15), and the dependence of the values of such areas on

the potential scan rate, are ascribable to diffusion of the electroactive species toward the bulk of the melt. Since this superoxide cannot be part of the precipitate itself because of the high solubility[23,24] of alkali metals superoxides in nitrate solvents, it must be a product of the electrooxidation (wave II) of the precipitate on the electrode. Two of the three possible precipitates reported in Fig. 6 *viz.* Na_2O and Na_2O_2 can, in theory, be easily oxidized to superoxide according to the following reactions:

$$Na_2O_{(solid)} = 2 Na^+ + \tfrac{1}{2} O_2^- + 1.5 \, e^-$$ (19)

$$Na_2O_{2(solid)} = 2 Na^+ + O_2^- + e^-$$ (20)

The actual precipitate can be deduced on the basis of the results reported in Fig. 4. The extrapolated value of R_{ext} represents, as previously seen, the ratio between the areas of peaks I and II in the absence of spontaneous dissolution. Under these limiting conditions, R is equivalent to the ratio between the electrons involved in the electro-formation (peak I) and in the successive electrodissolution (peak II) of the precipitate. In Fig. 4, R_{ext} is equal to 1.33 corresponding to an electron ratio of $2/1.5 = 1.33$, just as in the case of a precipitate formed uniquely by Na_2O (see Fig. 6 and eqn. (19)). A precipitate consisting of Na_2O_2 would give an electron ratio $2:1 = 2$. The precipitation of Na_3NO_3 seems quite improbable since its oxidation reaction would be expected to be:

$$Na_3NO_{3(solid)} = 3 Na^+ + NO_3^- + 2 \, e^-$$ (21)

which involves an electron ratio $2:2 = 1$ and does not produce superoxide. The suggestion that $R_{ext} = 1.33$ is due to a fortuitous precipitation of a $1:1$ mixture of Na_3NO_3 and Na_2O_2 instead of pure Na_2O has been rejected on the basis of the independence of R_{ext} on temperature (see curves a and b in Fig. 4). It is in fact likely that, if a mixed process were present, the relevant kinetics and equilibria involved [see Fig. 6 and reactions (19)–(21)] would be affected by a temperature variation of fifty degrees, with a consequent change in the ratio of the two precipitates and there-fore in the extrapolated value of R.

Thus, Na_2O is the only component of the precipitate. It can be electrooxidized to superoxide according to eqn. (19), and then to oxygen according to eqn. (17), giving rise to the two consecutive peaks II and III. If not electrooxidized, the deposit of Na_2O dissolves spontaneously in the melt. In pure $(Na, K)NO_3$ its physical dissolution is accelerated by the chemical reaction (c) in Fig. 6. In fact, working in excess of NO_2^- which is a product of reaction (c), the spontaneous solubilization effect decreases (compare the slope of curves b and c in Fig. 4), although the nature of the precipitate remains unchanged ($R_{ext} = $ constant).

Reaction path

The broad arrows in Fig. 6 indicate the sequential steps involved in the reduc-tion of NO_3^-, from the electrode reaction to the formation of the final products. Step (a) represents the overall electron-transfer reaction.

Analogously[25] to similar processes involving other oxygenated anions, the simplest primary cathodic process seems to be:

$$NO_3^- + 2 \, e^- = NO_3^{3-}$$ (22)

followed by a rapid decomposition of the intermediate orthonitrite (NO_3^{3-}) into

nitrite (soluble) and oxide (insoluble). This is in agreement with the finding that NO_3^- must be involved, as such, in the electron-transfer process; in fact, all the attempts[2,5,21] to invoke, in this reduction, the products of the possible dissociations [5,26,27] of NO_3^- (NO_2^+ or O_2):

$$NO_3^- = NO_2^+ + O^{2-} \tag{23}$$

$$NO_3^- = NO_2^- + \tfrac{1}{2} O_2 \tag{24}$$

have always failed. As seen, the oxide produced can precipitate on the electrode or dissolve in the melt because of the combined action of diffusion and reaction (c). During the recording of peak I the precipitation prevails, Na_2O is accumulated on the electrode and the reduction of NO_3^- is progressively inhibited. The after-peak limiting current[1,2,5] corresponds to a certain thickness of precipitate at which the rate of dissolution equals the rate of deposition. We have found that this thickness, calculated from the area of peak I (recorded at high potential scan rate to minimize the effect of spontaneous dissolution), is constituted by approximately 300 molecular layers at $229°C$. A steady-state similar to the after-peak situation can be readily reached also by polarizing, at a constant potential, an electrode in the region of peak I. It is the case of the massive electrolysis previously described.

Our finding that a chemical process—reaction (c)—is involved in the dissolution, offers a reasonable explanation for the value of 11 kcal* found[1,2] for the temperature coefficient of the limiting current. As pointed out by Swofford and Laitinen, this value is too high to be ascribed to a process uniquely governed by diffusion.

All the possible precipitates in Fig. 6 have been formulated as compounds with sodium and not with potassium, which is also present in the melt. This has been suggested by the fact that the reduction of NO_3^- results in the formation of a current peak only if sodium (or lithium) ions are present; if potassium alone is in the solvent, the current rises without formation of a peak[2,10]. The effect has been recently[10] tentatively explained by postulating a very large difference in solubility between K_2O and Na_2O (or Li_2O).

On the basis of the present study, the alternative interpretation that suggests itself is the difference in reactivity of oxide in the presence of the various alkali metal ions. The absence of the cathodic maximum in the presence of potassium alone can then be due to a fast production of superoxide which is a much more soluble species[23,24] than oxide. It is well known, on the other hand, that oxide (and hydroxide) react much more easily with strong oxidizing agents, such as molecular oxygen, in systems (both solid[28,29] or molten[30]) containing potassium rather than sodium or lithium. A quantitative study of the phenomenon appears, therefore, difficult of fulfilment because at the temperature necessary to work with pure KNO_3 the electrode reactions begin to be strongly complicated by a collateral process implying the corrosive attack[10] of any electrode surface.

Reproducibility and consistency of results

The reproducibility and the consistency of the results reported in this communication were critically contingent on the use of a perfectly dry melt; otherwise

---

* 1 kcal = 4.184 kJ.

the situation described could be modified by the concomitant reactions:

$$O^{2-} + H_2O = 2\,OH^- \tag{25}$$

$$O_2^{2-} + H_2O = 2\,OH^- + \tfrac{1}{2}\,O_2 \tag{26}$$

$$2\,O_2^- + H_2O = 2\,OH^- + \tfrac{3}{2}\,O_2 \tag{27}$$

Generally, the presence of small water concentrations does not substantially modify the processes of formation and precipitation of the oxide. In fact, as previously reported[2], the characteristics of the cathodic peak are practically independent of traces of moisture. This is probably due to the fact that only water, present in the vicinity of the cathode, can react according to eqn. (25). Precipitation is a fast process and most of the oxide produced can precipitate before additional water can diffuse to the electrode. The influence of moisture becomes much more important during the solubilization of the precipitate, governed as we have seen, by processes slower than precipitation and with which the diffusion of water can be competitive. For example, the presence of 0.02% w/w of water is sufficient to double the solubilization effect of a dry melt, *i.e.* the effects reported in Fig. 3 can be obtained with "waiting times" reduced by a half. Moreover, under a stirring regime (generally maintained during the massive electrolysis experiments reported in the literature) migration of both H_2O and O^{2-} is obviously accelerated, favouring their combination according to eqn. (25), which is certainly very fast and far[31] to the right. It is evident that beyond certain limits (moisture level, stirring, etc.) reaction (25) can prevail over process (c) in Fig. 6. This was very probably the case for the experiment presented in Fig. 2, for which [see eqn. (14)] the overall electrode process was:

$$NO_3^- + 2e^- + H_2O = NO_2^- + 2\,OH^- \tag{28}$$

Previously[4,9], the hypothesis of the formation of OH^- in the reduction of nitrate melts (supposedly wet) has also been formulated to interpret some potentiometric results.

Between the extreme limits exemplified by the mechanism of Fig. 6 and reaction (28) there exists a continuous spectrum of intermediate possibilities (depending on the accuracy in drying the melt *relative* to the final concentration of the electrolysis products) which can lead to spurious and inexplicable stoichiometries.

The all-platinum apparatus[15] that we used allowed us to avoid the side reactions with silica:

$$O^{2-} + SiO_2 = SiO_3^{2-} \tag{29}$$

$$O_2^{2-} + SiO_2 = SiO_3^{2-} + \tfrac{1}{2}\,O_2 \tag{30}$$

$$2\,O_2^- + SiO_2 = SiO_3^{2-} + \tfrac{3}{2}\,O_2 \tag{31}$$

We suggest that many of literature findings, which conflict with the model discussed in this paper, are interpretable in terms of side reactions such as (25)–(27) and (29)–(31). In fact it has been possible to reproduce a number of such earlier results by working in glass or silica vessels or by working with melts which had been insufficiently dried.

SUMMARY

Microcoulometric and voltammetric measurements have been carried out in the temperature range $229°-280°$ C, in a $(Na,K)NO_3$ eutectic melt, pure or containing species produced *in situ* by massive electrolysis. The following processes related to the electrochemical reduction of NO_3^- at a platinum cathode, have been substantiated:

$$NO_3^- + 2e^- = NO_2^- + O^{2-} \tag{a}$$

$$O^{2-} + 2\,Na^+ = Na_2O \text{ (solid)} \tag{b}$$

$$O^{2-} + NO_3^- = NO_2^- + O_2^{2-} \tag{c}$$

$$O_2^{2-} + 2\,NO_3^- = 2\,NO_2^- + 2\,O_2^- \tag{d}$$

The oxide ions, produced according to eqn. (a), precipitate on the electrode because of the low solubility of Na_2O and the kinetic prevalence of process (b) over (c). On the other hand, process (c) is sufficiently fast to accelerate considerably (subtracting oxide ions) the physical redissolution in the melt of the Na_2O accumulated on the electrode. Equation (d) represents a slow reaction which cannot influence the processes at the electrode. The sodium oxide formed on the electrode surface can be electro-oxidized according to the consecutive reactions: $2\,Na_2O$ (solid) $= 2\,Na^+ + O_2^- + 3e^-$; $O_2^- = O_2 + e^-$, responsible for two distinct anodic peaks.

This study is a further step toward a more comprehensive picture of "oxides chemistry" in molten solvents.

REFERENCES

1 G. J. HILLS AND K. E. JOHNSON, *Proceedings of the 2nd International Congress on Polarography, Cambridge, 1959*, Pergamon Press, London, 1961, p. 974.
2 H. S. SWOFFORD AND H. A. LAITINEN, *J. Electrochem. Soc.*, 110 (1963) 814.
3 H. S. SWOFFORD AND P. G. MCCORNICK, *Anal. Chem.*, 37 (1965) 970.
4 G. G. BOMBI AND M. FIORANI, *Talanta*, 12 (1965) 1053.
5 G. J. HILLS AND P. D. POWER, *J. Polarog. Soc.*, 13 (1967) 71.
6 A. M. SHAMS EL DIN AND A. A. EL HOSARY, *Electrochim. Acta*, 13 (1968) 135.
7 A. M. SHAMS EL DIN AND A. A. EL HOSARY, *J. Electroanal. Chem.*, 17 (1968) 238.
8 M. FRANCINI AND S. MARTINI, *Electrochim. Acta*, 13 (1968) 851.
9 G. A. MAZZOCHIN, G. G. BOMBI AND G. A. SACCHETTO, *J. Electroanal. Chem.*, 21 (1969) 345.
10 H. E. BARLETT AND K. E. JOHNSON, *J. Electrochem. Soc.*, 114 (1967) 64.
11 P. G. ZAMBONIN AND J. JORDAN, *J. Am. Chem. Soc.*, 89 (1967) 6365.
12 P. G. ZAMBONIN AND J. JORDAN, *J. Am. Chem. Soc.*, 91 (1969) 2225.
13 T. E. GECKLE, Thesis, Pennsylvania State University, University Park, Pa., 1964.
14 M. PELEG, *J. Phys. Chem.*, 71 (1967) 4553.
15 P. G. ZAMBONIN, *Anal. Chem.*, 41 (1969) 868.
16 G. DAVOLIO, W. GUERZONI AND P. PAPOFF, *Electrochim. Acta*, 5 (1961) 291.
17 J. A. CHRISTENSEN, *J. Am. Chem. Soc.*, 82 (1960) 5517.

18 V. G. LEVICH, *Physicochemical Hydrodynamics*, Prentice-Hall, Inc., Englewood Cliff, N.J., 1962.

19 J. HEYROVSKÝ AND J. KŮTA, *Principles of Polarography*, Academic Press New York, 1966.

20 P. G. McCORNICK AND H. S. SWOFFORD, *Anal. Chem.*, 41 (1969) 146.

21 L. E. TOPOL, R. A. OSTERYOUNG AND J. H. CHRISTIE, *J. Phys. Chem.*, 70 (1966) 2857.

22 P. DELAHAY, *New Instrumental Methods in Electrochemistry*, Interscience Publishers Inc., New York, 1954, pp. 120–137.

23 J. SAUKA AND V. BRUNERE, *Latvijas PSR Zinatnu Akad. Vestis Kim. Ser.*, 6 (1966) 615.

24 P. G. ZAMBONIN AND A. CAVAGGIONI, work in progress.

25 H. A. LAITINEN, *Talanta*, 12 (1965) 1237.

26 F. R. DUKE AND S. YAMAMOTO, *J. Am. Chem. Soc.*, 81 (1959) 6378.

27 D. INMAN AND J. BRAUNSTEIN, *Chem. Commun.*, (1966) 148.

28 I. I. VOL'NOV in A. W. PETROCELLI (Ed.), *Peroxide, Superoxide and Ozonides of Alkali and Alkaline Earth Metals*, English translation, Plenum Publishing Co. New York, 1966.

29 I. I. VOL'NOV, V. N. CHAMOVA, E. I. LATYSHEVA AND E. YA. FILATOV, *Russ. J. Phys. Chem., English Transl.*, 12 (1967) 1187.

30 H. LUX, R. KUHN AND T. NIEDERMEIER, *Z. Anorg. Allgem. Chem.*, (1959) 286.

31 J. JORDAN, W. B. McCARTHY AND P. G. ZAMBONIN in G. MAMANTOV (Ed.), *Characterization and Analysis in Molten Salts*, M. Dekker, New York, 1969, in press.

VOLTAMMETRY WITH DISC ELECTRODES AND ITS ANALYTICAL APPLICATION

I. BIAMPEROMETRIC EDTA-TITRATIONS IN ACIDIC SOLUTION USING GLASSY CARBON ELECTRODES

F. VYDRA AND P. PETÁK

J. Heyrovský Polarographic Institute, Czechoslovak Academy of Sciences and Ore Research Institute, Prague (Czechoslovakia)

Various electrode systems have been applied for the indication of biamperometric titrations[1–3]. On the basis of a voltammetric study the possibility of the application of two glassy carbon electrodes is demonstrated in the present paper for a biamperometric titration on the Fe^{3+}–EDTA system. Similar problems have been solved recently with platinum electrodes[1].

EXPERIMENTAL

Apparatus

The current and electrode potential during titration were measured with an apparatus consisting of two glassy carbon electrodes prepared from glassy carbon rods (Tokai Electrode Mfg., Tokyo, Japan) fixed in glass tubes with epoxide resin, of surface area 7 mm^2, which were rotated at the speeds of 600–1800 rpm, and two saturated calomel electrodes (SCE) with Luggin capillaries, the nozzles of which were 2 mm distant from the rotating electrodes.

The voltage was applied to the electrodes from a potentiometer and the current measured by a galvanometer of a flame photometer (K. Zeiss, Jena) with sensitivity control. The potential of the indicator electrodes against SCE during titration were measured by a compensation pH-meter THK-I (Mikrotechna, Praha).

The indicator electrode for the voltammetric measurement was a rotating disc made from glassy carbon. A glassy carbon rod was fixed in the Teflon tube at a higher temperature (100°C) to prevent leakage of water between the carbon rod and the Teflon tube. The glassy carbon disc (surface area 7 mm^2) was rotated at 2300 rpm. The resulting polarization curves were recorded using polarograph LP 60 (Lab. přístroje, Prague). The electrode surface was renewed before each measurement by polishing to a mirror-like finish with metallographic papers SIA (Switzerland) Nos. 1, 3 and 5.

pH measurements were carried out with pH meter PHK-1 (ČSSR) and a glass electrode.

Reagents

A 0.1 *M* solution of iron(III) was prepared by dissolving solid $Fe(NO_3)_3$

(analytical-grade purity) in water. Its concentration was verified gravimetrically. A 0.1 M solution of ethylenediaminetetraacetic acid (EDTA) was prepared by dissolving the solid compound in water and adjusting the pH to 5.

The buffer solutions were prepared by dissolving the solid salts in water to obtain a final concentration of about 1 M. The electrolytes used were: hydrochloric, nitric, trichloracetic and monochloroacetic acids, and buffer solution, acetic acid/ammonia, all prepared at a concentration of *ca.* 1.0 M.

EXPLANATION OF THE SHAPE OF THE TITRATION CURVES

During the titration of iron(III) with EDTA the external voltage, the current, and the potentials of both electrodes were measured. The volume of the solution titrated was always 100 ml and the concentration of Fe^{3+} ions 5×10^{-3} M. The titrations were carried out in the electrolytes described in the section *Reagents* and the polarization curves recorded. Various speeds of polarization were used; the best results were obtained at 400 mV min^{-1} and a chart speed of 40 mm min^{-1}.

In trichloracetic acid solution, where the shapes of waves are best developed, the height of the cathodic wave of Fe^{3+} is linearly dependent upon the iron concentration, in the range $1 \times 10^{-5} - 1 \times 10^{-3}$ M. At higher concentrations, the wave is deformed before reaching the limiting current. The height of the wave of the chelate FeY^- is also directly proportional to the concentration of the chelate, but in a considerably narrower range than in the case of Fe^{3+}. This can be seen in the Fig. 1 which shows the decrease of the height of the wave of Fe^{3+} as a function of the amount of EDTA added, and the corresponding increase of the chelate wave. The polarization curves from which this dependence was derived are given in the Fig. 2. The waves with $E_{\frac{1}{2}}$ of about $+0.4$ V are those of iron(III).

The voltammetric curves are also well developed and reproducible in monochloroacetic acid (pH 2.34) while in mineral acids the dependence of the height of the
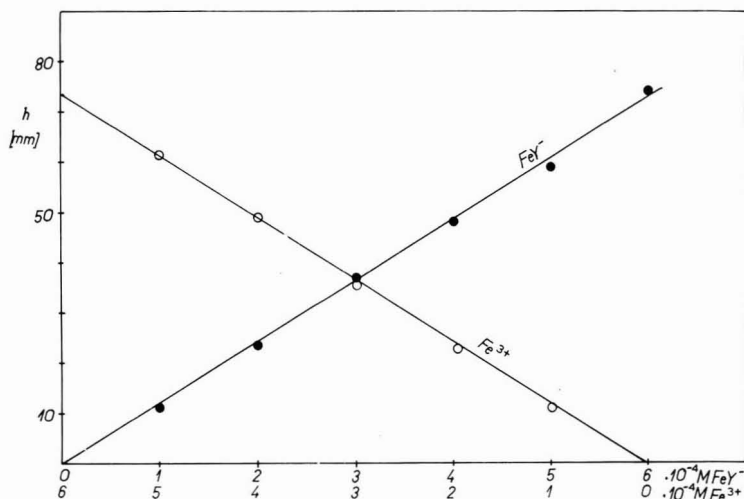
Fig. 1. The dependence of the wave height on the concn. of Fe^{3+} and FeY^- at pH 1.68.
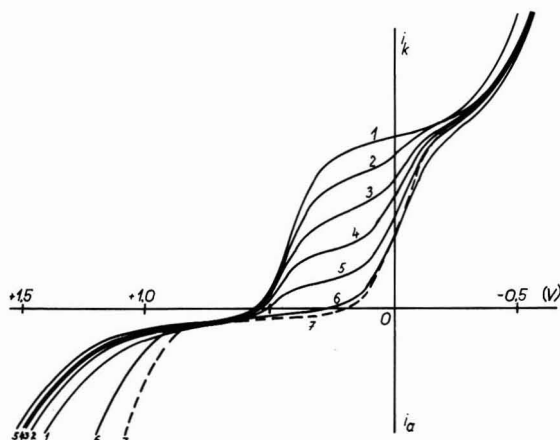
Fig. 2. Polarization curves during the titration of Fe^{3+} with EDTA. 0.1 M trichloracetic acid (pH 1.68); rate of polarization, 400 mV min^{-1}. (1) 6×10^{-4} M Fe^{3+}, (2) 5×10^{-4} M $Fe^{3+} + 1 \times 10^{-4}$ M FeY^-, (3) 4×10^{-4} M $Fe^{3+} + 2 \times 10^{-4}$ M FeY^-, (4) 3×10^{-4} N $Fe^{3+} + 3 \times 10^{-4}$ M FeY^-, (5) 2×10^{-4} M $Fe^{3+} + 4 \times 10^{-4}$ M FeY^-, (6) 6×10^{-4} M FeY^-, (7) 6×10^{-4} M $FeY^- + 6 \times 10^{-4}$ M EDTA.

waves on the concentration of Fe(III) ions and FeY^- is linear in a narrower concentration interval.

The polarization curve using trichloracetic acid as base electrolyte is given in Fig. 3. The foot of the reduction wave of dissolved oxygen is at a potential of -0.05 V; anodic evolution of oxygen starts at $+1.1$ V. The polarization curves (cathodic branch) of other acids are similar. The anodic evolution of oxygen starts at $+0.85$ V in nitric acid, in other acids at about $+1.1$ V.

Dissolved oxygen was found to affect neither the shape nor the position of the voltammetric curves of the titration system and therefore it was not removed from the solution[1].
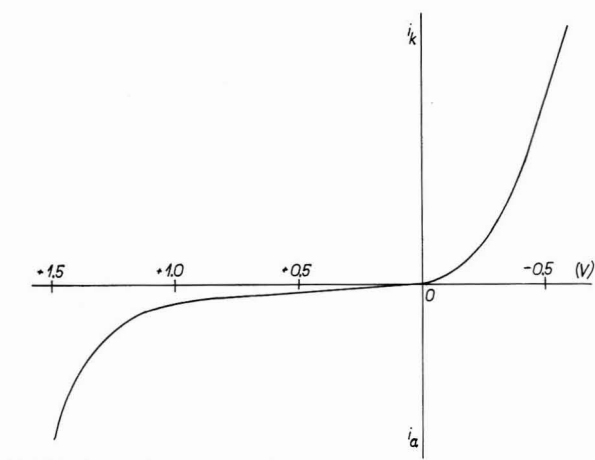
Fig. 3. Polarization curve of 0.1 M trichloracetic acid in the presence of dissolved oxygen.

After the insertion of both glassy carbon electrodes into the solution of iron(III) ions in a medium of 0.1 M trichloracetic acid, both the electrodes had a potential of $+0.5$ V *versus* SCE. The potential of the anode is shifted to more positive values and the potential of the cathode to more negative values during the step-wise increase of the applied voltage (measured with a circuit where no current flows). The shift of both potential values is approximately linear with respect to the values of applied voltage up to a value of 0.6 V (Fig. 4).
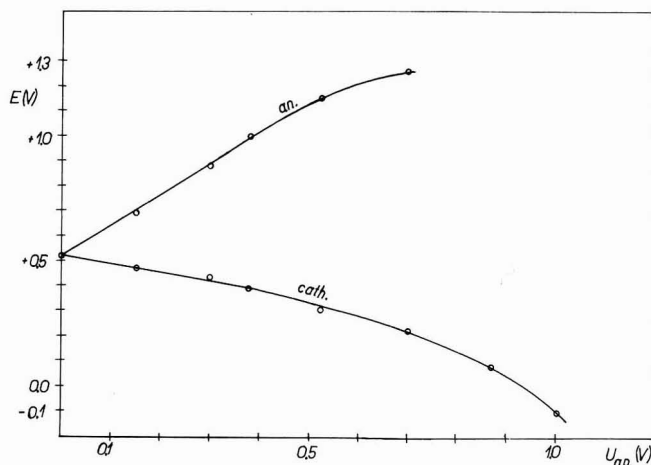
Fig. 4. The dependence of electrode potential upon the applied voltage for 5×10^{-4} M Fe^{3+} solution.

At an applied voltage of 0.6 V, the potential of the anode reaches the value $+1.2$ V (SCE), where the anodic evolution of oxygen starts (see Fig. 3). At this applied voltage the potential of the cathode is $+0.26$ V, *e.g.*, more negative than the value of the half-wave potential of the reduction of iron(III) ion ($+0.42$ V).

Under these conditions iron(III) ions are therefore reduced to iron(II) ions. As a result of these phenomena the dependence of the electrode potential on the applied voltage is not linear and the electrode reaction occurring at the applied voltage of 0.6 V influences the slopes of the curves presented in Fig. 4.

During the titration of iron(III) with EDTA in trichloracetic acid medium, a voltage of 0.4–1.0 V was applied to the electrode.

The explanation of the shape of the titration curve was arrived at by an analysis of the polarization curves corresponding to various phases of the titration (Fig. 2). The polarization curve corresponding to the beginning of the titration is shown in Fig. 5a which shows the reduction wave of Fe^{3+} with a half-wave potential of $+0.42$ V (SCE). At the point of titration of 50% of the total content of iron, the wave of Fe^{3+} decreased and a new wave corresponding to the reduction of the chelate FeY$^-$ ($E_{\frac{1}{2}} = 0.0$ V) (SCE) appeared (Fig. 5b). Up to the equivalence point no effect of this wave on the value of the measured current was observed. The current decreased with decrease in the concentration of free iron(III) ions during the titration.

At the equivalence point where (taking into account the high stability constant of FeY$^-$ at pH 1.68, $pK_{FeY} = 9.0$) virtually only the chelate is present, the residual current was recorded (Fig. 5c) and was higher at carbon than at platinum electrodes.

At this point the titration curve has a pronounced minimum but the corresponding current value is relatively high (approx. 5×10^{-7} A). On further addition of EDTA, the current value again increased as the titration curve shows. In this phase of the titration a shift in the anodic oxygen evolution from $+1.1$ to $+0.85$ V (SCE) was observed. At rotating glassy carbon electrodes no EDTA wave is observed probably as a result of the very slow electrode reaction and a preferential adsorption of oxygen. Polarization curves corresponding to various points of the titration curve are presented in Fig. 2.

In the case of a stationary electrode, there is a well developed wave with an $E_{\frac{1}{2}}$ of $+1.0$ V (Fig. 6). The voltammetry of EDTA and related compounds at a disc glassy carbon electrode will be presented in a separate paper.
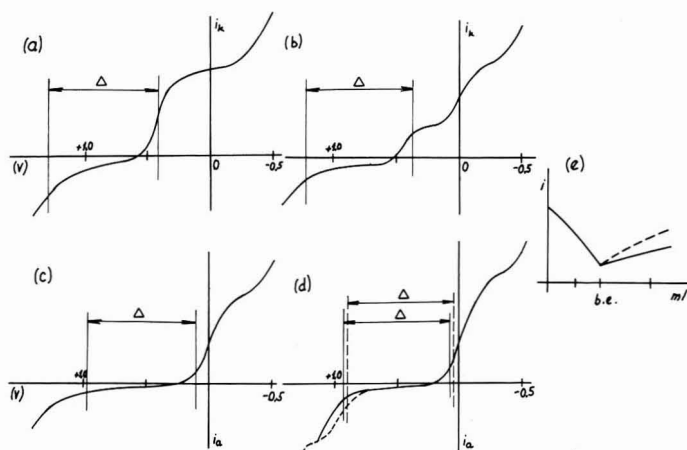
Fig. 5. Polarization curves of various phases of the titration of 6×10^{-4} M Fe^{3+} with EDTA in 0.1 M trichloracetic acid, pH 1.68. (a) Start, (b) half-equivalence, (c) equivalence, (d) 100% overtitrated, (e) resulting titration curve. (———) Rotating electrodes, (---) stationary electrodes, ($\triangle$) applied voltage.

The titration curves with stationary electrodes have a different shape after the equivalence point. Titration curves corresponding to the titration with rotating electrodes show a little increase of the current after the equivalence point owing to the shift of the anodic evolution of oxygen. On the other hand, this increase is higher on the curves corresponding to the titrations with the stationary electrode, because the wave of free EDTA is shifted to a more negative potential than the potential of the anodic evolution of oxygen (Fig. 5d, dotted line). The potential distance of the residual current between the reduction wave of FeY^- chelate and the titration wave of EDTA is therefore shortened, which at constant applied voltage results in an abrupt increase of the measured current (Fig. 5e, dotted line).

The potential of the indicator electrodes shifts to more negative values with decreasing concentration of free Fe^{3+} ions (Fig. 7). From Fig. 5 follows that at a constant potential difference of the anode and the cathode (Δ), the total current measured is:

$$i_c = i_a = i_\Sigma$$
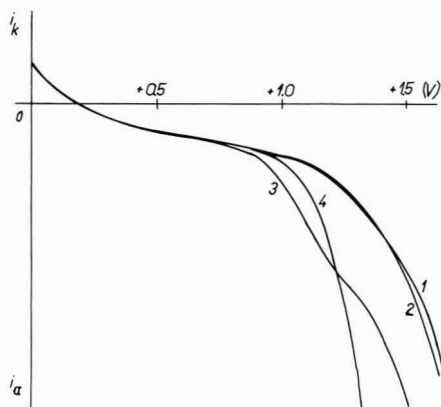
Fig. 6. Polarization curves of the oxidation of EDTA at rotating and stationary electrodes. (1) Base electrolyte 0.1 M trichloracetic acid at a rotating electrode, (2) the same at a stationary electrode, (3) 6×10^{-4} M EDTA at a stationary electrode, (4) the same at a rotating disc electrode. Polarization from 0.0 to 1.6 V with a speed of 400 mV min.$^{-1}$
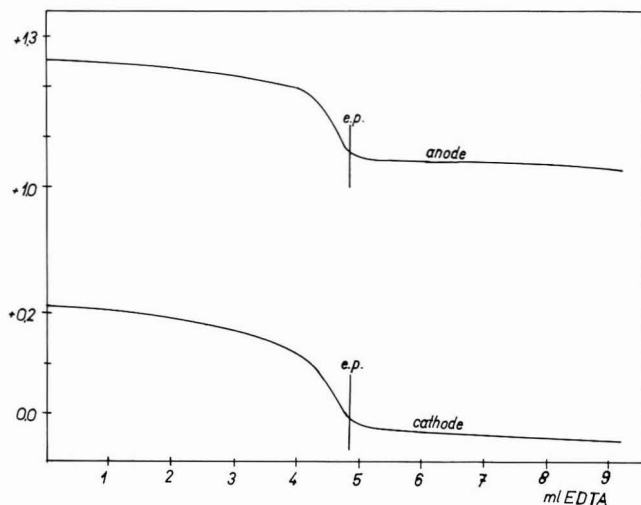
Fig. 7. The dependence of electrode potential on amount of EDTA added during the titration of 6×10^{-4} M Fe^{3+}; 0.1 M trichloracetic acid solution, applied voltage 0.7 V, titrated with 0.1 M EDTA.

This current represents the reduction of Fe^{3+} ions at the cathode and evolution of oxygen at the anode before equivalence; at equivalence it is virtually a background current, and after equivalence the current is given by reduction of the iron chelate and anodic oxygen evolution.

At stationary electrodes, the current after equivalence corresponds to the reduction of FeY^- and the oxidation of EDTA.

THE DEPENDENCE OF THE TITRATION CURVE OF FERRIC IONS ON THE pH

The pH-dependence of the titration of Fe^{3+} with EDTA could be followed only up to pH 2.5 because of the hydrolysis of ferric ions at higher pH values. In a solution of a pH below 1.5, there is a partial dissociation of the chelate FeY^-, the rate of the reaction of Fe^{3+} with EDTA decreases, and the stabilization of the current values takes a longer time. In spite of this, the results are satisfactory in solutions of both 0.1 M HCl and in 0.1 M HNO_3. The titrations were also carried out in trichloroacetic (pH 1.68) and monochloroacetic acids (pH 2.34).

The optimum titration medium from the point of view of indication is monochloroacetic acid, where the greatest current changes were observed during titration (Fig. 8). It is of interest that at high applied voltages (0.8–1.0 V) the greatest current changes were found in nitric acid solution. In this case the stabilization of current values is rather slow.
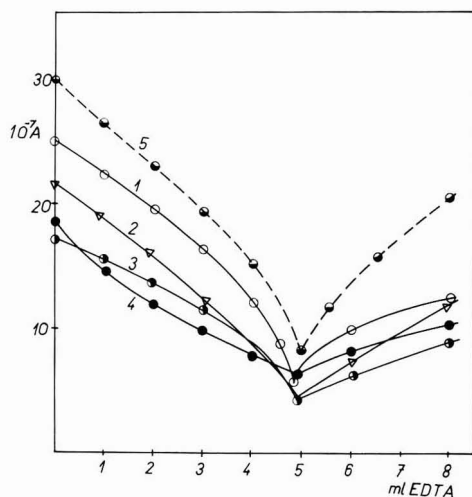
Fig. 8. The dependence of the titration curve of Fe^{3+} with EDTA on the composition of the base electrolyte. (1) 0.1 M monochloroacetic acid (pH 2.34), (2) 0.1 M HNO_3, (3) 0.1 M trichloracetic acid (pH 1.68), (4) 0.1 M HCl, (5) 0.1 M trichloracetic acid. (———) Rotating electrodes, (– – –) stationary electrodes; applied voltage 0.6 V.

The titration was also attempted in sodium acetate (pH 3.80). Owing to hydrolysis a colloidal solution of iron exists under these conditions. The titration is possible at high applied voltage (1.0 V) but the stabilization of the current value is very slow due to the slow reaction of dissolving hydroxo-complexes of iron during formation of the EDTA chelate.

On the other hand, only a lower applied voltage (0.6 V) can be used for the titration in HCl solution (pH 1.12) for obtaining reproducible titration curves because of interference from Cl^- ions similar to that observed with platinum electrodes[1]. In this case also it is necessary to wait rather a long time for current value stabilization.

DISCUSSION

The use of glassy carbon electrodes in biamperometry shows some differences and advantages with respect to platinum electrodes.

(1) Carbon electrodes are substantially cheaper than platinum electrodes.

(2) Pretreatment of carbon electrodes is easy and rapid. While platinum electrodes must be protected by electrolytic evolution of hydrogen and oxygen or by careful polishing, carbon electrodes are completely clean after simple polishing with a fine metallographic paper.

(3) The reduction of dissolved oxygen at platinum starts at about $+0.35$ V (SCE), but at a carbon electrode it does not do so until -0.05 V. Anodic oxygen evolution starts at both electrodes at $+1.1$ V. Thus a broader potential range is available.

(4) The voltammetric curves of Fe^{3+} and FeY^- have different shapes on carbon and platinum electrodes. FeY^- chelate yields a reduction wave ($E_{\frac{1}{2}}=0.0$) on a carbon electrode while on platinum electrode this wave does not appear in the potential interval studied. The half-wave potentials of the reduction waves of iron-(III) differ by 50 mV ($E_{\frac{1}{2}}$ $Fe^{3+}_{Pt} = +0.47$ V; $E_{\frac{1}{2}}$ $Fe^{3+}_C = +0.42$ V).

(5) The disadvantage of carbon electrodes is that they undergo recrystallization at high currents.

(6) The other disadvantage of carbon electrodes compared with platinum is the high value of the residual current. The residual current does not influence the shape of the biamperometric titration curves but, on the other hand, it may cause some trouble in the recording of the voltammetric curves. The titration curves of electroinactive metals (*e.g.* Al^{3+}) are similar to those obtained with platinum electrodes, *i.e.*, before the end point the current is approximately constant, increasing after the end point (reversed L-shaped curves).

REFERENCES

1 F. VYDRA AND K. ŠTULÍK, *J. Electroanal. Chem.*, 16 (1968) 375.
2 A. L. KIES, *J. Electroanal. Chem.*, 8 (1964) 325.
3 A. E. MARTIN AND R. C. REILLEY, *Anal. Chem.*, 31 (1959) 992.

DISPOSITIF AUTOMATIQUE D'ETUDE DE PROCESSUS ELECTROCHIMIQUES

BERNARD POINTU, MIREILLE BRAIZAZ et PIERRE PONCET

Section de Recherches de Mécanique Ondulatoire Appliquée, Faculté des Sciences de Lyon, 69 Villeurbanne (France)

INTRODUCTION

Les processus électrochimiques mettent en jeu des mécanismes décelables à travers les variations corrélatives de paramètres physico-chimiques mesurées expérimentalement.

Le nombre parfois élevé de grandeurs étudiées d'une part, le rôle privilégié de la variable temps d'autre part, suggèrent l'automatisation des montages. Celle-ci permet en particulier, la synchronisation des opérations de commande, l'obtention de mesures d'un grand nombre de variables, la connaissance de la date de chaque mesure et la possibilité d'observer simultanément des phénomènes présentant des vitesses d'évolution différentes. Dans divers cas, des méthodes automatiques ont été proposées[1-3]. Ces appareillages construits spécialement pour l'étude d'une variable demeurent souvent d'un emploi trop particulier pour justifier leur connexion avec des unités de calcul. Booman[4] a envisagé de façon générale l'adaptation de techniques digitales aux mesures électrochimiques et Breiter[5] a proposé une instrumentation appropriée aux mesures voltamétriques avec tension alternative superposée.

Le dispositif automatique décrit ci-dessous permet l'alimentation programmée d'une cellule électrochimique, la commande d'appareils annexes régissant l'évolution d'autres paramètres, la mesure automatique et à diverses vitesses d'une dizaine de variables, le "stockage" des valeurs mesurées et leur exploitation à l'aide d'un ordinateur.

1. DESCRIPTION ET FONCTIONNEMENT

La Fig. 1 représente les connexions entre les divers éléments constitutifs du montage. La plupart des appareils utilisés sont commercialisés; leurs performances essentielles sont résumées dans le Tableau 1.

Le montage de base comporte une cellule électrolytique B, son alimentation A et un appareil de mesure, C, pour lequel nous avons choisi un voltmètre numérique. Par suite de ce choix, toutes les grandeurs mesurées devront se présenter sous la forme de différences de potentiel.

1.1. *Origine des grandeurs mesurées*

La Fig. 2 est une représentation symbolique des branchements réalisés sur une

SCHEMA D'ENSEMBLE DU MONTAGE

Fig. 1.

EXEMPLE DE SYSTEME ETUDIE

CELLULE B

LEGENDE:

Th: thermocouple
R et R': électrodes de référence
V: électrode de verre
S: électrode sonde
K: cathode

A: anode
Sh: shunt (résistance étalon)
Cp: cellule photoélectrique
Am: amplificateur

E: éclairement
T: température
I: intensité
V_{ij}: différence de
   potentiel entre
   i et j
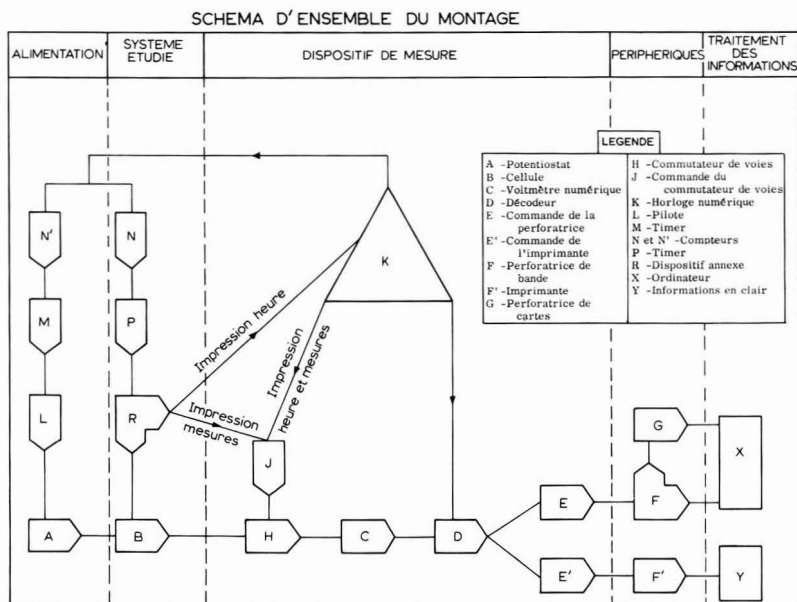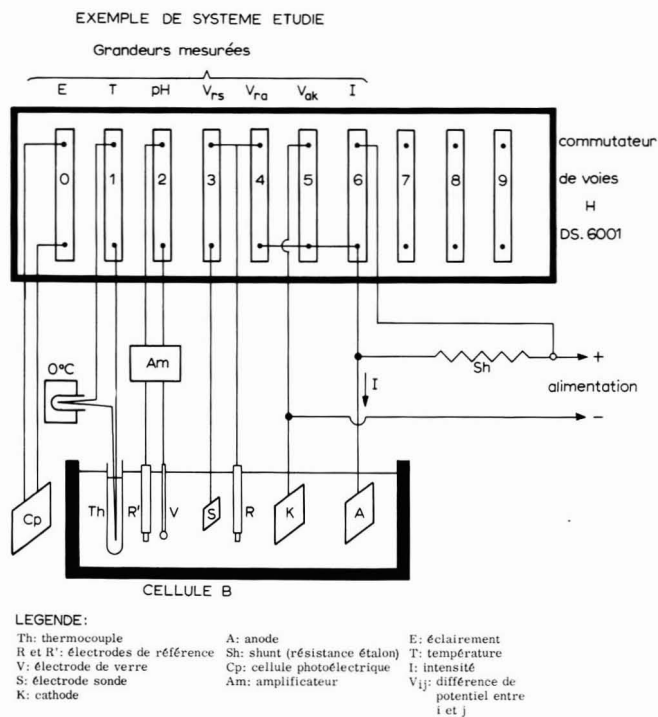
Fig. 2.

cellule à quatre électrodes munie également d'un contrôle de température, d'un contrôle de pH et d'un organe de détection de rayonnement lumineux. L'ensemble des grandeurs mesurées (E, T, pH, V_{rs}, V_{ra}, V_{ak} et I) ne constitue qu'un exemple et l'on peut le modifier en fonction du type d'alimentation choisi et de la nature des phénomènes étudiés. Ici le potentiostat A introduit une différence de potentiel contrôlée entre anode et cathode; les variations de cette tension sont commandées par le pilote, L, qui peut fonctionner en mode autonome ou, comme nous le verrons, selon un programme imposé par une commande extérieure.

Dans l'exemple de la Fig. 2 on a fait choix du paramètre éclairement d'une électrode pour présenter l'intervention dans le montage d'un dispositif annexe R. De façon plus générale R désigne tout dispositif régissant l'évolution d'un paramètre mécanique, thermique, optique ou chimique.

Un commutateur électronique, H, est placé entre B et C; il comporte un ensemble de voies permettant l'entrée de toutes les grandeurs à mesurer. L'organe de commande, J, du commutateur de voies, H, réalise diverses fonctions:

(a) il permet la commutation de l'ensemble des voies ou d'une partie seulement de celles-ci;

(b) il commande la scrutation automatique des voies selon trois modes distincts:
—exploration continue des voies affichées,
—exploration une seule fois de l'ensemble des voies,
—exploration continue d'une seule voie;

(c) il détermine la vitesse de scrutation des voies; celle-ci doit être compatible avec la vitesse d'enregistrement de l'organe de sortie.

1.2. *Mesures et enregistrement*

Le voltmètre numérique, C, est connecté au commutateur de voies et affiche les valeurs des grandeurs mesurées selon la mode et la vitesse d'exploration déterminées par J. Un panneau de programmation permet d'attribuer à chaque grandeur une gamme de mesure appropriée à sa valeur; le changement automatique des gammes est assuré par un module électronique.

L'enregistrement des mesures est obtenu par adjonction au voltmètre numérique, C, des éléments D, E, F, G d'une part, D, E', F' d'autre part. Le décodeur, D, transforme les informations enregistrées par le voltmètre pour les rendre assimilables par les organes de sortie (conversion parallèle-série). Ces données aboutissent à la perforatrice de bande F et à l'imprimante rapide F' par l'intermédiaire des commandes, E et E'; la bande perforée, produite en F, peut être transformée en cartes par la télébande perforatrice, G.

Cet appareillage constitue un ensemble effectuant des mesures précises, rapides et nombreuses des grandeurs connectées au voltmètre. Divers éléments viennent compléter le montage en vue de réaliser son automatisation totale, comme nous allons le voir.

1.3. *Mesure du temps et synchronisation*

L'horloge numérique, K, fournit l'impression du temps en heures, minutes et secondes par la liaison horloge décodeur K-D, que l'on peut réaliser à tout instant. Elle possède en outre différentes fonctions: elle fournit au décodeur D une mesure du temps qui date tout enregistrement; à des intervalles de temps égaux elle déclenche des

TABLEAU 1

	Appareils	Marque	Type	Caractéristiques
Alimentation	Potentiostat Intentiostat	A Tacussel Solea	PRT	—Tension de consigne réglable de −5 à +5 V. —Régulation meilleure que ±2 à 3 mV pour ±15% de variation de tension du réseau et 0–100% de variation de la charge. —Temps de réponse de 2–3 μs.
	Pilote	L Tacussel Solea	Servovit 9B	—Variations de 0.1–1100 mV min^{-1}.
Centralisateur de mesures: "Microscan 6400"	Commutateur de voies	H Dynamco	DS-6001	—Capacité maximum: 10 voies. Le "Microscan" peut contenir 10 commutateurs, soient 100 voies (une version améliorée comporte 600 voies).
	Commande du commutateur de voies	J Dynamco	DS-6002	—Vitesse de scrutation des voies variant de 1–17 voies par seconde. Possibilité d'exploration continue des voies ou d'une seule voie et d'exploration une seule fois de l'ensemble des voies.
	Décodeur	D Dynamco	DS-6003	
	Horloge numérique	K Dynamco	DS-6007	—Affichage lumineux des heures et minutes. —Impression des heures, minutes et secondes. —Déclenche des mesures à intervalles de temps constant (réglables de 1 min–5 h). —Fourni en affichant l'heure 2 impulsions de 1 ms, 2 impulsions de 7 s, toutes disponibles. —Peut être commandée par une impulsion extérieure.
	Electroniques de commande	E Dynamco E′ Dynamco	DS-6008 DS-6009	—Commande la perforatrice de bande. —Commande l'imprimante.
	Voltmètre numérique	C Dynamco	DM-2006	—Type intégrateur; 4 chiffres; 5 gammes de 10 μV–1000 V. Impédance d'entrée de 10,000 MΩ. Cadence de 20 mesures par seconde. —Précision: 0.02%. Changement automatique de gamme (Module D3) avec panneau de programmation des gammes (DS-6032) pour chaque voie scrutée.
Périphériques	Perforatrice de bande	F Data Dynamics	110	—110 caractères par seconde sur une bande à 8 canaux.
	Imprimante	F′ I.B.M.	B	—12 caractères par seconde.
	Perforatrice de cartes	G I.B.M.	47	—Perfore et imprime des cartes à partir de la bande perforée.
Mesures annexes	Voltmètre numérique	Dynamco	DM-2022	Type potentiométrique. 5 chiffres. 5 gammes. 10 μV–2000 V. Impédance d'entrée de 25,000 MΩ. Cadence de 50 mesures par seconde.

séries de mesure par la transmission d'impulsions à la commande J du commutateur de voies ; enfin, elle délivre simultanément d'autres impulsions que l'on utilise pour la synchronisation des appareils du montage (alimentation, dispositif annexe et dispositif de mesure).

Nous avons réalisé et adapté au matériel précédemment décrit un ensemble de modules électroniques (compteurs N et N', timers P et M, dispositif annexe R) assurant la synchronisation sur la base des impulsions produites par K. Ces différents modules sont schématisés sur la Fig. 3 ; nous allons préciser leurs rôles :
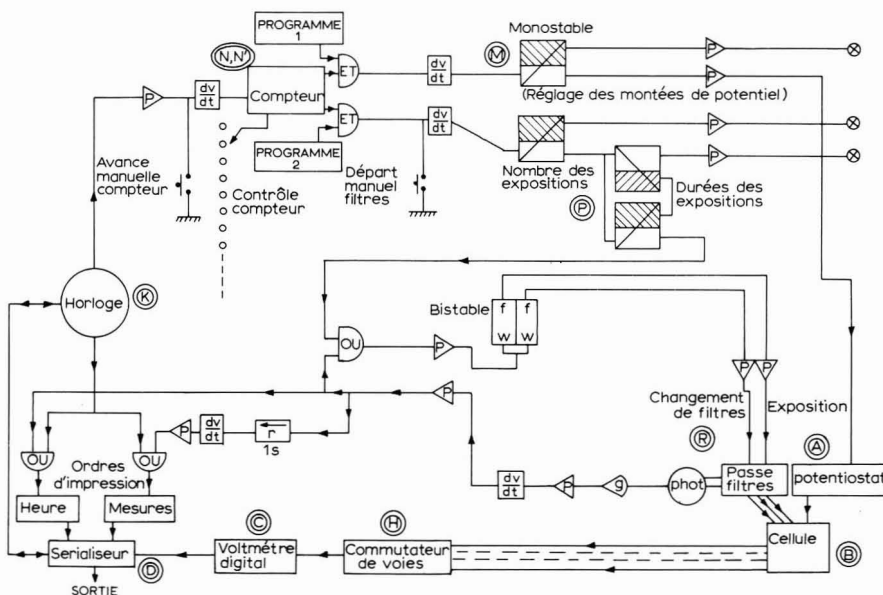
Fig. 3. Schéma électronique des dispositifs, N,N',P,M,R.

Les impulsions délivrées par l'horloge (à la fréquence choisie pour les séries de mesure) sont reçues par le compteur N' qui, pour certaines d'entre elles, met en oeuvre le timer, M ; ce dernier élément actionne le pilote, L, pendant un temps réglable. De cette manière l'alimentation est commandée par l'horloge : par exemple, si l'on enregistre les mesures toutes les trois minutes, on peut modifier les conditions d'alimentation toutes les douze minutes en utilisant, grâce au compteur, une impulsion sur quatre.

Ces impulsions sont également reçues par le compteur, N, qui commande, de la même manière, le timer, P, mettant en oeuvre le dispositif annexe. Les compteurs N et N' comportent des grilles de programmation permettant de situer les périodes de fonctionnement de R et de L dans le contexte de l'expérience, défini par l'horloge, K. Le programme général de fonctionnement du montage est donc essentiellement établi en fixant en J les modes d'exploration et en K les intervalles de commande des séries de mesures ; les fonctionnements de l'alimentation et du dispositif annexe R sont gouvernés par ce dernier choix. Un sous-programme définit le travail de R lors de chacune de ses interventions ; en outre, ce dernier module délivre lui même des

impulsions captées par l'horloge et la commande de commutateur de voies; on obtient ainsi des impressions de mesures datées rendant compte de l'action du dispositif annexe R.

Notons ici qu'il est possible d'intervenir, à tout moment, pour modifier le programme établi.

Nous venons d'analyser le déroulement d'une expérience automatique programmée, au cours de laquelle nous enregistrons à intervalles de temps donnés des séries de mesures de l'ensemble des grandeurs. L'horloge numérique joue un rôle essentiel dans ce mode de fonctionnement, elle est l'organe central de l'expérience. Il est important de noter que l'on peut toujours substituer à ce mode de fonctionnement, une exploration et un enregistrement continus de l'ensemble des voies ou même d'une seule voie. Ce dernier cas est particulièrement important car il permet l'enregistrement des variations d'un paramètre évoluant rapidement, en utilisant la vitesse maximale de fonctionnement de la perforatrice de bande; la mesure du temps n'est pas enregistrée mais se déduit aisément de l'intervalle de temps séparant deux mesures successives.

1.4. *Exploitation des résultats*

Lorsqu'il s'agit de mesures à vitesse lente, les deux modes d'enregistrement (perforatrice de bande et imprimante) sont utilisés simultanément et recueillent les mêmes mesures. L'expérimentateur suit le déroulement de la manipulation par lecture d'une part, des listes dressées par l'imprimante F′ et d'autre part des affichages numériques du voltmètre et de l'horloge; il dispose ainsi, à tout moment, de renseignements complets sur l'évolution des paramètres mesurés; sur la base de ces informations, il peut éventuellement modifier le cours prévu de l'expérience.

Dès que le nombre des résultats enregistrés devient important, l'exploitation proprement dite s'effectue à partir de la bande perforée, même si l'impression reste utile en tant que contrôle.

Dans le cas ou l'on désire enregistrer des variations rapides des paramètres mesurés on utilise la perforatrice de bande seule, à sa vitesse de perforation maximum.

Le traitement de la bande a généralement lieu en plusieurs étapes; elle n'est transmissible directement à l'ordinateur que s'il s'agit d'une suite régulière d'enregistrements, des mêmes grandeurs, effectués dans les mêmes conditions tout au long de l'expérience. La plupart du temps, une conversion en cartes perforées, préalable à tout traitement, est effectuée par la perforatrice de cartes G à partir de la bande initiale. Le traitement de l'information ainsi disponible est réalisé à l'ordinateur; la plupart des programmes de calcul étant euxmêmes entrés en machine par cartes perforées, il apparaît un nouvel intérêt de la conversion bande-cartes. Les techniques actuelles du calcul scientifique sur ordinateur apparaissent comme particulièrement adaptées pour la résolution de notre problème de traitement de l'information: il s'agit d'exploiter un très grand nombre de données; d'effectuer des calculs algébriques et de condenser l'information d'origine expérimentale en un nombre réduit de résultats significatifs. Ce mode de traitement présente une grande souplesse d'utilisation et pour chaque problème particulier on réalise un programme adapté aux besoins. Deux aspects intéressants doivent être signalés:

—la réalisation automatique de tracés de courbes; ces dernières sont obtenues soit directement à partir des valeurs expérimentales, soit à partir de valeurs résultant d'un calcul préliminaire.

—la possibilité d'appliquer les méthodes statistiques usuelles aux paramètres étudiés et d'apprécier, dans de bonnes conditions, les écarts entre répartitions expérimentales et théoriques.

Ce dernier point suggère de nombreux développements; l'utilisation de méthodes statistiques en électrochimie peut revêtir différents aspects : soit consister en l'analyse des résultats d'une expérience automatique, soit permettre la comparaison entre ceux de plusieurs manipulations successives ou simultanées; un échantillonage suffisant peut être obtenu, avec notre appareillage, en utilisant non pas une dizaine de voies, mais cent ou même six cents voies.

1.5. *Performances*

La commutation des voies (H) est très rapide et permet les mesures par le voltmètre des diverses variables avec les mêmes performances que les mesures d'une seule d'entre elles.

La vitesse de scrutation des voies, commandée en J, peut varier de une à dix-sept mesures par seconde. Cependant nous sommes limités par la vitesse d'impression des organes de sortie : 1 mesure par seconde avec l'imprimante et 10 mesures par seconde avec la perforatrice de ruban. Dans les exemples d'utilisation qui vont suivre ces performances sont suffisantes, mais pour aborder l'étude de phénomènes à évolution plus rapide, il faudrait avoir recours à un enregistrement sur bande magnétique permettant d'utiliser rationnellement les performances des voltmètres numériques.

2. EXEMPLES D'EMPLOI

Les trois exemples d'emploi introduits ci-dessous font actuellement l'objet de travaux au laboratoire. Nous indiquons brièvement ici les caractéristiques essentielles de chacun des montages et les modes de fonctionnement appropriés.

Le tracé des courbes courant–surtension peut se faire préalablement afin d'obtenir une définition précise des domaines à étudier; de plus, elle peut s'effectuer simultanément avec celle d'un phénomène particulier, grâce au grand nombre de paramètres enregistrés. Nous avons vu que le timer, M, met le pilote, L, en fonction à des intervalles de temps et pour des durées choisis par l'intermédiaire du compteur, N'; compte tenu de la possibilité de régler la pente "potentiel–temps", l'utilisation combinée du timer et du pilote permet d'obtenir une succession de variations de potentiel (de grandeur et de vitesse réglables) et de paliers, ou périodes de repos, durant lesquels le potentiel reste constant. Ce mode de fonctionnement est particulièrement important; il permet en effet :

—de décrire la caractéristique courant–surtension $i(\eta)$ du système en produisant des variations faibles du potentiel contrôlé et des périodes de repos suffisamment longues pour pouvoir atteindre l'équilibre thermodynamique;

—d'utiliser des périodes de repos pour étudier, à potentiel constant, l'évolution des autres paramètres ou l'action d'un phénomène extérieur au système.

Les phénomènes particuliers, envisagés ci-dessous, illustrent en fait l'emploi du matériel décrit, à des types de problèmes plus généraux :

—étude de phénomènes périodiques : cas des oscillations anodiques spontanées du potentiel et de la densité de courant;

—action d'une contrainte physique ou chimique sur le système : cas de l'éclairement (photocourants, photopotentiels).

2.1. *Oscillations anodiques du potentiel et de la densité de courant*

Nous avons complété les travaux de l'un de nous[6,7] portant sur les oscillations de potentiel anodique au cours du polissage électrolytique du cuivre en milieu phosphorique. Cette étude portait sur les oscillations du potentiel, V_{ra}, de l'anode par rapport à une électrode de référence ; le potentiel V_{ak} de l'anode par rapport à la cathode étant contrôlé. Ces oscillations, très reproductibles, sont situées sur le palier de densité de courant. La technique utilisée consistait à filmer les indications d'un voltmètre numérique mesurant cette seule grandeur ; le dépouillement des films était ensuite très long (vingt à trente mille images à dépouiller par expérience) et nous n'avions aucune mesure précise des autres paramètres. Les expériences que nous avons réalisées avec le système que l'on vient de décrire nous ont permis d'obtenir les améliorations suivantes :

—le nombre de courbes obtenues est beaucoup plus important et l'on peut suivre l'évolution des oscillations pendant un temps très long ;

—l'enregistrement simultané de plusieurs paramètres permet, en particulier, de tracer les courbes d'oscillation de potentiel en même temps que les courbes d'oscillation de densité de courant ; ainsi on a une mesure précise du déphasage entre ces deux grandeurs, précieuse pour l'interprétation du phénomène. Le tracé des courbes intensité–potentiel pendant les oscillations est alors possible.

—l'emploi conjugué du matériel décrit plus haut et d'un voltmètre numérique comme détecteur de limites, donne les valeurs des maximums et minimums des fonctions étudiées ;

—les particularités des courbes, telles que les points d'inflexion, sont situées par un traitement des informations à l'ordinateur ; les résultats obtenus permettent alors de préciser leurs significations physiques. Le choix des modes de fonctionnement du système dont nous disposons, permet l'enregistrement de l'ensemble des grandeurs à intervalles de temps reguliers ; nous pouvons ainsi tracer la caractéristique courant—surtension ; lorsque les oscillations à étudier apparaissent, on modifie la programmation du dispositif de façon à enregistrer, continûment et à la plus grande vitesse possible, les variations d'un seul paramètre (V_{ra} ou I) ou bien des deux.

La Fig. 4 reproduit un exemple de courbe obtenue par un traitement à l'ordinateur (traceur de courbe CALCOMP-ordinateur CDC 3600 de l'Institut Blaise Pascal du C.N.R.S. à Paris) ; il s'agit d'oscillations de V_{ra} en fonction du temps, tracées soit point par point, soit en trait continu.

2.2. *Effects photoélectrochimiques*

L'illumination d'une électrode produit des modifications des paramètres mesurés. L'éclairement agit simultanément sur l'intensité et le potentiel électriques, la température, etc. ; ceci implique la connaissance de ces paramètres et des grandeurs optiques caractérisant le rayonnement incident. Notre dispositif automatique convient à cette étude puisqu'il permet de mesurer quasi-simultanément un grand nombre de variables et de suivre leur évolution.

Deux facteurs importants, la longueur d'onde du rayonnement incident et le temps d'exposition, influencent ces effets : des radiations de différents domaines
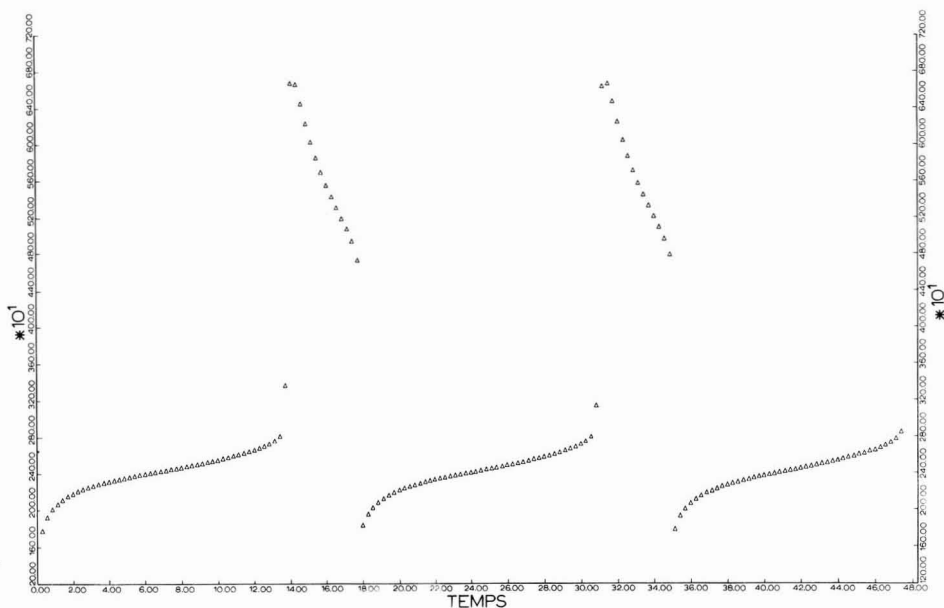
Fig. 4. Oscillations $V_{RA}(t)$. Graduations des axes: 40 mV et 0.5 s.

spectraux sont produites à l'aide de filtres interférentiels associés à une source appropriée; des illuminations de durées réglables, pouvant être en particulier très brèves, sont nécessaires pour rendre négligeable l'évolution de certains paramètres thermodynamiques (comme par exemple la température) au niveau de l'interface métal–solution; enfin la bonne marche de l'expérience est conditionnée par la reproductibilité des illuminations et leur parfaite synchronisation avec les mesures.

Le dispositif annexe R construit tient compte de ces diverses exigences; c'est un passeur automatique de filtres fonctionnant selon le principe suivant: le compteur N reçoit à intervalle de temps constant (par exemple 3 min), les impulsions produites par l'horloge K; une grille de programmation permet la sélection de certaines d'entre elles (par exemple une sur trois), pour mettre en fonction le timer P; ce dernier règle la durée des illuminations et met en oeuvre le dispositif R; lors du passage d'un filtre, R envoie des impulsions vers l'horloge et vers la commande J du commutateur de voies pour déclencher l'impression de l'heure et d'une série de mesures; après une période d'obscurité (facultative) un autre filtre est sélectionné et une série de mesures réalisée; le cycle de fonctionnement de R prend fin avant la commande par l'horloge (par l'intermédiaire de N', M, et L) d'une modification de l'alimentation. Ainsi, l'étude des photocourants est réalisée, après un temps de stabilisation réglable du potentiel d'électrode, sur des paliers du potentiel d'alimentation.

Le contrôle de divers paramètres et les mesures précises des photocourants et phototensions rendent possible une exploration des effets photoélectrochimiques. Cette étude concerne aussi bien le comportement général du système (vérification de lois proposées) que l'examen de phénomènes transitoires apparaissant localement. Ces deux aspects sont utiles pour préciser les mécanismes des photocourants à propos desquels de nombreuses théories sont proposées[8-10]. Ces questions sont d'ailleurs de

première importance car elles constituent une approche supplémentaire des processus aux interfaces métal–solution.

2.3. *Observation polarographique en courant variable*

L'expérience permet la mesure des grandeurs électriques caractéristiques d'une cellule électrolytique soumise à l'action de différences de potentiel continue et alternative superposées.

La cellule est composée d'une solution électrolytique aqueuse alimentée par deux électrodes de mercure. La variation de la distance goutte de Hg–surface de séparation Hg–solution, atténuée par l'emploi de vases communicants devient négligeable grâce à la rapidité des mesures.

L'alimentation est réalisée à partir d'un générateur T.B.F. débitant sur un circuit résistant. L'étude de la réponse de la cellule en fonction de la fréquence implique l'élimination des incertitudes de fréquence et de potentiel relatives aux mesures du temps. Ces différentes erreurs peuvent être affaiblies par des mesures annexes de fréquence et de potentiel sur oscilloscope, ainsi que par la détermination statistique du temps de chute des gouttes; mais le temps d'expérience devient important et introduit une modification non négligeable des conditions de l'expérience. Pour notre part, nous avons levé ces difficultés en adjoignant au dispositif automatique de mesure précédemment décrit, un générateur T.B.F. avec pilote (il remplace l'alimentation: potentiostat + pilote des deux autres expériences).

Ce générateur (WAVETEK 114) permet de connaître avec plus de précision les fréquences utilisées; elles sont calculées à partir de leurs valeurs initiale et finale, et du temps de balayage du pilote. La lecture des potentiels et la détermination du temps de chute des gouttes sont effectuées avec notre dispositif automatique:

—la première au $\frac{1}{100}$ mV (la date de la mesure étant connue au $\frac{1}{20}$ s)

—la seconde avec la précision de l'enregistrement des mesures (soit $\frac{1}{10}$ de seconde lorsqu'on utilise la perforatrice de bandes au maximum de ses possibilités).

La commande des mesures est réalisée à partir d'impulsions délivrées par l'horloge numérique K. Le mode d'utilisation le plus intéressant pour l'expérience décrite est le suivant: K émet périodiquement une impulsion qui met en fonctionnement le générateur et son pilote, et déclenche simultanément les mesures du Microscan. Les potentiels sont enregistrés continûment pendant la période où le balayage en fréquence est réalisé. A la fin de cette première série de mesures, une nouvelle série peut être effectuée dans une zone contiguë de fréquence. Une telle exploration de l'ensemble de la gamme des fréquences permet de localiser les résonances. Il est alors souhaitable d'effectuer plusieurs mesures successives dans une bande de fréquence plus restreinte. Dans ce dernier cas nous pouvons:

—étudier la stabilité du phénomène au cours du temps, en conservant les mêmes conditions d'expérience,

—noter son évolution lorsqu'un des paramètres varie (tension appliquée, résistance de la cellule, température, etc.),

—effectuer, quand le phénomène est stable, un calcul statistique pour améliorer encore la précision des mesures.

CONCLUSION

Nous avons décrit un appareillage comportant:

—un dispositif de mesure de tension : voltmètre numérique muni d'un commutateur de voies,

—des organes de sortie imprimant les valeurs mesurées et les perforant sur bande et sur cartes,

—une alimentation de cellule de type classique : potentiostat ou générateur pilotés,

—un dispositif annexe au montage produisant une variation programmée d'un paramètre physique ou chimique supplémentaire : température, éclairement, concentration, etc.,

—des organes de synchronisation dont l'élément essentiel est une horloge numérique permettant une connaissance précise du paramètre "temps" ; elle commande en outre les appareils mentionnés ci-dessus selon un programme préétabli.

Ce matériel peut être utilisé pour divers montages ; quelques exemples sont évoqués : oscillations de potentiel anodique, photocourants, polarographie ; l'adaptation à d'autres études est aisée si les grandeurs à mesurer sont des différences de potentiel ou peuvent être mises sous cette forme. Notons que l'enregistrement rapide d'un grand nombre de variables, y compris le temps, permet l'étude de phénomènes dont l'évolution est relativement rapide.

De telles expérimentations sont programmées à l'avance et se déroulent automatiquement et conformément au tableau de marche prévu ; néanmoins l'expérimentateur peut intervenir à tout moment et modifier manuellement telle ou telle condition de fonctionnement. Il en résulte souplesse et diversité d'emploi alliées à une reproductibilité parfaite dans le déroulement des différentes phases de l'expérience.

Les données brutes recueillies sont traitées à l'ordinateur ; on effectue ainsi, en particulier, le tracé automatique de courbes et tout calcul utile à la comparaison théorie–expérience. De plus, la validité des résultats obtenus peut être fondée sur des considérations statistiques grâce à la possibilité de faire de nombreuses expériences identiques, simultanées ou non, et d'obtenir pour chacune, un très grand nombre d'informations.

La limitation des performances de l'ensemble, provenant de la lenteur relative des organes de sortie, ne semble pas de grande importance dans beaucoup de cas ; il est d'ailleurs possible de limiter cette restriction par l'emploi d'un enregistreur à bande magnétique.

RÉSUMÉ

L'appareillage décrit conduit l'expérience sur la base d'un programme préétabli et enregistre les mesures de nombreux paramètres ; les données recueillies sont ensuite traitées à l'aide des techniques actuelles de l'informatique. Après la description du montage et l'analyse de son fonctionnement, quelques exemples d'utilisation sont brièvement donnés.

SUMMARY

The apparatus described carries out experiments based on a pre-determined programme and records the values of a number of parameters ; the data obtained are then treated with the aid of present techniques of information processing. After the description of the set-up and analysis of its behaviour, some examples of its use are briefly described.

BIBLIOGRAPHIE

1 J. P. Phillips, *Automatic Titrators*, Academic Press, London, 1959.
2 R. de Levie et A. A. Husovsky, *J. Electroanal. Chem.*, 20 (1969) 181.
3 E. Verdier, R. Grand et P. Vanel, *J. Chim. Phys.*, 66 (1969) 376.
4 G. L. Booman, *Anal. Chem.*, 38 (1966) 1141.
5 M. W. Breiter, *J. Electrochem. Soc.*, 112 (1965) 845.
6 B. Pointu, *Comp. Rend.*, 266 (1968) 669.
7 B. Pointu, *Electrochim. Acta*, 14, 12 (1969) 1207, 1213.
8 G. C. Barker, A. W. Gardner et D. C. Sammon, *J. Electrochem. Soc.*, 113 (1966) 1182.
9 A. M. Brodsky et Y. Y. Gurevich, *Electrochim. Acta*, 13 (1968) 1245.
10 H. Berg, *Electrochim. Acta*, 13 (1968) 1249.

THE DOUBLE LAYER REGION OF SINGLE CRYSTAL SILVER IN ALKALINE SOLUTIONS

R. D. GILES and J. A. HARRISON

Electrochemistry Research Laboratories, Department of Physical Chemistry, School of Chemistry, University of Newcastle upon Tyne, Newcastle upon Tyne, NE1 7RU (England)

INTRODUCTION

In general, the chemical nature of metal surfaces is important in determining the reaction mechanism and the properties of the double layer. Mercury is well known to behave as the bare metal over a wide potential range, whereas platinum shows a much narrower region where it is not covered with either adsorbed hydrogen or oxide. Other metals have been less well characterised. In the case of silver, the mechanism of oxygen reduction and the measurement of the point of zero charge are both complicated by the surface structure, and in practice depend on the pre-history of the electrode. We shall attempt to show in this paper that the effects are more serious, and the available potential range of silver in alkali metal containing solutions is more limited than previously assumed.

The anodic limit is determined by $Ag(OH)_2^-$ and Ag_2O formation[10], and the cathodic limit by alkali metal deposition and hydrogen evolution. The degree of reversibility of alkali metal deposition remains unresolved. Meaningful double layer capacity measurements cannot be made at potentials cathodic to the newly defined negative limit.

Kabanov and coworkers have presented considerable evidence for the incorporation of alkali metal into soft metal cathodes[1]. Specifically to silver it has been shown[2] that hydrogen overvoltage in alkaline solutions is time-dependent and has a Tafel slope increasing with cathodic polarisation especially negative to -1.75 V. The final value of hydrogen overvoltage at a fixed current density increases with atomic size of the alkali metal ion in the order $Li < Na < K < Cs < (CH_3)_4N$. Whilst the major effects on hydrogen evolution were observed at potentials negative to *ca.* -1.65 V (all potentials are quoted *vs.* $Ag_2O/Ag/OH^-$ reference electrode) it was shown[3] that smaller peaks than those at -1.65 V were observed at -0.85 V during anodic stripping voltammetry, but as the corresponding cathodic peaks were not observed no further analysis was attempted.

These workers[4,5] have shown that the amount of alkali metal that can be stripped from cathodes polarised at -1.65 V for various times passed through a maximum. As the hydrogen overpotential does not change with time there can be no change of surface properties. It was concluded that the oxidation of the alkali metals from the surface is retarded by slow formation of alkali metal–silver intermetallic compounds.

Zhutaeva *et al.*[6] have observed cathodic and anodic peaks containing a small

charge at *ca.* −400 and −750 mV during potential sweep voltammetry (P.S.V.) at 0.1 V s^{-1} on silver electrodes in deoxygenated 1 M KOH; but in later publications[7,8] they confirmed 2 anodic peaks (−350 and −600 mV), and only one cathodic peak (−650 mV). The anodic peak at −600 mV was ascribed to hydrogen desorption from surface intermetallics formed between alkali metal and silver. The peak at −350 mV was due to alkali metal removal. The cathodic peak was ascribed to co-deposition of alkali metal and hydrogen.

Koryta *et al.*[9], preliminary to work on oxygen reduction at a rotating silver disc electrode, studied its behaviour in 1 M KOH in the absence of oxygen. Not only was an indistinct cathodic peak found on P.S.V. at *ca.* −1000 mV with the corresponding anodic peak appearing at −750 mV, but the total charge during cathodic polarisation from 0 to −1500 mV was greater than the anodic charge. The anodic peak charge increased as the cathodic limit potential was shifted progressively negative. Limiting current for oxygen reduction, during measurements in the presence of oxygen, showed a minimum at the same potential as the anodic and cathodic peaks previously mentioned. Koryta attributed the larger cathodic charge to formation of a thin layer of surface silver oxide, but this cannot be the case, as it has been shown[10] that the Ag$_2$O monolayer is stable only 8 mV negative to the bulk reversible potential of Ag$_2$O. In addition, at potentials more negative than −1000 mV Koryta proposes that the peaks increase as a result of cathodic reduction of water and simultaneous adsorption of hydrogen, which subsequently affects the rate of oxygen reduction.

There is evidence[11,12] that silver has an equilibrium coverage of adsorbed hydrogen during hydrogen evolution, 10% at −1500 mV, but coverage anodic to −1500 mV is usually assumed to be zero. The only evidence to the contrary[13] is confused by Ag$_2$O phase formation.

On the other hand, there is some evidence that the double layer region extends past −1050 mV. A minimum at −1050 mV in the *C–E* curve has been identified[14] as the potential of zero charge (E_z). Investigations over a narrow potential range by Leikis *et al.*[15,16] have shown that this minimum at −1050 mV increases in depth with decreasing electrolyte concentration, and its potential is pH-independent, although the actual value of C_{dl} at E_z does increase with pH. The shape of the minimum on both polycrystalline and single crystal silver[17] roughly corresponds to the shape of the diffuse layer minimum at E_z on Hg in the same solution. However, the authors have made no comments about the direction of polarisation and pretreatments of the silver electrode, and it may be that this minimum is a slow faradaic pseudo-capacitance change.

Hampson *et al.*[18] also observed a minimum at −0.7 V (NHE) in the *C–E* curve for mechanically polished silver in 0.01 M NaClO$_4$ but only if the potential was swept from anodic potentials immediately before anodic dissolution. If the potential was swept from cathodic values no minimum was observed.

EXPERIMENTAL

The ⟨111⟩ silver single crystal electrode, hydroxide solutions, and cell were similar to those described previously[10] except that the Pt wire coil subsidiary electrode was replaced by a roughened Pt sheet electrode parallel to the silver electrode surface, with a geometric area ratio of 20 : 1. The roughening would cause the actual surface

area ratio to be considerably greater than this. The effect of H_2, O_2, and H_2O_2 dissolved in the solution was investigated in a similar cell, but with a sintered glass frit between working and subsidiary electrodes.

A.c. bridge measurements

Electrode impedance measurements were taken, using a conventional Wien bridge, the circuit of which has been detailed[19]. After the solution resistance had been subtracted out, the electrode impedance was almost entirely capacitative at all potentials, except those anodic to -100 mV where dissolution is taking place[10]. The large area of the silver crystal caused the inductance in the components of the bridge to be significant in dilute solutions ($< 0.01\ M$), and although the effect was minimised by measuring the C–E curves at low frequencies, the bridge was difficult to balance at the lowest frequencies due to a poor signal to noise ratio. The optimum frequency was 350 Hz. Even so the measured series capacities are probably low in dilute solutions,
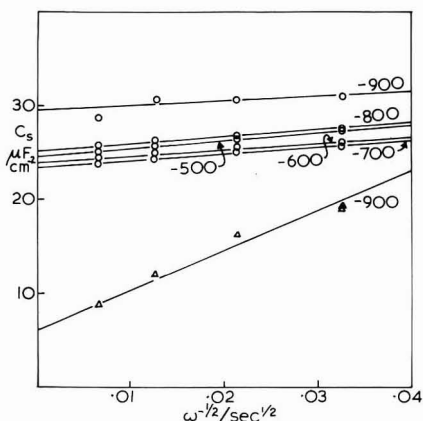
Fig. 1. C_s–$\omega^{-\frac{1}{2}}$. Typical frequency-dependence of silver single crystal electrodes. ($\bigcirc$) 1 M, ($\triangle$) 0.01 M NaOH. Numbers are potentials in mV (*vs.* Ag_2O/Ag).

but the shape of the C–E curves is correct. True values of capacity were obtained in 1.0 M solutions where the inductance effects were negligible.

In dilute solutions it was not possible to circulate the solution through a bed of charcoal, as this caused a significant drop in the electrolyte concentration. A few grains of charcoal were suspended in the solution without depleting it.

There was very little frequency-dependence of the electropolished silver electrodes in 1 M NaOH at potentials between -900 and -500 mV (Fig. 1), (3% change in C_s over the frequency range 100–1000 Hz), corresponding to a very flat, smooth electrode. The double layer capacity between -800 and -500 mV was $24.2 \pm 0.5\ \mu\mathrm{F\ cm^{-2}}$. The frequency-dependence of C_s in $10^{-2}\ M$ NaOH, when the inductance in the circuit becomes significant, is also shown in Fig. 1.

The shape of the C–E curves at fixed frequency (350 Hz) is determined largely by the electrodes previous polarisation history. The starting state of each electrode was a freshly electropolished surface which had been thoroughly washed with a jet of triply distilled water.

In a well de-aerated solution the electrode was switched into the circuit at the first quoted potential, then polarised as follows:

(a) $-550 \rightarrow -1350 \rightarrow -50$ mV in 10^{-3} M NaOH resulted in data shown in Fig. 2. There is a minimum during the cathodic sweep at -1150 mV, with 2 maxima either side of it at -900 and -1300 mV. C_s is sharply time-dependent at -1350 mV
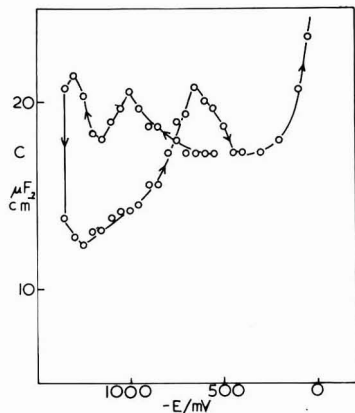
Fig. 2. C–E curve, 10^{-3} M NaOH. Polarised $-550 \rightarrow -1350 \rightarrow -50$ mV (350 Hz).
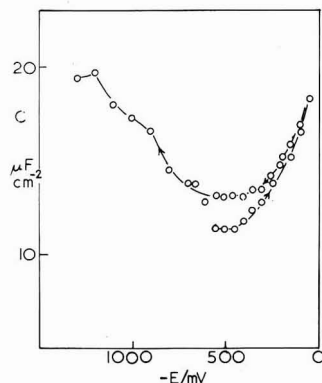
Fig. 3. C–E curve, 10^{-3} M NaOH. Polarised $-550 \rightarrow -50 \rightarrow -1350$ mV (350 Hz).

falling to a much lower stable value after 10 min. During the anodic sweep, a maximum is observed at -650 mV prior to the pseudocapacity rise due to dissolution at -200 mV.

(b) $-550 \rightarrow -50 \rightarrow -1300$ mV, 10^{-3} M NaOH (Fig. 3). No minimum is observed during the cathodic sweep, neither is there evidence for a rise in C_s at -650 mV during the anodic sweep.

(c) $-550 \rightarrow -1500$ mV, 10^{-3} M KOH (Fig. 4), the shape is the same as in 10^{-3} M NaOH.
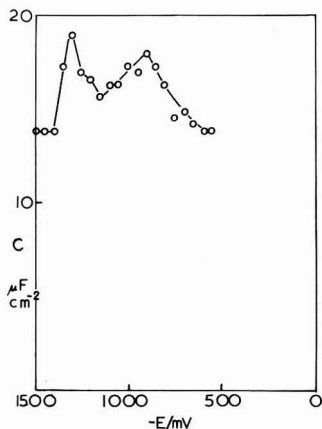
Fig. 4. C–E curve, 10^{-3} M KOH. Polarised $-550 \rightarrow -1500$ mV (350 Hz).
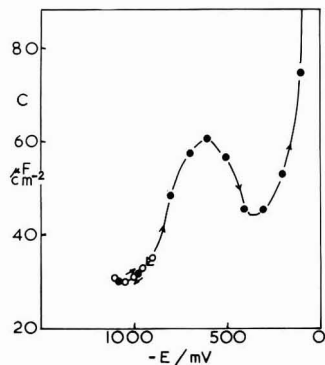
Fig. 5. C–E curve, 1.0 M NaOH. Polarised $-900 \rightarrow -1100 \rightarrow -50$ mV (350 Hz). (●) Anodic sweep, (○) cathodic sweep.

(d) $-900 \rightarrow -1100 \rightarrow -100$ mV, 1.0 M NaOH (Fig. 5). There appears to be a slight minimum at -1050 mV in this solution followed, on the anodic sweep, by a sharp maximum in C_s at -600 mV.

(e) $-900 \rightarrow -150$ mV, 1.0 M NaOH (Fig. 6). No anodic peak is observed on anodic sweep.

Clearly there is a minimum in the $C-E$ curves at -1050 mV (1.0 M NaOH) and -1150 mV (10^{-3} M NaOH) which deepen with dilution, and this has been identified by many authors[15,18] as the point of zero charge, E_z. The minimum does not appear after anodic polarisation (Fig. 3), nor after polarisation negative to -1200 mV. In spite of the minimum having approximately the correct shape for the diffuse layer minimum around E_z, there are clearly electrode capacity changes both before and after it. The maximum in the $C-E$ curves (Figs. 2 and 5) during the anodic sweep from a very negative potential, must involve a stripping process marking the return of the silver surface after some deposition has occurred. The peak is seen after polarisation to only -1100 mV in 1 M NaOH (Fig. 5) which is slightly beyond the potential of the minimum. An anodic peak is not seen after polarisation for 10 min at -900 mV (Fig. 6) but develops slowly after *ca.* 60 min.

It is concluded that it is unlikely that the minimum at -1150 mV (10^{-3} M NaOH), -1050 mV (1.0 M NaOH) corresponds to E_z. The rise in C_s on the cathodic side of the minimum in the $C-E$ curve is probably due to surface changes caused by
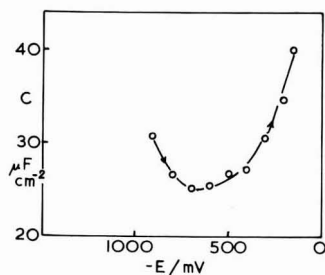
Fig. 6. $C-E$ curve, 1.0 M NaOH. Polarised $-900 \rightarrow -50$ mV (350 Hz).
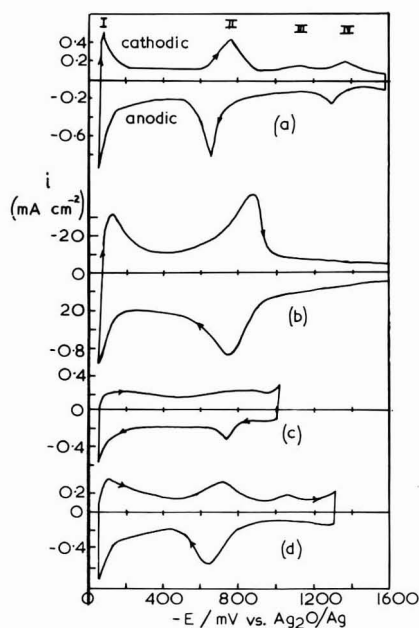
Fig. 7. $i-E$ curves in 1 M KOH after 2 min cycling. Anodic limit -50 mV. Cathodic limit: (a) (b) -1600. (c) -1000, (d) -1300 mV; (a) (c) (d) 3.0 V s^{-1}, (b) 300 V s^{-1}.

small faradaic processes occurring on the electrode surface. These have been further studied by potential sweep methods.

Potential sweep measurements

(*i*) *Steady state polarisations.* Evidence for faradaic processes occurring on a silver electrode in 1 M KOH is shown in Fig. 7a, b, c, d. Each *i–E* curve was obtained after freshly electropolishing the silver electrode followed by approximately 2 min continuous cycling. In Fig. 7a, b, when polarised between -50 and -1628 mV, there was no further change with time. Time-dependent measurements recorded before 2 min, will be described in a later section.

Two anodic and cathodic peaks were observed. The anodic and cathodic peaks (IA, IC, respectively) close to -50 mV correspond to dissolution of silver as $Ag(OH)_2^-$ and metal redeposition (as described in a previous paper[10]); these will not be discussed further. The peaks IIC, IIA have charges at all sweep rates approximating to a monolayer of material (after subtraction of the charging current).

In spite of the peak potential of II (E_p^{II}) lying at -800 mV, these peaks only occur to such a marked extent if the electrode is polarised strongly negative. On sweep from -50 to -1017 mV for 2 min, only shallow peaks of small charge are seen (Fig. 7c). These increase in magnitude after 2 min polarisation between -50 and -1326 mV (Fig. 7d), but the time-dependent peaks are still present on the $i-E$ curves. Clearly, the formation of the peaks II depend upon process(es) occurring at potentials more negative than itself.

(*ii*) *Time-dependent polarisations.* Figures 8, a–d confirm the existence of further faradaic processes other than those described in (i) above. On polarising a freshly electropolished electrode from -50 to -1640 mV, the *first* sweep (Fig. 8a, c) has cathodic peak II absent at both 3 V s^{-1} and 300 V s^{-1}, but 2 additional cathodic peaks, III and IV. These have corresponding anodic peaks on the reverse sweep. Subsequent sweeps show that peak II increases, but peak IV decreases with increasing time of polarisation towards their time-independent values. The charge for peak III also approximates to a monolayer of deposited material, and during each cycle the cathodic charge was greater than the anodic. The shift of E_p of II and III indicates that these two peaks coalesce with time, and this is further confirmed by measurements on the anodic peaks II and III at 0.03 V s^{-1} (Fig. 9a–c).

The *i–E* curves at 0.03 V s^{-1} (Fig. 9) are slightly different from those at 3.0 V s^{-1} and 300 V s^{-1}, in that peak IIC never coalesces with peak IIIC. The dissolution of Ag at the anodic end of the sweep does not allow any of the cathodically deposited material to remain on the surface before commencement of cathodic sweep. Hence, a fresh silver surface is always present at this point, and IIC is always absent. At -1600 mV, hydrogen is evolved and small bubbles are seen, but there is no corresponding anodic oxidation peak.

It has been concluded that the peaks II→IV correspond to surface faradaic processes. There is no change of E_p with sweep rate.

Peak II probably corresponds to deposition of hydrogen atoms (H·) on to a silver–alkali metal surface phase, left on the electrode after recycling according to (1)

$$H_2O + e \rightleftharpoons H^\cdot(MAg) + OH^- \tag{1}$$

where M is any alkali metal atom.

Peak III is the deposition of alkali metal ions on to preferred sites on the silver surface to form the surface phase MAg as in (2)

$$M^+ + e \rightleftharpoons MAg \tag{2}$$

with co-deposition of hydrogen atoms as in (1) above. The coalescence of the two peaks II and III is thus resolved, and its increase in size only after the electrode is polarised strongly negative is understandable.

Peak IV is attributed to the further deposition of alkali metal on to less preferred sites, to give full electrode coverage with the alkali metal. In addition, alkali metal atoms (M) will diffuse slowly into the silver and a further supply of these to the surface will be necessary. Deposition of alkali metal on to solids is strictly comparable with
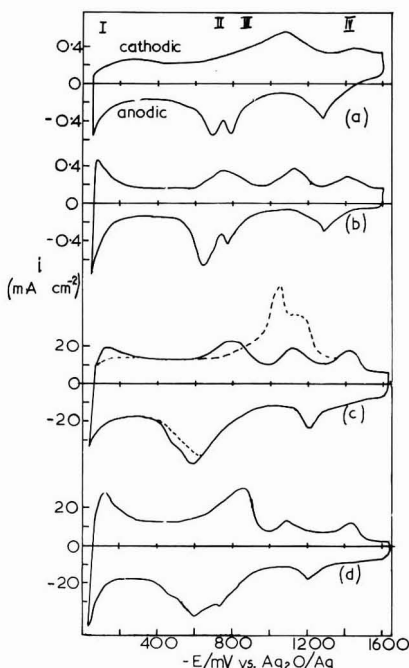
Fig. 8. i–E curves in 1 M KOH. Polarised -50 to -1600 mV. (a) 3.0 V s^{-1} first sweep, (b) 3.0 V s^{-1} multiple sweep after 5 s, (c) 300 V s^{-1} (---) 1st sweep, (——) after 5 s, (d) 300 V s^{-1} multiple sweep after 30 s.
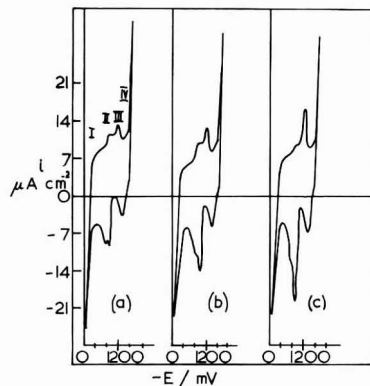
Fig. 9. i–E curves in 1 M KOH 0.03 V s^{-1}. Polarised $-50 \rightarrow -1620$ mV. (a) 1st, (b) 2nd, (c) 5th sweep.

alkali metal amalgams in the case of liquid mercury, and their free energy of formation must be sufficient to shift the equilibrium potential for deposition by $ca.$ -1300 mV. With increasing time, the deposition and partial dissolution of alkali metal from the silver will result in surface recrystallisation, with an associated increase in the number of preferential sites for M deposition according to peak III.

No separate hydrogen oxidation peak is observed when hydrogen saturated solutions are investigated. In spite of the reported high solubility of oxygen in silver,

the constancy of charge with sweep rate indicates that none of these peaks can be due to the reduction of oxygen coming from the bulk of the solid. Oxygen dissolved in aqueous solution caused quite separate peaks from the peaks II→IV and will be mentioned later.

A number of possible impurities were added to the solutions; Cl^- and CO_3^- had no effect in the double layer region. Surface active impurities from Araldite reduced the reproducibility of peaks. Excess CN^- caused only a small shoulder or peak at *ca.* -300 mV corresponding to thermodynamically reversible formation of AgCN. In all cases, the peaks II to IV were separate from these impurity effects.

Experiments were carried out in 1 M solutions of LiOH, NaOH and KOH but the alkali metal made little difference to the general shape of the peaks. On the *first* sweeps, peak IIIC in KOH and LiOH was separated from IIC by 100 mV more than in NaOH solutions, and IIIC appeared as a shoulder more than a peak. In LiOH, the surface phase was more difficult to remove by the anodic sweep, and the joint peak IIC and IIIC grew more rapidly than in other solutions.

A number of *i–E* curves were measured in the presence of dilute solutions of oxygen and hydrogen peroxide in 1 M KOH. At 3.0 V s^{-1} and 0.03 V s^{-1} a sharp fall occurred in the reduction currents of both of these compounds at *ca.* -800 mV, *i.e.* very close to the potential of the time-independent peak II. Koryta[9] concluded from rotating disc measurements that surface processes must be important. From our experiments it must be concluded that the co-deposition of alkali metal and hydrogen significantly retards the rate of both oxygen and hydrogen peroxide reduction.

SUMMARY

The behaviour of $\langle 111 \rangle$ silver single crystal electrodes in alkaline solutions has been investigated by a.c. bridge, and potential sweep voltammetry, in the so called double layer region. The measurements show that alkali metal is deposited at a potential of -1080 mV and is not easily reoxidised from the surface. The conclusion must be that there is the irreversible formation of a surface compound. Subsequent sweeps accumulate this compound at the surface together with hydrogen, presumably as hydrogen atoms. Because of the proximity of this effect to the observed capacity minimum in dilute alkaline, and neutral alkali metal ion containing solutions at -1050 mV, it is doubtful whether the zero point of charge can be measured.

The evidence points to there being no adsorption of hydroxide prior to $Ag(OH)_2^-$ and Ag_2O formation. Meaningful kinetic measurements can only be made upon bare silver in the potential range -100 to -900 mV in 1 M alkali metal hydroxide solutions (*vs.* Ag_2O/Ag). This is particularly relevant to recent work on oxygen reduction.

REFERENCES

1 B. N. KABANOV, *Electrochim. Acta*, 13 (1968) 19.
2 O. P. ALEXANDROVA, I. G. KISELEVA AND B. N. KABANOV, *Russ. J. Phys. Chem. English Transl.*, 38 (1964) 811.
3 I. G. KISELEVA, N. N. TOMASHOVA AND B. N. KABANOV, *Russ. J. Phys. Chem. English Transl.*, 38 (1964) 648.
4 I. G. KISELEVA, *Soviet Electrochem.*, 3 (1967) 241.
5 N. N. TOMASHOVA, I. I. ASTAKHOV, I. G. KISELEVA AND B. N. KABANOV, *Soviet Electrochem.*, 4 (1968) 1143.
6 N. A. SHUMILOVA, G. V. ZHUTAEVA AND V. J. TARASEVICH, *Electrochim. Acta*, 11 (1966) 967.
7 G. V. ZHUTAEVA AND N. A. SHUMILOVA, *Soviet Electrochem.*, 4 (1968) 87.
8 G. V. ZHUTAEVA, N. A. SHUMILOVA AND V. I. LUK'YANYCHEVA, *Soviet Electrochem.*, 4 (1968) 168.
9 M. BREZINA, J. KORYTA AND M. MUSILOVA, *Collection Czech. Chem. Commun.*, 33 (1968) 3397.
10 R. D. GILES, J. A. HARRISON AND H. R. THIRSK, *J. Electroanal. Chem.*, 22 (1969) 375.
11 H. GERISCHER AND W. MEHL, *Z. Elektrochem.*, 59 (1955) 1049.
12 M. A. V. DEVANATHAN, J. O'M. BOCKRIS AND W. MEHL, *J. Electroanal. Chem.*, 1 (1959) 143.
13 V. R. LOODNA, V. E. PAST AND M. E. KHAGA, *Soviet Electrochem.*, 2 (1966) 861.
14 L. RAMALEY AND C. G. ENKE, *J. Electrochem. Soc.*, 112 (1965) 947.
15 D. I. LEIKIS, E. S. SEVAST'YANOV AND I. G. DAGAEVA, *J. Electrochem. Soc.*, 113 (1966) 1341.
16 I. G. DAGAEVA, D. I. LEIKIS AND E. S. SEVAST'YANOV, *Soviet Electrochem.*, 2 (1966) 759.
17 E. S. SEVAST'YANOV AND T. VITANOV, *Soviet Electrochem.*, 3 (1967) 351.
18 N. A. HAMPSON, D. LARKIN AND J. R. MORLEY, *J. Electrochem. Soc.*, 114 (1967) 817.
19 R. D. ARMSTRONG, W. P. RACE AND H. R. THIRSK, *Electrochim. Acta*, 13 (1968) 215.

COMPARAISON ENTRE PROPRIETES DANS LE DIMETHYLFORMAMIDE ET PROPRIÉTÉS DANS LA N-MÉTHYLPYRROLODONE A L'AIDE DES COEFFICIENTS DE SOLVATATION

M. BRÉANT, C. BUISSON, M. PORTEIX, J. L. SUE et J. P. TERRAT

Laboratoire de Chimie Analytique et Industrielle, Institut National des Sciences Appliquées, Villeurbanne, Rhône (France)
Centre de Chimie Analytique de la Faculté des Sciences, Villeurbanne, Rhône (France)

Nous avons entrepris l'étude de quelques propriétés chimiques et électrochimiques dans les amides. A ce titre, Nguyen Van Kiet et Buisson ont examiné le comportement des composés du mercure dans le diméthylformamide (DMF)[1–3] et la N-méthylpyrrolidone (NMP)[4,5]. Dans ces deux solvants, nous avons mis en évidence la dismutation partielle des ions mercureux et déterminé les potentiels standards des couples Hg/Hg_2^{2+} et Hg_2^{2+}/Hg^{2+} [1,5]. En milieu complexant, nous avons examiné la formation des complexes mercuriques dont nous avons déterminé la formule HgX_4^{2-} (X = Cl, Br, I, SCN) et la constante de dissociation pK_c [2,5]. La comparaison entre les constantes vraies obtenues en milieu $LiClO_4$ et les constantes apparentes déterminées en milieu $HClO_4$ 0.1 N nous a conduit au calcul des constantes d'acidité des acides HX dans la NMP[5]. Nous nous proposons, dans le présent mémoire, d'analyser l'ensemble de ces résultats à l'aide des coefficients de solvatation, de façon à mettre en évidence le comportement individuel des divers ions étudiés dans le DMF et la NMP.

Rappelons tout d'abord la définition des coefficients de solvatation : Soit l'espèce i en solution dans un mélange eau–solvant. Par rapport à un état de référence défini dans l'eau, son potentiel chimique a pour expression :

$$(\mu_i)_E = (\mu_i^0)_E + RT \log a_i \tag{1}$$

et par rapport à l'état de référence défini dans le solvant S :

$$(\mu_i)_S = (\mu_i^0)_S + RT \log a_i' \tag{2}$$

a_i et a_i' étant les activités dans l'eau et dans le solvant. Le potentiel chimique du soluté dans le mélange est évidemment unique : $(\mu_i)_E = (\mu_i)_S$. Par ailleurs, l'enthalpie libre standard de transfert de l'espèce i, de l'eau dans le solvant S, peut être mise sous la forme :

$$\Delta G_t^0 = (\mu_i^0)_S - (\mu_i^0)_E = RT \log {}^E\Gamma_i^S \tag{3}$$

${}^E\Gamma_i^S$ est le coefficient de solvatation du soluté i dans le solvant S par rapport à l'eau. Nous définissons $p\Gamma_i = -\log \Gamma_i$.

Si $p^E\Gamma_i^S$ est négatif, i est moins solvaté dans S que dans l'eau, et contrairement si $p\Gamma_i$ est positif. La connaissance de ces coefficients de solvatation permettrait de

calculer toute constante dans le solvant S connaissant la constante analogue dans l'eau.

En effet, en comparant les éqns. (1), (2) et (3), il vient :

$$a_i = {}^E\Gamma_i^S a_i'$$

donc, si l'on considère la solubilité d'une molécule AB :

$$(pK_s)_S = (pK_s)_E + \log {}^E\Gamma_A^S + \log {}^E\Gamma_B^S \tag{4}$$

Pour l'équilibre :

$$A + B \rightleftarrows AB$$
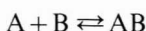
$$(K_c)_E = (K_c)_S \frac{{}^E\Gamma_A^S {}^E\Gamma_B^S}{{}^E\Gamma_{AB}^S}$$

soit

$$(pK_c)_S = (pK_c)_E + \log {}^E\Gamma_A^S + \log {}^E\Gamma_B^S - \log {}^E\Gamma_{AB}^S \tag{5}$$

Et pour les deux réactions d'oxydo–réduction :

$$M - ne \rightarrow M^{n+}$$

$$Ox + me \rightarrow Red$$
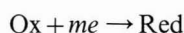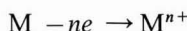
$$(\Delta E^0)_S = (\Delta E^0)_E - \frac{0.058}{n} \log {}^E\Gamma_{M^{n+}}^S + \frac{0.058}{m} \log \frac{{}^E\Gamma_{Ox}^S}{{}^E\Gamma_{Red}^S} \tag{6}$$

En fait, dans l'état actuel de nos connaissances, le calcul du coefficient de solvatation d'un ion pris isolément est thermodynamiquement impossible, l'ion considéré A étant toujours associé à un ion de signe contraire B. On n'atteint donc que le produit $\Gamma_A \Gamma_B$. Il est alors nécessaire de faire une hypothèse de travail extra-thermodynamique pour atteindre la valeur du coefficient de solvatation de chaque ion.

Nous avons utilisé l'hypothèse de Strehlow et ses collaborateurs[6] : le potentiel normal d'oxydo–réduction du couple ferrocène–ferricinium Fc/Fc$^+$ est indépendant du solvant considéré, ce qui sous-entend que les différences d'énergies de solvatation de chacun des composants du couple sont constantes, et se traduit par : $\log \Gamma_{Fc^+} = \log \Gamma_{Fc} = 0$. Si donc on utilise comme couple rédox de référence de potentiel dans S puis dans l'eau, le couple Fc/Fc$^+$, o'application de l'éqn. (6) au système Hg/Hg$_2^{2+}$ donne :

$$(\Delta E_i^0)_S - (\Delta E_i^0)_E = \frac{0.058}{2} \log {}^E\Gamma_{Hg_2^{2+}}^S \tag{7}$$

ce qui permet de déterminer ${}^E\Gamma_{Hg_2^{2+}}^S$.

Un calcul analogue conduit à ${}^E\Gamma_{Hg^{2+}}^S$ et à tous les coefficients du type ${}^E\Gamma_{M^{n+}}^S$. Connaissant cette dernière valeur, on en déduit les coefficients Γ_X—à partir des produits de solubilité des composés MX (éqn. (4)). Enfin l'éqn. (5) donne les coefficients de solvatation des complexes HgX$_4^{2-}$ à partir de leurs constantes de dissociation, de $\Gamma_{Hg^{2+}}$ et de Γ_{X^-} :

$$\log {}^E\Gamma_{HgX_4^{2-}}^S = (pK_c)_E - (pK_c)_S + \log {}^E\Gamma_{Hg^{2+}}^S + 4 \log {}^E\Gamma_{X^-}^S$$

Nous constatons que l'étude des composés du mercure nécessite la connais-

sance des coefficients de solvatation des ions complexants X^-. On peut atteindre ces valeurs à partir des produits de solubilité des sels MX et du coefficient de solvatation de l'ion M^+. Nous avions pensé utiliser les valeurs données dans la littérature pour les composés de l'argent, mais l'ensemble est assez hétérogène. En effet, Parker et ses collaborateurs[7,8] ont déterminé les coefficients Γ_{Ag^+} et Γ_{X^-} dans le DMF et la NMP, mais en supposant que les coefficients caractéristiques des ions tétraphénylborure et tétraphénylarsonium étaient égaux, hypothèse différente de celle que nous utilisons. Les travaux de Virtanen et al.[9] dans la NMP ne conduisent qu'à des valeurs relatives des coefficients Γ_{X^-} par rapport à Γ_{SCN^-}. Seuls Barraqué et al.[10] ont utilisé l'hypothèse de Strehlow pour déterminer Γ_{Ag^+} et Γ_{X^-} dans des mélanges eau–solvant (dont le DMF). Mais il semble que les valeurs proposées dans le solvant pur ne correspondent pas à celles obtenues par extrapolation à partir des mélanges. Dans ces conditions, il nous a semblé préférable de recalculer les coefficients Γ_{Ag^+} et Γ_{X^-} dans le DMF et la NMP, en utilisant la même hypothèse de travail que pour les coefficients $\Gamma_{Hg^{2+}}$ et $\Gamma_{Hg_2^{2+}}$ de façon à obtenir des résultats homogènes. Ceci nous a conduit à une étude préliminaire des composés de l'argent dans le DMF et la NMP, étude dont nous énumérons les résultats ci-après.

I. ÉTUDE DES COMPOSÉS DE L'ARGENT

Nous avons déterminé le potentiel standard du couple Ag/Ag^+ en milieu $HClO_4$ 0.1 N dans le DMF et la NMP en extrapolant jusqu'à $[Ag^+] = 1$ la droite $E = E_0 + 0.058 \log [Ag^+]$

Nous obtenons ainsi:

$E^0 = -0.100 \pm 0.005$ V dans le DMF

et $\quad E^0 = -0.028 \pm 0.005$ V dans la NMP

par rapport au potentiel standard du système Fc/Fc^+ dans le solvant considéré.

En suivant par potentiométrie à intensité nulle le dosage des ions X^- par les ions Ag^+, ou vice-versa, nous vérifions la formation des composés AgX_2^- et AgX. Dans le cas des iodures, il apparaît également un composé $Ag_3I_4^-$. Le Tableau 1 rassemble les constantes que nous avons obtenues en regard de celles données dans la littérature. Les constantes K correspondent au produit $[Ag^+][X^-]$ pour les composés AgX, à l'expression $[Ag^+][X^-]^2/[AgX_2^-]$ pour les complexes AgX_2^- et à $[Ag^+]^3[I^-]^4/[Ag_3I_4^-]$ pour les complexes $Ag_3I_4^-$. L'examen de ce Tableau appelle deux remarques: (a) la concordance entre nos valeurs, celles de Parker[7,8,11], de Butler[12], de Chateau et Moncet[13] et de Virtanen[9] est généralement très bonne; signalons cependant que ni Parker (DMF) ni Virtanen (NMP) n'ont mentionné l'existence du composé $Ag_3I_4^-$ dont cependant la formation apparaît nettement sur les courbes potentiométriques (Fig. 1); (b) il existe une différence systématique entre nos valeurs déterminées en milieu $LiClO_4$ 0.1 N (pK) et nos valeurs obtenues en milieu $HClO_4$ 0.1 N (pK'). Nous avions signalé un phénomène analogue lors de l'étude des composés HgX_4^{2-} dans la NMP[5] et nous en avions conclu que les acides HX n'étaient vraisemblablement pas forts dans ce solvant. Cette hypothèse est donc confirmée par l'étude des composés de l'argent.

Nous avons rassemblé dans le Tableau 2 les valeurs des constantes acide–base des couples HX/X^- déterminées à partir de la différence ΔpK entre les constantes

TABLEAU 1

CONSTANTES CARACTÉRISTIQUES DES COMPOSÉS DE L'ARGENT DANS LE DMF ET LA NMP

S	DMF				NMP			
Composé	pK'	pK	Valeurs de la littérature		pK'	pK	Valeurs de la littérature	
AgCl	12.8 ± 0.3	14.4 ± 0.3	14.5 ± 0.1[11]	14.49 ± 0.01[12]	12.5 ± 0.3	14.4 ± 0.3	14.4 ± 0.1[7]	14.4_5[9]
AgBr	$13.9_5 \pm 0.3$	14.9 ± 0.3	15.0 ± 0.1[11]		14.1 ± 0.3	14.6 ± 0.3		14.49[9]
AgI	15.6 ± 0.3	15.4 ± 0.3	15.8 ± 0.1[11]	16.44[13]	15.0 ± 0.3	15.2 ± 0.3	14.5 ± 0.1[7]	14.4[9]
AgSCN	$9.9_5 \pm 0.3$	11.0 ± 0.3	11.5 ± 0.1[11]			10.2 ± 0.3	10.0 ± 0.1[7]	10.26[9]
$AgCl_2^-$	13.0 ± 0.3	16.1 ± 0.3	16.3 ± 0.3[11]	16.29 ± 0.015[12]	13.1 ± 0.3	17.4 ± 0.3	17.6 ± 0.3[8]	17.73[9]
$AgBr_2^-$	15.2 ± 0.3	16.6 ± 0.3	16.6 ± 0.3[11]		16.3 ± 0.3	17.5 ± 0.3		17.53[9]
AgI_2^-	17.3 ± 0.3	$17.3_5 \pm 0.3$	17.8 ± 0.3[11]	18.12[13]	17.4 ± 0.3	17.8 ± 0.3		16.7[9]
$Ag(SCN)_2^-$	9.7 ± 0.3	11.1 ± 0.3	11.9 ± 0.3[11]			11.3 ± 0.3		11.3[9]
$Ag_3I_4^-$	46.6 ± 0.3	47.8 ± 0.3		51.55[13]	47.9 ± 0.3	48.6 ± 0.3		
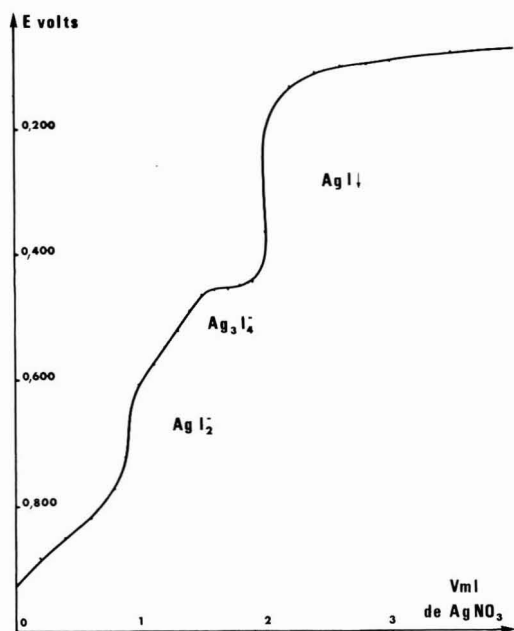
Fig. 1. Dosage d'une solution de chlorure par $AgNO_3$ suivi par potentiométrie à une électrode d'argent.

vraies et apparentes des composés AgX, AgX_2^- et HgX_4^{2-} [5]. En ce qui concerne les valeurs relatives aux composés HgX_4^{2-} dans le DMF, nous avons complété les valeurs obtenues par Nguyen Van Kiet[2]. Rappelons les formules qui conduisent aux valeurs du Tableau 2:

$$pK_A = pH + \log\left[10^{\Delta pKs} - 1\right]$$

à partir des constantes des composés AgX

TABLEAU 2

CONSTANTES ACIDE–BASE DES COUPLES HX/X^- OBTENUES PAR DIFFÉRENCE ENTRE LES CONSTANTES VRAIES ET LES CONSTANTES APPARENTES DE DIFFÉRENTS COMPOSÉS

S	DMF				NMP		
ΔpK de	AgX	AgX_2^-	HgX_4^{2-}	littérature	AgX	AgX_2^-	HgX_4^{2-} [5]
HCl/Cl$^-$	2.6 ± 0.2	2.6 ± 0.3	2.2 ± 0.6	3.4^{14}	2.8 ± 0.2	2.8 ± 0.3	2.9 ± 0.6
HBr/Br$^-$	1.9 ± 0.2	1.6 ± 0.3	1.9 ± 0.6	1.8^{14}	1.3 ± 0.2	1.5 ± 0.3	1.2 ± 0.6
HI/I$^-$	fort	fort	fort		0.8 ± 0.2	0.8 ± 0.3	0.8 ± 0.6
HSCN/SCN$^-$	2.0 ± 0.2	1.6 ± 0.3	1.5 ± 0.6				1.4 ± 0.6

$$pK_A = pH + \log \left[10^{\Delta pK_c/2} - 1 \right]$$

et

$$pK_A = pH + \log \left[10^{\Delta pK_c/4} - 1 \right]$$

à partir des constantes des complexes AgX_2^- et HgX_4^{2-}, respectivement.

Nous constatons que les valeurs obtenues sont très concordantes et que, dans le DMF comme dans la NMP, la force des hydracides HX décroît dans l'ordre : HI > HBr, HSCN > HCl. Contrairement à ce que nous avions précédemment supposé[3], l'acide HSCN ne serait donc pas fort dans le DMF.

II. DÉTERMINATION DES COEFFICIENTS DE SOLVATATION

Les constantes relatives aux composés du mercure sont rappelées dans le Tableau 3. Elles sont extraites des travaux de Nguyen Van Kiet[2] dans le DMF et de Buisson[5] dans la NMP. Les valeurs $p\Gamma_{M^{n+}}$ sont obtenues à partir de l'éqn. (7), les coefficients $p\Gamma_{X^-}$ à partir des $p\Gamma_{Ag^+}$ et des constantes K_S par l'intermédiaire de l'éqn. (4); enfin les valeurs $p\Gamma_{HgX_4^{2-}}$ et $p\Gamma_{AgCl^-}$ sont calculées à partir de l'éqn. (5). Tous ces coefficients sont rassemblés dans le Tableau 4. Nous constatons que les cations métalliques sont beaucoup plus solvatés par les solvants organiques que par l'eau. Le phénomène est plus important pour les ions mercuriques que pour les ions mercureux et il est plus marqué dans la NMP que dans le DMF. Ceci se traduit par la disparition progressive du domaine d'existence du dimère Hg_2^{2+} lorsqu'on passe de l'eau au DMF puis à la NMP. Les anions sont moins solvatés par les solvants or-

TABLEAU 3

CONSTANTES CARACTÉRISTIQUES DES COMPOSÉS DU MERCURE DANS DIFFÉRENTS SOLVANTS

Constante	Couple ou composé	Eau[15]	DMF[3]	NMP[5]
E_0(mV) par rapport au ferrocène	Hg/Hg$_2^{2+}$	390	73	29
	Hg/Hg^{2+}	450	90	25
K_c	HgCl$_4^{2-}$	15.2	33.8	37.1
	HgBr$_4^{2-}$	20.8	35.9	37.5
	HgI$_4^{2-}$	29.8	37.1	37.6
	Hg(SCN)$_4^{2-}$	19.8	22.5	25.6

TABLEAU 4

COEFFICIENTS DE SOLVATATION DES DIVERS COMPOSÉS ÉTUDIÉS

Composé	$H_2O\ DMF$ $p\Gamma$	$H_2O\ NMP$	Composé	$H_2O\ DMF$ $p\Gamma$	$H_2O\ NMP$ $p\Gamma$
Hg_2^{2+}	11.0	12.5	$AgCl_2^-$	-3.6	-3.4
Hg^{2+}	12.4	14.7	$AgBr_2^-$	-1.3	-0.9
Ag^+	5.1	6.2	AgI_2^-	$+2.2$	$+2.0$
			$Ag(SCN)_2^-$	-0.4	-0.3
Cl^-	-9.7	-10.8	$HgCl_4^{2-}$	-5.0	-6.6
Br^-	-7.7	-8.5	$HgBr_4^{2-}$	-0.5	-2.6
I^-	-4.5	-5.4	HgI_4^{2-}	$+3.3$	$+0.9$
SCN^-	-4.2	-4.5	$Hg(SCN)_4^{2-}$	-0.5	$+2.5$

ganiques que par l'eau; le phénomène est d'autant plus marqué que la taille de l'ion est plus petite; il est à l'origine de la très grande stabilité des complexes mercuriques dans le DMF et la NMP.

En conclusion de cette étude, nous constatons donc que le DMF et la NMP se comportent vis-à-vis des solutés comme les autres solvants dipolaires aprotiques et que tous les phénomènes observés sont plus importants pour la N-méthylpyrroli-done que pour le diméthylformamide.

RÉSUMÉ

Nous avons analysé, à l'aide des coefficients de solvatation, les résultats de nos travaux antérieurs sur les composés du mercure dans le diméthylformamide et la N-méthylpyrrolidone. Cette analyse nous a conduit à compléter les données de la littérature relatives aux composés de l'argent dans ces mêmes solvants. La comparaison des constantes obtenues dans différents milieux nous a permis de déterminer la constante acide–base des couples HX/X^- (X = Cl, Br, I, SCN). Les coefficients de solvatation ont été évalués à partir de l'hypothèse de Strehlow; leur examen montre que le diméthylformamide et la N-méthylpyrrolidone se comportent vis-à-vis des solutés comme les autres solvants dipolaires aprotiques.

SUMMARY

The results of our previous work on mercury compounds in dimethylformami-de and N-methylpyrrolidone were examined by means of solvent activity coefficients. This analysis enabled us to complete the literature data relative to silver compounds in DMF and NMP. By comparing the constants obtained in different media we were able to determine the acidity constant of the pairs HX/X^- (X = Cl, Br, I, SCN). Solvent activity coefficients were evaluated on the basis of Strehlow's hypothesis; they show that NMP and DMF behave towards solutes in the same way as other dipolar aprotic solvents.

BIBLIOGRAPHIE

1 M. Bréant et Nguyen Van Kiet, *Compt. Rend.*, 264 (1967) 1042.
2 M. Bréant et Nguyen Van Kiet, *Compt. Rend.*, 262 (1966) 492.
3 Nguyen van Kiet, Thèse, Lyon, 1967.
4 M. Bréant, M. Bazouin, C. Buisson, M. Dupin et J. M. Rebattu, *Bull. Soc. Chim. France*, (1968) 5065.
5 M. Bréant et C. Buisson, *J. Electroanal. Chem.*, 24 (1970) 145.
6 H. Strehlow, in J. J. Lagowski (Ed.), *The Chemistry of Non-Aqueous Solvents*, Vol. 1, Academic Press, New York, 1966, p. 129.
7 A. J. Parker et R. Alexander, *J. Am. Chem. Soc.*, 90 (1968) 3313.
8 R. Alexander, E. C. F. Ko, A. J. Parker et T. J. Broxton, *J. Am. Chem. Soc.*, 90 (1968) 5049.
9 P. Olavi, I. Virtanen et R. Kerkelä, *Suomen Kemistilehti B*, 42 (1969) 29.
10 C. Barraqué, J. Vedel et B. Trémillon, *Bull. Soc. Chim. France*, (1968) 3421.
11 R. Alexander, E. C. F. Ko, Y. C. Mac et A. J. Parker, *J. Am. Chem. Soc.*, 89 (1967) 3703.
12 J. N. Butler, *J. Phys. Chem.*, 72 (1968) 3288.
13 H. Chateau et M. C. Moncet, *J. Chim. Phys.*, 60 (1963) 1060.
14 B. W. Clare, D. Cook, E. C. F. Ko, Y. C. Mac et A. J. Parker, *J. Am. Chem. Soc.*, 88 (1966) 1911.
15 L. G. Sillén et A. E. Martell, *Stability Constants of Metal-Ions Complexes*, The Chemical Society, London, 1964.

ZUR THEORIE DER POLAROGRAPHISCHEN STRÖME BEI DISMUTATION DES ELEKTRODENREAKTIONSPRODUKTS

B. KASTENING*

Chemisches Institut der Hochschule, Bamberg (Deutschland)

(Eingegangen am 11. August, 1969)

EINLEITUNG

Die Grenzstromstärken polarographischer Kurven (sowie bei ähnlichen Verfahren, etwa der rotierenden Scheibe, etc.) werden in manchen Fällen durch eine Dismutationsreaktion bestimmt (Disproportionierung), der das primäre Produkt der Elektrodenreaktion unterliegt und durch die der ursprüngliche Depolarisator zum Teil zurückgebildet wird. Infolge dieser Rückbildung gehen dabei die Stromstärken—je nach der Geschwindigkeit der Dismutation mehr oder weniger stark—über den durch gewöhnlichen Antransport des Depolarisators und dessen Elektrodenreaktion bedingten Wert hinaus. Ein viel untersuchtes Beispiel stellt die Dismutation der Ionen von fünfwertigem Uran dar, das durch Reduktion der Ionen von sechswertigem Uran entsteht. Andere Fälle betreffen die Dismutation organischer Radikale, die als Primärprodukt der Elektrodenreaktion gebildet werden.

Die Kinetik der Dismutation folgt gewöhnlich dem Gesetz einer Reaktion zweiter Ordnung. Eine theoretische Behandlung des Problems ist infolgedessen erschwert, da die partiellen Differentialgleichungen, die den Stofftransport und die chemische Homogenreaktion beschreiben, nichtlinear sind. Die rigorose Berechnung, wie sie von Koutecký und Koryta[1] durchgeführt wurde, erfordert einen erheblichen Aufwand numerischer Rechnungen und vermag nur vergleichsweise langsame Reaktionen zu erfassen. Bei hinreichend raschen Reaktionen, bei denen die "Reaktionsschicht" klein gegenüber der Diffusionsschicht bleibt, kann eine Näherungsrechnung durchgeführt werden, wie Koutecký und Hanuš[2] gezeigt haben. Bislang ist dabei nur der Fall berücksichtigt worden, dass aus zwei Molekülen des primären Elektrodenreaktionsproduktes B je ein Molekül des ursprünglichen Depolarisators A und des Endproduktes C entstehen, gemäss dem Schema:

$$A + z e^- \rightarrow B \tag{1}$$

$$2 B \rightarrow A + C \tag{2}$$

In manchen Fällen verläuft die Dismutation jedoch nicht in dieser einfachen Weise, sondern es schliesst sich noch eine weitere Reaktion von C an, die eine zusätzliche Rückbildung von A ergibt, etwa gemäss

$$C + (m-2)B \rightarrow (m-2)A + D \tag{3}$$

---

* Jetzt: Forschungsabteilung Angewandte Elektrochemie, Kernforschungsanlage Jülich GmbH.

Als Beispiel sei die Dismutation des bei der Reduktion von Nitrobenzol gebildeten Radikalanions genannt[3,4], die im Bruttovorgang aus je 4 Radikalanionen 3 Nitrobenzol-Moleküle zurückliefert (im Falle von p-Nitranilin u.ä. aus je 6 Radikalanionen 5 Depolarisator-Moleküle). Die chemische Reaktion, die dem Elektrodenvorgang folgt, kann daher anstelle von Gl. (2) allgemeiner als

$$mB \rightarrow (m-1)A + D \tag{4}$$

formuliert werden, wobei der Vorgang (2) geschwindigkeitsbestimmend ist. Diese allgemeinere Dismutationsreaktion soll im folgenden theoretisch untersucht und das Resultat der Rechnung auf experimentelle Ergebnisse bei der Reduktion aromatischer Nitroverbindungen angewendet werden.

THEORETISCHE BERECHNUNG

I. Exakte Lösung für langsame Dismutation

Die exakte Lösung des Problems schliesst sich in ihrer Formulierung eng an die frühere Arbeit[1] für den Spezialfall $m = 2$ an. Die zugrundeliegenden Differentialgleichungen für die polarographische Tropfelektrode lauten hier allgemein

$$\frac{\partial a}{\partial t} = D \frac{\partial^2 a}{\partial x^2} + \frac{2x}{3t} \frac{\partial a}{\partial x} + (m-1)k_2 b^2 \tag{5}$$

$$\frac{\partial b}{\partial t} = D \frac{\partial^2 b}{\partial x^2} + \frac{2x}{3t} \frac{\partial b}{\partial x} - mk_2 b^2 \tag{6}$$

wo a und b die Konzentrationen der Stoffe A und B bedeuten. (Aus rationellen Gründen weicht die hier verwendete Geschwindigkeitskonstante k_2 in ihrer Bedeutung von der bei Koutecký und Koryta benutzten Konstante k ab, und zwar ist $k = 2 k_2$.) Bleiben die Vorgänge an der Elektrode auf die Reaktion (1) beschränkt und verläuft diese vollständig nach rechts, so erhält man für den Grenzstrom die Anfangs- und Randbedingungen

$$t = 0, \quad x > 0 \; :\} \tag{7}$$
$$\qquad\qquad\qquad a = a^*, \; b = 0$$
$$t \geqq 0, \quad x \rightarrow \infty : \} \tag{8}$$

$$t > 0, \quad x = 0 \; : \qquad a = 0, \; \frac{\partial a}{\partial x} + \frac{\partial b}{\partial x} = 0 \tag{9}$$

wo a^* die Konzentration von A im Innern der Lösung ist. Durch Einführung neuer unabhängiger Variabler

$$\psi = \frac{a + \dfrac{m-1}{m} b}{a^*}, \qquad u = \frac{1}{m} \frac{b}{a^*} \tag{10}$$

und Transformation der unabhängigen Variablen

$$s = \frac{x}{(\frac{12}{7}Dt)^{\frac{1}{2}}}, \qquad \eta = k_2 a^* t \tag{11}$$

erhält man die neuen Differentialgleichungen

$$\frac{\partial^2 \psi}{\partial s^2} + 2s \frac{\partial \psi}{\partial s} - \tfrac{12}{7}\eta \frac{\partial \psi}{\partial \eta} = 0 \tag{12}$$

$$\frac{\partial^2 u}{\partial s^2} + 2s\frac{\partial u}{\partial s} - \tfrac{12}{7}\eta\left(\frac{\partial u}{\partial \eta} + m^2 u^2\right) = 0 \tag{13}$$

mit den Randbedingungen

$$s=0 \ : \ \ \psi=(m-1)u, \ \ \ \frac{\partial \psi}{\partial s} + \frac{\partial u}{\partial s} = 0 \tag{14}$$

$$s\to\infty : \ \ \psi=1, \ \ \ u=0 \tag{15}$$

Die durch Reaktion (1) bestimmte Stromstärke ist gegeben durch

$$i = zFqD\left(\frac{\partial a}{\partial x}\right)_{x=0} = zFqD \frac{1}{(\tfrac{12}{7}Dt)^{\frac{1}{2}}} ma^*\left(\frac{\partial \psi}{\partial s}\right)_{s=0} \tag{16}$$

und mit dem rein transportbedingten Grenzstrom

$$i_{\mathrm{d}} = zFqD \frac{a^*}{(\tfrac{3}{7}\pi Dt)^{\frac{1}{2}}} \tag{17}$$

ergibt sich das Verhältnis

$$\frac{i}{i_{\mathrm{d}}} = \frac{\sqrt{\pi}}{2} m\left(\frac{\partial \psi}{\partial s}\right)_{s=0} \tag{18}$$

Die Lösung für die Variable ψ kann in der Form

$$\psi(s) = \sum_{i=0}^{\infty} a_i \Psi_{6i/7}(s)\eta^i + \frac{2}{\sqrt{\pi}} \int_0^s e^{-u^2}\,\mathrm{d}u \tag{19}$$

geschrieben werden, wo die Funktion $\Psi_\alpha(s)$ aus der zitierten Arbeit[1] bekannt ist (vergleiche auch ref. 5) und die Koeffizienten a_i durch die weitere Rechnung zu ermitteln sind; speziell ergibt sich leicht

$$a_0 = \frac{m-1}{m} \tag{20}$$

Durch Differentiation und unter Berücksichtigung von $(\mathrm{d}\Psi_\alpha/\mathrm{d}s)_{s=0} = -p_\alpha$ (für p_α vergleiche ref. 5) ergibt sich

$$\frac{i}{i_{\mathrm{d}}} = 1+(m-1)\sum_{i=1}^{\infty} C_i\eta^i \tag{21}$$

mit

$$C_i = -\frac{\sqrt{\pi}}{2}\frac{m}{m-1}\,a_i p_{6i/7} \tag{22}$$

und für die mittlere Stromstärke

$$\frac{i}{i_{\mathrm{d}}} = 1+(m-1)\sum_{i=1}^{\infty} D_i\eta_1^i \tag{23}$$

mit

$$D_i = \frac{7}{6i+7}\,C_i \tag{24}$$

$$\eta_1 = k_2 a^* \tau \tag{25}$$

wo τ die polarographische Tropfzeit bedeutet.

Die Berechnung der Koeffizienten a_i (und hieraus C_i und D_i) gestaltet sich völlig analog wie in der zitierten Arbeit[1]. Abweichend steht jedoch

$$s = 0: \quad \psi_i = (m-1)u_i \tag{26}$$

$$u_i(s) = -\frac{\Psi_{6i/7}(s)}{mp_{6i/7}} \int_0^\infty e^{u^2} G_i(u) \Psi_{6i/7}(u)\,du$$

$$\qquad\qquad - L_{6i/7}(s) \int_s^\infty e^{u^2} G_i(u) \Psi_{6i/7}(u)\,du$$

$$\qquad\qquad - \Psi_{6i/7}(s) \int_0^s e^{u^2} G_i(u) L_{6i/7}(u)\,du \tag{27}$$

und

$$a_i = -\frac{m-1}{mp_{6i/7}} \int_0^\infty e^{u^2} G_i(u) \Psi_{6i/7}(u)\,du \tag{28}$$

(Beim Vergleich mit Arbeit[1] ist zu berücksichtigen, dass neben den problem-bedingten Änderungen auch einige dort in Gln. (11) und (12) enthaltene Druckfehler eliminiert wurden.) Mit Gl. (22) folgt ferner

$$C_i = \frac{\sqrt{\pi}}{2} \int_0^\infty e^{u^2} G_i(u) \Psi_{6i/7}(u)\,du \tag{29}$$

Durch numerische Berechnung ergeben sich für die ersten drei Koeffizienten die Ausdrücke

$$C_1 = +0.3449$$

$$C_2 = -(0.1323 + 0.0339\ m)$$

$$C_3 = +(0.0483 + 0.0249\ m + 0.0050\ m^2)$$

woraus mit Gl. (24) auch leicht D_1, D_2 und D_3 erhalten werden. Bei geringfügiger Abweichung stimmen diese Werte mit den in der zitierten Arbeit[1] angegebenen überein, wenn $m=2$ gesetzt und die abweichende Formulierung für die Parameter η und η_1 sowie für i/i_d und $\bar{i}/\bar{i}_d$ berücksichtigt wird. Auf die umständliche Berechnung weiterer Koeffizienten wurde verzichtet, da sich an die mit den angegebenen Koeffizienten berechenbaren Werte für i/i_d bzw. $\bar{i}/\bar{i}_d$ für höhere Werte von η bzw. η_1 bald der Gültigkeitsbereich der im folgenden Abschnitt behandelten Näherungsmethode anschliesst.

II. Näherungsrechnung für rasche Dismutation

Erfolgt die Dismutation hinreichend rasch, so lassen sich in der partiellen Differentialgleichung für die Variable u

$$\frac{\partial u}{\partial t} = D\frac{\partial^2 u}{\partial x^2} + \frac{2x}{t}\frac{\partial u}{\partial x} - m^2 k_2 a^* u^2 \tag{30}$$

im Anschluss an Koutecký und Hanuš[2] die Glieder mit den ersten Differentialquotienten näherungsweise vernachlässigen, und man erhält hierauf nach geeignet durchgeführter Integration für den Bereich der Elektrodenoberfläche

$$x \to 0: \quad \left(\frac{du}{dx}\right)^2 = m^2 \frac{2k_2 a^*}{3D} u^3 + \text{const} \tag{31}$$

wo die Integrationskonstante "const" den Wert null besitzt. Bei Einführung der unabhängigen Variablen s nach Gl. (11) sowie

$$\xi = \left\{ \frac{8}{7} \frac{m^2}{(m-1)^3} k_2 a^* t \right\}^{\frac{1}{2}} \tag{32}$$

ergibt sich unter Berücksichtigung der Randbedingungen (14) die Differential-gleichung

$$\frac{\partial^2 \psi}{\partial s^2} + 2s \frac{\partial \psi}{\partial s} - \frac{6}{7}\xi \frac{\partial \psi}{\partial \xi} = 0 \tag{33}$$

mit den Randbedingungen

$$s = 0 \quad : \quad \frac{\partial \psi}{\partial s} = \xi \psi^{\frac{3}{2}} \tag{34}$$

$$s \to \infty : \quad \psi = 1 \tag{35}$$

Die bei Koutecký und Hanuš[2] angegebene Lösung für $m = 2$ kann auch auf beliebige Stöchiometrie mit $m \neq 2$ übertragen werden, da diese Autoren ihre Berechnungen nicht auf den Grenzstrom beschränkten, sondern für ein beliebiges Verhältnis a/b an der Elektrodenfläche und damit auch für beliebiges ψ/u wie in Gl. (14) formulierten. (Bei Anwendung ihrer Formulierungen für die Dismutation sind einige Rechen- bzw. Druckfehler kritisch zu berücksichtigen.) Einfacher noch ist es, sich unmittelbar auf ihre Berechnung einer nachfolgenden Dimerisierung des Depolarisationspro-duktes zu beziehen, da das hierfür angeführte Gleichungssystem (23) der Arbeit[2] formal identisch ist mit dem oben durch Gln. (33)–(35) formulierten Problem. Das Stromstärke-Verhältnis ist wiederum durch Gl. (18) gegeben. Durch Vergleich mit den entsprechenden Ansätzen für i/i_d in Arbeit 2 zeigt sich, dass im vorliegenden Falle

$$\frac{i}{i_d} = m f_2(\xi) \tag{36}$$

wobei der Parameter ξ nach Gl. (32) mit demjenigen in Tabelle III der Arbeit 2 zu identifizieren ist. Entsprechend ist das Verhältnis der mittleren Stromstärken aus Tabelle IV der Arbeit 2 zu entnehmen

$$\frac{i}{i_d} = m \bar{f}_2(\xi_1) \tag{37}$$

wobei

$$\xi_1 = \left\{ \frac{8}{7} \frac{m^2}{(m-1)^3} k_2 a^* \tau \right\}^{\frac{1}{2}} \tag{38}$$

III. Näherung mit der Methode der Reaktionsschicht

Für eine sehr schnelle Dismutation, wenn die "Reaktionsschicht" μ klein ist gegenüber der Diffusionsschicht δ,

$$\mu = \left(\frac{D}{mk_2 b_{x=0}}\right)^{\frac{1}{2}} \ll \delta = (\tfrac{3}{7}\pi Dt)^{\frac{1}{2}} \tag{39}$$

kann auch die Näherungsmethode mit dem Konzept dieser Reaktionsschicht angewendet werden. Dabei ist anzusetzen, dass die Konzentrationsveränderungen sowohl für die Spezies A als auch B in der Reaktionsschicht infolge Stofftransports, chemischer Reaktion und Elektrodenreaktion zusammen jeweils null ergeben. Diese Bilanzen sind wie folgt zu formulieren:

$$0 \leqq x \leqq \mu: \quad \frac{\mathrm{d}n_A}{\mathrm{d}t} = \bar{q}D\left(\frac{\partial a}{\partial x}\right)_{x=0} + \bar{q}\mu(m-1)k_2\bar{b}_{x=0}^2 - \frac{i}{zF} = 0 \tag{40}$$

$$\frac{\mathrm{d}n_B}{\mathrm{d}t} = \bar{q}D\left(\frac{\partial b}{\partial x}\right)_{x=0} - \bar{q}\mu m k_2\bar{b}_{x=0}^2 + \frac{i}{zF} = 0 \tag{41}$$

Die jeweils ersten Glieder der rechten Gleichungsseiten, die das Herein- bzw. Hinausdiffundieren in die/aus der Reaktionsschicht beschreiben, können näherungsweise durch die gewöhnlichen Transportbeziehungen beschrieben werden:

$$\bar{q}D\left(\frac{\partial a}{\partial x}\right)_{x=0} = \bar{q}D\frac{a^* - a_{x=0}}{\delta} = \bar{q}D\frac{a^*}{\delta} = \frac{i_d}{zF} \tag{42}$$

$$\bar{q}D\left(\frac{\partial b}{\partial x}\right)_{x=0} = \bar{q}D\frac{-b_{x=0}}{\delta} = -\frac{b_{x=0}}{a^*}\frac{i_d}{zF} \tag{43}$$

Ferner kann in den jeweils zweiten Gliedern der Gln. (40)/(41) die mittlere Elektrodenfläche durch den transportbedingten Grenzstrom i_d beschrieben werden:

$$\bar{q} = 0.81\frac{i_d\tau^{\frac{1}{2}}}{zFD^{\frac{1}{2}}a^*} \tag{44}$$

Durch Einsetzen der Beziehungen (42)–(44) in Gln. (40) und (41) berechnet man

$$b_{x=0} = a^*\frac{m - \dfrac{i}{i_d}}{m-1} \tag{45}$$

und ferner

$$\frac{\left(\dfrac{i}{i_d} - 1\right)^2}{\left(m - \dfrac{i}{i_d}\right)^3} = \frac{0.66}{m(m-1)}k_2 a^*\tau \tag{46}$$

In Abb. 1 sind für $m=2$, 4 und 6 die sich zufolge Gln. (23), (37) und (46) ergebenden Werte der relativen mittleren Stromstärke dargestellt. Die ausgezogenen Kurvenäste I entsprechen dem mit den berechneten Koeffizienten zugänglichen Bereich der exakten Beziehung (23), die ausgezogenen Äste II und III dem Gültigkeitsbereich der oben unter II und III angegebenen Näherungen; dazwischen ist gestrichelt interpoliert. Punktierte Linien deuten den weiteren Verlauf der Näherungen ausserhalb ihres Gültigkeitsbereichs an.
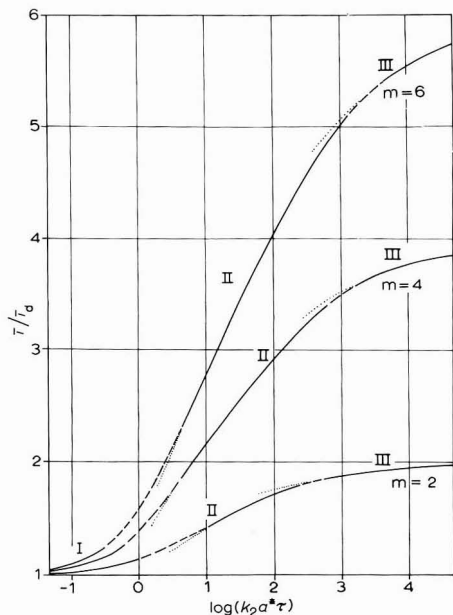
Abb. 1. Mittlerer polarographischer Grenzstrom in Abhängigkeit vom Parameter $k_2 a^* \tau$ bei Dismutation des Depolarisationsproduktes, für die stöchiometrischen Faktoren $m = 2$, 4 und 6. (——— I, II, III) berechnet nach den in Abschnitt I, II, III abgeleiteten Funktionen; (– – –) interpolierter Verlauf; (· · · · ·) Verlauf der Näherungsfunktionen ausserhalb ihres Gültigkeitsbereichs.

ANWENDUNG AUF EXPERIMENTELLE ERGEBNISSE

Die vorstehenden Berechnungen wurden angewendet auf die unter geeigneten Bedingungen zu beobachtende Dismutation der Radikalanionen, die bei der Reduktion aromatischer Nitroverbindungen entstehen. Nach früheren Untersuchungen[4,6,7] kommt nur dann ein durch die Dismutation bestimmter Grenzstrom zustande, wenn heterogene Abreaktionen der Radikalanionen an der Elektrode verhindert werden, und zwar: (a) die unmittelbare Weiterreduktion des Radikalanions nach

$$(R-NO_2^-)_{ad} + e^- \rightarrow R-NO_2^{2-} \rightarrow \text{schnelle chemische Folgereaktionen und Weiterreduktion}$$
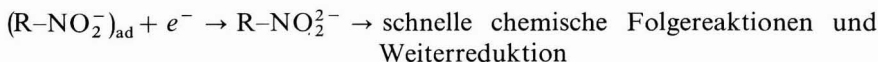
sowie (b) die heterogene Protonenübertragung mit sofortiger anschliessender Weiterreduktion:

$$(R-NO_2^-)_{ad} + H^+ \rightarrow R-NO_2H \rightarrow \text{schnelle Weiterreduktion}$$
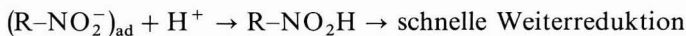
Beide Heterogenreaktionen lassen sich durch grenzflächenaktive Stoffe als Inhibitoren ausschalten. Während aber der Vorgang (a) schon durch mässig wirksame Inhibitoren verhindert wird, indem sich die Weiterreduktion dann erst bei negativeren Potentialen bemerkbar macht, erfordert die Unterdrückung der Reaktion (b) die Anwendung stark wirkender Inhibitoren (wie Campher oder Triphenylphosphinoxid); auch dann kann bei sehr kleinen Konzentrationen a^* und niedrigen pH-Werten die Reaktion (b) mit der homogenen Dismutation in Konkurrenz treten[6,7].

Bei der Anwendung der theoretischen Beziehungen ist zu berücksichtigen,

dass ein Protonisierungsgleichgewicht

$$R-NO_2^- + H^+ \rightleftharpoons R-NO_2H \tag{47}$$

der geschwindigkeitsbestimmenden bimolekularen Reaktion

$$R-NO_2^- + R-NO_2H \xrightarrow{k} R-NO_2 + R-NO_2H^- \tag{48}$$

vorgelagert ist; an letztere schliesst sich dann die schnelle Reaktion mit weiteren Radikalanionen entsprechend Gl. (3) unter Bildung des entsprechenden Hydroxylamins ($m=4$) bzw. Amins ($m=6$) an. (Erst in stärker alkalischen Lösungen, bei etwa pH $\geq$ 12, wird auch die direkte Dismutation zwischen zwei Radikalanionen merkbar.) Die experimentell beobachtete Geschwindigkeitskonstante k_2 enthält daher neben der wahren bimolekularen Geschwindigkeitskonstante k für die Reaktion (48) noch die Säure-Dissoziationskonstante K_S für das ungeladene Radikal nach Gl. (47)

$$k_2 = \frac{[H^+]}{K_S} k \tag{49}$$

und ist der Wasserstoffionen-Aktivität proportional.

In Abb. 2 sind Messergebnisse für Nitrobenzol und p-Nitrochlorbenzol ($m=4$) sowie p-Nitranilin ($m=6$) wiedergegeben, die bei verschiedenen pH-Werten und Konzentrationen a^* erhalten und zum Teil früheren Arbeiten[3,4] entnommen
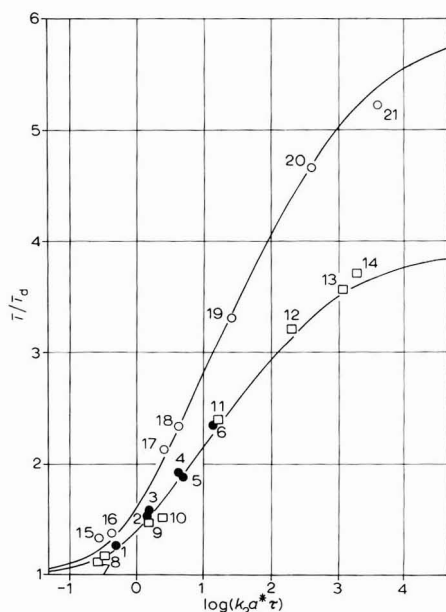
Abb. 2. Wiedergabe experimenteller Ergebnisse für aromatische Nitroverbindungen bei Annahme der im Text angegebenen Werte für k_2. Im folgenden sind für die einzelnen Messpunkte der pH-Wert und die Konzentration a^* (M) angegeben: ($\bullet$) Nitrobenzol: (1) pH = 9.20, $a^* = 10^{-3}$ M; (2) 9.20, $3 \cdot 10^{-3}$; (3) 8.72, 10^{-3}; (4) 8.72, $3 \cdot 10^{-3}$; (5) 9.20, 10^{-2}; (6) 8.72, 10^{-2}. ($\square$) p-Nitrochlorbenzol: (7) 8.90, 10^{-4}; (8) 9.81, 10^{-3}; (9) 8.10, 10^{-4}; (10) 8.90, 10^{-3}; (11) 8.10, 10^{-3}; (12) 6.99, 10^{-3}; (13) 6.20, 10^{-3}; (14) 5.98, 10^{-3}. ($\bigcirc$) p-Nitranilin: (15) 8.2, 10^{-5}; (16) 9.0, 10^{-4}; (17) 8.2, 10^{-4}; (18) 9.0, 10^{-3}; (19) 8.2, 10^{-3}; (20) 7.0, 10^{-3}; (21) 6.0, 10^{-3}.

wurden. Die Messpunkte folgen gut den theoretisch berechneten Kurven. Für die Konstante k_2 wurden folgende Werte zugrundegelegt:

Nitrobenzol: $\qquad k_2 = 2.7 \times 10^{11}[H^+] \ M^{-1}s^{-1}$
p-Nitrochlorbenzol: $k_2 = \quad 7 \times 10^{11}[H^+] \ M^{-1}s^{-1}$
p-Nitranilin: $\qquad k_2 = 1.5 \times 10^{12}[H^+] \ M^{-1}s^{-1}$

Die Werte für Nitrobenzol und p-Nitrochlorbenzol stehen in guter Übereinstimmung mit denjenigen, die mittels Elektronenspinresonanz durch unmittelbare Verfolgung der Abreaktion in homogener Lösung erhalten wurden[6,8]. (Beim Vergleich mit den Angaben in Arbeit 8 ist zu berücksichtigen, dass dort der stöchiometrische Faktor 4 in die Konstanten mit einbezogen ist.)

Zur Ermittlung der wahren Geschwindigkeitskonstanten k ist die Kenntnis der Dissoziationskonstanten K_S erforderlich. Für Nitrobenzol wurde der Wert p$K_S = 3.2$ angegeben[9]. Nimmt man einen gleich grossen Einfluss der *para*-ständigen Substituenten auf die Dissoziationskonstante wie im Falle der entsprechenden Benzoesäuren an (bei denen der Zusammenhang Δp$K_S = -\sigma$ mit dem Hammettschen σ-Koeffizienten gut erfüllt ist), so lassen sich hieraus für p-Nitrochlorbenzol- und p-Nitranilin-Radikale p$K_S = 3.0$ bzw. 3.93 abschätzen. Damit ergeben sich für die Geschwindigkeitskonstante k die Werte

Nitrobenzol: $\qquad k = 1.7 \times 10^8 \ M^{-1}s^{-1}$
p-Nitrochlorbenzol: $k = \quad 7 \times 10^8 \ M^{-1}s^{-1}$
p-Nitranilin: $\qquad k = 1.7 \times 10^8 \ M^{-1}s^{-1}$

Neben den mittleren Stromstärken lassen sich auch die Strom–Zeit-Kurven am einzelnen polarographischen Tropfen durch die im theoretischen Teil abgeleiteten Beziehungen gut beschreiben. Dies ist in Abb. 3 veranschaulicht, in der für p-Nitranilin in einer früheren Arbeit[3] erhaltene Messwerte sowie die theoretisch mit $k_2 = 2 \times 10^{12}$ $[H^+]$—leicht abweichend von obiger Angabe—berechneten Kurven eingezeichnet sind. Berücksichtigt man, dass sämtliche Kurven der Abb. 3 mit einem einzigen Wert des willkürlichen Parameters berechnet wurden, während in Arbeit 3 zunächst die am besten angepasste Kurve aufgesucht und der Parameter erst nachträglich durch
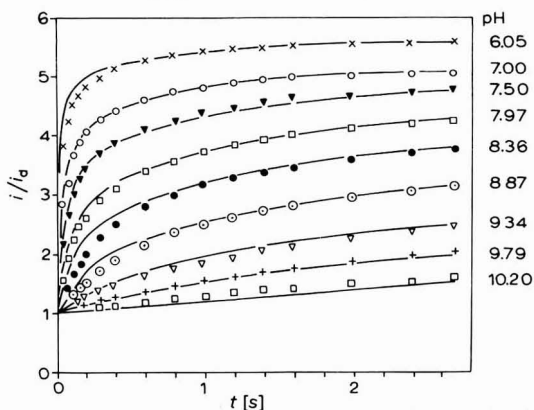
Abb. 3. Strom–Zeit-Kurven am polarographischen Einzeltropfen für p-Nitranilin. Messwerte aus einer früheren Arbeit[3]. Ausgezogene Kurven berechnet nach den in Abschnitt I, II und III abgeleiteten Funktionen für den momentanen Strom unter Annahme des im Text angegebenen Wertes für k_2; $a^* = 10^{-3} \ M$.

Mittelung erhalten wurde, so ist die Anpassung erheblich besser als bei der damals zugrundegelegten Annahme einer geschwindigkeitsbestimmenden Reaktion erster Ordnung.

EXPERIMENTELLES

Sämtliche Messergebnisse wurden in wässrigen Lösungen mit einem Gehalt von 10% Methanol sowie 0.1–0.15% Campher oder Triphenylphosphinoxid als Inhibitor erhalten.

ZUSAMMENFASSUNG

Die Theorie kinetisch bedingter polarographischer Ströme, die auf der Rückbildung des Depolarisators infolge Dismutation des Depolarisationsproduktes beruhen, wird verallgemeinert für beliebige Stöchiometrie der Dismutationsreaktion. Durch Anwendung der exakten Berechnung für langsame und zweier Näherungsmethoden für schnelle Dismutation kann die Überhöhung der polarographischen Stufen für beliebige Werte des Parameters $k_2 a^* \tau$ (k_2 = Geschwindigkeitskonstante der Dismutation, a^* = Depolarisator-Konzentration, τ = Tropfzeit) und des stöchiometrischen Faktors m angegeben werden. Die Theorie wird auf die Dismutation der Radikalanionen aromatischer Nitroverbindungen angewendet. Die hiernach erhaltenen Werte der Geschwindigkeitskonstanten stehen in Übereinstimmung mit denjenigen, die bei direkter Verfolgung der Homogenreaktion beobachtet wurden.

SUMMARY

The theory of polarographic currents controlled by the kinetics of dismutation of the depolarization product with regeneration of the depolarizer, has been generalized for any stoichiometry of the dismutation reaction. The currents exceeding the diffusion-controlled values can be given for any value of the parameter $k_2 a^* \tau$ (k_2 = rate constant of dismutation, a^* = depolarizer concentration, τ = drop time) and of the stoichiometric factor m, by applying the rigorous solution for slow, and two approximate methods for fast dismutation. The theory has been applied to the dismutation of anion radicals of aromatic nitro compounds. The rate constants calculated from the currents agree with those obtained from direct observation of the dismutation reaction in homogeneous solution.

LITERATUR

1 J. KOUTECKÝ UND J. KORYTA, Collection Czech. Chem. Commun., 19 (1954) 845.
2 J. KOUTECKÝ UND V. HANUŠ, Collection Czech. Chem. Commun., 20 (1955) 124.
3 B. KASTENING UND L. HOLLECK, Z. Elektrochem., 63 (1959) 166.
4 B. KASTENING, Electrochim. Acta, 9 (1964) 241.
5 J. KOUTECKÝ, Collection Czech. Chem. Commun., 18 (1953) 311, 597.
6 B. KASTENING UND S. VAVŘIČKA, Ber. Bunsenges. Physik. Chem., 72 (1968) 27.
7 B. KASTENING, Vortrag 19. CITCE-Tagung, Sept. 1968, Detroit/USA, Extended Abstracts, p. 81;
   B. KASTENING UND L. HOLLECK, in Vorbereitung.
8 D. KOLB, W. WIRTHS UND H. GERISCHER, Ber. Bunsenges. Physik. Chem., 73 (1969) 148.
9 K. D. ASMUS, A. WIGGER UND A. HENGLEIN, Ber. Bunsenges. Physik. Chem., 70 (1966) 862.

PHOTO-POLAROGRAPHIE

XXIII. MITT.* ÜBER DIE URSACHEN VON PHOTO-RESTSTRÖMEN

H. BERG

Deutsche Akademie der Wissenschaften zu Berlin (D.D.R.)

P. REISSMANN

Institut für Mikrobiologie und experimentelle Therapie, Abteilung Biophysikochemie, Jena (D.D.R.)

(Eingegangen am 12. April 1969; revidiert am 19. August 1969)

In unserer Übersichtsarbeit zur Photo-Polarographie[1] wurde abschliessend darauf hingewiesen, dass sich aus elektrochemischen Daten unter Lichteinwirkung "neue Konsequenzen vor allem für die Elektrodenkinetik ergeben werden". Inzwischen wurde diese Voraussage bestätigt durch neuere Arbeiten aus den photoelektrochemischen Laboratorien von Delahay[2], Frumkin[3,4], de Levie[5] und Perone[6]. Mit Ausnahme der letzten Gruppe hat man sich auf das Teilgebiet der nichtabsorbierenden Lösungen konzentriert und die Potential-, Frequenz- und Ionenabhängigkeit des Photostromes studiert, wobei Scavenger (N_2O, H_3O^+) zwecks Verbesserung der Messempfindlichkeit absichtlich zugesetzt wurden. In unserer Terminologie der Photo-Polarographie sprechen wir bei nichtabsorbierenden Lösungen von einem Photo-Reststrom $i_v = i_e + i_{cv} + i_s$, der sich aus einem Photoemissionsstrom i_e, einem Kapazitätsstromanteil i_{cv} und einem Scavenger-Strom i_s zusammensetzt; letzterer wird bei gereinigten Grundlösungen hauptsächlich durch unvermeidbare Spuren von O_2, H_3O^+ verursacht. Unsere Untersuchungen hierüber zielten darauf ab, zwischen den seit 1963 bestehenden drei ursprünglichen Hypothesen von Barker[7], Berg[8] und Heyrovský[9] über die Ursachen von Photo-Restströmen entscheiden zu helfen.

Ihre Hauptunterschiede bestehen darin:

(*a*) Barker und Berg nehmen gegenüber Heyrovský eine Elektronenemission bei geeigneter Wellenlänge und Elektrodenpotential an. Danach solvatisiert das Elektron (Barker) oder kann damit konkurrierend direkt als e^- mit nichtabsorbierenden Photo-Depolarisatoren bzw. Scavengern (z.B. H_3O^+) reagieren (Berg, vgl. Reaktionsschema S. 432).

(*b*) Heyrovský nimmt langwelligere Absorption von Grenzflächen-CT-Komplexen an, um das Auftreten anodischer Photo-Oxidationsströme zu erklären, während Berg zusätzlich die Photodesorption bei anderen Substanzen nach Energieaufnahme der Elektrodenoberfläche postuliert. Allgemein führen Belichtungsstörungen der Doppelschicht auch zu Kapazitätsstromänderungen[1] (Berg).

Anhand eigener Messungen und obengenannter neuer Ergebnisse soll nun der heutige Stand unter Berücksichtigung der neuesten Ergebnisse von De Levie

---

* XXI. Mitt. s. ref. 18. XXII. Mitt. s. ref. 19.

charakterisiert werden. Gemäss unserer Konzeption der "heissen Elektrode" unter Belichtung versuchten wir, Änderungen ihrer Eigenschaften wie Oberflächenspannung (Tropfzeit) und Kapazitätsstrom nachzuweisen.

EXPERIMENTELLES

Eine mittels Filterflüssigkeit (30% Essigsäure) temperierbare Quarzzelle mit Normalkalomelelektrode (NCE), umgeben von ringförmigem monochromatischem Quecksilberniederdruckbrenner[10] oder von U-förmigem polychromatischem Quecksilberhochdruckbrenner, wurde möglichst erschütterungsfrei aufgestellt. Der Quecksilberfaden in der Tropfkapillare wurde durch Aluminiumbedampfung der Glaswandung gegen Belichtung geschützt. Das Quecksilbervorratsgefäss war temperierbar. Der ebenfalls temperierbare Quecksilberniederdruckbrenner emittiert mit der Intensität von 6.7×10^{-6} Einstein cm^{-2}min^{-1} fast nur $\lambda = 254$ nm $\cong 5$ eV in Dauerbelichtung, was zu 40% absorbiert wird. Die Entlüftung der Grundlösungen (0.1 M K$_2$SO$_4$) erfolgte mittels Argon. Isopropanol wurde über Natrium destilliert.

Zur Registrierung dienten:

für die Tropfzeit: Digitalvoltmeter mit Impulsverstärker als Eigenbaugerät, sowie das Zählgerät nach Nygard[11] im Vorversuch, jedoch ohne Temperaturkonstanz des Tropfquecksilbers;

für die Stromzeitkurven: modifiziertes Gerät mit Styloschleifen ($S = 3.9 \times 10^{-8}$ A mm^{-1}) nach Hans[12];

für die Breyer-Wechselstrompolarogramme: Wechselstrompolarograph GWP 563 (78 Hz, 20 mV Wechselspannung) der Akademiewerkstätten (Berlin).

ERGEBNISSE

Die Versuche basierten auf:

1. Nachweis von Oberflächenspannungsänderungen am belichteten Quecksilbertropfen.

2. Nachweis von Kapazitätsstromänderungen bei Photodesorption. Bisher dienten als Indikationen: Tropfzeitmessungen für (1); Stromzeitkurven für (2).

1. *Zur Beeinflussung der Tropfzeit durch Belichtung*

Obwohl im Vorversuch durch Tropfzeitbestimmung mit dem Zählgerät nach Nygard zunächst eine Verkürzung um 0.01 s bei -0.6 V infolge Belichtung von 1×10^{-3} M Natriumlaurylsulfonat in 0.1 M Na$_2$SO$_4$-Lösung angezeigt wurde, stellte sich unter weitgehender Ausschaltung systematischer Fehlerquellen (Temperaturinkonstanz des Tropfquecksilbers) heraus, dass der Belichtungseffekt bei reinen Leitelektrolyten nur innerhalb der Grössenordnung der Ungenauigkeit unserer Eigenbau-Zähleinrichtung von ± 0.004 s liegt. Um den möglichen Einfluss von Temperaturänderungen auf die Tropfzeit modellmässig vergleichen zu können, wurde einmal die gesamte Messzelle auf 35°C erwärmt und dabei das "Tropfquecksilber" vor der Kapillare auf konstanter Temperatur (25°C) gehalten, während im zweiten Fall umgekehrt verfahren wurde, so dass nur die Temperatur des "Tropfquecksilbers" um 10°C über der Lösungstemperatur lag. Die resultierende Verkürzung der Tropfzeit zwischen 25°C und 35°C war in beiden Fällen nahezu dieselbe, nämlich 0.004–

0.0037 s/grd trotz jeweils entgegengesetzter Wärmeflüsse durch die Elektroden-grenzfläche. Bei kurzen und mittleren Tropfzeiten (2–4 s) reicht daher die belichtungs-abhängige Erwärmung des ausfliessenden Quecksilbers am Tropfenhals nicht aus, um seine Ausflussgeschwindigkeit so stark zu erhöhen, dass die Verkürzung der Tropfzeit 0.1% des Dunkelwertes überschreitet.

2. Beeinflussung des Kapazitätsstromes

Unter allen Belichtungsbedingungen[16,17] treten stets Störungen an der Grenzschicht Elektrode/Lösung und damit Kapazitätsstromänderungen auf. Damit sollten auch Adsorptionsgleichgewichte nach Energieabsorption der Elektroden-oberfläche verschoben werden. Am Adsorptionsverhalten von Isopropanol, welches schon in etwa 1 M-Lösung die Quecksilberoberfläche unter Orientierung der OH-Gruppe in Richtung Lösung vollständig bedeckt, lässt sich die Lichtbeeinflussung des Kapazitätsstromes in folgender Weise zeigen. Während bei Potentialen auf dem negativen Ast der Elektrokapillarkurve der bekannte katodische Photoemissions-strom anwächst, fanden wir in ihrem positiven Bereich mittlere anodische Photo-
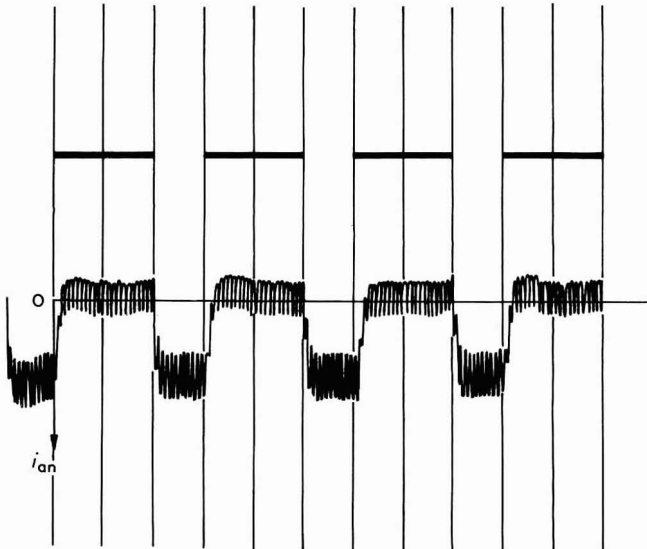
Abb. 1. Anodischer Photo-Reststrom (i_{an}) bei intermittierender polychromatischer Belichtung mit Hg-Brenner U-500. Lösung 0.1 M KCl, 40% Isopropanol, konstantes Potential $\pi = -0.4$ V gegen NCE.

ströme von 10^{-7}–10^{-9} A. In Abb. 1 ist das Ansprechen eines mittleren anodischen Photostromes bei intermittierender Belichtung enthalten. Abbildung 2 bringt eine Gegenüberstellung von Photoströmen ohne und mit hohem Isopropanolgehalt bei drei verschiedenen Leitlösungen. In jedem Fall wird mit Isopropanol der katodische Photo-Reststrom erniedrigt oder in einen anodischen umgewandelt. Über die Ursache dieser der Elektronenemission entgegengerichteten Photo-Restströme gaben Strom-zeit-Kurven des Einzeltropfens bei konstantem Potential Aufschluss. Als Mess-bedingungen wurden gewählt:

Potential 0 V, 0.64 M-Isopropanol in 0.1 M K_2SO_4, entlüftet (d.h. unvoll-
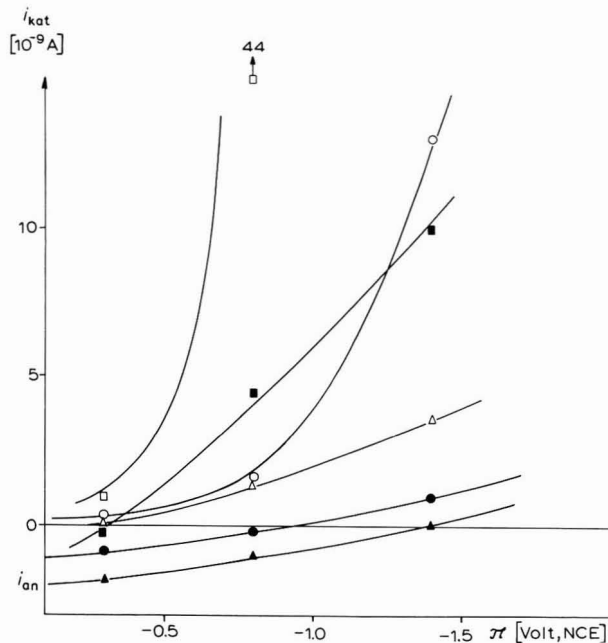
Abb. 2. Einfluss von Isopropanol (40%) auf den Photo-Reststrom i_{kat}, i_{an} in den Grundlösungen: ($\bigcirc$) Phosphatpuffer pH 7, ($\bullet$) +Isopropanol; ($\square$) 0.1 M-H_2SO_4, ($\blacksquare$) +Isopropanol; ($\triangle$) 0.1 M-NaOH, ($\blacktriangle$) +Isopropanol, bei verschiedenen Potentialen π der Tropfelektrode.

ständige Bedeckung der Elektrode), Belichtungswellenlänge 254 nm (d.h. starke Einstrahlung).

Die resultierenden anodischen Kapazitätsstrom–Zeitkurven (i_c = const. $t^{-\alpha}$) behielten unter Belichtung den Exponenten von $\alpha = \frac{1}{3}$ bei und ergaben am Ende der Tropfzeit einen Photodesorptionsstrom von 1.2×10^{-7} A als Differenz zum Dunkelstrom. Demgegenüber beträgt die Desorptionsstromänderung allein durch Temperaturerhöhung im Dunkeln nur etwa 0.04×10^{-7} A/grd Lösungstemperatur.

DISKUSSION

Da die Genauigkeit unserer Tropfzeitmessung nicht ausreichte, um die Erwärmung der Tropfenoberfläche aus der Tropfzeitverkürzung berechnen zu können, wurde folgende Abschätzung vorgenommen und mit der gemessenen Temperaturabhängigkeit der Tropfzeit verglichen. Mit den Daten unseres Versuches

absorbierte Lichtenergie $I = 0.5 \times 10^{-2}$ cal cm^{-2}s^{-1},
Quecksilberausflussgeschwindigkeit $m_t = 2.86 \times 10^{-3}$g s^{-1},
Tropfzeit $\tau = 3.227$ s
Absorptionsvermögen bei 254 nm = 0.4
spezifische Wärme $c_{Hg} = 0.03325$ cal g^{-1} grd^{-1}

ergibt sich unter der Annahme einer gleichmässigen Aufheizung des Tropfens eine Temperaturerhöhung gegen Ende von τ zu $\Delta T = 1.2$ grd, wenn die Wärmeableitung[13] unberücksichtigt bleibt. Damit würde aus dem gemessenen Temperaturkoeffizienten

der Tropfzeit von -0.004 s pro grd eine maximale Tropfzeitverkürzung von 0.0048 s resultieren. Andererseits entspräche obiger Temperaturerhöhung eine Verminderung des Bedeckungsgrades von Isopropanol um etwa 2%. In Wirklichkeit jedoch dürfte schliesslich gegen Ende der Tropfzeit eine so beträchtliche Temperaturdifferenz zwischen Oberfläche und Tropfinnerem herrschen, wie aus obigem Vergleich von Photodesorptionsstrom und Temperaturdesorptionsstrom hervorgeht, dass ihr unmittelbarer Einfluss auf die Desorption z.B. von Isopropanol gegenüber einer Verkürzung der Tropfzeit stärker ist. Hinzu kommt eine Anregung der Elektronen im Metall, wodurch die Adsorptionskräfte ebenfalls verändert werden. Beide Licht-effekte: Elektronenanregung und Aufheizung der Grenzfläche modifizieren den Aufbau der Doppelschicht und damit das ψ_1-Potential[14] nach Frumkin, sowie die Lage von Adsorptionsgleichgewichten.
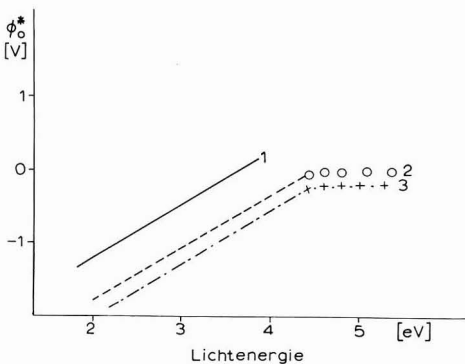
Abb. 3. Diskussionsschema über die qualitative Abhängigkeit des Schwellenpotentials ϕ_0^* für den Elektro-nenaustritt von der eingestrahlten Lichtenergie. (1) mit Scavengerzusatz (Fall C); (2) ohne Scavengerzusatz, im Lichtenergie-Bereich ○○○ ist der Kurvenverlauf noch unbestimmt, vgl. Text (Fall A); (3) ohne Scaven-gerzusatz, jedoch mit Adsorbendum. Im Lichtenergie-Bereich + + + wurde bei Isopropanolzusatz eine Stromumkehr registriert (Fall B).

Nunmehr lässt sich unsere Kenntnis über Photoströme in nichtabsorbierenden Grundlösungen einfacher Elektrolyte unter Verwendung von Quecksilber- oder Amalgamelektroden durch folgendes Diskussionsschema (Abb. 3) charakterisieren, in welchem über der eingestrahlten Lichtenergie Schwellenpotentiale für Photoströme dargestellt sind. Das Schwellenpotential ϕ_0^* gewinnt man aus der experimentell in Gegenwart von Scavengern am besten verifizierbaren Beziehung[4]:

$$i_v = A[hv - hv_0 - e(\phi^* - \psi_1^*)]^{\frac{5}{2}} \tag{1}$$

durch Extrapolation von i_v über $(\phi^* - \psi_1^*)$ nach $i_v \to 0$.

In (1) bedeuten:

A —lichtintensitätsabhängige Konstante

hv —eingestrahlte Lichtenergie

hv_0—Schwellenenergie für $(\phi^* - \psi_1^*) = 0$

ϕ^* —Elektrodenpotential bei Belichtung

ψ_1^*—Frumkin-Potential bei Belichtung.

Die Messungen von De Levie und Kreuser[5] unter Zuhilfenahme von N_2O als

Scavenger, wodurch der Rückfluss solvatisierter Elektronen in die Elektrode verhindert wird, geben in prinzipieller Übereinstimmung mit Pleskov und Rotenberg[4] die Kurve 1. Unsere früheren Untersuchungen[15,16] mit 1 M-H_3O^+ als Scavenger lassen im Vergleich zu neutralen Elektrolytlösungen (10^{-7} M-H_3O^+) abschätzen, dass letzteres Schwellenpotential ohne zugesetzten Scavenger beträchtlich negativer liegt und ein mittlerer Elektronen-Emissionsstrom nach positiveren Potentialen nicht mehr messbar ist ($\bigcirc\bigcirc\bigcirc$, Kurve 2). Schliesslich bewirkt ein Zusatz adsorbierbarer organischer Substanzen—wiederum ohne Scavenger—eine weitere Negativierung der Kurvenlage und sogar die von uns gemessene Umkehr der Stromrichtung ($+++$, Kurve 3) infolge Überkompensation der Elektronenemission durch kapazitative Photodesorption.

Die von Heyrovský aufgefundene (Faradaysche) Stromumkehr bei bestimmten organischen Substanzen möchten wir hingegen als eine photosensibilisierte Elektrooxydation unter die Gruppe der Photo-Durchtrittsreaktionen mit (adsorbierten) Photo-Depolarisatoren einreihen[1].

Wenn z.Z. auch noch zu wenig experimentelles Material zu obigem Schema vorliegt, zeichnet sich dennoch folgendes ab:

(A) Der Photo-Reststrom (nach unserer Definition[1]) in reiner neutraler wässriger (oder nichtwässriger) Elektrolytlösung ohne Scavenger-Zusatz beruht auf den unbeeinflussten Reaktionen:
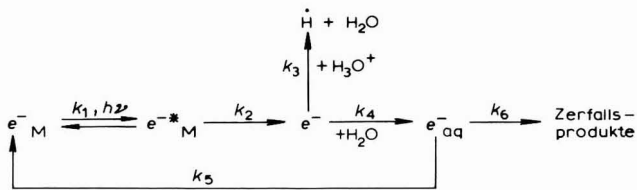
Der ϕ_0^*–hv-Verlauf (entsprechend Kurve 2) wurde noch nicht genau bestimmt. Bei positiven Elektrodenpotentialen ist zu erwarten, dass die erzwungene Emission durch hohe Lichtenergie direkt nicht registriert werden kann, weil Elektronen wieder in die Elektrode zurückkehren ($k_5 > k_6$; die dem k_2 entsprechende Rückreaktion ist zu vernachlässigen[17]).

(B) Für den Photo-Reststrom mit Zusatz von Adsorbendum zur Lösung von (A) überlagert sich ein verstärkter Photodesorptionseffekt, der an der positiven "heissen" Elektrodenoberfläche einen anodischen kapazitativen Photo-Reststrom i_{cv} hervorruft (im Lichtenergiebereich $+++$ der Kurve 3).

(C) Für den Photostrom mit Zusatz von Scavenger wird die Rück-Durchtrittsreaktion k_5 weitgehend eliminiert und damit kann selbst bei positiven Elektrodenpotentialen noch eine Elektronenemission gemessen und nach Gl. (1) berechnet (Gerade 1) werden.

Aus dieser Differenzierung folgt, dass der Versuch von de Levie[5], unsere Desorptionshypothese für die heisse Elektrode durch Nachweis von Kapazitätsströmen zu prüfen, unter solchen Bedingungen fehlschlagen musste, wo der Elektronenemissionsstrom überwiegt. Aussicht auf Erfolg für Kapazitätsstromnachweise besteht nur im Falle (B), d.h.

1. positive Ladung der Elektrodenoberfläche,

2. intensive Belichtung mit $\lambda < 300$ nm,

3. Besetzung der Quecksilberelektrode durch nichtabsorbierendes Adsorbendum, oder aber unter den Bedingungen von Korschunov et al.[17].

Wenn kein Scavenger anwesend ist, ist die Rückkehr von emittierten Elektronen in die Elektrode leichter möglich (Fall A). Aus diesem Grund ist noch zu prüfen, ob Gl. (1) auch für Lösungen ohne Scavengerzusatz bei positiven Potentialen Gültigkeit besitzt und ob eine lineare Extrapolation von $i^{0.4}$ noch zulässig ist. Nach unseren Vorstellungen[1] sollte die logarithmische Abhängigkeit von i_v über $(\phi^* - \psi_1^*)$ in diesem Bereich wieder an Bedeutung gewinnen, was durch höchstempfindliche Strommessungen entschieden werden muss.

DANK

Herrn Dipl.-Phys. E. Stutter danken wir für wertvolle Hinweise. Herr Dr. B. Nygard nahm an den Vorversuchen in Uppsala entscheidenden Anteil.

ZUSAMMENFASSUNG

Um zwischen den ursprünglichen drei Hypothesen über die Ursache des Photo-Reststromes entscheiden zu können, wurden die Konsequenzen der "heissen Elektrode" durch Tropfzeitbestimmungen und Stromzeitkurven geprüft. Während die Änderung der Tropfzeit in der Messfehlergrenze lag, zeigten die anodischen Kapazitätsstromkurven den erwarteten Effekt einer Photodesorption infolge "Aufheizung" der Elektrodenoberfläche. Diese Stromumkehr in Abwesenheit von Scavenger hat Konsequenzen für die Beziehung zwischen Photo-Reststrom und Elektrodenpotential, sowie Schwellenpotential und Wellenlänge.

SUMMARY

The consequences of the "hot electrode"-hypothesis concerning the origin of photo-residual current were tested by drop time measurements and current–time curves. Although the very low changes of drop time are in the limits of error of our apparatus the anodic capacity current shows the effect of photo desorption. This inversion of photocurrent without scavengers influences the relations between photo-residual current and electrode potential or threshold potential and wave length.

Added in proof. G. Bomchil, J. d'Alessio, D. Schiffrin (Buenos Aires) were able to follow the return of hydrated electrons to the electrode by submicrosecond light pulses (Preprint 20, CITCE, Strasbourg, 1969, p. 106).

LITERATUR

1 H. Berg, H. Schweiss, E. Stutter und K. Weller, J. Electroanal. Chem., 15 (1967) 415.
2 V. Sharma, P. Delahay, G. Susbielles und G. Tessari, J. Electroanal. Chem., 16 (1968) 285.
3 Yu. Gurevich, A. Brodsky und B. Levich, Elektrokhimiya, 3 (1967) 1302.
4 Yu. Pleskov und Z. Rotenberg, J. Electroanal. Chem., 20 (1969) 1.
5 R. de Levie und J. Kreuser, 21 (1969) 221.
6 S. Perone und J. Birk, Anal. Chem., 38 (1966) 1589.

7 G. BARKER, A. GARDNER UND D. SAMMON, *J. Electrochem. Soc.*, 113 (1966) 1182.

8 H. BERG, *Electrochim. Acta*, 13 (1968) 1249.

9 M. HEYROVSKÝ, *Proc. Roy. Soc. London, Ser. A*, 301 (1967) 411.

10 L. KITTLER UND H. SCHWEISS, *Photochem. Photobiol.*, 5 (1966) 771.

11 B. NYGARD, E. JOHANSSON UND J. OLOFSON, *J. Electroanal. Chem.*, 12 (1966) 564.

12 W. HANS, W. HENNE UND E. MEURER, *Z. Elektrochem.*, 58 (1954) 836.

13 E. STUTTER, Privatmitteilung.

14 A. FRUMKIN, V. BAGOTSKY, Z. JOFA UND B. KABANOV, *Kinetika Elektrodynkh Prozessov*, Izd. Moskovskogo, Moscow, 1952.

15 H. BERG, 14. CITCE, Moskau, 1963, Preprint.

16 H. BERG UND H. SCHWEISS, *Electrochim. Acta*, 9 (1964) 425.

17 L. KORSCHUNOV, J. ZOLOTOVICKIJ AND V. BENDERSKIJ, *Elektrokhimiya*, 4 (1968) 499.

18 E. STUTTER, *Elektrokhimiya*, 4 (1968) 151.

19 E. STUTTER, *Z. Wiss. Phot. Photophysik Photochem.*, 62 (1968) 47.

A POLAROGRAPHIC STUDY OF THE COPPER–TETREN SYSTEM

D. GATTEGNO, A. M. GIULIANI AND M. R. IMPERATORI

Istituto di Chimica Generale ed Inorganica dell' Università di Roma e Laboratorio di Teoria e Struttura Elettronica e Comportamento Spettrochimico dei Composti di Coordinazione del C.N.R., Università di Roma (Italia)

The polarographic behaviour of complex ions in the presence of a metal excess has recently been dealt with in some detail by several authors[1–8]. Macovschi[1–4] examines, from a theoretical point of view, different cases of complex reduction, all leading to amalgam formation. He works out wave equations applicable in the whole range of ligand concentration, *i.e.* from the pure metal ion solution to large excesses of ligand. In all cases he considers that the metal ion and the complexes give rise to only one wave.

Other authors[5–8], on the other hand, examine the case when the metal ion and the complex are reduced at quite different potentials. They propose wave equations for several mechanisms of electrode reaction, when the complex species in solution are stable and of definite composition.

The proposed wave equations have been applied to elucidate the mechanism of polarographic reduction of metal chelates of aminopolyacetic acids. We thought it would be interesting to check if the explanation given for the shift of $E''_{\frac{1}{2}}$ towards less negative values holds also in the case of a system with a different type of chelating agent. A polyamine seemed well suited for our purposes.

Since the formation of complexes between copper(II) and polyamines, like ethylenediamine and homologues, has been extensively studied, copper(II) was chosen as metal ion. In particular, the complexing ability of tetraethylenepentamine (tetren) towards copper(II) has been investigated by means of several techniques[9–11]. Stable complexes of definite composition are formed between the metal and tetren. We have therefore selected the copper(II)–tetren system for our study, as all fundamental requirements for the applicability of an appropriate wave equation are satisfied and the stability constants of the chelates are known.

EXPERIMENTAL

A. Reagents and instruments

Technical grade tetren obtained from Fluka AG was purified as the penta-hydronitrate following the procedure described by Reilley and Holloway[9]. The analysis of the product gave the following results: Calcd.: C 19%, H 5.6%, N 27.7%; found: C 19.1%, H 5.8%, N 26.6%. All other chemicals were reagent grade and were used without further purification. Copper(II) solutions were standardized against a

0.1 M EDTA solution using aqueous murexide as indicator. Cell, electrodes and buffers have been described in a previous paper[6].

Polarograms were recorded on a Polariter PO4 Radiometer instrument; pH measurements were made with a Beckmann research pH-meter.

The capillary constant was 2.49 $mg^{\frac{2}{3}} sec^{-\frac{1}{2}}$ in the potential range $-0.1/-0.5$ V vs. SCE in all acetate buffers used. All limiting currents have been determined at the maximum of the oscillations. Gelatine, in small concentrations, was added to suppress maxima.

B. Results

In the presence of excess ligand the copper complex is reduced in one irreversible two-electron step. With increase in ligand excess (Fig. 1) the half-wave potential shifts to more negative values.

Polarograms at different pH values in buffered solutions have been recorded for several metal : ligand ratios; the results are plotted in Fig. 2.

When a metal excess is present in the solution two waves appear at pH > 4. For lower pH values the two waves are only slightly, or not at all, separated. The first step is due to the slightly irreversible two-electron reduction of acetato–copper(II)
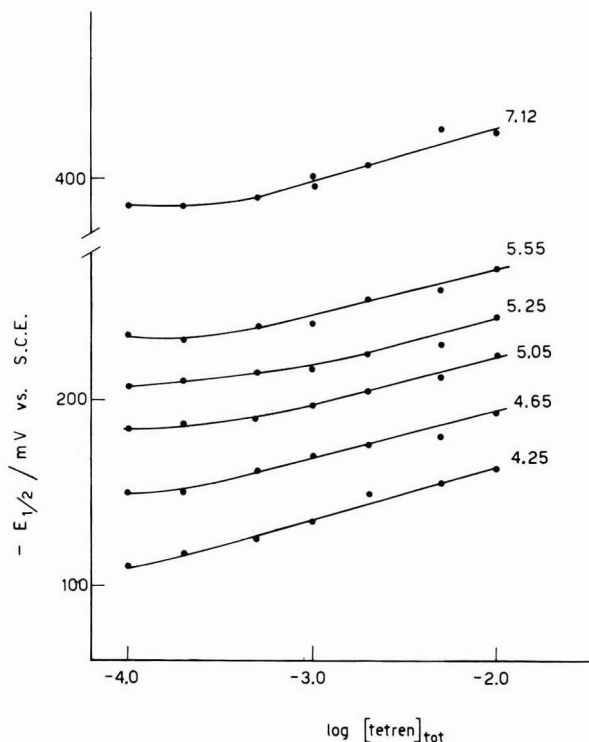
Fig. 1. Dependence of $E_{\frac{1}{2}}$ on the logarithm of the analytical concn. of tetren in presence of ligand excess. $[Cu^{2+}] = 1 \times 10^{-4}$ M, $\mu = 0.5$ with $NaClO_4$, $t = 25.0 \pm 0.1\,^{\circ}C$; acetate buffers; numbers on curves are pH values.
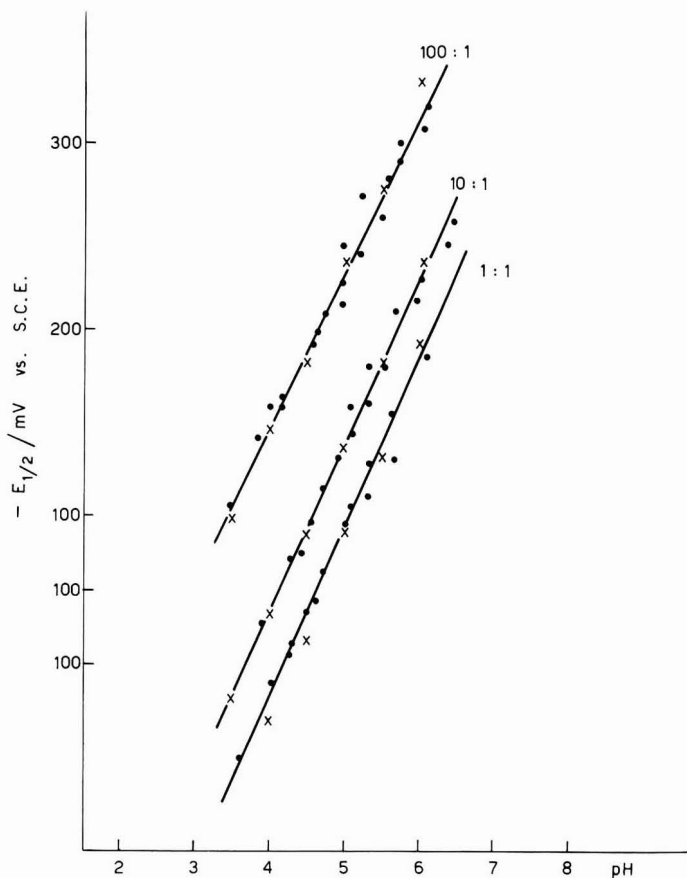
Fig. 2. Dependence of $E_{\frac{1}{2}}$ on pH in presence of ligand excess. $[Cu^{2+}] = 1 \times 10^{-4}$ M, $\mu = 0.5$ with $NaClO_4$, $t = 25.0 \pm 0.1\,°C$; acetate buffers; numbers on plots are ligand : metal ratios. ($\bullet$) Exptl. points, ($\times$) calcd. according to eq. (1).

complex to amalgam. The second wave is due to the irreversible two-electron reduction of the copper–tetren complex.

The diffusion current of the first wave decreases linearly as the ligand : metal ratio increases and becomes zero at a copper/tetren ratio of 1 : 1, while the limiting current of the second wave increases linearly as the ligand/metal ratio varies from 1 : 20 to 1 : 1 and then remains constant. The displacement of $E_{\frac{1}{2}}$ of the second wave as a function of log $[\text{tetren}]_{\text{tot}}$ is shown in Fig. 3 for several pH values.

In Fig. 4 the dependence of the half-wave potential of the complex wave on pH is shown for several copper/tetren ratios.

DISCUSSION AND CONCLUSIONS

The dissociation constants of tetren have been determined by several authors[9–11]; Jonassen et al.[12] report the following values, measured at $25°C$: $pK_1 = 2.65$, $pK_2 = 4.25$, $pK_3 = 7.87$, $pK_4 = 9.08$, $pK_5 = 9.92$.
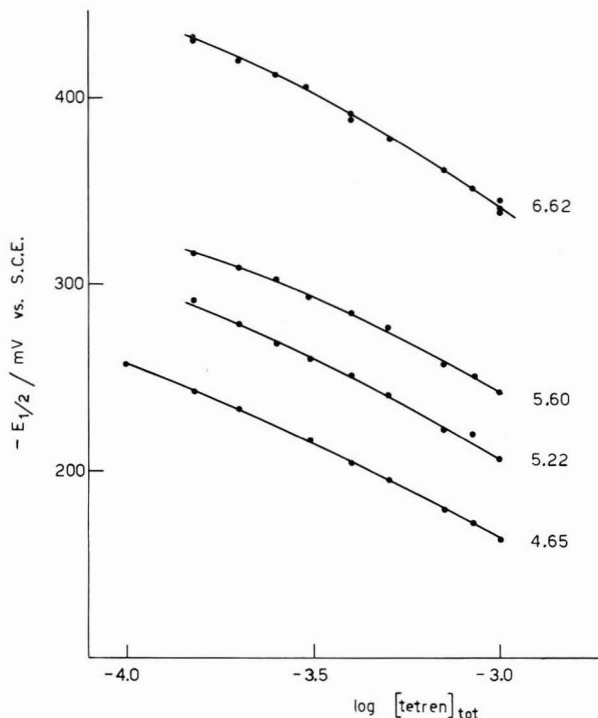
Fig. 3. $E_{\frac{1}{2}}$ as a function of the logarithm of total tetren concn., at different pH values. $[Cu^{2+}] = 1 \times 10^{-3}\ M$. $\mu = 0.5$ with $NaClO_4$, $t = 25.0 \pm 0.1\,°C$; acetate buffers; numbers on curves are pH values.

The distribution curves of the protonated forms of tetren are plotted in Fig. 5. The dissociation constants of copper(II) complexes with tetren

$$\beta_0 = \frac{C_M f_M \cdot C_X f_X}{C_{MX} f_{MX}}, \quad \beta_1 = \frac{C_M f_M \cdot C_{HX} f_{HX}}{C_{MHX} f_{MHX}} \text{ and } \beta_2 = \frac{C_M f_M \cdot C_{H_2X} f_{H_2X}}{C_{MH_2X} f_{MH_2X}}$$

have been determined by different authors. Jonassen and coworkers[13] give log β_0 $= -24.25$ at 25°C in 0.1 M NaCl, determined polarographically. Paoletti and Vacca[10] give the following values determined potentiometrically at 25°C in 0.1 M KCl: $\beta_0 = 10^{-22.8}$, $\beta_1 = 10^{-18.3}$ and $\beta_2 = 10^{-13}$.

From our polarographic data of wave height in the presence of a metal excess it is evident that a 1:1 complex is formed quantitatively between copper(II) and tetren even at pH *ca.* 4. For lower pH values nothing can be deduced from the polarographic data owing to the poor separation of the two waves. Nevertheless it is evident from potentiometric titrations that complex formation is virtually complete even at pH *ca.* 3, at least for $\mu = 0.1$.

In the Appendix a wave equation has been deduced for our system which is applicable for ligand:metal ratios $\geq 1:1$.

When a large excess (tenfold or more) of ligand is present in solution, the wave equation takes the form (eqn. (xxii) in the Appendix):

$$E'' = E_{\frac{1}{2}}^{M} - \frac{RT}{\alpha n_{M} F} \ln \frac{i''}{i_{d}'' - i''} - \frac{RT}{\alpha n_{M} F} \ln \frac{\sum\limits_{n} (C_{H} f_{H})^{n}/\alpha_{n} \beta_{n}}{\sum\limits_{p} R_{p}} +$$

$$- \frac{RT}{\alpha n_{M} F} \ln C_{X}^{\text{tot}} - \frac{RT}{\alpha n_{M} F} \ln \frac{h_{C} f_{M} f_{X}}{f_{C} h_{M}} \tag{1}$$

A log-plot according to eqn. (1) gives a value $\alpha = 0.78 \pm 0.04$ for the transfer coefficient.

When the metal ion and the ligand are in the stoichiometric ratio, the wave equation becomes (eqn. (xxv) in the Appendix):

$$E'' = E_{\frac{1}{2}}^{M} - \frac{RT}{\alpha n_{M} F} \ln \frac{i''^{2}}{i_{d}'' - i''} - \frac{RT}{\alpha n_{M} F} \ln \frac{\sum\limits_{n} (C_{H} f_{H})^{n}/\alpha_{n} \beta_{n}}{\sum\limits_{p} R_{p}} +$$

$$- \frac{RT}{\alpha n_{M} F} \ln \frac{h_{C} f_{M} f_{X}}{f_{C} h_{L} k_{M}} \tag{2}$$

Using eqn. (2) to evaluate α from plots of E'' vs. $\log [i^{2}/(i_{d} - i)]$, we obtain values of the transfer coefficient changing from 0.6 to 0.7 as the Cu(II) concentration is varied from $5 \cdot 10^{-5}$ M to $1 \cdot 10^{-3}$ M.

Although α is generally found to be constant at different concentrations of the electroactive species, thus making possible the evaluation of the kinetic parameters of the reaction, there is no theoretical justification for this[14]. In our case it is obviously necessary to admit a non-constant value of α.

When a metal excess is present in solution, eqn. (2) has to be modified to take into account the difference in the amalgam concentration due to the free copper ion reduction. The wave equation becomes therefore

$$E'' = E_{\frac{1}{2}}^{M} - \frac{RT}{\alpha n_{M} F} \ln \frac{i''(i'' + i_{d}')}{i_{d}'' - i''} - \frac{RT}{\alpha n_{M} F} \ln \frac{\sum\limits_{n} \frac{(C_{H} f_{H})^{n}}{\alpha_{n} \beta_{n}}}{\sum\limits_{p} R_{p}} +$$

$$- \frac{RT}{\alpha n_{M} F} \ln \frac{h_{C} f_{M} f_{X}}{f_{C} h_{L} k_{M}} \tag{3}$$

The expression for the half-wave potential is:

$$E_{\frac{1}{2}}'' = E_{\frac{1}{2}}^{M} - \frac{0.054}{\alpha n_{M}} \log (i_{d/2}'' + i_{d}') +$$

$$- \frac{0.059}{\alpha n_{M}} \log \frac{\sum\limits_{n} \frac{(C_{H} f_{H})^{n}}{\alpha_{n} \beta_{n}}}{\sum\limits_{p} R_{p}} \tag{4}$$

It is virtually impossible to calculate the theoretical shift of $E_{\frac{1}{2}}$ with tetren concentration from eqn. (4) and to compare it with the experimental data (Fig. 3), because, as has been shown before, α is not constant through a series of measurements. Never-
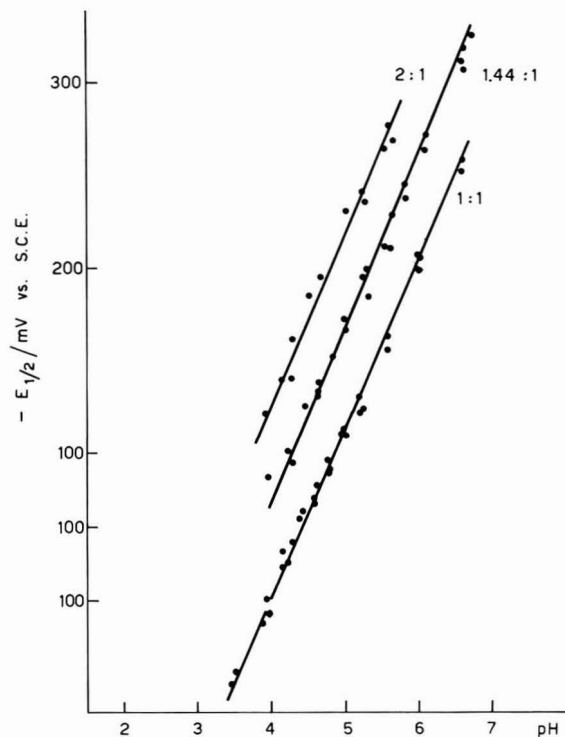
Fig. 4. $E_{\frac{1}{2}}$ as a function of pH, for different metal : ligand ratios. $[Cu^{2+}] = 1 \times 10^{-3}$ M, $\mu = 0.5$ with NaClO$_4$, $t = 25.0 \pm 0.1$ °C; acetate buffers; numbers on curves are metal : ligand ratios.
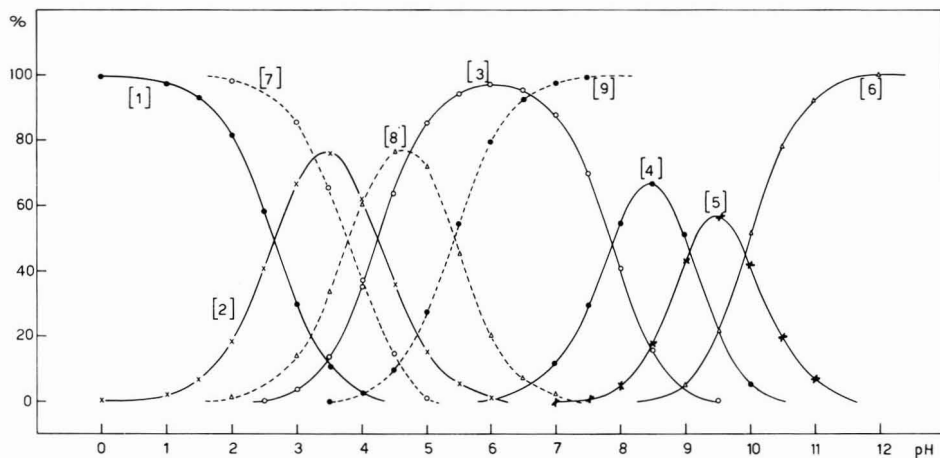
Fig. 5. Distribution curves of tetren and copper(II)–tetren complexes. [1] H$_5$tetren^{5+}, [2] H$_4$tetren^{4+}, [3] H$_3$tetren^{3+}, [4] H$_2$tetren^{2+}, [5] H tetren$^+$, [6] tetren, [7] CuH$_2$ tetren^{4+}, [8] CuH tetren^{3+}, [9] Cu-tetren^{2+}.

theless, a careful examination of the plots of Fig. 3 prompts the following considera-tion. The shift of $E_{\frac{1}{2}}$ with tetren concentration, at constant pH, calculated according to eqn. (4), using an average α value of 0.65 is much smaller (*ca.* 15 mV) than the experi-mental value (90–100 mV).

Such a large experimental shift towards less negative values as the ligand concentration increases, may be justified only if the electrode process is partly, if not completely, independent of the ligand concentration. Indeed, if a rapid dissociation of ligand precedes the electron transfer, the term i'', which causes a shift of $E_{\frac{1}{2}}$ towards more negative values as the ligand concentration increases, disappears from eqn. (4).

On the other hand, the hypothesis of a partial dissociation of the complex prior to the electrode reaction when the ligand excess is very low, might be an ex-planation for the difference in the α values found at high concentrations of the com-plexing agent and at the stoichiometric copper/tetren ratio, and also for the shape of the plots in Fig. 1.

Another point to be considered is the dependence of $E_{\frac{1}{2}}$ on pH. $E_{\frac{1}{2}}$ is not a linear function of pH and the average number of protons involved in the electrode process cannot be simply evaluated. The theoretical shift of $E_{\frac{1}{2}}$ with pH may be calculated by means of the wave equations already discussed and then compared with the experi-mental plots of Fig. 2. The shifts have been calculated for metal : ligand ratios of $1:100$ ($\alpha=0.80$), $1:10$ ($\alpha=0.77$) and $1:1$ ($\alpha=0.70$) and the values obtained are plotted in Fig. 2 to fit the experimental curves. The agreement is fairly good. The calcula-tions have not been performed for lower ligand : metal ratios, because of the dissocia-tion process which we have supposed to take place before the reduction and which would change the form of the wave equation.

In view of the preceding discussion a tentative scheme may be proposed for the electrode process. In the presence of a large excess of ligand, the overall reaction may be written as :

$$CuH_nX^{(n+2)+} + (p-n)H^+ + 2e + Hg \rightarrow Cu(Hg) + H_pX^{p+} \tag{a}$$
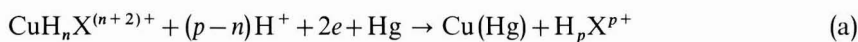
when n takes the values 0, 1 and 2, and, for each n, p takes all the values between 0 and 5. When the ligand excess is low, or the metal is in excess, the following reactions may take place together with (a):

$$CuH_nX^{(n+2)+} + (p-n)H^+ \rightarrow Cu^{2+} + H_pX^{p+} \qquad n=0, 1, 2; \ p=0, \ldots, 5 \tag{b}$$
$$\downarrow {\scriptstyle +2e+Hg}$$
$$Cu(Hg)$$
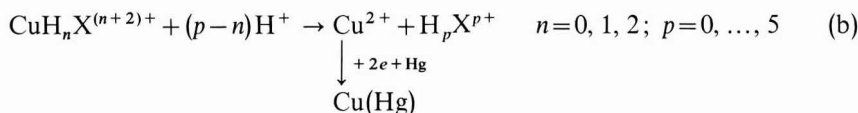
Our results do not agree with the conclusions of Jonassen and coworkers[13], mainly on one point. They consider a reversible electrode process, while at the same metal : ligand ratio we observe an irreversible reduction with an α value of 0.77.

In conclusion the wave equations based on the reduction mechanism proposed are a fairly satisfactory fit for the experimental results.

It has been impossible to carry out theoretical calculations, based on eqn. (4), to evaluate quantitatively the shift of $E_{\frac{1}{2}}''$ with ligand concentration. Nevertheless, the usefulness of measurements in the presence of a metal excess to reveal fast chemical reactions, preceding the electron transfer, has once more been demonstrated.

SUMMARY

   The polarographic behaviour of the copper(II)–tetren system has been thoroughly investigated in a variety of experimental conditions. The effects of pH, concentration of electroactive species and ligand : metal ratio have been studied both in the presence of metal ion excess and of ligand excess. The transfer coefficient has been found to change with the concentration of electroactive species. A wave equation has been deduced following the scheme proposed by Macovschi. A tentative scheme is presented for the mechanism of the electrode process.

APPENDIX

   To derive our wave equation we will follow the scheme proposed by Macovschi. The notations of this author will be used and, for simplicity, the charge of the ions will be omitted.

   We will consider the case of a hydrolysable ligand forming a series of differently protonated 1 : 1 complexes with a metal ion. We assume that the metal ion is reduced to amalgam and that the solution is well buffered.

   Also, we examine the case of metal ions and complexes reduced at different potentials. The dissociation constants of the complexes and of the ligand, which are the same at the electrode surface and in the bulk solution, are respectively:

$$\beta_n = \frac{C_M f_M C_{H_n X} f_{H_n X}}{C_{MH_n X} f_{MH_n X}} = \frac{C_M^0 f_M C_{H_n X}^0 f_{H_n X}}{C_{MH_n X}^0 f_{MH_n X}} \quad n = 0, 1, 2 \tag{i}$$

$$\alpha_p = \frac{C_X f_X (C_H f_H)^p}{C_{H_p X} f_{H_p X}} = \frac{C_X^0 f_X (C_H^0 f_H)^p}{C_{H_p X}^0 f_{H_p X}} \qquad p = 0, 1, ..., 5 \tag{ii}$$

We assume an electrode reduction of the following type:

$$MH_n X + (p-n)H + 2e \rightarrow M(Hg) + H_p X \qquad n = 0, 1, 2 \tag{iii}$$
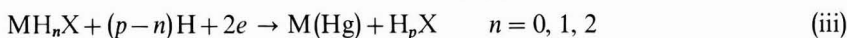
which may be formally written as:

$$MH_n X + (p-n)H \rightleftarrows M + H_p X$$
$$M + 2e + Hg \rightarrow M(Hg) \tag{iv}$$

For the dissociation equilibrium, the constant is:

$$\gamma_p^n = \frac{C_M f_M C_{H_p X} f_{H_p X}}{C_{MH_n X} f_{MH_n X} (C_H f_H)^{p-n}} = \frac{C_M^0 f_M C_{H_p X}^0 f_{H_p X}}{C_{MH_n X}^0 f_{MH_n X} (C_H^0 f_H)^{p-n}} \tag{v}$$

For each value of n, p may assume all values from 0 to 5; therefore the total concentration of $MH_n X$ is given by the summation:

$$(C_{MH_n X}^0)^{tot} = \sum_{p=0}^{5} \frac{C_M^0 f_M C_{H_p X}^0 f_{H_p X}}{(C_H^0 f_H)^{p-n} f_{MH_n X} \gamma_p^n} \tag{vi}$$

The complexes with different n values exist simultaneously in solution, in different ratios depending on the pH. They are all reduced at the electrode at the same potential.

   The reduction process leads to concentration variations at the electrode; therefore

$$\begin{cases} C^0_{MH_nX} = C_{MH_nX} - \Delta C_{MH_nX} \\ C^0_{H_pX} = C_{H_pX} + \Delta C_{H_pX} \end{cases} \tag{vii}$$

The current inside the mercury drop is given by:

$$i = n_M F j_{am} = n_M F h_{am} C^0_{am} \tag{viii}$$

The total current passing through the solution is:

$$i = \sum_{n=0}^{2} i_{MH_nX} = n_M F \sum_{n=0}^{2} j_{MH_nX} = n_M F \sum_{n=0}^{2} (C_{MH_nX} - C^0_{MH_nX}) \tag{ix}$$

In quasi-stationary conditions the following relations hold for the mass-currents:

$$\begin{cases} j_{am} = \sum_n j_{MH_nX} & \text{(i.e. all the metal ions reduced at the mercury surface} \\ & \text{diffuse toward the center of the drop)} \\ \sum_n j_{MH_nX} = \sum_p j_{H_pX} & \text{(i.e. all the ligand carried at the DME surface as complex is} \\ & \text{carried back into the bulk solution as more or less pro-} \\ & \text{tonated ligand)} \end{cases} \tag{x}$$

The protons involved in the electrode process do not change the hydrogen concentration, as the medium is well buffered (i.e. $C_H = C^0_H$).

The equation for the electrode potential (supposing an irreversible process) is:

$$E = E_0 - \frac{RT}{\alpha n_M F} \ln \frac{C^0_{am} f_{am}}{C^0_M f_M} \tag{xi}$$

Introducing the expression for $E_{\frac{1}{2}}$ of the simple metal ion gives:

$$E = E^M_{\frac{1}{2}} - \frac{RT}{\alpha n_M F} \ln \frac{i}{k_M C^0_M} \tag{xii}$$

where

$$E^M_{\frac{1}{2}} = E_0 - \frac{RT}{\alpha n_M F} \ln \frac{f_{am} k_M}{k_{am} f_M}$$

From eqns. (ix) and (vi) we obtain:

$$i = i_d - n_M F \sum_{n=0}^{2} h_{MH_nX} C^0_M f_M \sum_{p=0}^{5} \frac{C^0_{H_pX} f_{H_pX}}{(C^0_H f_H)^{p-n} f_{MH_nX} \gamma^n_p} \tag{xiii}$$

Keeping in mind eqns. (i), (ii) and (vii), and using the notation $kC^0_M = y$ the following equation results:

$$i = i_d - n_M F \sum_n \frac{h_{MH_nX}}{f_{MH_nX}} \frac{f_M}{k_M} f_X y \frac{(C_H f_H)^n}{\alpha_n \beta_n} [C_X + \Delta C_X] \tag{xiv}$$

From eqn. (x):

$$j_{am} = \frac{i}{n_M F} = \sum_n j_{MH_nX} = \sum_p j_{H_pX} = \sum_p h_{H_pX} \Delta C_{H_pX} \tag{xv}$$

Introducing (vii) into eqn. (ii):

$$\alpha_p = \frac{\Delta C_X f_X (C_H f_H)^p}{\Delta C_{H_pX} f_{H_pX}} \tag{xvi}$$

Substitution in eqn. (xv) gives:

$$\Delta C_X = \frac{i}{n_M F \sum_p h_{H_p X} R_p} \quad \left(\text{with } R_p = \frac{f_X}{f_{H_p X}} \frac{(C_H f_H)^p}{\alpha_p}\right) \tag{xvii}$$

On the other hand, we have:

$$C_X^{tot} = \sum_n C_{MH_n X} + \sum_p C_{H_p X} \tag{xviii}$$

We are dealing with very stable complexes and ligand: metal ratios higher than or equal to the stoichiometric one, therefore

$$C_X^{tot} = C_M^{tot} + \sum_p \frac{C_X f_X (C_H f_H)^p}{f_{H_p X} \alpha_p} \tag{xix}$$

and one obtains for C_X:

$$C_X = \frac{C_X^{tot} - C_M^{tot}}{\sum_p R_p} \tag{xx}$$

Introducing (xx) and (xvii) in (xiv):

$$\Phi(y) = n_M F \sum_n \frac{h_{MH_n X}}{f_{MH_n X}} \frac{f_M}{k_M} f_X y \frac{(C_H f_H)^n}{\alpha_n \beta_n} \times$$

$$\left[\frac{C_X^{tot} - C_M^{tot}}{\sum_p R_p} + \frac{i}{n_M F \sum_p h_{H_p X} R_p}\right] + i - i_d = 0 \tag{xxi}$$

The solution φ of eqn. (xxi) introduced into (xii) furnishes the desired wave equation. Let us find the solution of (xxi) in special cases.

A. *The ligand is in great excess* (*Lingane type approximation*)

$$C_X^{tot} \gg C_M^{tot}; \quad C_X^{tot} \gg \frac{i}{n_M F}$$

$$\varphi = \frac{(i_d - i) \sum_p R_p}{n_M F \sum_n \frac{h_{MH_n X}}{f_{MH_n X}} \frac{f_M}{k_M} f_X \frac{(C_H f_H)^n}{\alpha_n \beta_n} C_X^{tot}}$$

The wave equation takes the form:

$$E = E_{\frac{1}{2}}^M - \frac{RT}{\alpha n_M F} \ln \frac{i}{i_d - i} - \frac{RT}{\alpha n_M F} \ln C_X^{tot} +$$

$$- \frac{RT}{\alpha n_M F} \ln \frac{\sum_n (C_H f_H)^n / \alpha_n \beta_n}{\sum_p R_p} - \frac{RT}{\alpha n_M F} \ln \frac{f_M f_X h_C}{f_C k_M} \tag{xxii}$$

where we have supposed

$$\begin{cases} h_{MX} \simeq h_{MHX} \simeq h_{MH_2X} = h_C \\ f_{MX} \simeq f_{MHX} \simeq f_{MH_2X} = f_C \end{cases} \tag{xxiii}$$

For the half-wave potential we obtain the expression:

$$E''_{\frac{1}{2}} = E^M_{\frac{1}{2}} - \frac{RT}{\alpha n_M F} \ln C^{tot}_X - \frac{RT}{\alpha n_M F} \ln \frac{\sum_n (C_H f_H)^n / \alpha_n \beta_n}{\sum_p R_p} +$$

$$- \frac{RT}{\alpha n_M F} \ln \frac{f_M h_C f_X}{h_M f_C} \tag{xxiv}$$

B. The ligand is in the stoichiometric amount for a 1 : 1 *complex formation*

$$C^{tot}_X = C^{tot}_M$$

$$\varphi = \frac{(i''_d - i'') \sum_p h_{H_pX} R_p}{i'' \sum_n \frac{h_{MH_nX}}{f_{MH_nX}} \frac{f_M}{k_M} f_X \frac{(C_H f_H)^n}{\alpha_n \beta_n}}$$

Considering eqn. (xxiii) and putting $h_X \simeq h_{HX} \simeq \ldots = h_L$ we get the equation:

$$E'' = E^M_{\frac{1}{2}} - \frac{RT}{\alpha n_M F} \ln \frac{i''^2}{i''_d - i''} - \frac{RT}{\alpha n_M F} \ln \frac{\sum_n (C_H f_H)^n / \alpha_n \beta_n}{\sum_p R_p} +$$

$$- \frac{RT}{\alpha n_M F} \ln \frac{h_C f_M f_X}{h_L f_C k_M} \tag{xxv}$$

For $E''_{\frac{1}{2}}$ we have

$$E''_{\frac{1}{2}} = E^M_{\frac{1}{2}} - \frac{RT}{\alpha n_M F} \ln i''_d / 2 - \frac{RT}{\alpha n_M F} \ln \frac{\sum_n (C_H f_H)^n / \alpha_n \beta_n}{\sum_p R_p} +$$

$$- \frac{RT}{\alpha n_M F} \ln \frac{h_C f_M f_X}{h_L f_C k_M} \tag{xxvi}$$

REFERENCES

1 M. E. MACOVSCHI, *J. Electroanal. Chem.*, 16 (1968) 457.
2 M. E. MACOVSCHI, *J. Electroanal. Chem.*, 18 (1968) 47.
3 M. E. MACOVSCHI, *J. Electroanal. Chem.*, 19 (1968) 219.
4 M. E. MACOVSCHI, *J. Electroanal. Chem.*, 20 (1969) 393.
5 A. M. GIULIANI, D. GATTEGNO AND A. FURLANI, *Gazz. Chim. Ital.*, 97 (1967) 1076.
6 A. FURLANI, D. GATTEGNO AND A. M. GIULIANI, *J. Electroanal. Chem.*, 15 (1967) 381.
7 A. M. GIULIANI, D. GATTEGNO AND A. FURLANI, *J. Electroanal. Chem.*, 18 (1968) 151.
8 D. GATTEGNO AND A. M. GIULIANI, *Electrochim. Acta*, in press.
9 C. N. REILLEY AND J. H. HOLLOWAY, *J. Am. Chem. Soc.*, 80 (1958) 2917.

10 P. PAOLETTI AND A. VACCA, *J. Chem. Soc.*, (1964) 5051.
11 H. B. JONASSEN AND L. WESTERMANN, *J. Am. Chem. Soc.*, 79 (1957) 4275.
12 H. B. JONASSEN, F. W. FREY AND A. SCHAAFSMA, *J. Phys. Chem.*, 61 (1957) 504.
13 H. B. JONASSEN, J. AARON BERTRAND, F. R. GROVES AND R. I. STEARNS, *J. Am. Chem. Soc.*, 79 (1957) 4279.
14 H. GERISCHER, *Z. Physik. Chem. Frankfurt*, 26 (1960) 223, 325.

DIE ANWENDUNG VON KOMPLEXBILDNERN IN DER POLARO-GRAPHISCHEN ANALYSE ANORGANISCHER VERBINDUNGEN

XIV.* POLAROGRAPHISCHES STUDIUM VON KOMPLEXEN DER *l*-ASKORBINSÄURE

J. MUSIL

Kovohutě, Mníšek pod Brdy (ČSSR)

J. DOLEŽAL

Institut für analytische Chemie, Naturwissenschaftliche Fakultät der Karlsuniversität, Prag (ČSSR)

J. VORLÍČEK

Institut für Erzforschung, Prag (ČSSR)

(Eingegangen am 9. Juli 1969)

EINLEITUNG

l-Askorbinsäure, $C_6H_8O_6$, d.h. die enol-Form des 3-keto-1-Gulonsäure-Laktons[22] wurde von Erdey als reduktometrisches Reagens in die analytische Chemie eingeführt[8–10,12–14,18,40,41,46,47,57,63,65]. Diese Säure wurde als ein vorteilhaftes Reduktionsmittel in der Photometrie eingeführt[4,6,10,35]. Bei Anwendung dieses Stoffes zum Maskieren von Eisen[33,42,43,61,62,64,68–70], Kupfer[1,29,38] oder Chrom[39] ist es häufig schwer die eigentliche reduktive Wirkung vom tatsächlichen Maskieren zu unterscheiden, wobei das letztere mit der Bindung des störenden Elementes im Askorbatkomplex verbunden ist.

Auf die komplexbildenden Eigenschaften der *l*-Askorbinsäure hat bereits Ettori[15] aufmerksam gemacht. Später wurden die Komplexe mit Titan[19,20,28,34,51–53], Antimon[2,7], Wolfram[58] und Uran[17,48] spektrophotometrisch untersucht. Qualitativ wurde mittels dieser Methodik eine Reihe von Komplexen mit anderen Elementen nachgewiesen[55]. Einige Askorbatkomplexe wurden ferner mittels Ionenaustauscher-Chromatographie[26,27,44] bzw. potentiometrisch[50,59] untersucht.

In der Polarographie wurde einmal das Verhalten der eigentlichen *l*-Askorbinsäure[3,24] beschrieben, ferner wurde ein Grundelektrolyt auf Askorbatbasis zur Bestimmung von Uran[56], Bismuth[49,67], Kupfer[25], Arsen[60] und Spurenverunreinigungen in reinem Indium[32] vorgeschlagen.

Die analytische Anwendung der *l*-Askorbinsäure haben Pilipenko und Kladnitskaja[36] in einem Referat zusammengefasst.

Zweck der vorliegenden Mitteilung war das Studium des polarographischen Verhaltens geläufiger Kationen in einem *l*-Askorbinsäure enthaltenden Elektrolyten mit Rücksicht auf gewisse Informationen über die Askorbatkomplexe, die mittels dieser Methodik erzielt werden können.

---

* Mitteilung XIV: s. Lit. 71.

THEORETISCHER TEIL

Untersuchung der Zusammensetzung von Askorbatkomplexen

Das polarographische Studium von Kationen in einem *l*-Askorbinsäure (ferner nur H_2A) enthaltenden Elektrolyten war auf das Gebiet von pH < 6 beschränkt, wo man annehmen kann dass HA^- Teilchen und Hydroxylgruppen die Funktion von Liganden haben.

Unter Vernachlässigung der Dissoziation zur 2. Stufe und der Herabsetzung der Konzentration von HA^- Teilchen infolge ihres Eintrittes in Komplexe, gilt:

$$c_{H_2A} = [HA^-] + [H_2A] \tag{I}$$

wo c_{H_2A} die analytische Konzentration der *l*-Askorbinsäure ist.

Aus der Beziehung (I) und der Definition der 1. Dissoziationskonstante K_1^A der *l*-Askorbinsäure folgt

$$[HA^-] = \frac{K_1^A c_{H_2A}}{[H^+] + K_1^A} \tag{II}$$

Die Zusammensetzung der einzelnen Komplexe $M^{z+}(HA^-)_i$, wo $i = 1, 2, \ldots x$ ist, kann jetzt aus der Abhängigkeit des Wertes $\Delta E_{\frac{1}{2}}$ der kathodischen Welle von dem $[HA^-]$ Werte bestimmt werden. Der $\Delta E_{\frac{1}{2}}$ Wert wurde durch graphische Extrapolation aus der folgenden Beziehung ermittelt:

$$E_{\frac{1}{2}} = (E_{\frac{1}{2}})_{[HA^-]} - \lim_{[HA^-] \to 0} (E_{\frac{1}{2}})_{[HA^-]}; \quad pH = \text{konst.}$$

so dass es möglich war, im gesamten untersuchten Bereich von pH < 6 zu arbeiten, ohne die Gefahr der Hydrolyse in Abwesenheit des komplexbildenden Reagens (z.B. bei pH-Werten von etwa 4 im Falle von Bi^{III}).

Bestimmung der Anzahl von koordinierten OH^--Gruppen aus der Abhängigkeit des $E_{\frac{1}{2}}$ Wertes der Komplexwelle vom pH-Wert

Wir wollen annehmen, dass ein polarographisch aktives Ion M^{z+} aus einem Komplex der Zusammensetzung $M^{z+}(HA^-)_x(OH^-)_y$ mittels folgender Reaktion entsteht (die Gesamtladung des Komplexes wurde ausgelassen)

$$M^{z+}(HA^-)_x(OH^-)_y \to M^{z+} + x \, HA^- + y \, OH^-$$
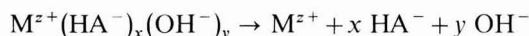
Die Gleichgewichtskonstante der Reaktion ist

$$K = \frac{M^{z+}[HA^-]^x[OH^-]^y}{[M^{z+}(HA^-)_x(OH^-)_y]} \tag{III}$$

Unter Anwendung des daraus folgenden Ausdruckes für $[M^{z+}]$ zum Ableiten der Gleichung für das Halbwellenpotenzial der kathodischen Welle erhalten wir die Beziehung

$$E_{\frac{1}{2}} = E_{\frac{1}{2}}(\text{frei}) - \frac{RT}{nF} \ln \left(\frac{D}{D^*}\right)^{\frac{1}{2}} + \frac{RT}{nF} \ln K - \frac{RT}{nF} \ln [OH^-]^y - \frac{RT}{nF} \ln [HA^-]^x$$

wo D, D^* die Diffusionskoeffizienten des freien Ions und des Komplexes sind.

Nach Substitution in dieser Gleichung, und zwar für $[OH^-] = 10^{-14} \times [H^+]^{-1}$

und für $[HA^-]$ aus der Beziehung (II), bekommen wir

$$E_{\frac{1}{2}} = E_{\frac{1}{2}}(\text{frei}) - \frac{RT}{nF}\left\{\ln\left(\frac{D}{D^*}\right)^{\frac{1}{2}} + \ln K\right\} + y\frac{RT}{nF}\ln 10^{-14} \times [H^+] -$$

$$- x\frac{RT}{nF}\ln\frac{1}{K_1^A}\left(1 + \frac{[H^+]}{K_1^A}\right)$$

Die konstanten Glieder werden in einer neuen Konstante $E_{\frac{1}{2}}^0$ zusammengefasst. Das vorletzte Glied wird in dekadische Logarithmen umgerechnet. Im letzten Glied kann der Ausdruck $\ln(1+[H^+]/K_1^A)$ mit dem Wert $[H^+]/K_1^A$ approximiert werden, und zwar mit der Stirlingschen Formel mit einem Fehler von weniger als 10%, unter Bedingung

$$\frac{[H^+]}{K_1^A} \leqq 0.230, \quad \text{d.h. für pH} \geqq 4.82 \tag{IV}$$

Nach Einsetzen des Wertes $K_1^A = 6.8 \times 10^{-5}$ [16] ist

$$E_{\frac{1}{2}} = E_{\frac{1}{2}}^0 + 0.058\frac{y}{n}\log[H^+] + 3.7 \times 10^2\frac{x}{n}[H^+]$$

daher

$$\frac{dE_{\frac{1}{2}}}{d\,pH} = -0.058\frac{y}{n} - 8.5 \times 10^2\frac{x}{n}[H^+] \tag{V}$$

Wenn wir die Steigung der Tangente zum Graph der Funktion $E_{\frac{1}{2}}$ (pH) in Betracht ziehen, z.B. im Punkt pH = 5 (der der Bedingung (IV) genügt) erhalten wir

$$\frac{dE_{\frac{1}{2}}}{d\,pH} = -0.058\frac{y}{n} - 8.5 \times 10^{-3}\frac{x}{n}; \quad pH = 5 \tag{VI}$$

Wenn die Werte x und n bekannt sind, ist es möglich aus der Beziehung (IV) das Verhältnis $y = OH^- : M^{z+}$ auf Grunde der experimentell ermittelten Abhängigkeit von $E_{\frac{1}{2}}$ vom pH-Wert bei konstanter analytischer Konzentration der Askorbinsäure zu bestimmen.

EXPERIMENTELLER TEIL

Angewandte Reagenzien

1 M Lösungen der *l*-Askorbinsäure (Produkt der Fa. SPOFA ČSSR, Reinheit nach ČSL) wurden immer unmittelbar vor Anwendung bereitet: 17.61 g der Substanz wurden in redestilliertem Wasser gelöst, aus dem der Sauerstoff entfernt worden war. Je nach Bedarf wurde der pH-Wert mit 2 M NaOH eingestellt und die Lösung auf 100 ml aufgefüllt. Der wirkliche Askorbinsäuregehalt wurde jodometrisch ermittelt[11].

Gelatinelösung (0.05%) wurde ebenfalls unmittelbar vor der Anwendung bereitet.

Die weiteren verwendeten Chemikalien waren: NaOH, KOH, HNO_3, H_2SO_4, HCl, $NaNO_3$ und $HClO_4$, insgesamt inländischer Herkunft und des Reinheitsgrades p.a.

Sauerstoff wurde mittels zweistufig mit Chromsulphatlösung gereinigtem

Stickstoff aus den Lösungen beseitigt.

0.01–0.05 M Metallösungen wurden aus p.a. Stoffen bereitet, in der Form von Nitraten (Cu^{II}, Bi^{III}, U^{VI}, Pb^{II}, Tl^{I}), Chloriden (V^{IV}, Ti^{IV}), oder Sulphaten (Cd^{II}, Sb^{III}, Ti^{IV}). Der Metallgehalt der Lösungen wurde meistens chelatometrisch kontrolliert[37].

Geräte und Apparatur

Es wurde der Modell LP 55 Polarograph, Erzeugniss der Fa. Laboratorní přístroje, Prag, verwendet. Die Konstanten der stumpfen Kapillare waren: Innendurchmesser 0.06 mm, Tropfdauer $t_1 = 2.98$ s in destilliertem Wasser, Durchflussgeschwindigkeit $m = 2.83$ mg s^{-1} bei einer Reservoirhöhe von $h = 55$ cm. Die Korrektion für den Rückdruck war $h_z = 1.5$ cm. Zur Arbeit mit der stationären Quecksilberelektrode wurde die Apparatur nach Kemula[23] der Fa. Radiometer, Kopenhagen, verwendet.

Polarographiert wurde in Gefässen nach Kalousek, in einem Gesamtvolumen von etwa 50 ml. Alle Messungen wurden gegen eine gesättigte Kalomelelektrode vorgenommen und entsprechend dem gefundenen Halbwellenpotenzial der Tl^+-Welle in 0.1 M NaNO$_3$ ($E_{\frac{1}{2}} = -0.456$ V) korrigiert. pH-Werte wurden mit dem Elektronenröhren-pH-Meter "Multoskop III" tschechoslowakischer Erzeugung mit einer hochohmigen Glaselektrode gemessen.

Allgemeiner Arbeitsgang

Sofern nicht anders angeführt wird, wurde der folgende Arbeitsgang eingehalten: Der pipettierten Standardmetallösung wurden 50 ml 1.0 M H$_2$A oder Askorbatpuffer mit demselben H$_2$A-Gehalt, 10 ml 0.05% Gelatinelösung zugegeben und die Lösung wurde auf 100 ml aufgefüllt. Es wurde der pH-Endwert gemessen. Der gelöste Sauerstoff wurde im Polarographiegefäss sofort mit einem Stickstoffstrom beseitigt (*ca.* 5 Min) und danach wurden die polarographischen Kurven registriert. Die Temperatur variierte zwischen 19 und 21°C.

Der diffuse Charakter der erzielten Wellen wurde durch ein Studium der Abhängigkeit der Wellenhöhe von der Höhe der Quecksilbersäule und der Depolarisatorkonzentration überprüft. Je nach Bedarf wurde die Ionenstärke der Lösung mittels Zugabe von NaNO$_3$ auf einen Wert von $\mu = 1$ eingestellt. Alle Messungen wurden mindestens dreimal wiederholt, und das arithmetische Mittel wurde aus den Resultaten gezogen.

ERGEBNISSE

Die Grundeigenschaften der polarographischen Wellen einiger Ionen in Askorbatelektrolyt sind in Tabelle 1 zusammengefasst. Die Zusammensetzung und Beständigkeitskonstanten der untersuchten Askorbatkomplexe sind in Tabelle 2 angeführt.

Wismut

Bei pH-Werten rund 1 ist die Höhe und der Halbwellenpotenzial der Wismutwelle in 0.5 M H$_2$A mit den Werten für die $Bi^{3+} \rightarrow Bi^0$ in einem Milieu von HNO$_3$ allein identisch[66]. Mit steigendem pH verringert sich die Wellenhöhe einigermassen (etwa um 15%). Das Ergebnis zyklisch-voltametrischer Messungen mit der statio-

TABELLE 1

HALBWELLENPOTENZIALE EINIGER METALLE IN $0.5\ M$ ASKORBATPUFFER-MILIEU

Element	$E_{\frac{1}{2}}/SCE$			Reaktion	Anmerkung
	pH, 1.2*	pH, 2.0	pH, 4.0		
Cu	+0.01	...	...	$2 \to 0$	k.
Bi	+0.01	−0.05	−0.16	$3 \to 0$	k.
U	−0.28	−0.20	−0.32	$6 \to 5$	k.
Pb	−0.40	−0.42	−0.42	$2 \to 0$	k.
Tl	−0.46	−0.46	−0.46	$1 \to 0$	k.
Ti	−0.38	−0.47	...	$4 \to 3$	k., nicht Dif.-Str.
	...	(−0.67)	−0.86	$4 \to 3$	k., nicht Dif.-Str.
	...	−0.85	...	$4 \to 3$	k., nicht Dif.-Str.
Mo	...	−0.15	−0.32	$6 \to 5$ (?)	k.
	−0.38	−0.49	−0.70	$5 \to 3$ (?)	k.
V	...	...	−0.17	$3 \leftrightarrow 4$	a.-k.
	−0.90	−0.81	−0.87		k.
As	...	−0.88	−0.88		k.
Cr	−0.9	...	...		k., schlecht entwickelte Welle
Sb	−0.18	...	...		k., Anzeichen einer Doppelwelle

* $0.15\ M\ H_2A$, $0.1\ M\ HNO_3$.
W, Ni, Co, Mn, Fe, Zn, Ga, Zr und Nb sind im erreichbaren Potenzialbereich nicht polarographisch aktiv.

TABELLE 2

ZUSAMMENSETZUNG VON KOMPLEXEN TEILCHEN IN ASKORBATLÖSUNGEN BEI $pH = 4$

M^{z+}	$M:HA^-$	Werte der scheinbaren Beständigkeitkonstanten	$M:OH^-$
Bi^{3+}	1:1	$K_1 \doteq 17.5$	
	1:2	$K_2 \doteq 6.4 \times 10^2$	
	1:3	$K_3 \doteq 3.2 \times 10^3$	
	1:4	$K_4 \doteq 4.5 \times 10^4$	1:2
Pb^{2+}	1:1	$K_1 = 3.7$	
	1:2	$K_2 = 11.7$	
	1:3	$K_3 = 23.5$	
UO_2^{2+}	1:1	$K_1 = 30.3$	1:2

nären Quecksilberelektrode bestätigt, dass die Reduktion bis zum Metall verläuft.

Die Steigungswerte der logarithmischen Analyse bewegen sich zwischen 0.032 V und 0.040 V in Abhängigkeit vom $c_{H_2A}:[Bi^{III}]$ Verhältniss, so dass die Welle nicht perfekt reversibel ist. Trotzdem kann die Komplex-Untersuchungsmethode nach DeFord und Hume[5] mit der Beschränkung angewandt werden, dass nur die Zusammensetzung der Komplexe ermittelt wird, während die Werte der Beständigkeitskonstanten nur grössenordnungsmässig gesichert sind. Die Ergebnisse dieser Untersuchung waren für pH = 3.70 und pH = 4.10 identisch.

Die Steigungswert der pH-Abhängigkeit des $E_{\frac{1}{2}}$-Wertes der untersuchten Welle ist −0.055 V/pH (Abb. 1), woraus nach Substitution in die Beziehung (VI) mit den Werten $x = 4$, $n = 3$ der Wert $y = 2.2$ resultiert. Es darf also angenommen werden,

dass im kompliziertesten Teilchen neben vier HA^- Anionen zwei Hydroxylgruppen koordiniert sind.

Die untersuchte Wismutwelle ist von diffusem Charakter und kann analytisch verwendet werden.
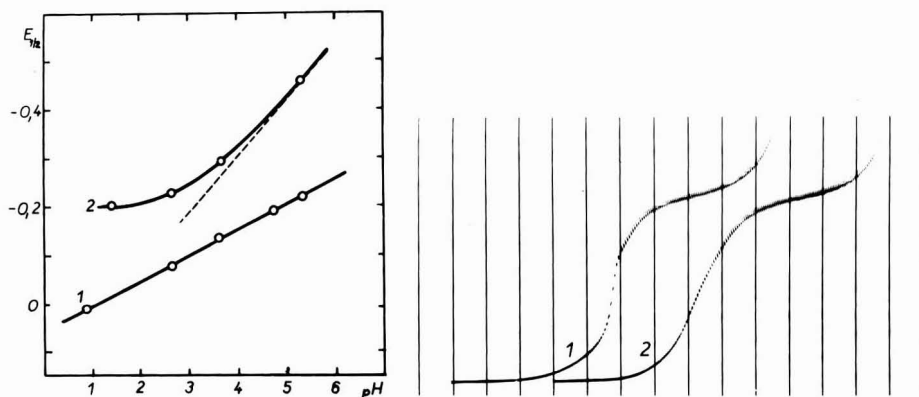
Abb. 1. Abhängigkeit des Halbwellenpotenziales vom pH. (1) 10^{-3} M Bi^{III}, 0.4 M H_2A Puffer; (2) 5×10^{-4} M UO_2^{2+}, 0.2 M H_2A Puffer.

Abb. 2. Abhängigkeit der Form der Ti^{IV}-Welle vom im Elektrolyten anwesenden Kation. (1) 2.5×10^{-4} M Ti^{IV} (Lösung in HCl), 0.1 M H_2A Puffer, pH = 4.05 mit KOH eingestellt; Anfang der Kurve bei -0.5 V, 100 mV/Absz.; (2) als (1), pH = 4.05 mit NaOH eingestellt.

Blei

Im Askorbatelektrolyten bietet der Bleikomplex eine gut entwickelte diffuse Welle $Pb^{II} \rightarrow Pb^0$. Der Steigungswert der logarithmischen Analyse ist 0.036 V, so dass der Elektrodenprozess annähernd polarographisch reversibel ist.

Die Bleiwelle im Askorbatelektrolyten ist in der analytischen Chemie sehr gut anwendbar.

Uran

Es ist gefunden worden, dass die Uranwelle im Perchloratelektrolyten $(U^{VI} \rightarrow U^V; E_{\frac{1}{2}} = -0.20$ V$)^{66}$ sich nach Zugabe von H_2A zum Perchlorat in eine Welle mit $E_{\frac{1}{2}} = -0.32$ V umwandelt, wobei sich die Wellenhöhe praktisch nicht verändert. Die Abhängigkeit des $E_{\frac{1}{2}}$-Wertes vom pH ist in Abb. 1 dargestellt. Šušić und Mitarbeiter[56] verwendeten diese gut ausgeprägte U^{VI}-Welle im Askorbatelektrolyten zu analytischen Zwecken.

Wenn U^{VI} vorher in H_2SO_4-Milieu mittels Zn-Amalgame zu U^V reduziert wird, verschwindet die genannte Welle im Askorbatelektrolyten fast gänzlich. Daraus kann gefolgert werden, dass diese Welle der Reaktion $U^{VI} \rightarrow U^V$ entspricht. Der Steigungswert der logarithmischen Analyse ist 0.068 V (pH = 3.05). Die Welle kann also als annähernd reversibel betrachet werden, und ist analytisch gut verwendbar.

Kupfer

In einem 0.1 M HNO_3 und 0.4 M H_2A enthaltenden Elektrolyten bildet Kupfer eine gut entwickelte diffuse kathodische Welle von $E_{\frac{1}{2}} = +0.01$ V, deren Höhe

und $E_{\frac{1}{2}}$-Wert denjenigen der Cu^{2+}-Welle in 0.1 M $NaClO_4{}^{54}$ ähnlich sind. In beiden Fällen handelt es sich um die Reduktion $Cu^{II}\rightarrow Cu^0$. Die Steigung der logarithmischen Analyse ist 0.037 V, die Welle ist also nicht reversibel.

Die Kupferwelle in Askorbatmilieu ist analytisch gut verwertbar, sofern der pH-Wert der Lösung nahe 1 ist.

Bei Steigen des pH-Wertes in die Nähe von 2 reduziert die Askorbinsäure das Kupfer zum Metall, u.z. auch in Anwesenheit von z.B. NO_3^-, SO_4^{2-}, NH_4^+, Na^+ und K^+. In Anwesenheit von Cl^--Ionen findet keine Reduktion statt. Die Reduktionsgeschwindigkeit wurde amperometrisch untersucht, mit der Quecksilbertropfelektrode bei $E = -0.5$ V. Die Reduktionsgeschwindigkeit steigt mit dem steigenden pH. Durch Anwesenheit von Sauerstoff wird die Reduktion zum Metall verlangsamt.

Titan

In Askorbatelektrolyt bilden Titankomplexe bis zu drei kathodischen Wellen, deren Höhe sowie $E_{\frac{1}{2}}$-Wert pH-abhängig sind.

Bei pH < 1 existiert eine einzige, gut entwickelte Diffusionswelle. Im Bereich von pH 1.5–2 ist eine Doppelwelle an der Kurve klar zu erkennen. Die Abhängigkeit der Höhe der Doppelwelle vom $\sqrt{h}$ Wert ist linear, und die Gerade verläuft durch den Anfang des Koordinatensystems. Im Falle der einzelnen Wellen ist die Abhängigkeit aber nicht notwendigerweise linear. Bei pH = 3.5–5.5 existiert in 0.5 M H_2A in Anwesenheit von SO_4^{2-} oder Cl^- eine einzige Ti^{IV}-Welle von semikinetischem Charakter. Es ist interessant, dass die Form und Steilheit dieser Welle weitgehend von anwesenden Kation abhängen: bei Anwendung von KOH zur pH-Einstellung ist die Welle bedeutend steiler als wenn zu diesem Zwecke NaOH verwendet wurde (Abb. 2). Dasselbe erfolgt auch wenn ein neutrales Kaliumsalz zugegeben wird (z.B. KCl oder K_2SO_4) zu einem Na^+-Elektrolyten, während die Zugabe eines Natriumsalzes derselben Konzentration auf den Kurvenverlauf ohne Einfluss bleibt. Ähnlich wie ein Kaliumsalz, aber in weit geringerem Masstab, wirkt auch die Anwesenheit von Magnesiumsalz.

Die logarithmische Analyse beweist die Irreversibilität aller beschriebenen Wellen des Titaniums, wobei der Einfluss des Kations sich auch in der graphischen Form der logarithmischen Analyse der entsprechenden Welle klar ausdrückt.

In allen untersuchten Fällen führte die Anwesenheit von NO_3^--Ionen zu einem Anstieg der Wellenhöhe um eine weitere kinetische Komponente, wahrscheinlich als Folge der Reaktion zwischen Ti^{III} und Nitrationen.

Analytisch verwertbar ist nur die Titan-Diffusionswelle bei pH-Werten von rund 1.

Molybdän

In Askorbatelektrolyt bildet das Natriummolybdenat zwei kathodische Wellen, deren $E_{\frac{1}{2}}$-Werte vom pH Abhängig sind. Die Abhängigkeit der Höhe jeder dieser Wellen vom $\sqrt{h}$-Wert ist linear, aber nur im Falle der negativeren Welle verläuft die Gerade durch den Anfang des Koordinatensystems. Die negativere Welle ist von diffusem Charakter und kann zu analytischen Zwecken verwendeten werden.

Vanad

An der polarographischen Kurve des V^{IV} entstehen zwei diffuse Wellen, wobei

die positivere Welle reversibel, anodisch-kathodisch ist. Das Verhältniss der Höhe dieser Wellen sowie ihre $E_{\frac{1}{2}}$-Werte sind pH-abhängig. Es ist klar dass in der Lösung in Abhängigkeit vom pH zwischen den beiden Oxydationsstufen des Vanads ein Gleichgewicht entsteht.

Nach vorgehender Reduktion mit Zn-Amalgam verschwindet die negativere Welle. Die Steigung der logarithmischen Analyse der positiveren (anodisch–kathodischen) Welle ist 0.064 V. Die Welle bleibt auch nach vorgehender Reduktion mit Zn-Amalgam bestehen. Diesen Angaben entspricht die Elektrodenreaktion $V^{IV} \leftrightarrow V^{III}$.

Die untersuchten Vanadwellen sind analytisch anwendbar.

Arsen

Das dreiwertige Arsen bildet eine kathodische Welle mit $E_{\frac{1}{2}} = 0.88$ V. Das Halbwellenpotenzial ist im Bereich von 2.5–4.5 vom pH unabhängig. In diesem Bereich sinkt die Wellenhöhe mit steigendem pH. Diese Welle wurde nicht eingehend untersucht, da sie bereits Šušič und Mitarbeitern[60] verwendet hatten.

DISKUSSION DER ERGEBNISSE

Sobkowska untersuchte das polarographische Verhalten von Bi^{III} in Askorbatelektrolyt auf oscillopolarographischem Wege[49]. Aus der Stellung des kathodischen und des nicht besonders gut entwickelten anodischen Einschnittes folgert sie, das es sich um einen reversible Prozess handelt. Das Ergebniss der logarithmischen Analyse interpretiert die Authorin dann so, dass sie einen Zweielektronprozess ohne weitere Erklärung voraussetzt. Diese Schlussfolgerung widerspricht den Ergebnissen der zyklischen Voltametrie an der hängenden Hg-Tropfenelektrode. Auch der Unterschied von 15% zwischen der Höhe der Bi^{III}-Welle in 0.1 M HNO_3 und im Askorbatelektrolyt entspricht den zwei ausgetauschten Elektronen nicht: eine ausreichende Erklärung dieser Höhenverringerung bietet aber eine Veränderung des Diffusionskoeffizienten die mit dem Entstehen eines komplexen Wismutions zusammenhängt. Eine ausreichende Interpretation der Welle ist also die Reaktion $(Bi^{3+}(HA^-)_4 (OH^-)_2)^{3-} \rightarrow Bi^0$.

Im Zusammenhang mit der beschriebenen Reduktion von Cu^{II}-Ionen in einem Milieu von l-Askorbinsäure bei pH > 2 ist noch der Reaktionsmechanismus zu klären. Für die katalytische Wirkung des Kupfers bei der Oxydation von H_2A wurde ein Reaktionsmechanismus vorgeschlagen[31], in dem das Kupferchelat zur Wirkung kommt. Der erste Schritt führt zur Bildung von einwertigem Kupfer mit gleichzeitiger Bildung der Semichinonstruktur A:
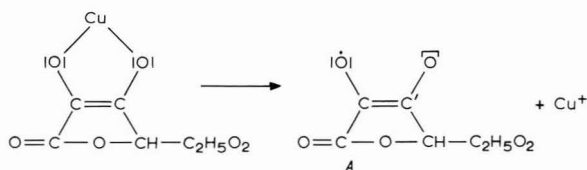
Im zweiten Schritt wird unter Mitwirkung von H^+ und Luftsauerstoff die Reduktion zu Dehydroaskorbinsäure beendet, wobei dem einwertigen Kupferion ein weiteres Elektron entnommen wird und der Katalysator, d.h. Cu^{II} wird so erneuert. Es ist

anzunehmen, dass unter den Bedingungen der Reduktion zum Metall, d.h. in einem Milieu mit niedriger H^+-Ionen-Konzentration und in Abwesenheit von Luftsauerstoff dieser zweite Schritt blockiert wird und die Reduktion dann durch Übertragung eines ungeraden Elektrons aus der Struktur A auf das Cu^+-Ion unter Bilden von metallischem Kupfer weitergeht. Dieser Schritt kann durch Ansteigen des Redox-Potenziales infolge der Bindung von Kupfer in einem Chlorid-Komplex unmöglich werden, was eine mögliche Erklärung des beobachteten Einflusses der Cl^--Ionen wäre. Bei eingehendem Studium der Kinetik wäre es notwendig, auch dem möglichen Einfluss der Beleuchtung auf die Geschwindigkeit des zweiten Reaktionsschrittes (Übertragung des ungeraden Elektrons) Aufmerksamkeit zu widmen.

Vollkommen ungeklärt bleibt bisweilen der Einfluss von Kationen auf die Wellenform des Titans. Es scheint dass der beschriebene Effekt mit Adsorption nicht zusammenhängt.

Die Existenz von relativ festen Bi^{III}-Komplexen mit Askorbinsäure ist im Einklang mit der allgemeinen Fähigkeit des Wismuts, Komplexe mit grösserer Zahl von OH-Gruppen enthaltenden organischen Stoffen zu bilden. Die Existenz ähnlicher Komplexe kann auch bei As und Sb angenommen werden. Unter der Annahme, dass das Askorbation gegenüber Bi^{III} die Rolle eines eindonorigen Reagens spielt, und mit Hinsicht auf zwei koordinierte Hydroxylgruppen, erfolgt beim höchsten Komplex die Formel $(Bi^{3+}(HY^-)_4(OH^-)_2)^{3-}$ und die Koordinationszahl 6. Es muss betont werden, dass die Konstante K_1 des niedrigsten Komplexes bedeutend niedriger ist als die nachfolgende Konstante K_2 (Tabelle 2). Die Ergebnisse der weiteren Analyse wären kaum anders, wenn wir $K_1 = 0$ annähmen, d.h. die Existenz des niedrigsten Komplexes kann nicht als nachgewiesen betrachtet werden.

Die Zusammensetzung des Bleikomplexes $Pb : HA^- = 1 : 3$ folgt auch aus einer einfacheren Analyse[70]: Der Graph der Abhängigkeit $E_{\frac{1}{2}}$ von $\log HA^-$ nähert sich bei höheren H_2A Konzentrationen einer Geraden, deren Steigung, 0.088 V mit der Theorie im Einklang steht (0.0885 V) für die Komplexzusammensetzung 1 : 3. Die effektive Atomzahl von Pb^{II} im Komplex $(Pb(HA^-)_3)^-$ ist e.A.Z. $= 82 + 3 + 1 = 86$, so dass der Komplex der Sidgwickschen Regel genügt (A.Z. Rn ist 86). Unter den zwei möglichen Strukturen (Dreieck und dreiseitige Pyramide) kommt für die Struktur des komplexen Teilchens die pyramidale Struktur eher in Betracht, dass es sich um ein geladenes Teilchen handelt.

Die ermittelte Zusammensetzung des Urankomplexes $(UO_2)^{2+}(HA^-)(OH^-)_2^-$ stimmt mit den auf spektrophotometrischem Wege erzielten Literaturangaben[17] gut überein.

Durch Anwendung des Askorbatelektrolyten wird es in der analytischen Praxis möglich, in saurem Milieu polarographisch einige Kationen zu bestimmen, z.B. Cu^{II}, die sonst in einem ammoniakalen Elektrolyten bestimmt werden. Diese Möglichkeit ist insbesondere dann vorteilhaft, wenn eisen- bzw. aluminiumhaltige Stoffe analysiert werden, da die genannten Metalle, sowie auch andere Elemente im Ammoniakelektrolyt Hydroxydniederschläge bilden, deren Adsorptivität stören könnte. Die Koinzidenz der Kupfer- und Wismutwellen kann durch Zugabe von EDTA beseitigt werden (der $E_{\frac{1}{2}}$-Wert von Bi^{III} verschiebt sich zu den negativeren Potenzialen), wobei die Wellenhöhe von Bi^{III} und Cu^{II} praktisch unverändert bleibt[67]. Es zeigt sich, dass durch Anwendung des Erkenntnisses über das Ausscheiden von Kupfer aus Askorbatlösungen die Möglichkeit geboten wird, Wismut noch bei einem

1000fachen Überschuss von Kupfer zu bestimmen. Es ist dabei nachgewiesen worden, dass Wismut quantitativ in der Lösung bleibt. Der kleine Rest an nicht-ausgeschiedenem Kupfer stört in der Regel nicht mehr. In einigen Fällen könnte es zweckmässig sein, das Ausscheiden von metallischem Kupfer mittels Askorbinsäure als Trennmethode zu modifizieren.

ZUSAMMENFASSUNG

Es wurden die Grundeigenschaften von polarographischen Wellen geläufiger Kationen in einem *l*-Askorbinsäure enthaltenden Elektrolyten untersucht und die entsprechenden Halbwellen-Potenziale wurden gemessen. Die Zusammensetzung und angenäherte Werte der Beständigkeitskonstanten von Wismut-, Blei- und Uran-Askorbatkomplexen wurden polarographisch bestimmt. Im theoretischen Teil der Mitteilung wurde eine Methode zum Bestimmen der Zusammensetzung von solchen Komplexen ausgearbeitet, die neben dem Anion einer schwachen Säure auch OH⁻ Gruppen als Liganden enthalten. Mittels der vorgeschlagenen Methode wurde die Zusammensetzung ternärer Hydroxyl-Askorbatkomplexe des Wismuts und Urans bestimmt.

SUMMARY

The basic properties of the polarographic waves of some common cations in an electrolyte containing *l*-ascorbic acid were investigated and the corresponding half-wave potentials were measured. The composition and the approximate value of the stability constants of bismuth, lead and uranium ascorbate complexes were determined polarographically. In the theoretical part a method is worked out for the determination of the composition of complexes which contain OH⁻ as well as the anion of a weak acid as ligands. By means of this method, the composition of ternary hydroxyl–ascorbate complexes of bismuth and uranium was determined.

LITERATUR

1 B. K. AFGHAN, R. M. DAGNALL UND K. C. THOMPSON, *Talanta*, 14 (1967) 715.
2 J. BASSET UND J. CH. JONES, *Analyst*, 91 (1966) 176.
3 R. BRDIČKA in: *Sammelbuch des 1. internationalen polarographischen Kongresses*, Praha, NČSAV, 1952, B. III., S. 301.
4 M. L. CAP, *Zavodsk. Lab.*, 21 (1955) 10.
5 D. DeFORD UND D. N. HUME, *J. Am. Chem. Soc.*, 73 (1951) 5321.
6 S. ELINSON UND L. POBIEDINA, *Zavodsk. Lab.*, 25 (1959) 909.
7 A. ELKIND, K. H. GAYER UND D. F. BOLTZ, *Anal. Chem.*, 25 (1953) 1744.
8 L. ERDEY UND E. BODOR, *Magy. Kem. Folyoirat*, 56 (1950) 277.
9 L. ERDEY UND E. BODOR, *Z. Anal. Chem.*, 136 (1952) 109.
10 L. ERDEY UND E. BODOR, *Magy. Kem. Folyoirat*, 58 (1952) 295.
11 L. ERDEY UND E. BODOR, *Anal. Chem.*, 24 (1952) 418.
12 L. ERDEY UND E. BODOR, *Anal. Chem.*, 24 (1952) 419.
13 L. ERDEY UND A. KARSAY, *Acta Chim. Acad. Sci. Hung.*, 9 (1956) 43.
14 J. ERDEY UND G. SVEHLA, *Chemist-Analyst*, 52 (1963) 24.
15 J. ETTORI, *Compt. Rend.*, 202 (1936) 852.
16 J. FRAGNER (Ed.), *Vitamine, ihre Chemie und Biochemie, B.II*, 1. Ausg., Praha, NČSAV, 1961, S. 694.
17 I. J. GAL, *Bull. Inst. Nuclear Sci. "Boris Kidrich"*, 6 (1956) 173.

18 Z. A. GALLAJ, V. G. TIPTCOVA UND V. M. PEŠKOVA, *Zh. Analit. Khim.*, 12 (1957) 469.
19 Z. GREGORRCZYK, *Acta Polon. Pharm.*, 15 (1958) 129.
20 Z. GREGORRCZYK, *Acta Polon. Pharm.*, 15 (1958) 333.
21 J. HEYROVSKÝ UND J. KŮTA, *Grundlagen der Polarographie*, 1. Ausg., Praha, NČSAV, 1962, S. 112.
22 E. L. HIRST, *Chem. Ind. London*, 52 (1935) 221.
23 W. KEMULA UND Z. KUBLIK, *Anal. Chim. Acta*, 18 (1958) 104.
24 E. KODIČEK UND K. WENIG, *Nature*, 142 (1938) 35.
25 M. KOPANICA UND J. VORLÍČEK, *Chemist-Analyst*, 54 (1965) 105.
26 J. KORKISCH, A. FARAG UND F. HECHT, *Microchim. Acta*, (1958) 415.
27 J. KORKISCH UND A. FARAG, *Microchim. Acta*, (1958) 659.
28 J. KORKISCH, *Microchim. Acta*, (1961) 262.
29 A. KOVÁCH, *Magy. Kem. Folyoirat*, 70 (1964) 252.
30 A. I. LAZAREV UND V. I. LAZAREVA, *Zavodsk. Lab.*, 24 (1958) 798.
31 A. E. MARTELL UND M. CALVIN, *Metallchelatenchemie*, 1. Ausg. Praha NČSAV, 1959, S. 372.
32 J. MUSIL UND M. KOPANICA, *Chemist-Analyst*, 55 (1966) 9.
33 J. MUSIL, *Hutnické Listy*, 23 (1968) 649.
34 E. NINES UND D. F. BOLTZ, *Anal. Chem.*, 24 (1952) 947.
35 M. OTOMO, *Bull. Chem. Soc. Japan*, 36 (1963) 137.
36 A. T. PILIPENKO UND M. B. KLADNITSKAJA, *Zavodsk. Lab.*, 32 (1966) 3.
37 R. PŘIBIL, *Komplexometrie*, B.I., 1. Ausg. Praha SNTL, 1957.
38 R. PŘIBIL, *Talanta*, 13 (1966) 1223.
39 R. PŘIBIL UND V. VESELÝ, *Talanta*, 8 (1961) 565.
40 N. K. PŠENITSYN UND N. A. EZERSKAYA, *Zh. Analit. Khim.*, 14 (1959) 81.
41 B. V. PTITSYN UND V. A. KOZLOV, *Zh. Analit. Khim.*, 4 (1949) 35.
42 H. N. RAY, M. S. GHOSCH, K. BISWAS UND S. RAY, *Z. Anal. Chem.*, 217 (1966) 189.
43 J. REŘICHA UND J. MAYER, *Hutnické Listy*, 12 (1962) 883.
44 J. SCHUBERT UND A. LINDENBAUM, *J. Am. Chem. Soc.*, 74 (1952) 3529.
45 D. SINGH, *J. Sci. Res. Banaras Hindu Univ.*, 10 (1959–60) 6.
46 D. SINGH UND A. VARMA, *J. Sci. Res. Banaras Hindu Univ.*, 11 (1960–61) 202.
47 D. SINGH UND A. VARMA, *J. Sci. Res. Banaras Hindu Univ.*, 12 (1961–62) 267.
48 D. SINGH, J. HAVEL UND L. SOMMER, *Collection Czech. Chem. Commun.*, im Druck.
49 A. SOBKOWSKA, *Chim. Anal. Warsaw*, 7 (1962) 959.
50 A. SOBKOWSKA UND J. MINCZEWSKI, *Roczniki Chem.*, 36 (1962) 17.
51 L. SOMMER, *Z. Anal. Chem.*, 171 (1960) 410.
52 L. SOMMER, *Z. Anorg. Algem. Chem.*, 321 (1963) 191.
53 L. SOMMER, *Collection Czech. Chem. Commun.*, 28 (1963) 449.
54 B. P. NIKOLSKIŸ (Ed.), *Spravočnik chimika*, 2. Ausg., B. IV. Moskva-Leningrad, Khimija, 1965, S. 502.
55 K. P. STOLYAROV UND I. A. AMANTOVA, *Talanta*, 14 (1967) 1237.
56 M. V. SUŠIĆ, I. GAL UND E. CUKER, *Anal. Chim. Acta*, 11 (1954) 586.
57 M. V. SUŠIĆ UND D. Ž. DJURDJEVIĆ, *Bull. Soc. Chim. Belgrade*, 23-24 (1959) 297.
58 M. V. SUŠIĆ, D. S. VESELINOVIĆ UND D. Z. SUŽNJEVIĆ, *Bull. Soc. Chim. Belgrade*, 29 (1964) 121.
59 M. V. SUŠIĆ, D. S. VESELINOVIĆ UND D. Z. SUŽNJEVIĆ, *Bull. Soc. Chim. Belgrade*, 29 (1964) 311.
60 M. V. SUŠIĆ UND M. G. PJEŠČIĆ, *Analyst*, 91 (1966) 258.
61 V. N. TIKHONOV, *Zh. Analit. Khim.*, 21 (1967) 275.
62 V. N. TIKHONOV UND M. J. GRANKINA, *Zavodsk. Lab.*, 32 (1966) 278.
63 J. I. USATĚNKO UND G. E. BEKLEŠOVA, *Zavodsk. Lab.*, 19 (1953) 147.
64 J. I. USATĚNKO UND G. E. BEKLEŠOVA, *Zavodsk. Lab.*, 24 (1958) 1189.
65 J. I. USATĚNKO u.a., *Zavodsk. Lab.*, 21 (1955) 25.
66 A. A. VLČEK, *Chem. Listy*, 50 (1956) 400.
67 J. VORLÍČEK, J. PETÁK UND J. MUSIL, *Hutnické Listy*, 22 (1967) 263.
68 J. VORLÍČEK UND J. VYDRA, *Chemist-Analyst*, 54 (1965) 87.
69 J. VORLÍČEK UND J. VYDRA, *Microchem. J.*, 9 (1965) 152.
70 J. VORLÍČEK UND J. VYDRA, *Talanta*, 12 (1965) 671.
71 D. SUŽNJEVIĆ, J. DOLEŽAL UND M. KOPANICA, *J. Electroanal. Chem.*, 20 (1969) 279.

pH-METRIC STUDIES ON THE REACTION OF SILICIC ACID SOLS WITH HEMOGLOBIN AND SOYBEAN PROTEINS

WAHID U. MALIK AND JAI PAL SINGH ARORA

Department of Chemistry, University of Roorkee, Roorkee, U.P. (India)

(Received June 2nd, 1969)

The reaction between silicic acid and proteins has been studied qualitatively by a number of workers[1-5]. It is now fairly well established that the reaction product is not merely a precipitate obtained through mutual coagulation but is formed as a result of the combination of the silicic acid with the protein. The recent work of Clark and co-workers[6,7] on the reaction of silicic acid with insulin, albumin and nylon monolayers using surface pressure measurements, has provided evidence for the formation of hydrogen bonds between keto-imino groups of the proteins and the -OH groups of the silicic acid. Bergman and Nelson[8] have investigated the binding power of a silica sol for both fibrillar and globular proteins over a wide pH range and have reported data on the stoichiometry of the reaction. More recently, Shvaiger[9] has used the reaction of gelatin with silicic acid for the gravimetric estimation of the latter.

The aim of the present communication is to show that the pH-metric method is of more general application than the methods so far used in investigating the silicic acid–protein reactions. This method not only provides a means of determining the extent of binding but also throws light on the mechanism of the reaction. For this purpose two proteins, *viz.* hemoglobin, a protein of physiological importance, and soybean, a protein of high food value, were allowed to react with silicic acid sols at·pH 2.0, 2.5 and 3.0.

EXPERIMENTAL

Silicic acid sols were prepared by slowly mixing and stirring 75 ml of 25.0% sodium metasilicate solution in 125 ml of 3.5 N hydrochloric acid. The resulting solution was dialysed till the desired pH was attained. The concentration of the sol was determined by drying a known volume in an air oven at 105–110°C. The dry mass was then washed repeatedly for the removal of electrolyte. The amount of silica was determined after drying again at 105°C. The concentration of the sol was adjusted to the value required by adding doubly-distilled water.

Protein solutions

Soybean protein was isolated from soybean seeds (BDH) by the method of Kunihiko Suminokura[10]. A solution was prepared in dilute KOH and the pH was adjusted to 12.0. The concentration of the protein solution was determined by drying a known volume at 105°C.

Hemoglobin (E. Merck) was dissolved in KOH solution according to the method of Steinhardt and Zaiser[11] to prepare a 2% solution. The pH of the protein solution was adjusted to 12.0 by dialysing it for some time. The protein concentration was determined as above. Dilute solutions of carbonate-free KOH (pH 12.0) were prepared using Kolthoff's method[12].

pH-metric measurements were carried out using a Beckman Model H, pH-meter in conjunction with a wide range glass electrode. The pH-meter was standardised against 0.05 M potassium hydrogen phthalate (pH 4.0) and 0.5 M sodium borate (pH 9.2) for the acid and basic ranges, respectively.

Procedure

Different volumes of 2% silicic acid sol of different initial pH values, *viz.* 2.0, 2.5 and 3.0, were taken in different Pyrex boiling tubes. Two similar sets were prepared, each having the same amount of the sol; to one set was added 3.0 ml of 2% protein solution (pH 12.0); the other contained 3.0 ml of KOH (pH 12.0). The total volume was made up to 15 ml in each case by adding the requisite amount of conductivity water.

RESULTS AND DISCUSSION

Table 1 gives the initial and the final pH values of the protein–silicic acid sol mixtures. The curves for pH-metric titrations are shown in Fig. 1, a–c.

TABLE 1

COMPARISON OF pH VALUES FOR HEMOGLOBIN AND SOYBEAN PROTEIN WHEN TITRATED WITH SILICIC ACID SOL OF DIFFERENT INITIAL pH

Initial pH of the silicic acid sol	Hemoglobin		Soybean		KOH	
	Initial pH	Final pH	Initial pH	Final pH	Initial pH	Final pH
2.0	11.20	3.00	11.20	7.50	11.15	2.15
2.5	11.20	7.50	11.20	8.75	11.15	6.48
3.0	11.20	8.10	11.20	8.80	11.15	7.70
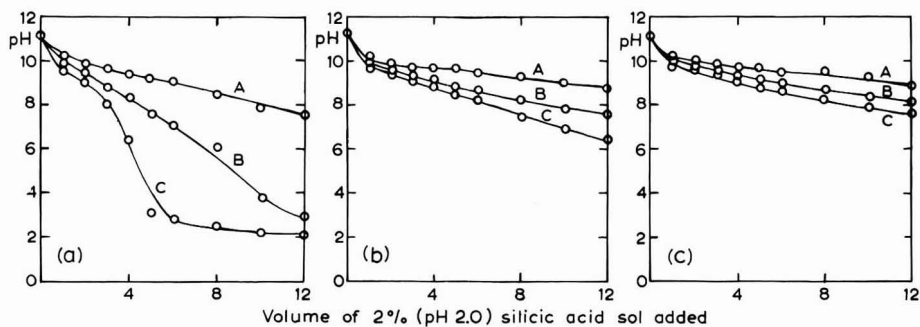
Fig. 1. pH-metric titration curves: (A) soybean + sol, (B) hemoglobin + sol, (C) KOH + sol.

On titrating a 2% silicic acid sol at pH 2.0 with KOH of the same pH as the protein solution (pH 12.0) a typical acid–base titration curve with a sharp inflexion in the pH range 2.5–9.5 was obtained (Fig. 1a). In this region silicic acid exists in the form of polysilicic acid[13-15]. There is another small inflexion in the pH range 9.5–11.0; this represents the depolymerised state of the silicic acid which results in the formation of disilicate $(Si_2O_5^{2-})$ ions.

On replacing KOH with hemoglobin of the same pH (pH 12.0) there is a shift in the titration curve towards a higher pH (Fig. 1a). The two curves almost coincide up to pH 9.5 showing that disilicate ions do not react with this protein. After pH 9.5 the two curves start to separate and binding occurs in the intermediate pH range 3.0–7.0. The binding involves interaction between the hydrogen of the silanol group of polysilicic acid and the reactive groups of the protein. Since the silanol group shows a slight tendency to ionisation, the reaction also takes place through the SiO^- groups of the silicic acid. Also, since polymerisation is catalysed at high pH, the reaction of silicic acid with the protein would bring about its rapid polymerisation.

The groups available from the protein for the reaction in the pH range 3.0–7.0 are carboxyl (both ionised and unionised), protonated and unprotonated imidazol, amino and guanidino. Their reactions with the silanol groups of the polysilicic acid can be represented as follows:

(i)　$-\overset{|}{\underset{|}{Si}}-OH + \underset{HO}{\overset{O}{>}}C- \rightarrow -\overset{|}{\underset{|}{Si}}-O-H\cdots\underset{HO}{\overset{O}{>}}C-$　(at low pH)

(ii)　$-\overset{|}{\underset{|}{Si}}-OH + \underset{O}{\overset{O}{>}}C \rightarrow -\overset{|}{\underset{|}{Si}}-O-H\cdots\underset{O}{\overset{O}{>}}C-$　(above pH 5.0)

(iii)　$-\overset{|}{\underset{|}{Si}}-OH + N-H_2 \rightarrow -\overset{|}{\underset{|}{Si}}-O-H\cdots NH_2$　(uncharged nitrogen atom)

(iv)　$-\overset{|}{\underset{|}{Si}}-\overset{-}{O} + H-\underset{H}{\overset{|}{N}}- \rightarrow -\overset{|}{\underset{|}{Si}}-\overset{-}{O}\cdots H-\overset{H}{\overset{|}{N}}-$

(v)　$-\overset{|}{\underset{|}{Si}}-\overset{-}{O} + H-\underset{H}{\overset{+}{N}}- \rightarrow -\overset{|}{\underset{|}{Si}}-\overset{-}{O}\cdots H-\underset{H}{\overset{+}{N}}-$
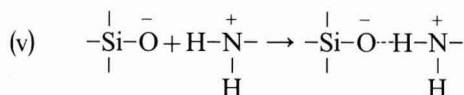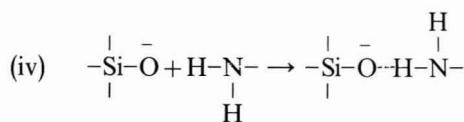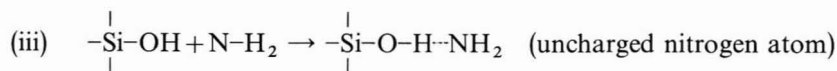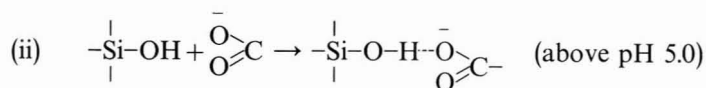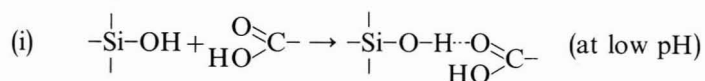
In the last case the presence of a positive charge on the nitrogen atom significantly enhances the strength of the hydrogen bond[16]. Since the nitrogen atoms in the pH range 3.0–7.0 are mostly positively charged and the silanol group may be in the ionised form $(SiOH = SiO^- + H^+)$ hydrogen bond formation between positive nitrogen atoms and the SiO^- groups is possible.

The titration curves of silicic acid with soybean protein are of a similar nature; the only difference is that the curves are shifted towards a higher pH. This means that soybean proteins bind more silicic acid than hemoglobin. The mechanism of the reaction would, however, be the same as in the case of hemoglobin.

The variations in pH are quite marked with a silicic acid sol of pH 2.0 and the binding can be calculated fairly well. The amount of silicic acid bound per gram of each protein has been determined from the difference in the amount of silicic acid taken up by alkali at any particular pH and that consumed by the proteins for binding at the same pH. The binding data for the two proteins are given in Table 2.

TABLE 2

AMOUNT OF SILICIC ACID BOUND PER GRAM OF PROTEIN AT DIFFERENT pH VALUES

pH	Silicic acid combined per g hemoglobin/g	Silicic acid combined per g of soybean/g
7.5	0.50	2.20
8.0	0.45	1.80
8.5	0.32	1.40
9.0	0.20	1.00
9.5	0.125	0.675
10.0	0.102	0.200
10.5	0.05	0.075

From Table 2 it is evident that soybean protein binds a larger amount of silicic acid than hemoglobin in the pH range 7.5–10.5. The difference in behaviour between the two proteins towards silicic acid is understandable since silica is well known for its role in forming the structural framework of certain plants (*e.g.* bamboos, equisetum, chara, etc.) and also in enhancing their phosphorus metabolism.

Silicic acid solutions of pH 2.5 and 3.0 should exist in a much more polymerised form than those at pH 2.0. Here the possibility of interaction of the proteins with silicic acid through hydrogen bond formation should be enhanced. The titration curves (Figs. 1b and 1c) in these two cases are shifted to higher pH values than in the case of silicic acid of pH 2.0 but it is not possible to calculate the binding owing to the nature of the silicic acid–KOH curves. It appears that silicic acid at pH 2.5 and 3.0 is devoid of its acidic character and the polymerised state with its predominantly siloxane groups (Si O–Si) is present. The presence of these groups does not allow interaction with the hydroxyl ions of the alkali.

SUMMARY

A comparison of the pH titrations of proteins or KOH of the same pH (12.0) with silicic acid sol of different initial pH, *i.e.* 2.0, 2.5 and 3.0, has shown that silicic acid of pH 2.0 reacts in a different way to that of solutions at pH 2.5 and 3.0. The titration curves of silicic acid sols of pH 2.0 with KOH of pH 12.0 show two inflexions corresponding to polysilicic acid (pH 2.5–9.5) and a depolymerised state, *i.e.* disilicate ions (pH 9.5–11.0). The binding of silicic acid to proteins is realised in the pH range 3.0–7.0. It has also been shown that soybean protein binds a larger amount of silicic acid than hemoglobin.

REFERENCES

1 W. PAULI, *Trans. Faraday Soc.*, 26 (1930) 723; W. PAULI AND P. DESSAWAR, *Helv. Chim. Acta*, 25 (1942) 225.
2 E. I. KRYAT, *Colloid J. (USSR)*, *English Transl.*, 5 (1939) 399, 449.
3 T. GRAHAM, *J. Chem. Soc.*, 15 (1862) 216.
4 F. MYLIUM AND E. GRASSCHUFF, *Ber. Deut. Chem. Ges.*, 39 (1906) 116.
5 W. J. LESLEY, *Trans. Faraday Soc.*, 25 (1929) 507; 26 (1930) 69.
6 S. G. CLARK, P. F. HOLT AND C. W. WENT, *Trans. Faraday Soc.*, 53 (1957) 1500.
7 S. G. CLARK, P. F. HOLT AND C. W. WENT, *Trans. Faraday Soc.*, 53 (1957) 1509.
8 I. BERGMAN AND E. S. NELSON, *J. Colloid Sci.*, 17 (1962) 823.
9 M. I. SHVAIGER, *Novye Metody Analiza na. Met.*, (1964) 117 (Russ).
10 KUNIHIKO SUMINOKURA, *J. Agr. Chem. Soc.*, *Japan*, 15A (1939) 133.
11 J. STEINHARDT AND E. M. ZAISER, *J. Am. Chem. Soc.*, 75 (1953) 1599; *J. Biol. Chem.*, 190 (1951) 197.
12 I. M. KOLTHOFF AND E. B. SANDELL, *Text Book of Quantitative Inorganic Analysis*, The Macmillan Co., New York, 3rd edn., 1952.
13 W. D. TREADWELL AND W. KONING, *Helv. Chim. Acta*, 16 (1933) 468.
14 H. T. S. BRITTON, *J. Chem. Soc.*, (1927) 425.
15 B. CHATTERJI, *J. Ind. Chem. Soc.*, 16 (1939) 586.
16 L. PAULING, *Nature of the Chemical Bond*, Cornell University Press, Ithaca, N.Y., 1940, p. 307.

SHORT COMMUNICATIONS

Studies on the composition and stability of uranyl, vanadyl and titanous complexes with some aminoacids

A number of papers on the metal complexes of amino acids[1-4] have appeared in the literature in recent years. These studies are mainly concerned with the determination of the stability constant of a complex by various electrometric methods, *viz.* potentiometry, pH-metry, polarography, etc. References to studies on the complexes of Cu, Zn, Fe, Ni, Co, Mn, Cd and other transition metals are available but no attempt has yet been made to investigate possible complex formation between VO^{2+}, UO_2^{2+} and Ti^{3+} ions with amino acids.

The present communication deals with the behaviour of these ions towards some amino acids. Formation of 1 : 1 complexes has been indicated by conducto-metric titrations, and the stability constants of the complexes have been computed from the results of pH-metric titrations.

Experimental

Amino acids such as glycine, β-alanine, DL-α-alanine, L-asparagine, DL-serine, L-leucine, DL-valine and L-proline (B.D.H. biologically pure) were used for the experiments, and their solutions (0.01 *M*) were prepared in doubly-distilled water.

Uranyl sulphate (B.D.H. AnalaR), and vanadyl sulphate (B.D.H.) were employed and solutions of these salts were analysed gravimetrically as the metal oxides[5,6]. An aqueous solution of titanium(III) chloride was prepared by dissolving crystals[7] of $TiCl_3 \cdot 6 H_2O$ in air-free doubly-distilled water, and the solution standardized[8]. Fresh solutions were always prepared before use and kept covered with a layer of kerosene oil or toluene throughout the investigations to avoid oxidation.

Carbonate-free KOH solution was used for pH-metric titrations. It was stored in a Pyrex bottle fitted with a KOH tube for protection against atmospheric CO_2. The solution was standardized by titrating with standard oxalic acid solution, and the strength was checked periodically before carrying out pH-metric titrations.

The conductometric titrations were performed using a Philips conductivity bridge model PR 9500/90 and a dip type conductivity cell (cell constant 1.48). The pH-metric titrations were carried out with a direct reading EIL pH-meter model 23A using glass and calomel electrodes. All the titrations were carried out in a specially designed cell, with provision for adding metal salt solutions from a burette, to a stirred oxygen-free system.

Results and discussion

The composition of the vanadyl, uranyl and titanous complexes with various amino acids was determined conductometrically. The conductometric titrations were reversible. In all cases a ratio of 1 : 1 (metal : amino acid) was established. Typical curves are given in Fig. 1. The pH-metric titrations were performed in triplicate for each amino acid. The titrations were carried out in the order: (a) amino acid (0.01 *M*),
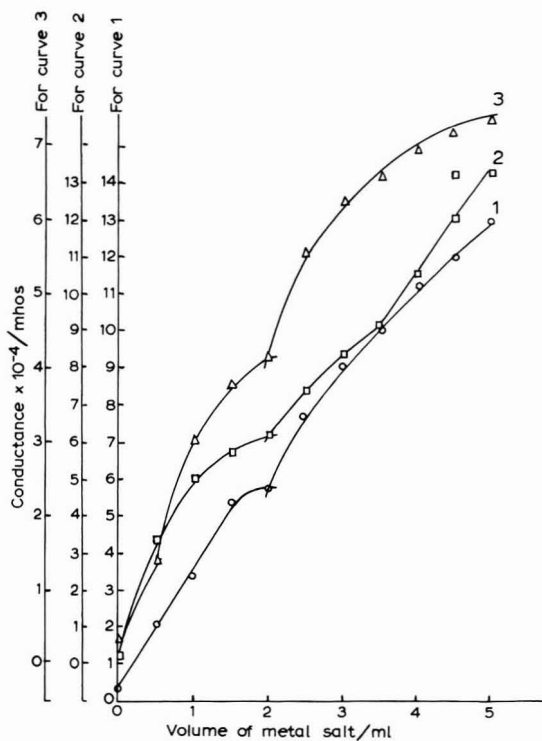
Fig. 1. Reverse conductometric titrations: (1) $M/15$ $TiCl_3$ added to 40 ml of $M/300$ DL-serine, (2) $M/12$ UO_2SO_4 added to 40 ml of $M/240$ DL-α-alanine, (3) $M/15$ $VOSO_4$ added to 40 ml of $M/300$ DL-valine.
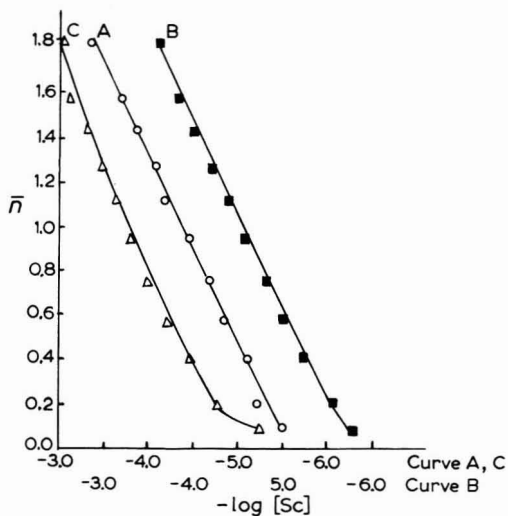
Fig. 2. Formation curves: (A) DL-valine–$VOSO_4$ complex, (B) DL-α-alanine–UO_2SO_4 complex, (C) DL-serine–$TiCl_3$ complex.
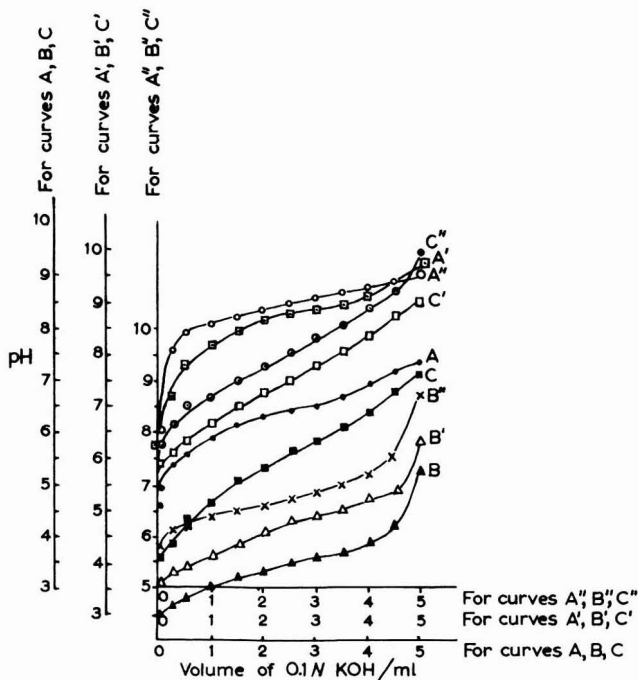
Fig. 3. pH-metric titrations: (A, B, C) DL-serine–TiCl$_3$, (A', B', C') DL-α-alanine–UO$_2$SO$_4$, (A'', B'', C'') DL-valine–VOSO$_4$.

TABLE 1

VALUES OF LOG $(K_s/\text{mol}^2\,\text{l}^{-2})$ FOR VANADYL, URANYL AND TITANOUS AMINO ACIDS COMPLEXES OBTAINED BY TWO METHODS

Amino acids	Vanadyl sulphate		Uranyl sulphate		Titanous chloride	
	Theo-retical	Graphi-cal	Theo-retical	Graphi-cal	Theo-retical	Graphi-cal
L-Asparagine	6.95	6.90	6.88	6.85	7.25	7.20
β-Alanine	9.77	9.80	9.92	9.90	9.72	9.70
DL-α-Alanine	8.75	8.70	9.00	9.00	8.53	8.50
Glycine	× ×	× ×	8.62	8.65	8.52	8.50
L-Leucine	9.08	9.10	8.61	8.60	8.55	8.50
L-Proline	10.33	10.30	10.46	10.45	10.08	10.05
DL-Serine	7.54	7.50	6.86	6.90	7.60	7.60
DL-Valine	8.65	8.65	8.59	8.60	8.12	8.20

(b) metal salt (0.005 M) and (c) metal salt and amino acid (total concentration 0.005 M and 0.01 M, respectively), employing 0.1 N KOH as titrant. The pH-titration curves show appreciable shifts, indicating the formation of complexes with the amino acid (Fig. 3). The complex formation constant K_s was evaluated by the method modified by Albert[4].

The values of log K_s at $\bar{n}=1$, where $\bar{n}$ is the average number of molecules of

amino acid bound by one atom of the metal ion, were calculated from the values of $-\log[Sc]$ obtained by plotting $\bar{n}$ vs. $-\log[Sc]$ (Fig. 2). $[Sc]$ is the concentration of the free amino acid. The values of $\log K_s$ for various amino acids evaluated from the formation curves, and those calculated are given in Table 1.

The values of the overall stability constants $\log K_s$ obtained from the formation curves (Fig. 2), are in good agreement with those calculated.

Uranyl sulphate, vanadyl sulphate and titanous chloride form 1 : 1 complexes with various amino acids (L-asparagine, β-alanine, DL-α-alanine, glycine, L-leucine, L-proline, L-serine and DL-valine). In the vanadyl and titanous complexes the values of $\log K_s$ vary from L-asparagine (6.95, 7.25) to L-proline (10.33, 10.08), whereas in uranyl complexes the variation is from DL-serine (6.86) to L-proline (10.46). There does not seem to be any correlation between the nature of the aminoacids and the K_s values although, with a few exceptions, the latter decreases with increase in chain length of carbon atoms. The real nature of bonding in these complexes is a matter of speculation as no complex could be isolated in a sufficiently pure form.

Department of Chemistry,   Omar Farooq
Aligarh Muslim University,   A. U. Malik
Aligarh (India)   N. Ahmad*
                                                             S. M. F. Rahman

1 D. J. PERKIN, *Biochem. J.*, 51 (1952) 487.
2 J. B. GILBERT, O. CLYDE AND J. Z. HEARON, *J. Am. Chem. Soc.*, 77 (1955) 2599.
3 A. A. KHAN AND W. U. MALIK, *J. Indian Chem. Soc.*, 40 (1963) 565.
4 A. ALBERT, *Biochem. J.*, 47 (1950) 531.
5 A. C. CUMMING AND S. A. KAY, *Quantitative Chemical Analysis*, Oliver and Boyd, London, IX edn., 1945, p. 367.
6 N. H. FURMAN (Ed.), *Standard Methods of Chemical Analysis, Vol. 1*, D. van Nostrand, New York, VI edn., 1962, p. 1189.
7 J. W. MELLOR, *Inorganic and Theoretical Chemistry, Vol. VII*, Longmans, London, 1963, p. 74.
8 N. H. FURMAN (Ed.), *Standard Methods of Chemical Analysis, Vol. 1*, D. van Nostrand, New York, VI edn., 1962, p. 984.

---

* Present address: Department of Chemistry, Louisiana State University, Baton Rouge, La. 70803, U.S.A.

COMMENTS ON "ELECTROCHEMICAL REDUCTION AND HYDROGEN EVOLUTION ON GERMANIUM ELECTRODES"*

BY R. MEMMING AND G. NEUMANN

In a recent publication on the effect of hydrofluoric acid on the surface properties of germanium electrodes during anodic dissolution[1] we described an experiment which showed that after anodic polarisation oxidation products could be detected in the electrolyte by applying a ramp shaped potential–time profile to a germanium disc electrode. The potential of the electrode was held for 15 s at $+650$ mV $vs.$ NHE, then a linear potential sweep was applied until the electrode potential fell to -950 mV $vs.$ NHE. For 1 N H_2SO_4 it was observed that the current was stirring dependent. It had the effect of splitting a rather broad current maximum at about -350 mV into two less prominent ones at -250 and -450 mV. (Notice that in Fig. 4 the captions for curves 1 and 4 should be interchanged.) Our explanation for this effect was that oxidation products, the exact nature of which we did not investigate, build up at the surface of the electrode while it was kept at $+650$ mV. During the cathodic sweep these products will be reduced leading to a large current maximum. At the rotating disc electrode these products cannot accumulate so that a smaller current maximum is observed which is caused by the reduction of surface groups mainly.

These findings have recently been criticized[2]. The authors concluded that our results implied the formation of a surface film, probably germanium oxide, which should be detectable with an ellipsometer. As such a film was shown not to exist it was stated that the reduction of oxygen was a more reasonable explanation for the cathodic maximum. It seems to us that the discussion of our measurements by these authors contains two flaws:

1. It is highly unlikely that a stirring dependent reduction current is caused by an oxide film. Thus looking for one with an ellipsometer does not seem to be a very sensible experiment.

2. On stirring the reduction current decreased in magnitude. Thus it must be caused by products which diffuse away from the surface and not oxygen which would diffuse to the surface and cause an increase of the current on stirring.

Thus we conclude that the reduction of oxygen does not appear to be a valid explanation for our experiments.

Orbisphere Corporation,   W. Mehl
91, route de la Capite,
CH 1223 Cologny, Geneva (Switzerland)

CIBA A.G.,   F. Lohmann
CH 4000 Basel 7 (Switzerland)

1 W. MEHL AND F. LOHMANN, *Ber. Bunsenges. Physik. Chem.*, 71 (1967) 1055.
2 R. MEMMING AND G. NEUMANN, *J. Electroanal. Chem.*, 21 (1969) 295.

* *J. Electroanal. Chem.*, 21 (1969) 295.

REPLY TO DR. MEHL'S COMMENT ON OUR PAPER "ELECTROCHEMI-CAL REDUCTION AND HYDROGEN EVOLUTION ON GERMANIUM ELECTRODES"*

As mentioned in their comment Mehl and Lohmann interpreted their results assuming oxidation products to be built up at the germanium surface during anodic polarization in H_2SO_4. Moreover these authors observed a decrease of the corresponding reduction current stirring the electrolyte.

First of all it should be mentioned it is rather difficult to compare our results with those obtained by Mehl and Lohmann because of several reasons:

(1) As we have shown in our paper the pretreatment of the electrode (etching, orientation, *etc.*) is very important for the measurements.

(2) We used *n*-type Ge whereas Mehl and Lohmann performed corresponding measurements with *p*-type Ge. For our investigations of cathodic processes *n*-type Ge turned out to be much better than *p*-type material.

Therefore we did not want to criticise Mehl and Lohmann's interpretation. As mentioned in our paper we only could not interpret our results using the same model. We observed several current peaks sweeping the potential into the cathodic direction. Whereas two peaks are due to the formation of a hydride surface the third current peak depends on the concentration of oxygen and increased on stirring. It may be that much less oxidation products are formed on *n*-Ge than on *p*-Ge.

As far as the sensitivity of ellipsometric measurements is concerned it is certainly true that this is not a useful tool for detecting oxidation products dissolved in the electrolyte. Since Mehl and Lohmann mentioned that oxidation products are built up at the surface we expected germanium oxides which are not very soluble in acid solutions to remain as a spongy layer, *e.g.* at the surface. Nevertheless our results indicate—as outlined above—that the germanium hydroxide is transformed into a hydride surface during cathodic polarization and oxygen is reduced as soon as the hydride surface is complete.

Philips Zentrallaboratorium GMBH,   R. Memming
2 Hamburg 54,   G. Neumann
Vogt-Kölln-Strasse 30, (Deutschland)

---

* *J. Electroanal. Chem.*, 21 (1969) 295.

ANNOUNCEMENTS

IUPAC INTERNATIONAL CONGRESS ON ANALYTICAL CHEMISTRY

KYOTO, APRIL 3-7, 1972

Organized by The Japan Society for Analytical Chemistry

To celebrate its Twentieth Jubilee, the Japan Society for Analytical Chemistry is planning to hold an International Congress on Analytical Chemistry in 1972. It will be held from the 3rd to the 7th of April at the Kyoto International Conference Hall. About one thousand participants, including several hundred from abroad, are expected.

Proposed programme

The scientific programme will cover most areas of analytical chemistry. Topics will include various types of electrochemical analysis including polarography, optical analysis including mass spectroscopy, radiochemical analysis, chromatography, and organic analysis. Special emphasis will be given to trace analysis and the use of non-aqueous solvents.

Further information

Those wishing to obtain information regarding the Congress are requested to contact the Organizing Committee:

Organizing Committee,
International Congress on Analytical Chemistry,
Kyoto International Conference Hall,
Takaraike, Sakyo-ku,
Kyoto, Japan.

FUTURE MEETINGS OF CITCE

21ST MEETING OF CITCE

Prague, Czechoslovakia,
September 28 to October 2, 1970

This will be a full meeting. The main themes will be:
- Structural effects in inorganic and organic electrochemical processes.
- Non-aqueous solvents (with the main emphasis on instrumentation and the role of the solvent in the mechanisms of electrode reactions).
- Double layer influence on the mechanisms of electrode processes.

Besides the sessions on the main themes, there will be sessions under the auspices of the Sections of CITCE.

For further information and registration please apply to: Dr. J. Kůta, Polarographic Institute, Czechoslovak Academy of Sciences, Vlašská 9, Prague 1, Czechoslovakia.

22nd Meeting of CITCE, Dubrovnik, Yugoslavia, September 21 to 27, 1971

This will be a restricted meeting, devoted to "Electrochemistry of non-metallic electrodes".

CITCE Colloquium, Rome, Italy, Spring 1971

This colloquium will be devoted to "Biological aspects of electrochemistry". The exact date will be announced in due course.

23rd Meeting of CITCE, Stockholm, Sweden, Autumn 1972

This will be a full meeting. Two symposia will be held:
- Accelerated corrosion testing with electrochemical methods.
- Electrochemical engineering.

Besides the two symposia, sessions under the auspices of the Sections of CITCE will be held. The exact data will be announced in due time.

For further information, please apply to the Secretary General of CITCE: Dr. H. Tannenberger, Institut Battelle, 7, route de Drize, 1227 Carouge-Genève, Switzerland.

BOOK REVIEW

Practical Polarography, by J. Heyrovský and P. Zuman, Academic Press, London and New York, 1968, viii + 237 pages, 50s.

This volume is a translation of the second Czech edition published in 1964, with some additional material. The approach is limited to the practical aspects of polarography; some doubts about the wisdom of the complete neglect of theory are voiced by the junior author in his preface. Even if the view that the text should be comprehensible to the average technician is accepted, present day training would require some knowledge of theory as surely we are trying to move away from the concept of technician as a pair of hands only. The other aspect which has a dated flavour is contained in the twenty or so pages devoted to photographic recording polarographs, in contrast to a much abbreviated discussion of pen-recording instruments inserted for this edition.

Certainly for a laboratory taking up polarography with no previous practical experience the first three chapters devoted to handling and interpretation abound in useful tips which could save much time and frustration. A section on hazards contains the questionable suggestion that a vacuum cleaner is essential in keeping down mercury contamination, it is also an extremely effective means of introducing large quantities of mercury vapour into the laboratory atmosphere from small quantities of spilled mercury. There is a section on a fairly representative selection of simple determinations which might be useful for teaching at an elementary level. An indication of applications to real problems is given with experimental details. The collection of half-wave potentials and buffers would be useful to laboratories not possessing library facilities, but the bibliography will not help those with limited resources as most of the references are to the Czech literature. This may be justifiable on grounds of priority but is hardly helpful in an edition for western countries.

All in all this is a rather disappointing book. It will be useful mainly for those starting from scratch who wish to use polarography as a very routine analytical method and they will find little help in extending their knowledge outside the book's boundaries.

M. E. Peover, National Physical Laboratory

JOURNAL OF ELECTROANALYTICAL CHEMISTRY AND INTERFACIAL ELECTROCHEMISTRY, VOLUME 24, 1970

AUTHOR INDEX

JOURNAL OF ELECTROANALYTICAL CHEMISTRY AND INTERFACIAL ELECTROCHEMISTRY, VOLUME 24, 1970

SUBJECT INDEX

Preliminary Note

Anodic oxidation of the product(s) of the scavenger-solvated electron reaction at an irradiated mercury electrode in electrolytes

I. LEVIN and P. DELAHAY

Department of Chemistry, New York University, 4 Washington Place, New York, N.Y. 10003 (U.S.A.)

Since Barker's fundamental paper[1] on photocurrents at an ideal polarized mercury electrode in aqueous electrolyte solutions progress has been made on detailed studies, quantum mechanical interpretation and instrumentation. There is not universal agreement on the mechanism proposed by Barker – photoelectron emission followed by electron solvation and subsequent reaction with a scavenger – but his views are widely accepted for a number of processes. Not much attention was paid to the electrode processes subsequent to the scavenger-solvated electron reaction. Barker[2] did infer from his results that the product(s), presumably H-atoms and/or H_2^+, of the hydrogen ion-solvated electron scavenger reaction is oxidized at the electrode, at least when the potential is not too negative. He also elaborated on the reactions with N_2O as a scavenger. A method for *measuring* such anodic currents is described here and is applied to two scavengers, namely, hydrogen ion and nitrous oxide. The sign of the ionic valence of the species being oxidized is tentatively ascertained from double-layer effects.

The technique was the same as in a previous study[3], but equipment was completely redesigned and improved. The principle is as follows:

A dropping mercury electrode (to minimize electrode contamination) is set at a given potential against a reference electrode (0.1 NCE); the electrode circuit is open at a given stage of the drop life, and the electrode is flash-irradiated with polychromatic light for less than 1 ms; potential–time variations are recorded with an oscilloscope from a time before irradiation (≈ 20 ms) to some time afterwards (≈ 50 ms). The current for double-layer charging, caused by expansion of the mercury drop, as well as any spurious faradaic current, is compensated for. The potential–time curve in the absence of any complication thus is a step function. A charge-injection (coulostatic) experiment is also performed under identical conditions but without irradiation. The electronic charge lost by photoelectron emission is directly computed from the two potential steps observed separately with irradiation and with injection of a known charge without irradiation.

It is observed that coulostatic potential–time curves in presence of scavenger have the expected shape of a step function when double-layer charging is properly compensated for. However, the curves obtained by flash irradiation with scavenger show
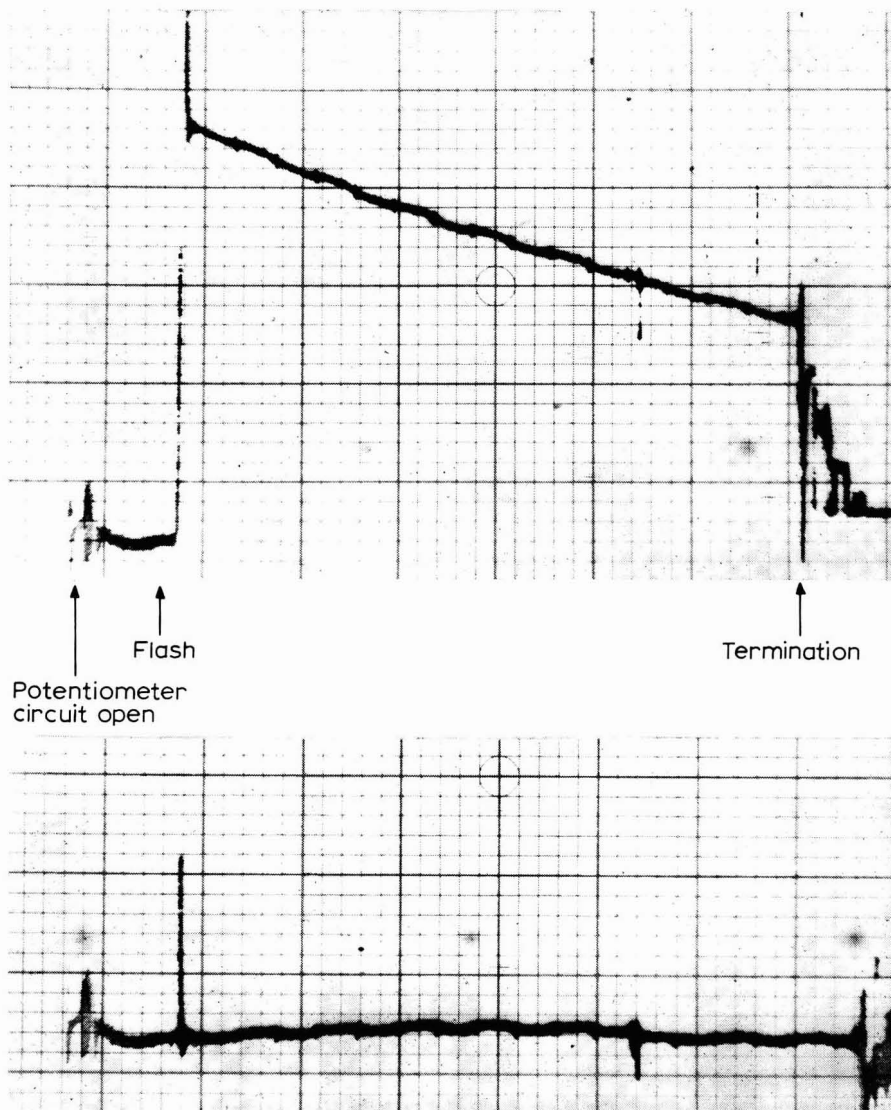
Fig.1. Potential–time trace for 0.1 M NaF saturated with N_2O at –1.2 V $vs.$ 0.1 NCE in Pyrex cell. Scales: 20 ms per main horizontal division; 2 mV per main vertical division. Upper trace obtained with electrode irradiation; lower trace obtained with flash operating but with opaque screen in front of cell (thus showing good compensation setting).
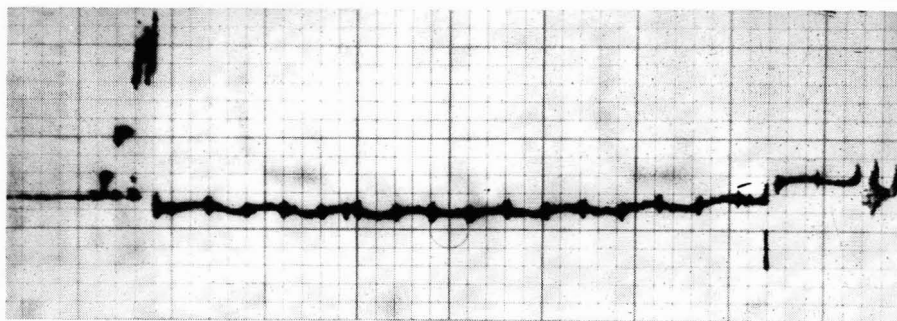
Fig.2. Potential–time trace for 0.1 M NaF without N_2O at –1.4 V $vs.$ 0.1 NCE in quartz cell. Scales: 20 ms per main horizontal division; 1 mV per main vertical division. Maximum flash intensity.

a pronounced drift of potential toward cathodic values when the initial segment, prior to irradiation, is horizontal★ (Fig.1). Several possible interpretations can be ruled out.

(*a*) Inadequate compensation cannot be invoked since the usual rectangular pulse was obtained by coulostatic charge injection with the same compensation setting as that used in flash irradiation. In the absence of irradiation or charge injection, the trace is practically horizontal, exhibiting only a slight curvature presumably caused by the variation of the double-layer charging current as a result of the drop growth.

(*b*) Leakage through the oscilloscope input does not account for the drift as was shown with a capacitor working as a dummy cell under charge-injection conditions. The resulting drift did not exceed 10% of the values in actual experiments with scavenger and flash irradiation.

(*c*) Operation of the flash did not cause any interference accounting for the decay. This was verified with a dummy cell and with the actual cell (Fig.1, bottom trace).

(*d*) The heating effect reported★★ by Korshunov *et al.*[4] is not the cause of decay of potential in this work. This effect would result in a decay of potential toward positive values in the range of potentials studied here. However, potential–time curves with irradiation but without scavenger did not exhibit any significant decay (Fig.2). The presence of the scavenger would cause the heating effect to show up if the heat of the scavenger-solvated electron reaction was sufficient. This point was not investigated further.

(*e*) Changing conditions at the mercury thread–solution interface, as a result of heating of the capillary by irradiation★★★, do not account for the decay of potential. This effect would show up in experiments without scavenger, but this was not the case (Fig.2).

★This drift was not detected in our previous work[3] because the segment of the potential–time curve before irradiation was too short. Thus, the compensating current, in that work, was adjusted to a value resulting in a horizontal trace after irradiation. The magnitude of the potential step is hardly affected by the choice of compensation procedure – that is, horizontal trace either before or after irradiation – but the information on anodic processes is lost with the procedure previously applied.

★★We are indebted to Dr. R. de Levie[5], Georgetown University, for calling this paper to our attention and for suggesting the experiment without scavenger.

★★★We are indebted to Dr. G.C. Barker, Harwell, for pointing this out as well as the possibility of the photolysis processes discussed below and the possible effect of impurities.

(*f*) One could assume that the decay of potential is caused by the anodic oxidation of the product(s) of some solution photolysis process: solvent photolysis, electron transfer to solvent, photolysis of scavenger in the case of nitrous oxide. All these processes require shorter wavelengths than those transmitted by glass. Actually, the decay of potential was observed as well with glass or quartz cells (Fig.1) and even with an additional glass filter (7 mm thick).

One possibility cannot be ruled out completely: some impurity may be present which would yield a species undergoing anodic oxidation. This is not impossible, but it is noted that experiments were repeated many times with a variety of chemicals over an eight-month period. Consistent results were always obtained.

Unless some overlooked artifact turned out to account for the decay of potential one can reasonably conclude that there is a net anodic process which continues long after flash extinction (flash duration < 1 ms). Moreover, the drift toward the value which the potential had prior to irradiation is significant.

A mathematical model for mixed control by mass transfer and some postulated electrode reaction could be set up with a varying degree of realism, but this is not our purpose here. More simply, we note that the decay of potential appears quite linear for some time after flash irradiation. The corresponding anodic current density is $i = C \, dE/dt$, where C is the differential capacity of the double layer per unit area, and dE/dt is constant for a linear decay. This equation holds for an excursion of potential not exceeding a few millivolts, *i.e.*, for a constant C. The value of C needed to calculate i is obtained directly from the coulostatic experiment. (Of course, it could be determined independently.)

Plots of i against the charge ΔQ lost by flash irradiation, at constant potential are linear. This relationship was verified for 0.1 M KCl saturated with N_2O at -1.0, -1.2 and -1.5 V (vs. 0.1 NCE) for $0 < \Delta Q \leq 3.4$ nanocoulombs and $0 < I \leq 0.044$ μA (Q and I are actual charge and current, not densities). Q was varied by changing the flash intensity. Similar plots, but for a smaller range of Q, are shown below.

The effect of potential and concentration is shown in Fig.3a and 3b for the $NaF–N_2O$ system and in Fig.4a and 4b for $Na_2SO_4–H_2SO_4$. Similar results to those of Fig.4a were also obtained for 0.1 M KCl + 0.05 M HCl and for saturated KCl + 0.05 M HCl. Unless the anodic currents result from some spurious, unsuspected effect, the results of Fig.3 and 4 seem to indicate★ that the species being oxidized is an anion for N_2O and a cation for H_2SO_4. No mechanism is proposed here.

The influence of H^+-concentration is shown in Fig.4c. Increase of H^+-concentration enhances the current, *i.e.*, the effect is in the opposite direction of that shown in Fig.4b. Significant concentration polarization of scavenger is unlikely, especially for 0.05 and 0.5 M H_2SO_4. The results of Fig.4c seem to indicate that H^+-ions participate in the anodic process.

In conclusion, the foregoing observations seem to substantiate an interpretation based on an anodic process. It should be noted that the effects would be hard to detect

---

★The interpretation is based on sole consideration of double-layer effects on the concentration of the species being oxidized. In the range of potentials studied herein (especially for the H_2SO_4 system), the anodic current is probably controlled by the supply of reactant to a first approximation. The effect of potential is then reflected only in the change of double-layer structure.
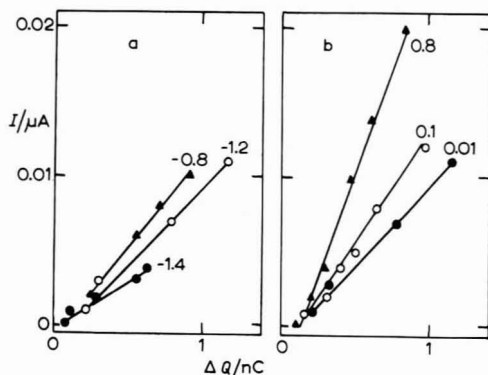
Fig.3. Plot of anodic current I against the charge ΔQ lost by photoelectron emission for a mercury electrode in NaF solution saturated with N_2O at room temperature. Quartz cell: (a) 0.01 M NaF at 3 potentials (V $vs.$ 0.1 NCE), (b) 3 NaF molar concentrations at -1.2 V $vs.$ 0.1 NCE.
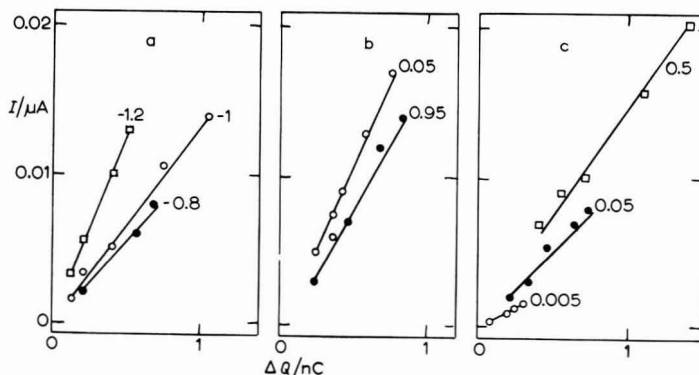
Fig.4. Plot of I against ΔQ for $Na_2SO_4 + H_2SO_4$ at room temperature. Quartz cell:
(a) 0.05 M Na_2SO_4 + 0.025 M H_2SO_4 at 3 potentials (V $vs.$ 0.1 NCE), (b) 0.05 M H_2SO_4 + Na_2SO_4 ((○) 0.05 M, (●) 0.95 M) at -1.1 V $vs.$ 0.1 NCE, (c) 1 M Na_2SO_4 + H_2SO_4 ((○) 0.005 M, (●) 0.05 M, (□) 0.5 M) at -0.9 V $vs.$ 0.1 NCE.

directly upon square pulse irradiation, as used by Barker[6], because the anodic current is quite negligible in comparison with the photocurrent. It is seem from Figs. 3 and 4 that $I \approx 0.01$ μA for $\Delta Q = 1$ nanocoulomb. Since the flash duration was shorter than 1 ms, the average photocurrent was ≈ 1 μA, $i.e.$ $I \approx 1\%$ of the photocurrent.

1 G.C. Barker and A.W. Gardner, paper presented at the 1963 Moscow meeting of C.I.T.C.E.
2 G.C. Barker, A.W. Gardner and D.C. Sammon, $J.$ $Electrochem.$ $Soc.,$ 113 (1966) 1182
3 V.P. Sharma, P. Delahay, G.G. Susbielles and G. Tessari, $J.$ $Elektroanal.$ $Chem.,$ 16 (1968) 285.
4 L.I. Korshunov, Ya,M. Zolotovitskii and V.A. Benderskii, $Elektrokhimiya,$ 4 (1968) 499.
5 R. De Levie, private communication.
6 G.C. Barker, private communication.

Preliminary Note

Adsorption of maleate and fumarate ions at the mercury—water interface

ROGER PARSONS and J.T. REILLY

Department of Physical Chemistry, University of Bristol, Bristol BS8 1TS (Great Britain)

(Received December 3rd, 1969)

Recent work[1] on the adsorption of the optical isomers of dibenzoyl tartaric acid indicated that their behaviour at the interface was identical but that marked differences were observed with the racemic mixture. It was proposed that this was due to the adsorption of D–L couples. The geometrically isomeric acids, maleic and fumaric, were studied by Korchinsky[2] by the electrocapillary method. Differences were observed which were compatible with the structure of the isomers. No detailed study has yet been made of the adsorption of isomeric *ions*. The present work was undertaken to investigate the properties of the mercury—aqueous solution interface when such ions are adsorbed.

Water was purified by triple distillation. Sodium maleate and sodium fumarate (British Drug Houses Ltd.) were recrystallized from this water after treatment of the solutions with activated charcoal. The salt was dried finally in a desiccator over silica gel. Mercury was purified as described previously[3]. The reference electrode was a dip-type saturated calomel electrode. It was dipped into a 0.1 mol l^{-1} solution of salt (maleate or fumarate); contact with the working solution being then made in a glass tap. Capacities were measured using the bridge previously described[4]. No significant dispersion with frequency was observed. The point of zero charge was found using a streaming mercury electrode[5].

The capacity curves for solutions containing 1 mol l^{-1} of each salt at 25°C are shown in Fig.1. It is evident that the two anions yield capacity curves which differ considerably in shape in the region where specific adsorption of the anions would be expected. In the presence of fumarate the capacity shows a large 'hump' close to the point of zero charge followed on the positive side by a deep minimum. This behaviour is similar to that shown by perchlorate or hexafluorophosphate ion but the peak value of the capacity is higher. On the other hand in the presence of maleate ion the 'hump' is almost suppressed while the steep rise in capacity occurs at a potential 0.25 V more negative than in the presence of fumarate. Preliminary measurements of electrocapillary curves suggest that the two isomers are adsorbed approximately equally. Thus the difference in the capacity curves must be due to the difference in the location of the adsorbed charge in the inner layer. General considerations suggest that the carbon—carbon axis in both anions is probably oriented parallel to the plane of the interface. In the fumarate ion the carboxyl groups will then both be close to the mercury surface while those of the
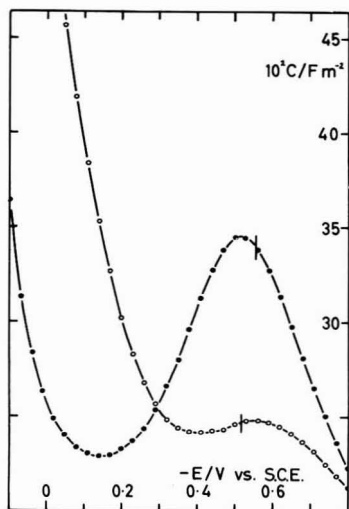
Fig.1. Capacity per unit area of a mercury electrode in contact with aqueous solutions containing: (o−o) 1 mol l^{-1} sodium maleate; (●−●) 1 mol l^{-1} sodium fumarate. Measurements were made at 1 kHz and 25° C against a saturated calomel electrode dipping into a 0.1 mol l^{-1} solution of the appropriate salt. The potential of zero charge is indicated by the vertical bar on each curve.

maleate ion are able to project towards the solution. The centre of gravity of adsorbed negative charge is thus closer to the mercury when fumarate is adsorbed than when maleate is adsorbed. This is consistent with the more negative position of the point of zero charge in the presence of the former, but does not in itself explain the variation in the magnitude of the 'hump'. A possible explanation of the latter is that it is due to the interaction of water molecules with the adsorbed anions (cf. ref.6). The maleate ion with the negative charge further from the mercury may stabilise the orientation of water molecules with the oxygen atom towards the mercury. This is the orientation stable at positive charge on the electrode so that no re-orientation occurs in the region in which the anion is specifically adsorbed. On the other hand when the adsorbed negative charge is very close to the metal surface as with the fumarate the opposite orientation of water molecules will be favoured. As the charge becomes more positive these water molecules will be re-oriented, the result being a large 'hump' in the capacity curve.

This explanation is at present tentative; more detailed measurements and further analysis are necessary to confirm this. It is hoped to present these in the near future.

REFERENCES

1 A. Inesi, F. Rallo and L. Rampazzo, *Trans. Faraday Soc.*, 64 (1968) 3340.
2 G.A. Korchinsky, *Ukrain. Khim. Zh.*, 29 (1963) 1031.
3 J.D. Garnish and R. Parsons, *Trans. Faraday Soc.*, 63 (1967) 1754.
4 G.J. Hills and R. Payne, *Trans. Faraday Soc.*, 61 (1965) 316.
5 D.C. Grahame, R.P. Larsen and M.A. Poth, *J. Am. Chem. Soc.*, 71 (1949) 2978.
6 E. Schwartz, B.B. Damaskin and A.N. Frumkin, *Zh. Fiz. Khim.*, 36 (1962) 2419.

Preliminary Note

Mechanism of the oxygen electrode in molten salts
A unitary interpretation of potentiometric findings in unbuffered melts

PIER GIORGIO ZAMBONIN

Istituto di Chimica Analitica, via Amendola 173, Universita' di Bari, Bari (Italy)

Recently, Wrench and Inman[1] have presented a convincing experimental study on the oxygen electrode in molten chlorides. These authors, adding Li_2O to a $(Li,K)Cl$ eutectic melt at $723°K$ under oxygen flow at the pressure of one atmosphere, observed a slope $2.3 RT/F$ for the plot of E (the equilibrium potential of a platinum or gold electrode dipping in the system) *versus* the logarithm of the added oxide concentration. The same Nernst slope has been previously obtained in molten potassium nitrates at $623°K$ by Shams El Din and Gerges[2]. These authors also report that similar (unpublished) results had been obtained in other laboratories.

Such potentiometric findings, unexpected on the basis of previous theories concerning oxygen—oxide systems, have been tentatively explained by the various authors in different ways, mainly on the basis of an irreversible behaviour of the system. Since then it has been suggested[3,4] that the electrode process:

$$O_2 + e = O_2^- \tag{1}$$

which has been demonstrated[4,5] to be polarographically reversible on noble metal electrodes at high temperature, might offer an interpretation for these potentiometric data.

In effect, this last hypothesis seems reasonable if analyzed in the light of the most recently acquired knowledge on oxygen—oxides systems. In ionic solvents, the oxide ion can be oxidized[4–6] to peroxide and superoxide according to the reactions:

$$2 O^{2-} + O_2 = 2 O_2^{2-} \quad K_2 = [O_2^{2-}]^2/[O_2] [O^{2-}]^2 \tag{2}$$

and
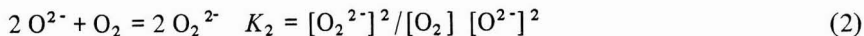
$$O_2^{2-} + O_2 = 2 O_2^- \quad K_3 = [O_2^-]^2/[O_2^{2-}] [O_2] \tag{3}$$
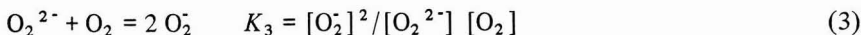
So, when oxygen flows in an oxide (or peroxide) solution, all the species: O^{2-}, O_2^{2-}, O_2^-, O_2 can be simultaneously present. The corresponding potential-determining electrode processes are summarized in Table 1 (column 1). The Nernst equation for each of them can be expressed in the form:

$$E = E' \, f(\alpha, \beta) + \gamma \, \ln [O^{2-}] \tag{4}$$

TABLE 1

VALUES OF E AND γ IN EQUATION 4

Electrode reactions		E'	γ
(a)	$\frac{1}{2}O_2 + 2e = O^{2-}$	$E^0_{O_2/O^{2-}} + (RT/2F)\ln([O_2]^{1/2}/(1-\alpha-\beta))$	$-RT/2F$
(b)	$O_2 + 2e = O_2^{2-}$	$E^0_{O_2/O_2^{2-}} + (RT/2F)\ln([O_2]/\alpha)$	$-RT/2F$
(c)	$O_2 + e = O_2^-$	$E^0_{O_2/O_2^-} + (RT/F)\ln([O_2]/2\beta)$	$-RT/F$
(d)	$O_2^- + 3e = 2O^{2-}$	$E^0_{O_2^-/O^{2-}} + (RT/3F)\ln(2\beta/(1-\alpha-\beta)^2)$	$-RT/3F$
(e)	$O_2^- + e = O_2^{2-}$	$E^0_{O_2^-/O_2^{2-}} + (RT/F)\ln(2\beta/\alpha)$	$-$
(f)	$O_2^{2-} + 2e = 2O^{2-}$	$E^0_{O_2^{2-}/O^{2-}} + (RT/2F)\ln(\alpha/(1-\alpha-\beta)^2)$	$-RT/2F$

where $[O^{2-}]$ is the concentration of the total oxide introduced in the melt, and α and β are the fractions of $[O^{2-}]$ oxidized to peroxide and superoxide respectively. The function E' and the values of γ in the different cases are reported in Table 1 (columns 2 and 3). It follows that E can be a linear function of $\ln[O^{2-}]$, *as experimentally found,* only if E' can be considered a constant. This seems possible for the following conditions:

$$\alpha \simeq 0, \qquad \beta \simeq 0 \quad \text{(low values of } K_2 \text{ and } K_3) \tag{5}$$

$$\alpha \simeq 1, \qquad \beta \simeq 0 \quad \text{(high value of } K_2, \text{ low value of } K_3) \tag{6}$$

$$\alpha \simeq 0, \qquad \beta \simeq 1 \quad \text{(high value of } K_3) \tag{7}$$

for which (see Table 1) the probable potential determining electrode reactions would be (a), (b) and (c) respectively. The third of these limiting situations might explain the experimental slope RT/F. In this case most of the oxide is converted to superoxide and relation (4) becomes:

$$E = E^0_{O_2/O_2^-} + (RT/F)\ln[O_2]/2 - (RT/F)\ln[O^{2-}] \tag{8}$$

where $[O_2]$ is a constant at equilibrium conditions.

Actually, a quite complete and relatively fast oxidation of oxide to superoxide, under the experimental conditions at which the above-mentioned potentiometric measurements were performed, seems to be a real possibility on the basis of the thermodynamic data[7] reported in Fig. 1 and of the kinetic information in the literature[4,6]. The value of K_3, at the temperature of the nitrate solvent experiments of Shams El Din and Gerges, extrapolated from the data in Fig. 1, is 5×10^4 (K_2 is certainly very high, *e.g.* it is $\simeq 10^{17}$ mol^{-1} kg in nitrates[4] at 500°K). At the same temperature the oxygen concentration, under one atmosphere pressure, can be supposed to be of the order of magnitude of 10^{-4} mol kg^{-1} (from voltammetric measurements it has been found to be $\simeq 10^{-5}$ mol kg^{-1} at 502°K and the temperature coefficient for gas solubility[8] in molten solvents is usually of the order of +10 kcal). These data indicate that more than 90% superoxide★ can be present up to an

---

★The contribution of the reaction[4,9] $NO_3^- + O_2^- = NO_2^- + 2O_2^-$ is not considered because it is probably, negligible at this temperature.
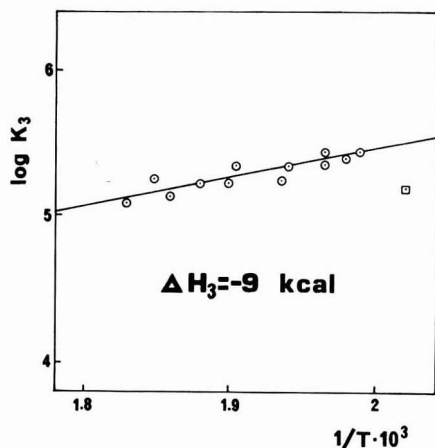
Fig. 1. Plot of lg K_3 vs. $1/T$. Values calculated from experimental data[4-7] obtained in $(Na,K)NO_3$ (⊙) and $(Li,K)NO_3$ (⊡) eutectic solvents.

added concentration of oxide of the order of 10^{-1} mol kg^{-1}. This value, in effect, corresponds approximately to the upper limit of the concentration range, at which Shams El Din and Gerges verified an RT/F slope. An upper limit of the same order of magnitude was found by Wrench and Inman working in molten chlorides at higher temperature ($723°K$). Since a large solvent effect is not to be expected★ the non-existence of a remarkable temperature effect on the limit value of concentration (which depends on the completeness of reaction (3)) can be explained considering that the effect of a decrease of K_3 with the temperature (ΔH negative) can be balanced by an increase in the oxygen solubility (ΔH positive).

The inconsistency of the results obtained at low oxide concentrations (approximately 10^{-3} and 10^{-2} mol kg^{-1} in nitrates and chlorides solvent, respectively) is in agreement with the extreme difficulty in obtaining perfectly dry melts. In the presence of traces of water part of the oxide is "stabilized" by the reaction:

$$O^{2-} + H_2O = 2OH^-$$ (9)

which is fast and practically complete[1,10]. Other anomalies can be due to SiO_2 present because of vitreous components of the cell.

In the work of Wrench and Inman the oxygen electrode was found to respond very slowly to changes in the partial pressure of oxygen and no real stable potentials could be attained in a reasonable lapse of time. The fact seems in accord with the model proposed here, considering that the measurements at lower oxygen pressures were performed pumping down the system after that steady, reproducible potentials were attained (which implies an

★The probable small influence of solvent anions on equilibria involving negative ions and/or uncharged species has been previously pointed out[4]. Certainly the solvent cations are expected to play a major role on such equilibria. However, from Fig. 1 it seems that in the case of Na$^+$ and Li$^+$ (which are involved in this discussion) their substitution affects the equilibrium constant K_3 in a way which is not very significant in the context of the qualitative interpretation attempted in the present paper.

equilibrium situtation for process (3)) under 1 atmosphere of oxygen. This reduction of pressure promotes the decomposition (very probably a slow kinetic process) of the super-oxide previously formed giving rise to a "persistent" non-equilibrium situation.

In this discussion we have considered only the possibility of an homogeneous electrode mechanism, although a metallic oxide film has been noted on the electrode surface. The possibility of a second kind electrode does not seem very likely in fact, as pointed out by Wrench and Inman, since the same potential values have been observed with gold or platinum electrodes.

REFERENCES

1 N.S. Wrench and D. Inman, *J. Electroanal. Chem.*, 17 (1968) 319.
2 A.M. Shams El Din and A.A. Gerges, in *Electrochemistry, Proceedings of 1st Australian Conference on Electrochemistry 1963,* Pergamon, London, 1964.
3 P.G. Zambonin, Comments on literature reports at 156th Meeting of the Am. Chem. Soc.; section *Characterization and Analysis in Molten Salts,* Atlantic City, Sept. 1968.
4 P.G. Zambonin and J. Jordan, *J. Am. Chem. Soc.,* 91 (1969) 2225.
5 P.G. Zambonin and J. Jordan, *J. Am. Chem. Soc.,* 89 (1967) 6365.
6 J. Goret and B. Trémillon, *Bull. Soc. Chim. France,* (1966) 67.
7 P.G. Zambonin and V.L. Cardetta, Unpublished data (1969), work in progress.
8 G.J. Janz, *Molten Salts Handbook,* Academic Press, London, 1967.
9 P.G. Zambonin, *J. Electroanal. Chem.,* 24 (1970) 365.
10 J. Jordan, W.B. MacCarthy and P.G. Zambonin, in G. Mamantov (Ed.),*Characterization and Analysis in Molten Salts,* M. Dekker, New York, N.Y., 1969.

Preliminary note

Glow-discharge electrolysis in molten salts

L.W. HAMILTON and M.D. INGRAM

Department of Chemistry, University of Aberdeen, Aberdeen, AB9 2UE (Great Britain)

(Received November 28th, 1969)

We are reporting preliminary results of the first study of the chemical effects of glow-discharge electrolysis (GDE) in molten salts. Typically, the anode is a short distance (10 mm) above the surface of the melt, the space being occupied by argon at reduced pressure (25 mm), and a substantial current (35 mA) is passed through the cell on application of a high voltage – around 350 V, depending on conditions. We are investigating a number of systems including "hydrate" melts such as the bisulphate eutectic, $NH_4HSO_4-KHSO_4$ (83:17), and also anhydrous nitrate melts, KNO_3-NaNO_3 (1:1) and $KNO_3-Ca(NO_3)_2$ (2:1). There is no truth in an earlier report[1] that GDE is difficult to establish with molten-salt electrolytes; and therefore it should be possible to obtain interesting chemical effects similar to those reported for GDE in aqueous systems[2].

One reaction of interest is the anodic evolution of iodine from solutions of iodide in molten nitrates. The yield is unaffected by temperature but is markedly dependent on the iodide concentration, as can be seen from the data in Fig.1, which refer to the $KNO_3-Ca(NO_3)_2$ (2:1) melt. Following the usual convention for GDE[2], the current efficiency is expressed as a "G-value" in equiv. F^{-1}, and from the reciprocal graph (b) it is seen that as $1/[I^-] \to 0$, $1/G \to 0.33$. This corresponds to a hypothetical limiting G-value of 3 equiv. F^{-1} as the iodide concentration tends to infinity.

This high yield of anodic oxidation (in excess of Faraday's law) is understood in terms of the iodide ions *scavenging* the free radicals produced in the melt by the glow-discharge. One mechanism which could account for the above results will now be discussed. Ar^+ ions entering the melt from the discharge undergo a charge transfer reaction:

$$Ar^+ + NO_3^- \to Ar + NO_3 \tag{1}$$

Assuming that iodide ions are reacting with all the available free radicals, the experimental limiting G-value can be predicted on the basis of the following reactions:

$$NO_3 \to NO_2 + O \tag{2}$$

$$NO_2 + I^- \to NO_2^- + \tfrac{1}{2}I_2 \quad \text{(see ref. 3)} \tag{3}$$

$$O + 2I^- \to O^{2-} + I_2 \tag{4}$$
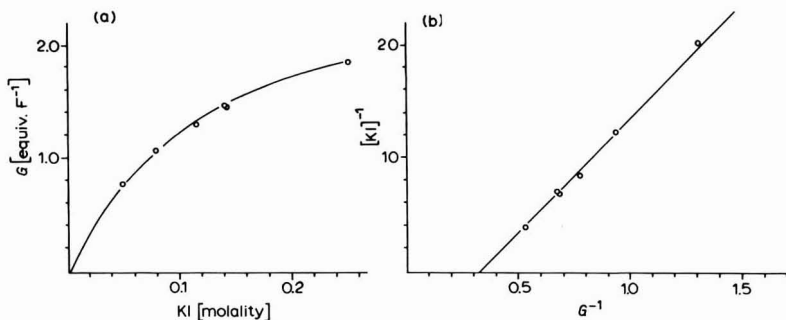
Fig. 1. Yields of iodine during GDE of molten $KNO_3-Ca(NO_3)_2$ (2:1) at 180°C, 25 mm of Ar, and 35 mA: (a) G-value (equiv. F^{-1}) is plotted *versus* molality of KI; (b) $1/G$ is plotted *versus* $1/[KI]$.

The electrolytic products, however, are strikingly dependent on the composition of the nitrate melt; and thus in the $NaNO_3-KNO_3$ melt the G-value of iodine is always zero. It is apparent either that the proposed reaction mechanism is incorrect or else that in different melts different reaction schemes are operative.

In aqueous GDE the high yields of electrolysis are ascribed to the break-up of water molecules into H and OH radicals, and it is possible that in the nitrate melts a similar process occurs, thus:

$$NO_3^- \rightarrow NO_2^- + O \tag{5}$$

The high yields of iodine in the $KNO_3-Ca(NO_3)_2$ melt could then arise entirely from reaction (4), and the absence of an iodine yield in the $NaNO_3-KNO_3$ melt could be caused by the disappearance of O atoms in a competitive reaction, thus:

$$O + NO_3^- \rightarrow O_2 + NO_2^- \tag{6}$$

In this second reaction scheme, the existence of an iodine yield is seen to depend on the non-occurrence of reaction (6), which in turn may be related to the existence of nitrato complexes of calcium in the $KNO_3-Ca(NO_3)_2$ melt[4]. A detailed discussion of this question must await the results of a polarographic study of the nitrate melts, which is now in progress.

The role of free-radical reactions in molten salt chemistry has previously received almost no attention, although Ubbelohde and his co-workers[5] have recently stressed the importance of chain reactions in the thermal decomposition of molten acetates and a report has appeared[6] on the γ-radiolysis of molten nitrates. GDE could provide a valuable new tool in the elucidation of free-radical reactions in molten salts.

REFERENCES

1 B.S.R. Sastry, *J. Electroanal. Chem.*, 10 (1965) 248.
2 A. Hickling and M.D. Ingram, *J. Electroanal. Chem.*, 8 (1964) 65.
3 R.F. Bartholomew and D.W. Donigian, *J. Phys. Chem.*, 72 (1968) 3545.
4 M.D. Ingram and J.A. Duffy, *J. Am. Ceram. Soc.*, submitted.
5 J.J. Duruz, H.J. Michels and A.R. Ubbelohde, *Chem. Ind.*, (1969) 1386.
6 V.M. Moralev and L.T. Bugaenko, *Khim. Vys. Energ.*, 1 (1967) 557.

CONTENTS

20.ᛃᛃ.25